NNT/NL : 2020AIXM0361/110ED62

THÈSE DE DOCTORAT

Soutenue à Aix-Marseille Université
Le 18 Novembre 2020

Alexandre Chuyen

Molecular and cellular basis of pattern establishment in a vertebrate epithelium.

Discipline

Biologie santé

Spécialité

Biologie du Développement

École doctorale 62

Sciences de la vie et de la santé

Laboratoire

Institut de Biologie du Développement de Marseille (IBDM)/CNRS – UMR 7288

Composition du jury

Roberto MAYOR UCL, Londres	Rapporteur
Cécile GAUTHIER-ROUVIERE CRBM, Montpelier	Rapporteuse
Marc BILLAUD CRCL, Lyon	Examinateur
Laurence RÖDER TAGC, Marseille	Examinatrice
Sophie CHAUVET IBDM, Marseille	Présidente du jury
Andrea PASINI IBDM, Marseille	Directeur de thèse

Affidavit

I, undersigned, Chuyen Alexandre, hereby declare that the work presented in this manuscript is my own work, carried out under the scientific direction of Andrea Pasini, in accordance with the principles of honesty, integrity and responsibility inherent to the research mission. The research work and the writing of this manuscript have been carried out in compliance with both the French national charter for Research Integrity and the Aix-Marseille University charter on the fight against plagiarism.

This work has not been submitted previously either in this country or in another country in the same or in a similar version to any other examination body.

Place Marseille, date 19 août 2020

Cette œuvre est mise à disposition selon les termes de la Licence Creative Commons Attribution - Pas d'Utilisation Commerciale - Pas de Modification 4.0 International.

Résumé

L'un des défis majeurs de la biologie du développement est de comprendre les mécanismes contrôlant la distribution des cellules dans un embryon. Les distributions cellulaires régulières ont été particulièrement étudiées, notamment dans le contexte de complexes réseaux de régulation des gènes dictant le destin des cellules à une position donnée. Cependant, comment des patrons globaux peuvent émerger de comportements individuels restent mal compris.

Lors du développement de l'épiderme mucociliaire chez l'amphibien *Xenopus laevis*, les cellules multiciliées (MCCs), s'intercalent radialement de la couche interne où elles naissent, à la couche épithéliale externe. Fait remarquable, ces MCCs s'intercalent entre les jonctions d'au moins trois cellules de la couche externe (vertex), et respectent une règle stricte de non-contiguïté, ce qui se traduit par un patron de distribution semi-régulier.

Durant ma thèse, j'ai étudié les mécanismes contrôlant la distribution régulière des MCCs. Avant de s'intercaler, les MCCs sont distribués en amas irréguliers au sein de la couche mésenchymateuse interne et se dispersent progressivement. Par modélisation mathématique, nous avons suggéré que l'intégration de la répulsion mutuelle des MCCs et leur affinité avec les jonctions de cellules de la couche externe suffis pour récapituler une distribution régulière. La vidéomicroscopie a démontré que les MCCs se séparent les unes des autres par un mécanisme de type inhibition de contact de la locomotion alimenté par le remodelage de l'actine Arp2/3 dépendant. En parallèle, les MCC se déplacent en remodelant le cytosquelette d'actine pour suivre les jonctions extracellulaires. Des approches fonctionnelles multiples, ont démontré que la voie de signalisation dépendant du récepteur de la tyrosine kinase Kit et de son ligand associé Scf sont tous deux nécessaires à la bonne distribution spatiale des MCCs. Scf est exprimé par les cellules épithéliales de la couche externe, tandis que Kit n'est exprimé que par les MCCs. Altérer la voie Scf/Kit entraîne de graves anomalies de distribution des MCCs, causées par la perte de répulsion mutuelle, d'une réorganisation de l'actine altérée et d'une affinité réduite pour les jonctions extracellulaires. Alors que Scf se comporte comme un puissant signal adhésif pour les MCCs, l'expression de Kit est suffisante pour conférer de l'ordre à une population de cellules hétérologues désordonnées. Ces travaux révèlent comment un seul système de signalisation peut mettre en œuvre une structuration auto-organisée à grande échelle.

Mots clés : développement du Xénope, morphogénèse de la peau, intercalation cellulaire radiale, patron cellulaire régulier, patron d'espacement, dispersion cellulaire, migration cellulaire, répulsion cellulaire mutuelle, remodelage du cytosquelette, inhibition de contact de la locomotion

Abstract

One of the major aims of developmental biologists is to understand the mechanisms controlling the distribution of cells in an embryo. Regular cell distribution patterns have been widely studied, particularly in the context of complex genes regulatory networks which dictate the fate of cells at a given position. However, how global patterns can emerge from individual behaviors remains poorly understood.

During the development of the mucociliary epidermis in the amphibian Xenopus laevis, multiciliated cells (MCCs), intercalate radially from the inner layer where they are born, to the outer epithelial layer. Remarkably, these MCCs intercalate at the junctions between at least three cells of the outer layer (vertex) and follow a strict rule of non-contiguity, resulting in a semi-regular distribution pattern.

During my thesis, I studied the mechanisms that control the regular distribution of MCCs. Before intercalation, MCCs are distributed in irregular clusters within the internal mesenchymal layer and progressively disperse. By mathematical modeling, we suggested that the integration of the mutual repulsion of MCCs and their affinity with the cell junctions of the outer layer is sufficient to summarize a regular distribution. Live-imaging shows that MCCs separate from each other through contact-inhibition-like mechanism powered by Arp2/3-mediated actin remodelling. Concomitantly, MCCs follows the extracellular junctions and stabilize beneath vertices by remodelling actin cytoskeleton. Using multiple functional approaches, we showed that the signalling pathway dependent on the tyrosine kinase receptor c-KIT and its cognate ligand Scf are both required for the proper spatial distribution of MCCs. Scf is expressed by the outer layer epithelial cells, while the expression of c-KIT is restricted to MCCs. The disruption of the Scf/c-KIT pathway results in severe abnormalities in the distribution of MCCs, which stem from loss of mutual repulsion, impaired actin reorganization and reduced affinity for vertices. While Scf behaves as a potent adhesive cue for MCCs, Kit expression is sufficient to confer order to a disordered heterologous cell population. Our work reveals how a single signalling system can implement self-organized large-scale patterning.

Keywords: Xenopus development, skin morphogenesis, radial cell intercalation, regular cell pattern, cell dispersion, cell migration, mutual cell repulsion, cytoskeleton remodelling.

Remerciements

First, I would like to acknowledge the members of my thesis jury, Dr. Roberto Mayor, Dr. Cécile Gauthier-Rouviere, Dr. Marc Billaud, Dr. Laurence Röder, Dr. Sophie Chauvet and Dr. Andrea Pasini for spending time reviewing this manuscript.

Je remercie infiniment tous ceux qui de près ou de loin ont contribué à cette thèse.

Aux membres de mon comité de thèse, **Marc Billaud, Laurence Röder, Claudio Collinet, Andrea Pasini Laurent Kodjabachian**. Vos conseils et encouragements ont grandement contribué à la maturation de ce projet et j'espère avoir utilisé au mieux ces deux après-midis d'échanges stimulants dans l'aboutissement du projet, merci à vous.

Laurent Kodjabachian, merci de m'avoir accueilli dans ton équipe, tes conseils et ton soutien m'auront fait grandir tout au long de cette thèse. Merci infiniment d'avoir soutenu mes prolongations de contrats et d'avoir fait de ton mieux pour assurer un bon environnement de travail depuis le premier jour de mon recrutement jusqu'à ma soutenance ainsi que la chance que tu m'as offerte de participer à plusieurs congrès.

Andréa Pasini, depuis six ans, tu m'accompagnes, me guides et me conseilles, merci infiniment d'avoir été mon maitre de stage, puis mon directeur de thèse. Que ce soit au labo, au téléphone, ou dans un bar la veille d'un oral pour répéter, tu as été le mentor qu'il me fallait. En me laissant travailler en autonomie, j'ai pu découvrir de quoi j'étais capable. Bien sûr, tu veillais au grain afin que je garde le cap. En Master, je doutais énormément de moi et ce gage de confiance m'aura considérablement aidé. J'ai grandement apprécié ta pédagogie qui m'a fait grandir et m'épanouir dans les sciences, tu m'auras aidé à trouver ma voie. Enfin, merci de ta patience pour la relecture de ce long manuscrit.

Merci à toute l'équipe pour votre accompagnement et tous ces moments partagés.
Virginie, pour tes conseils techniques, tu fais tourner l'équipe et on peut toujours compter sur toi.
Camille, merci pour tous tes conseils techniques et scientifiques j'ai beaucoup apprécié nos longues conversations en tous genres ainsi que tes derniers conseils lors de l'organisation de la thèse et des figures.
Olivier, Diego et Juliette et Athulia, merci pour tous vos conseils qui ont contribué à cette thèse.
Claire, tu es arrivée en fin de thèse mais merci pour ta bonne humeur et nos conversations philosophiques variées. J'ai beaucoup apprécié nos réflexions sur les poursuites de carrières et le monde de la recherche.
Marie Zilliox, merci infiniment pout ta joie de vivre lors de tes stages j'ai été heureux de participer à ton encadrement et même si je comprends parfaitement tes choix de partir sur de nouveaux projets, sache que j'aurais beaucoup aimé travailler avec toi sur cette fin de thèse, je serais ravi que nos routes se croisent dans le futur.
Pour finir, **Aude**, le meilleur binôme qui soit ! Malgré nos tentatives respectives d'assassinat (toi t'échouant sur une digue en paddle ou moi poussé dans le canal à vélo), qui aurait cru que ce début de thèse conduirait à une amitié si forte ? Merci pour tous ces bons moments partagés au labo, en congrès et en dehors du travail. Je suis heureux de t'avoir trouvée et même si nos routes se séparent en post-doc, le « frog binôme » restera.

Merci **Raphaël, Charlotte et Fabrice** pour votre contribution à l'article et nos échanges

Merci à tous les autres encadrants qui au fil de mes stages, m'ont guidé pas à pas :
Vincent Bertrand, j'ai pu découvrir la recherche grâce à ce premier stage dans ton équipe, je garde encore de très bons souvenirs de toi et Pauline m'apprenant les bases.
Manos Mavrakis, j'ai énormément apprécié travailler avec toi et les techniques que tu m'as apprises m'auront aidé tout au long de cette thèse.
Dominique Massey-Harroche, tes conseils m'auront aidé à gagner en organisation.
Laurent Perrin, Laurence Roder et Ramy Ragheb, Merci encore pour l'ambiance exceptionnelle lors de ce stage avec vous.
Laurence tu m'as trouvé alors que j'étais perdu et m'auras permis de transformer ce que je voyais comme un échec en une réussite, tu as été une vraie marraine de thèse, toujours là à me conseiller ou simplement rire autour d'un café. Je suis heureux d'avoir fait ce deuxième Master sans lequel je ne serais jamais arrivé dans votre équipe et bien que je sois parti lors de ma thèse j'apprécie de vous retrouver en toutes occasions.

Merci à tous les amis du **TAGC et d'Hippo'thèse** ! Ce temps consacré à une association en plus de ma vie au labo aura été d'un grand épanouissement. Merci à **Florian, Laurianne et Eva** pour m'avoir insidieusement conduit à en prendre la présidence, je n'aurais jamais imaginé faire ça un jour et je vous en suis fort reconnaissant car j'ai adoré pouvoir gérer ce beau projet. J'espère que l'asso nous survivra encore longtemps. En mémoire de tous ces afterlabs ! **Quentin**, merci beaucoup pour tes conseils en stats, j'ai trouvé ça très stimulant, merci beaucoup aussi pout tous les moments passés.

Merci à toi **Elsa** pour tout ton soutien et tes conseils depuis le Master.
Un grand merci également à **Charlotte, Caroline, Claudio, Marwa, Lucrezia, Lucie, Sara, Catarina, Anissa, Alain et Veronika** pour tous ces moments partagés au labo, dans les transports, ou en dehors j'ai beaucoup aimé vivre cette aventure avec vous.

Je ne pouvais finir ces remerciements sans mentionner ma famille, mon premier et plus grand soutien. Au-delà de la fierté d'être allé si loin, ces études représentent beaucoup de sacrifices et aussi un petit sentiment parfois amer par mon passage en Médecine, heureusement vite balayé et avantageusement remplacé par ma fabuleuse année de licence à Montréal jusqu'à la thèse… Dix ans passés en un éclair...
Caro, **Cloé**, vous étiez enfants vous voilà femmes ! Merci de m'avoir soutenu pendant tout ce temps, sans vous je n'aurais sans doute pas dépassé le collège ! Je sais que vous êtes fières de moi mais vous n'avez pas idée à quel point je le suis de vous !
Ana, je sais que plus tard tu veux « être un scientifique comme ton grand frère », je te souhaite de trouver ta voie.
Papa, **maman**, merci pour votre éducation, cette force de ne jamais baisser les bras et de se battre pour ses rêves c'est à vous que je le dois.
Merci aussi à ces mauvais profs me poussant à l'abandon, c'est peut-être mon esprit de défi et de revanche qui m'a mené si loin ?
Merci à **Magalie** d'avoir croisé ma route. Tu partages ma vie et m'épaules au quotidien sans faille. J'espère que ma thèse ne t'a pas trop soulée. Tu as vu ce projet grandir et auras tout fait pour que je puisse m'y consacrer dans les meilleures conditions possibles. Merci de ta patience, particulièrement pendant ce confinement où je n'ai fait que travailler et écrire... Encore désolé pour toutes ces soirées, weekend et mêmes parfois vacances où je restais bloqué au labo, promis c'est fini, maintenant on va profiter ensemble, quoi que, le post-doc arrive ^^

Table of contents

AFFIDAVIT **2**

RÉSUMÉ **3**

ABSTRACT **4**

REMERCIEMENTS **5**

TABLE OF CONTENTS **7**

Abbreviations list **9**

INTRODUCTION **11**

1. CELLULAR PATTERNS IN DEVELOPMENT AND THEIR CONTROLLING MECHANISMS **12**

1.1 Principles of mathematical modelling of pattern formation 13

1.2 Principles of biological mechanisms of pattern formation 15

1.2.1. Genetically controlled cell positioning: when cell pattern is pre-printed 15

1.2.1.1. Long range intercellular communication: the morphogen-dependent patterning 17

1.2.1.2. Short range tissue communication 27

1.2.2. Spacing pattern by controlled cell and tissue remodelling 31

2. PATTERN MORPHOGENESIS THROUGH CELL MOVEMENT: ACTORS AND MECHANISMS **38**

2.1. The cytoskeleton 38

2.1.1. Intermediate filaments 40

2.1.2. Microtubules 42

2.1.3. Actin filaments 47

2.1.3.1. The modular architecture of the actin cytoskeleton in migrating cells. 48

2.1.3.2. Actin-based structures involved in cell motility 52

2.2. Morphogenetic processes that shape tissue 57

2.2.1. The Acto-Myosin contractility generates cell shape changes and cell movement. 57

2.2.2. Epithelium remodeling through cell shape changes and movements. 58

2.2.3. Cell migration 63

2.3. Avoiding one's neighbors: the mechanisms of cell repulsion 75

2.3.1. Contact inhibition of locomotion 75

3.MULTICILIATED CELLS IN *XENOPUS LAEVIS* EMBRYONIC EPIDERMIS: A MODEL OF REGULAR CELL DISTRIBUTION PATTERN **81**

3.1. Mucociliary epithelium 82

3.1.1. The composition of Xenopus MCE 84

3.1.1.1. Mucus producing cells 84

3.1.1.2. Multiciliated cells (MCCs) 85

3.1.1.3. Ionocytes 86

3.1.1.4. Small secretory cells 87
3.1.1.5. Basal cells 88
3.2. The development of Xenopus mucociliary epithelium: a multistep process 88
3.2.1. Ectodermal layer segregation 88
3.2.2. Cell fate specification 89
3.2.3. Cell intercalation 92
3.2.4. Cell differentiation 98
3.3. MCC patterning. 99
4. THE SCF/KIT SIGNALING PATHWAY IN CELL MIGRATION AND CELL REPULSION 101
4.1. The Stem Cell Factor (SCF) ligand 101
4.2. The tyrosine kinase receptor KIT 103
4.3. The SCF/c-KIT signaling pathway controls cell adhesion, migration and cytoskeletal reorganization. 105
5. AIM OF MY WORK 109
6. RESULTS 110
6.1. Manuscript under revision at Dev Cell 110
6.2. Experiments required for manuscript revision 111
6.2.1. The affinity of MCCs for outer layer cell junctions is a non-random behavior 111
6.2.2. Quantification of cell speed 113
6.2.3. Does the cleaved version of Scf stimulate the mutual dispersion of MCCs? 116
6.3. Unpublished data 119
6.3.1. Wiskott–Aldrich syndrome protein does not regulate the mutual repulsion of MCCs 119
7. DISCUSSION 121
8. CONCLUSION AND PERSPECTIVES 135
9. MATERIAL AND METHOD 137
BIBLIOGRAPHIE 139

Abbreviations list

+TIP: microtubules plus-end tracking protein

α-DG: α-DistroGlycan

α-tub: α-tubulin

ADAM: Disintegrin and metalloproteinase domain-containing protein
ADF: Actin-Depolymerizing Factor
ADP/ATP: Adenosin Di/Tri Phosphate

AKT: Protein Kinase B
APC: Adenomatous Polyposis Coli
aPKC: atypical Protein Kinase C
ARP: Actin Related Protein

BB: Basal Body
Bcd: Bicoid
bHLH: basic Helix-Loop-Helix

BMMCs: Bone Marrow–derived Mast Cells
BMP: Bone Morphogen Protein

C3a: Complement component 3a
C3aR: C3a anaphylatoxin chemotactic Receptor
ca12: carbonic anhydrase 12
CC: Ciliated Cells
CIL: Contact Inhibition of Locomotion

CP: Capping Proteins
CR: Cajal-Retzius cells
CSL: CBF1, Suppressor of Hairless, Lag-1
CXCL12: C-X-C motif chemokine 12

DMSO: Dimethyl Sulfoxide
dn: dominant negative

DNA: DesoxyriboNucleic Acid
DRG: Dorsal Root ganglia

EB: End-Binding protein
ECM: Extracellular Matrix
EDA: Ectodysplasin A
EDAR: Ectodysplasin A Receptor
EDNRB: endothelin receptor B

EMT: Epithelial-to-Mesenchymal Transition
Ena: Drosophila enable
ERK: Mitogen-activated protein kinase
ERM: Ezrin, Radixin, Moesin

FAK: Focal Adhesion Kinase
FGF: Fibroblast Growth Factor
FISH: Fluorescent in situ Hybridization

FoxA1: Forkhead box protein A1
FoxJ1: Forkhead box protein J1

GCL: Ganglion Cell Layer
GCRP: G-Protein-coupled-receptor
GDP / GTP: Guanosine Di/Tri Phosphate
GEF: Guanine nucleotide Exchange Factor
GEF-Vav2: vav Guanine nucleotide Exchange Factor 2
Gemc1: Geminin coiled-coil domain-containing protein 1

GFP: Green Fluorescent Protein
GliA/R: transcription factor Gli (activator / Repressor form)
Gmnc: Geminin coiled-coil domain-containing protein 1 coding gene
GPI: GlycosylPhosphatidylInositol
GRN: Gene Regulatory Network

HC: Retinal Horizontal cells

Hpf: Hours' post-fertilization

INL: Inner Nuclear Layer
IPL: Inner Plexiform Layer

ISH: In Situ Hybridization

KIF13B: Kinesin-like protein KIF13B

KitL: Kit Ligand

LGL2: scribble cell polarity complex component 2
LPA: LysoPhosphatidic Acid

Lrp6: Low-density lipoprotein receptor-related protein 6

MAPK : Mitogen-Activated Protein Kinase
MAPs: Microtubule-Associated Proteins
MCCs: MultiCiliated Cells
MCE: MucoCiliary Epithelia
MCI: Multicilin
MEK: Dual specificity mitogen-activated protein kinase kinase
MGF: Mastocyte Growth Factor
miR: microRNA
MOs: antisens Morpholono-modified oligonucleotides
mRNA: messenger RiboNucleic Acid
MSA: Migration staging area
MSCs: Malanocytes Stem Cells
MTOC: Microtubules organizing center
MTs: Microtubules
Myb: MYB proto-oncogene, transcription factor

N: nucleus
NC: Neural Crest
NCCs: Neural Crest Cells
NECD: Notch ExtraCellular Domain
NFL: Nerve Fiber Layer
NICD: Notch Intracellular Domain
NPFs : Nucleating Promoting Factors
Nrp1/2: Neuropilins 1 and 2
NSPC: Neuronal Stem/Progenitor Cell
NT: Neural Tube

OLM: Outer Limiting Membrane
ONL: Outer Nuclear Layer
OPL : Outer Plexiform Layer
ORF: Open Reading Frame
OS: Outer Segment

PCP: Planar Cell Polarity
PCR: Poly Chain Reaction
PDGF: Platelet-Derived Growth Factor
PGCs: Primordial Germ Cells
PI3K: PhosphoInositide 3-Kinase
PIP2: PhosphatidylInositol 4,5-bisphosphate
Pk3: Prickle3
PKC: Protein Kinase C
PLCγ: Phosphoinositide phospholipase C γ
PN: Peripheral Nerves
PR: PhotoReceptor
Ptch: Protein patched

Rab11: Ras-related protein Rab-11
RFP: Red Fluorescent Protein
Rfx: Regulatory factor X
RH: Retinal Horizontal cells
RNA: RiboNucleic Acid
ROBO: Roundabout
ROCK: Rho-associated protein kinase
RPE: Retinal Pigment Epithelium
RTK: Receptor Tyrosine Kinase
RT-PCR: Reverse Transcription-Poly Chain Reaction

SCF: Stem Cell Factor
SCPs: Schwann Cell Precursors
SDF1: Stromal cell Derived Factor 1
Sema: Semaphorin
SGPs: Somatic Gonadal Precursors
SHH: Sonic HedgeHog
SLF: Steel Locus Factor (SCF)
SLIT: Slit homolog 2 protein
Smo: Smoothened
SoxB: Sarcosine oxidase subunit beta
Src: Proto-oncogene tyrosine-protein kinase sarc
SSC: Small Secretory Cell

TFs: Transcription Factors
TK: Tyrosine Kinase
TRE1: Protein Trapped in Endoderm-1
tTJ: Tri-cellular Tight Junctions
Tyr: Tyrosine

Vangl2: Vang-like protein 2
VASP: Vasodilatator-Stimulated Phosphoproteine
v-ATPase: Vascular proton pumps
VEGF: Vascular Endothelial Growth Factor
VEGFR: Vascular Endothelial Growth Factor Receptor.

WASP: Wiskott-Aldrich Syndrome Protein

ZO-1: Zonula Occludens protein 1

Introduction

1. Cellular patterns in development and their controlling mechanisms

Patterns in nature, defined as visible regularities of form found in the natural world, have always been topic of interest and already captured the attention of the early Greek philosophers Plato, Pythagoras and Empedocles.

In multicellular organisms, regular patterns are the consequence of millions of years of evolution driven by the process of natural selection. From the initial determination of embryonic layers to later organ formation and functioning, the generation of patterned cell populations is crucial to every aspect of development and physiology.

Throughout their variety of body shapes, Metazoans (multicellular animals) present many striking cases of patterning such as appendages and integument pigmentation patterns, regular distribution of cell populations, cell layering, or body segmentation (Figure 1).

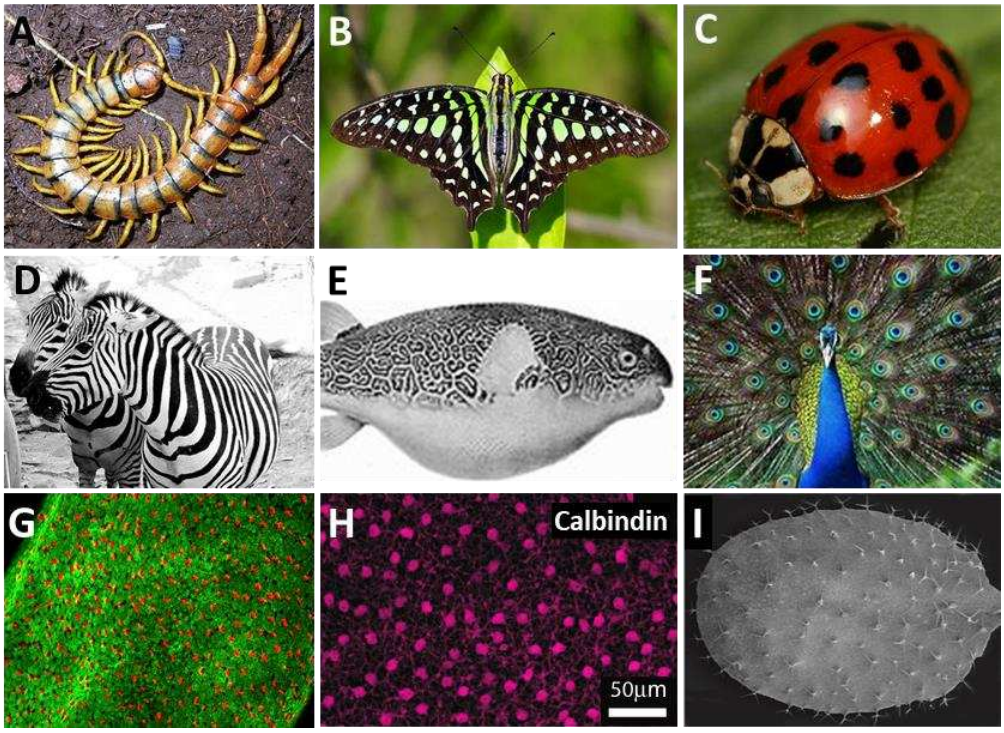

Figure 1: Regular patterns in multicellular organisms.

Representation of the diversity of macroscopic scale regular patterns in invertebrates: **(A)** repetitive segments in arthropod (centipede), **(B,C)** pigmentation pattern in insects such as stripes (butterfly,) or spots (ladybug) and in vertebrates: **(D)** Zebra pigmentation stripes, **(E)** elaborate labyrinth-like skin patterns in adult giant pufferfish, and **(F)** "eyespot" on the train feather of peafowl. Highly organized cellular patterns establish during the formation of specific structures in tissues and organs as the result of single cell distribution: **(G)** Fluorescent i*n situ* hybridization for α-tubulin shows the regular spacing of multiciliated cells throughout the skin of *Xenopus* tadpole (image from Kodjabachian lab). **(H)** Calbindin immunofluorescence of mouse retinal flat-mount showing the horizontal cells somata and processes and reveals the non-random distribution of these cells across the retina (from Poché et Reese, 2009). **(I)** Regular distribution pattern in plants: example of the epidermal hair of *Arabidopsis thaliana* shown by scanning electron micrograph of a two-week-old wild-type leaf displaying regularly spaced trichomes with three to four branches, leaf base to the bottom (Grebe, 2012).

Generally, regular cell distribution patterns arise during embryogenesis through processes such as cell specification and cell movements, which are controlled by a variety of underlying mechanisms.

Over the past centuries, scientists from different disciplines and backgrounds (biologists, physicists, mathematicians) have tried to explain the occurrence of regular patterns in development. In particular, unravelling the molecular and genetic mechanisms of pattern formation has been a major goal of cell and developmental biology. Also, mathematical modelling such as that proposed by Alan Turing has provided major clues in our understanding of pattern formation (Turing, 1952).

In this first chapter, I will briefly present some non-exhaustive examples of regular patterns in multicellular organisms and their underlying developmental mechanisms.

1.1 Principles of mathematical modelling of pattern formation

In parallel to the experimental work of biologists, physicists and mathematicians have provided fundamental work to explain the formation of developmental patterns. Indeed, many aspects of the process by which a a single cell (the zygote) forms a fully differentiated multicellular organism with elaborated shapes and patterns can be recapitulated by mathematical models based on sets of equations. Giving too many details about modelling would be far beyond the aim of my work, so I will go straight to the main principles. Indeed, theoretical models provide a good entry point into the developmental concepts and the main examples that will be presented throughout this chapter.

In 1952, Alan Turing's work proposed a theoretical model to explain the formation of regular patterns. At a time when DNA structure was not yet fully revealed, Turing postulated that the formation of living beings must respect some logic and developed "a mathematical theory of embryology" (Turing, 1952). In his work, Turing postulated that natural patterns such as stripes and spots result from the reaction of chemical species with particular characteristics and proposed the so-called 'reaction-diffusion' model. This model hypothesizes diffusing molecules as responsible for the generation of growing shapes and structures in developing organisms. Such diffusing molecules, named "morphogens" were later identified *in vivo* (Wolpert, 1969). Turing's diffusion-reaction model requires two components, an activator and an inhibitor, that freely diffuse within the tissue with different kinetics. The activator auto-amplifies by positive feedback and, after a certain threshold, it produces the repressor, which turns off the activator. Also, the diffusion of the repressor is faster than that of the activator. In the initial system, the interacting agents are stable and homogeneous but diffusion induces fluctuations that give to the system the potential to spontaneously reorganize. This model relies on self-

organization, since it only requires the interaction of two diffusive components without any initial asymmetry or any pre-printed pattern in the system, (Meinhardt & Gierer, 2000).

While the reaction-diffusion model is rather simple, changing some parameters produces a variety of patterns such as stripes, spots or even more complex structures such as digits (Kondo & Miura, 2010; Sheth et al., 2012; Raspopovic et al., 2014). Taking for example the cheetah, it harbours spots on its body and stripes on its tail and Turing's reaction-diffusion model can predict both types of pattern. As previously mentioned, the condition of the system will govern the type of pattern generated. The size of the system is one of the variables of the reaction-diffusion model. The tail can be considered as a tube with a progressively decreasing radius. As for the rest of the body, the basis of the tail is large enough to support two-dimensional patterns like spots. When the radius becomes smaller, the region of high activator concentration spreads all the way around and joins up with itself so that spots become stripes. Interestingly, the reaction diffusion model adapts the generated pattern to the shape of the tissue (Gierer & Meinhardt, 1972; Murray, 1988).

Turing's model theoretically accounts for most of the patterns observed in living systems. However, in reality a "simple" two component reaction-diffusion system *per se* cannot fully explain the complex morphogenetic programs which depend on multiple genetic and molecular regulators, a common criticism of experimental biologist (Landge et al., 2020). Turing himself was critical about his own model: "This model will be a simplification and an idealization, and consequently a falsification. It is to be hoped that the features retained for discussion are those of greatest importance in the present state of knowledge" (Turing, 1952).

Therefore, the biological relevance of his work has been extensively challenged over the last seventy years: *"Well the stripes are easy. But what about the horse part?" – Alan Turing, in reaction to the enthusiasm regarding his work on reaction-diffusion systems, as supposedly quoted by Francis Crick in 1972*. It was then proven that systems where the initial conditions comport asymmetries such as local enrichment of maternal transcript don't follow the reaction-diffusion model (Carroll, 2005; Fox Keller, 1999; Salazar-Ciudad et al., 2001). This is the case of the antero-posterior segmentation of the drosophila embryo, where the regular pattern doesn't depend on self-organization process, as it will be shown later in this chapter. The observation of asymmetrically distributed gradients of diffusive morphogens gave rise to the concept of "positional information" through a new model of pattern generation, the "French flag" (Wolpert, 1969). In this model, each cell in a line of cells exposed to a morphogen gradient has the potential to be "blue, white or red". The cells take up different identities depending on their position along the axis in response to the concentration profile of the diffusing morphogen (the positional information) and thus become "blue, white or red".

On the other hand, many biological processes have been shown to follow Turing's reaction diffusion principle, such as skin patterns: hair follicle in mice, feather in birds, stripes formation in zebrafish, labyrinth-like pigment patterns on the epidermis of the giant pufferfish and mouse digits as previously mentioned (Sick et al., 2006; Sheth et al.,

2012; Watanabe & Kondo, 2015; Aragón et al., 1998; Ishida et al., 2019; Marcon & Sharpe, 2012). Also, we cannot exclude combinations of positional-information and reaction diffusion models *in vivo* (Green & Sharpe, 2015). As we saw here, theoretical models inspired developmental biologists by suggesting mechanisms not yet proven at the molecular level while in turn biologists also inspired mathematicians, thus leading to mutual enrichment between experimental and theoretical approaches (Marcon & Sharpe, 2012).

1.2 Principles of biological mechanisms of pattern formation

The purpose of this chapter is to present a general view of the several developmental ways to generate a regular pattern. We can schematize three main developmental mechanisms that account for the establishment of the vast amount of regular pattern that can be observed:

- The first one is pattern specification, where cells become committed to a specific position following a specific developmental program by a pre-patterning mechanism that cannot be visualised simply by looking at physical properties of the undifferentiated cells but may be driven by the creation of a genetic pre-pattern.
- The second one involves the morphogenetic events that take place to generate regular patterns from populations of initially disorderly distributed but already fated cells. For example, changes in adhesion molecule concentration, cell motility, and cell rearrangements that will favour transition from an initial unordered cell distribution to an ordered pattern.
- Often the two mechanisms cannot be separated; genetic pre-patterns irreversibly mark the position of a presumptive pattern by cell specification, and cells undergo morphogenetic events that remodel the tissue and generate the final regular pattern (Baker et al., 2009).

1.2.1. Genetically controlled cell positioning: when cell pattern is pre-printed

Patterns in developing embryos often arise from the action of Gene Regulatory Networks (GRNs), which control the specification of cells with respect to their spatial positioning (Davidson, 2010). GRNs depend on spatiotemporal cues allowing a tightly organized spatial distribution of cells essential for the developmental processes and control both cell fates and their position at the same time. Also, *de novo* formation of

embryonic territories requires GNRs based on several sub-circuits organized in successive 'layers' of processes (Davidson, 2010).

To reproducibly construct patterns in the embryo, cell communication is required to organize individual cells throughout the tissue. Therefore, pattern can arise from long- and short-range cell communication under the control of GNRs. Long range signalling requires the secretion of diffusing molecules to coordinate patterning at the whole tissue scale while short-range signalling mostly relies on direct cell-cell contact and the ensuing signal transduction (Figure 2) (Inomata, 2017). In the following section I will develop how long- and short-range signals control regular patterning in developing tissues. Of note, *in vivo* these two mechanisms are not exclusive and can work in combination to establish patterns.

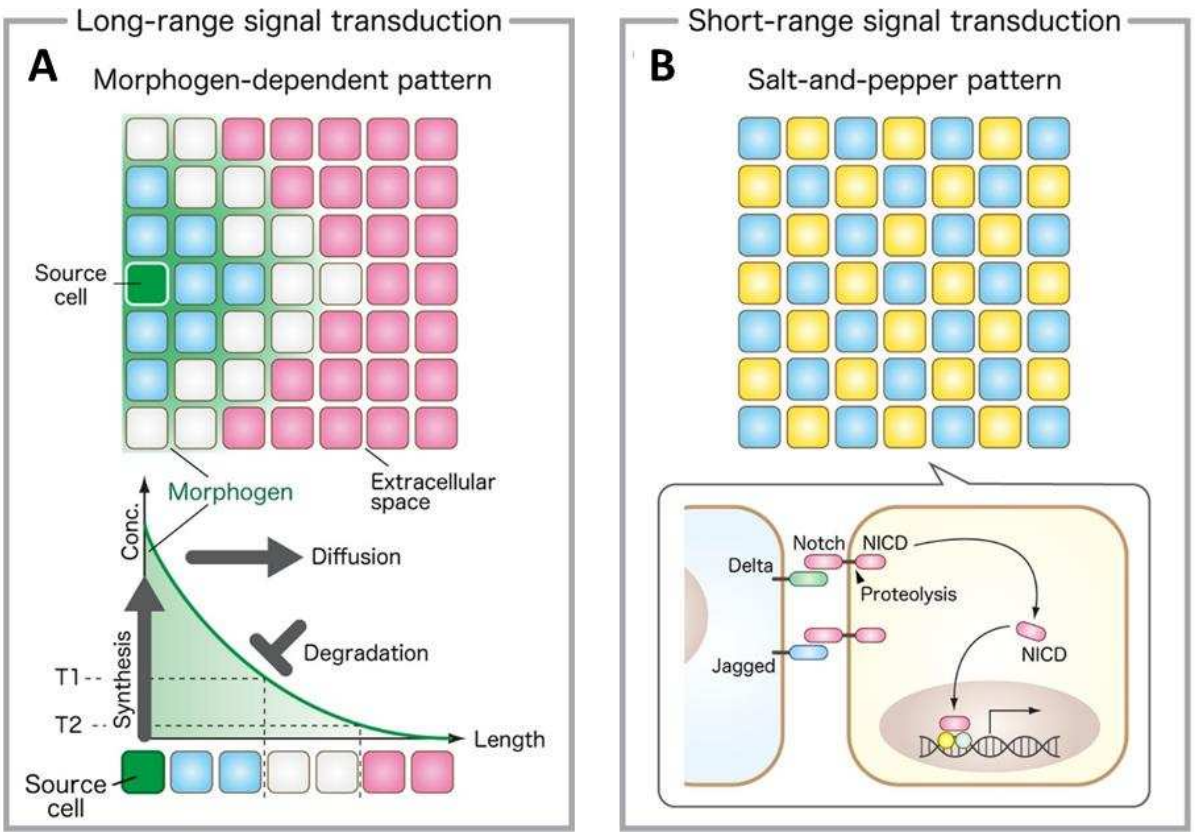

Figure 2: Schematic of long-range and short-rage signal transduction in pattern formation.

(A) Secreted morphogens diffuse from the source cells into the extracellular space, creating a gradient. Cells differentiate into three different types according to the threshold (T1 and T2) of morphogen concentration: blue cells (high), white cells (middle), and red cells (low). The shape of the gradient is mainly regulated by synthesis, diffusion, and degradation.

(B) Salt-and-pepper patterns (blue and yellow pattern) can arise by lateral inhibition, mediated by Notch signaling. Interaction between Delta/Jagged and Notch causes proteolysis of the Notch intracellular domain (NICD). NICD forms a transcriptional activator complex in the nucleus and activates Notch target genes (Adapted from from Inomata, 2017)

1.2.1.1. Long range intercellular communication: the morphogen-dependent patterning

In the 1950's, the theoretical concept of gradients of soluble factors called 'morphogens' that control the embryo development depending on their concentration emerged (Turing, 1952). This was further validated *in vivo* by biologists who developed the concept of 'positional information' derived from the cell interpretation of external signals (Wolpert, 1969) and proposed diffusion as the motor of molecular gradient throughout tissues (Crick, 1970). This unified concept has been extensively studied to understand pattern generation in many developmental contexts (Figure 3).

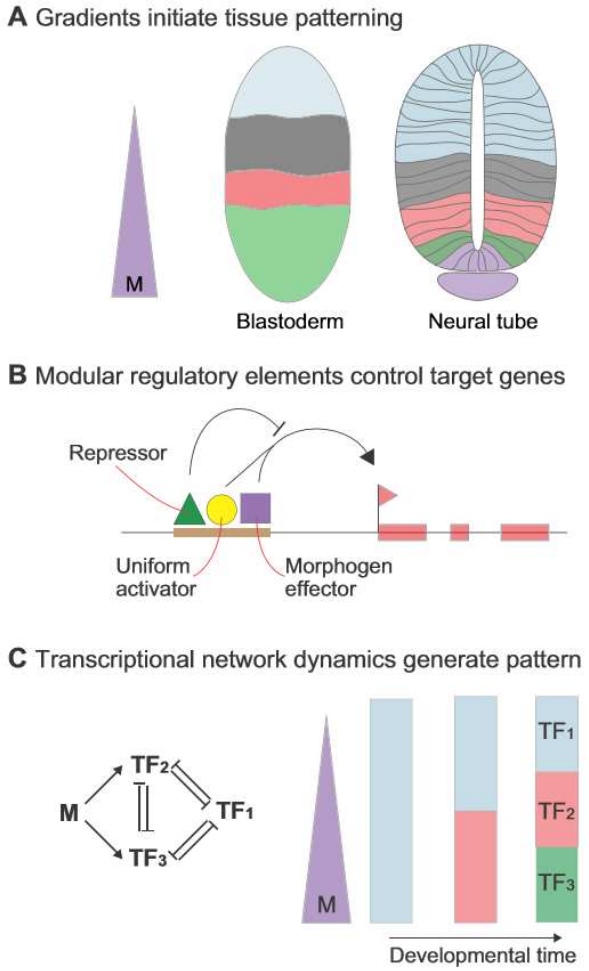

Figure 3: Design principles of patterning in the Drosophila blastoderm and vertebrate neural tube.

(A) Signaling gradients polarize tissues by initiating and orienting gene expression patterns. A morphogen (M, left), Bcd in the case of the blastoderm (center) and Shh for the neural tube (right), forms a gradient. This asymmetry initiates the division of the tissue into domains of gene expression (colored blocks) arrayed along the patterning axis (anteriorposterior in the blastoderm and ventral-dorsal in the neural tube). (B) Patterns of target gene expression are controlled by modular regulatory elements containing binding sites for multiple distinct TFs. These elements integrate transcription inputs from morphogen effectors, uniformly expressed factors, and the transcriptional repressors that comprise the morphogen-regulated transcriptional network. (C) The dynamics of the transcriptional network transform broadly distributed activation and localized repression mechanisms into precisely positioned boundaries of gene expression. This directly links spatial and temporal mechanisms of pattern formation. (From Briscoe & Small, 2015)

- ***Pattern establishment through morphogen gradients in Drosophila.***

Nowadays, one of the most studied examples of developmental pattern is the antero-posterior segmentation in *Drosophila melanogaster* embryo (Sanson, 2001; Briscoe & Small, 2015) which is quite conserved among arthropods (Clark et al., 2019). In *Drosophila*, the initial uniform population of cells of the early embryo blastoderm sustains a break of symmetry by adoption of a series of alternative cell fates along the antero-posterior axis. Then, a precise and regular pattern of stripes which prefigures the future segments of the larval body arises at cellular-level resolution by an elaborated process (Davidson, 2010). The development of such compartmentalized regions requires precise patterning cues to initiate GRNs that determine the localization where each cell type should develop. Here, the final patterning along the embryo antero-posterior axis is the result of the birthplace readout of GNRs for each single cell (Davidson, 2010).

The *Drosophila* embryo presents a peculiarity: following fertilization, nuclear division is uncoupled from cell division. Four hours post-fertilization, the embryo is a multinucleate syncytium with about 6000 nuclei distributed below the surface of the egg's membrane. At that stage, individual cells are formed by invagination of the plasma membrane (cellularization) that will envelop each single nucleus resulting in a monolayered cell epithelium.

Interestingly, the antero-posterior axis is already established before the cellularization starts and does not require intercellular signalling. Before fertilization, the future antero-posterior axis of the embryo is set up by localized deposits of specific mRNA transcripts, coding for transcription factors which act as "morphogens". Morphogens are diffusive molecules that give a dose-dependent response depending on their concentration along the axis of diffusion (Turing, 1952; Wolpert, 1969, Crick, 1970).

The future anterior pole is enriched in mRNA coding for the Bicoid protein, which diffuses away from its source to form a concentration gradient with its maximum at the anterior end of the egg. Conversely, the future posterior end of the embryo contains a high concentration of mRNA coding for Nanos, which sets up a posterior gradient in the same way. Therefore, antiparallel gradients of the two maternal transcription factors emanate from the two poles of the embryo and induce discrete domains expressing distinct sets of zygotic transcription factors. These zygotic transcription factors act as a second layer of diffusing molecules, which will divide the tissue into molecularly distinct arrays of cells perpendicular to the antero-posterior axis. Subsequently, the combination of maternally localized and zygotically expressed diffusing morphogens distributed in the syncytial embryo in gradients will serve as a spatiotemporal cue for nuclei along the body axis. In the end, each stripe of activated gene will generate a specific cell fate depending on the cell position.

Cis-regulatory modules are DNA elements that have transcriptional regulatory activity upon binding of transcription factors. During *Drosophila* segmentation, the cells within each stripe respond to a given range of value for each morphogen, which binds to cis-regulatory modules and activates or represses the expression of specific genes. Thus, the

future multicellular embryonic territories depend on the cis-regulatory responses to different combinations of morphogens and their respective concentrations.

In this system, the transcription factors Nanos and Bicoid are important initial inputs. The state of the transcriptional network depends on the position of cells relative to the two morphogen gradients which determine the expression of activating and repressing transcription factors. The successive step refines the spatial stripes of regulatory gene expression along the anterior-posterior axis. Each territory activates target genes depending on the combination of transcription factors binding to their regulatory elements. After the initial gradients of Bicoid and Nanos have defined the antero-posterior axis, different waves of segmentation genes are zygotically expressed by subsets of cells in the embryo to refine the pattern. Over time, segmentation genes are activated by successive groups of morphogens, progressively defining increasingly smaller regions. Moreover, these successive morphogen waves overlap and contribute to refine the pattern.

First comes a set of six genes, the so-called 'gap genes' (knirps, Krüppel, hunchback, giant, huckebein and tailless) regulated by the maternal Nanos and Bicoid gradients. They are expressed in ordered bands along the anterior-posterior axis and encode transcriptions factors, which regulate each other to achieve their precise expression pattern.

The second wave is formed by the 'pair-rule' genes, which subdivide the embryo in seven bands perpendicular to the anterior-posterior axis. Here again, the encoded transcriptions factors regulate each other to achieve their precise expression pattern. The end of this step coincides with the end of the syncytial embryo and the start of cellularization.

After cellularization is completed, the newly-formed cells express the final class of segmentation genes, the segment-polarity genes, which refine the boundaries between the newly formed cell bands into 14 parasegments. Together, the segmentation genes form a complex GRN that subdivides the embryo into progressively smaller domains along the antero-posterior axis, distinguished by different patterns of gene expression.

For each gene expressed in stripes, the cis-regulatory modules that control it at a given range of morphogen concentration have been isolated. The positions of the stripes are determined by the quantitative values of the morphogen concentrations read by these cis regulatory systems at those locations. Cis-regulatory modules only activate their target gene expression in the region that coincides with a given morphogen concentration. For example, Bicoid binding sites have been identified in the cis-regulatory elements of more than 50 different target genes, most of which are expressed in the anterior and ventral part of the embryo (Ochoa-Espinosa et al., 2009; Briscoe & Small, 2015).

When Bicoid-binding *cis*-regulatory modules of several Bicoid target genes driving the expression of reporters are introduced into the egg, they generate stripes of expression at fixed positions along the antero-posterior axis (Ochoa-Espinosa et al., 2009). When Bicoid concentration is changed throughout the embryo, the *cis* regulatory module

activity does not seem to depend on specific Bicoid threshold but rather on combinatorial activator and repressor inputs. Indeed, except for the highest value, the local concentration of morphogens alone is not by itself enough to predict the spatial expression domains of their target genes (Ochoa-Espinosa et al., 2009). The concept of position-dependent expression of target genes determined solely by the quantitative value of the morphogen is too simplistic and only works in extreme cases.

As we have seen earlier, there are successive waves of morphogens and several transcription factors can be present in a cell at the same time. They are called pattern-determining transcription factors and work as transcriptional networks that play central roles in the morphogen interpretation (Briscoe & Small, 2015). Thus, the overall pattern results from the properties of the GRN rather than being a property of individual cis-regulatory modules that independently and quantitatively read single gradient values (Davidson, 2010). However, when we consider the evolutionary point of view, the emergence of new patterns is unlikely to arise through mutation of genes from the regulatory network but rather by changes in the sequence of cis-regulatory modules. Indeed, changing the activity of these pathways might occasionally lead to useful new patterns or structures, but is far more likely to disrupt existing developmental processes (Jiggins et al., 2017). The study of wing patterns in flies and butterflies provides a window into evolutionary changes without disrupting the existing gene functions (reviewed in Jiggins et al., 2017). As for segmentation, morphogen gradients give positional information read by cis-regulatory modules and translated into the local activation of specific transcription factors and pigment-synthesizing enzymes (Figure 4). The major difference is that these patterning events arise in the imaginal disc precursors of the wing long after cellularization through the activity of gradients of local morphogen such as Wnt. Among few examples that I will not develop in depth, it is worth mentioning the dorso-ventral patterning of *Drosophila,* which depend on dorsal morphogens (Roth et al., 1989)

- ***Pattern establishment through morphogen gradients in vertebrates.***

Vertebrates also present archetypal examples of morphogen-derived tissue patterning. Among them is the neural tube, where several cell types form a precise spatial arrangement. This pattern results from cells fated at a given position related to the dorso-ventral axis and depends on morphogen gradients originated from the two opposite poles of the tissue. Interestingly, the dorso-ventral patterning of the neural tube in vertebrates presents striking similarities with the antero-posterior segmentation of *Drosophila* (Briscoe & Small, 2015). However, both patterning systems are analogous but they derive from distinct evolutionary origins, with striking different time scales of development and molecular players. They rely on morphogen gradients and initiate transcriptional GRNs that integrate broadly distributed activators and localized repressors. Also, in both cases, the precise positioning of boundaries depends on the temporal and spatial dynamics of the transcriptional network (Briscoe & Small, 2015).

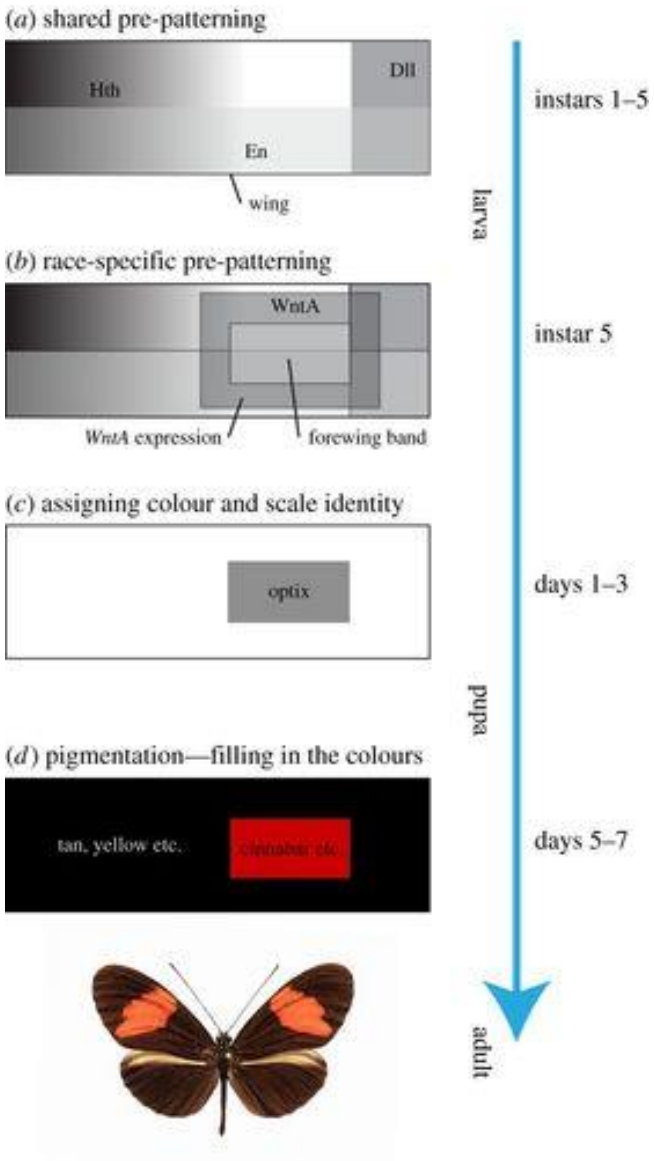

Figure 4: Summary of wing pattern development in *Heliconius*.
(*a*) Early in larval development, many of the genes involved in early wing patterning are shared across the insects and, therefore, highly conserved in their expression domains. (*b*) Late larval stages start to differentiate in gene expression patterns between different wing pattern forms within *Heliconius*, such as at *WntA*. (*c*) During pupal stages, early patterning information is interpreted into different colours—notably *optix*, which defines presumptive red wing regions. (*d*) Finally, in the second half of pupation, the expression of patterning genes such as *optix* is converted into colours via localized expression of pigment synthesis enzyme genes such as *cinnabar* (red) and *tan* (black).
(Adapted from Jiggins et al, 2017)

The ventral half of the forming spinal cord is one of the simplest and most conserved parts of the neural tube. The neuroepithelium that composes it is divided into 6 discrete domains, spatially restricted by the expression of a set of homeodomain and bHLH transcription factors arrayed along the dorso-ventral axis. Each domain expresses a distinct combination of transcription factors which regulate the differentiated cell type that each progenitor generates (Placzek & Briscoe, 2018).

As for *Drosophlia* antero-posterior patterning, the cell fate specification of the neural tube follows a precise template to array these six discrete progenitor domains along the dorso-ventral axis (Dessaud et al., 2008). The dorso-ventral patterning of the vertebrate neural tube relies on well characterized morphogen gradients: Sonic hedgehog (Shh) ventrally (Dessaud et al., 2008) and Bone Morphogenetic Protein (BMP)/Wnt dorsally(Alvarez-Medina et al., 2008; Zagorski et al., 2017).

A strong difference between *Drosophila* antero-posterior and vertebrate dorso-ventral patterning is the presence of cell membranes. In the syncytial blastoderm of *Drosophila,* long-range signals diffuse directly to cell nuclei. In contrast, in the vertebrate neural tube, cells form a pseudostratified epithelium. In that context, long-range signalling relies on protein secretion and requires the expression by the receiving cell of membrane-associated receptors. These receptors help to read morphogen gradients and transduce it into complex intracellular signalling to the nuclei.

For example, Shh is secreted by the notochord, a mesodermal-derived embryonic structure localized ventrally to the neural tube and form a ventral-dorsal decreasing gradient. The intracellular transduction of Shh signals requires it binding to the transmembrane receptor Ptch. In the absence of Shh, a second transmembrane protein, Smo, induces the degradation of the transcription factor Gli and the formation of a transcriptional repressor (GliR). The binding of Shh to Ptch inactivates Smo, allowing a switch of Gli from its repressing form to its activating form (GliA) (Briscoe & Thérond, 2013). In response to Shh gradient and the following Gli activity, various transcription factors are activated or repressed along the dorso-ventral axis. Neural progenitor target genes cis-regulatory elements contain binding sites for Gli, homoeodomain proteins and SoxB proteins (Placzek & Briscoe, 2018). The SoxB family is composed of transcriptional activators broadly expressed throughout the neural tube. Homeodomain proteins on their side mediate repressive activity. Taken together, the GRNs control the dorso-ventral patterning of the vertebrate neural tube by integrating the combination of Shh-Gli signalling and other activators and repressors bound to the cis-regulatory elements relative to the morphogen gradient. This results in the induction of position-specific cell fates along the morphogen gradient axis and controls the subsequent development of the tissue. (Placzek & Briscoe, 2018). This example stresses the complexity of intracellular signalling in patterning events, but, since it is far beyond my thesis work, it was a simplification of the process and I will not develop it any further.

Interestingly all three morphogens, Shh, BMP and Wnt, participate to other patterning events such as inner ear patterning (Ohta & Schoenwolf, 2018) Together with the antero-posterior patterning of the vertebrate spinal cord, which depends on retinoic acid and FGF gradients, these examples are worth mentioning but I will not develop them.

In conclusion, the general concept of antiparallel morphogen gradient, even if it came from distinct evolutionary origin, is broadly used in the development of spatial patterns (Briscoe & Small, 2015).

- ***A combination of Turing's reaction-diffusion model of morphogen gradient and cell movement regulates spacing patterns***

Spacing patterns result from the maintenance of a regular distance between repetitive neighbouring elements and represent one of the simplest and most frequently observed embryonic patterns (Wolpert, 1998). Spacing patterns exist in many repeated structures such as teeth, glands and skin appendages. Epidermal regular spacing patterns are well represented by structures such as gustatory papillae, hair follicles in mammals or avian feather buds (H.-S. Jung et al., 2003; Sick et al., 2006; Sengel, 1975). Interestingly, many genes related to patterning events in vertebrate epithelia and insect limbs are also involved in establishing spacing patterns (Wolpert, 1998). In this section, I will present the feather bud spacing pattern formation while the hair follicle patterning, which shares many similarities, will be developed in another context in Chapter 2.

In the chick embryo, feathers form in the dorsal skin from a hexagonally patterned array of feather buds (Sengel, 1976). The proper patterning of feather buds requires coordinated follicle spacing with appropriate gene expression profiles into stereotypical anatomical sites. Feather buds first appear as dense row-like regions on the skin surface of the dorsal midline and develop with a strict spatiotemporal order in well-defined lines, the feather tracts (Figure5 A) In each tract, a primary bud forms in the lumbar region at the level of the hindlimbs. Then, a wave of patterning symmetrically spreads out bi-directionally and bilaterally along the midline axis (Jiang et al., 1999; Lin et al., 2006, 2009; Inaba et al., 2019). (Figure 5 A,B).

Each bud forms from an aggregation of mesenchymal cells from the dermis beneath a thickening of the skin, the epidermal placode (Figure 5 C) (Ho et al., 2019). The top layer of the skin is made from adherent epithelial cells unable to move, whereas the underlying mesenchymal cells are motile and can move around in the extracellular matrix (ECM) (Wolpert, 1998). Before feather bud formation, both epithelium and mesenchyme are homogeneous and multipotent with an equal probability of becoming bud or interbud (Jiang et al., 1999). Subsequently, the combined structure of epithelial and mesenchymal cells becomes identifiable by tight packing and specific gene expression and forms the feather primordium from which the feathers will grow.

Many cases of pattern of skin appendages including mammalian follicles and avian feather buds require morphogens such as Wnt, FGF, Follistatin, BMP and Ectodysplasin A (EDA) (Figure 6). In avians, the pattern of buds and interbuds is defined by the distribution pattern of activators and inhibitors, which promote and suppress bud formation (Jung et al., 1998). Some morphogens are initially homogeneously expressed by outer epidermal cells and become spatially restricted as the patterning proceeds. This is the case of FGF and Follistatin, two activators of dermal condensation (Song et al., 2004). BMPs on their side, inhibit feather formation (Jung et al, 1998). The pathway initiated through EDA binding to its receptor EDAR has been shown to be crucial in feather bud formation (Drew et al., 2007).

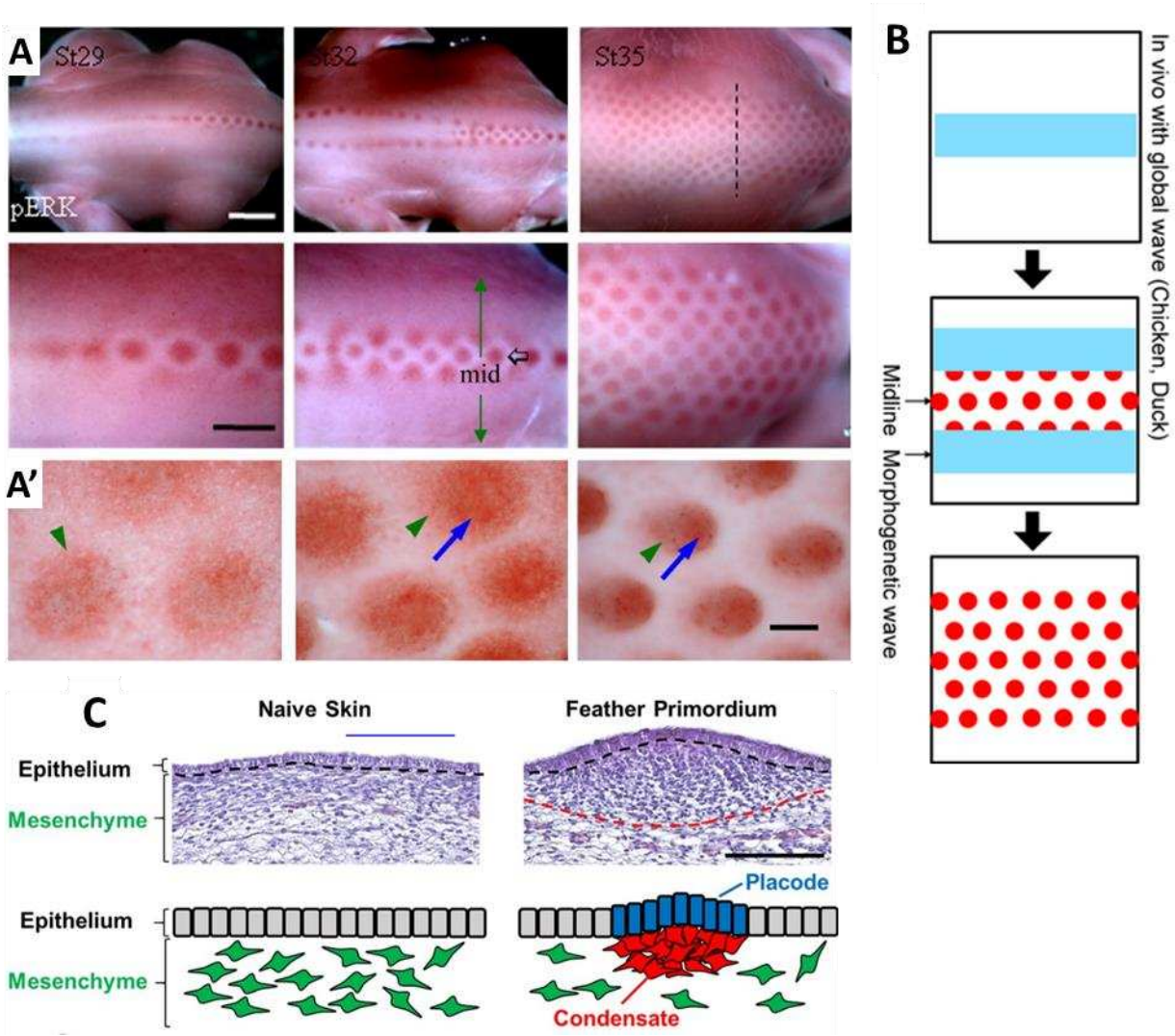

Figure 5: Generation of the feather bud pattern in chicks

(A) Whole-mount immunostaining shows expression of phosphorylated ERK at different feather development stages. Staining marks the feather placodes, which initiate along the dorsal midline at stage 29 and spread bilaterally from the midline (black arrow) with developmental progression (green arrows). Scale bar is 2 mm in the upper row, and 1 mm in the lower row. (A′) High power view of p-ERK in different stages of feather buds. p-ERK is first expressed in a wider region and at a medium level. Then it becomes enriched in the central bud domain (blue arrow) while the peripheral expression (green arrowheads) gradually decreases. Scale bar is 100 μm. (Lin et al, 2009)
(B) Schematic representation of the feather array formation as a global wave: the high ordered feather array (red) is formed sequentially from the midline to lateral regions by the morphogenetic waves (blue) that travel bilaterally. (adapted from Inaba et al, 2019).
(C) Sections of embryonic skin showing cell distribution before and after feather primordium formation. Cell nuclei are stained purple. Black dashed lines indicate the epithelial-mesenchymal boundary. Schematic below. Scale bar: 100 μm. (Ho et al, 2019)

This suggest that spaced feathers represent an example of Turing's pattern (Turing, 1952; Michon et al., 2008; Inaba et al., 2019; Ho et al., 2019) as it was demonstrated for mammalian hair follicles in which a pure reaction-diffusion system with no reliance on cell movement normally patterns the primary hair follicles (Glover et al., 2017). In mammalian hair follicles, the morphogen gradient initiates the pattern formation in the

overlaying epidermis and subsequently induces mesenchymal migratory behaviour (Glover et al., 2017; Nogare & Chitnis, 2017). However, the feather bud pattern is not strictly defined by pre-pattern of cell specification at a given position. The initial density of mesenchymal cells plays a role, but some cell-movements are also required. Previous studies have suggested that first, the pattern arises and dictates where epithelial cells over the tract (the feather forming region) should become competent and then competent cells initiate inner mesenchymal cells migration to form individual feather primordial (Widelitz & Chuong, 1999).

In chick embryos, feather buds form as a wave of patterning suggesting that two mechanisms are at work *in vivo*: a positional information gradient, which renders cells competent to form primordia, overlying a local morphogenetic patterning mechanism which is dependent on a number of parameters: activators, inhibitors, cell adhesion molecules but also cell density, cell migration and proliferation (Kim et al., 2005; Baker et al., 2009; Ho et al., 2019). However, whether the patterning mechanisms can be divided into two separate phases of pattern specification followed by cell differentiation/rearrangement, or whether the processes are intimately coupled remains debated (Shyer et al., 2017). It was suggested that the expression of morphogens responsible for follicle fate determination in the avian skin accompanies rather than precedes the earliest morphogenetic changes associated with follicle formation (Shyer and al., 2017; Nogare and Chitinis., 2017). For example, it was demonstrated that the formation of cellular aggregates is not necessarily dependent on Wnt signalling in the epidermis in birds as it is for mammalian skin (Shyer et al., 2017).

It has been known for long that the initial patterning signal arises from the mesenchyme (Sengel, 1976). It was proposed that the mesenchyme determines the number, size and location, as well as the structural identity, of each appendage, while the epithelium determines the orientation and the competence status (Jiang et al, 1999). While the chemical bases of Turing reaction-diffusion model have been investigated for over 60 years, it was recently suggested that mechanical forces also contribute to morphogenesis in this model (Howard et al., 2011). It was shown that mechanical forces initiate a pattern of dermal condensation in the dermis (Shyer et al., 2017). In this model, cellular contractility serves as a local activator, while substrate stiffness serves as long-range inhibitor of follicle aggregate formation. (Shyer et al., 2017). The pattern assembly in this system is not strictly speaking a Turing's reaction-diffusion model, since it relies on cellular, rather than molecular interactions. The proposed model suggests that mechanical instability spontaneously generates an increase in morphological complexity (Shyer et al., 2017). In response to mechanical compression of dermal mesenchymal cells, the outer epithelial cells react via β-catenin, a sensor that, upon nuclear translocation, translates mechanical stimuli into primordium-specific gene expression (Brunet et al., 2013; Noramly et al., 1999; Shyer et al., 2017). Then the dermis mesenchymal condensations coupled to the surface epithelia through basement membrane initiate Wnt

signalling in the overlaying epidermis. This reinforces and/or refines the periodic pattern of developing feather bud follicles (Nogare & Chitnis, 2017).

At the start of feather bud formation, the appearance of cell aggregates neither precedes nor follows local changes in gene expression, rather both features emerge synchronously. A so called "reaction-diffusion-taxis" system was proposed to explain the periodic pattern establishment. The model combines reaction-diffusion-mediated prepatterning and mesenchymal cell motility, integrating them into a unified periodicity-generating mechanism (Ho et al., 2019).

The feather periodic patterning system relies on FGF20, which attracts mesenchymal cells to form an aggregate, a crucial role in avian skin patterning (Wells et al., 2012). FGF20 is secreted by epithelial cells to attract mesenchymal cells that aggregate under the midline (Figure 6A top panel). Focal clustering of mesenchymal cells results in the compression of epidermal cells, which respond through β-catenin, thus in turn reinforcing and intensifying *FGF20* expression (Shyer et al, 2017). The positive feedback of FGF20 upon mechanical cell compression represents an integration point between Turing/reaction-diffusion and mechanical systems (Brinkmann et al., 2018). Aggregated mesenchymal cells produce BMP that diffuses and inhibits FGF20 production, limiting the condensation expansion (Figure 6A) (Michon et al., 2008; Ho et al., 2019).

The initial condensation formation along the midline requires the EDA signal to trigger periodic patterning by lowering the threshold of mesenchymal density. EDA spreads as a wave, which induces a transient stripe of FGF20 production where the advancing EDA wave meets the receding β-catenin/EDAR wave (Figure 6A, lower panel). This low FGF20 stripe initiates mesenchymal cell aggregation, which in turn promotes FGF20 expression through epidermal compression-response thus leading in turn to enhanced mesenchymal attraction.

The regulation of cell aggregation by BMP suppression of FGF production, together with the local depletion of mesenchymal cells from the region surrounding the aggregates, results in the formation of discrete and characteristically spaced feather primordia. Then, along the midline, epidermal and dermal cells compress into rows under the antagonistic action of FGF20 and BMP (Figure 6B) (Ho et al., 2019). As the EDA wave spreads laterally, it produces a periodic patterning by the effect of the inhibition exerted by the preceding feather primordium row through BMP production and local mesenchymal cell depletion. The inhibitory template of each newly formed row places out of register the new one. Repeated iterations of this process produce hexagonally patterned array of feather buds (Figure 6C).

This system incorporates aspect of both reaction-diffusion and mesenchymal condensation into a hybrid model capable of breaking symmetry to produce *de novo* formation of a periodic pattern. (Ho et al, 2019). However, I presented here only a simplified view of the system that does not include all known regulators of the feather bud patterning process. A few of those that I didn't present in detail deserve to be at least mentioned. This is the case of cell adhesion molecules, which have been shown to play a role in pattern formation, their expression becoming progressively restricted to the feather buds as development proceeds (Jiang et al, 2004). Furthermore, the Notch lateral

inhibition system stabilizes the follicular domain identity by strengthening its boundaries (Crowe et al., 1998; Michon et al., 2007); this system correspond to a short range signalling and will be presented in the next section.

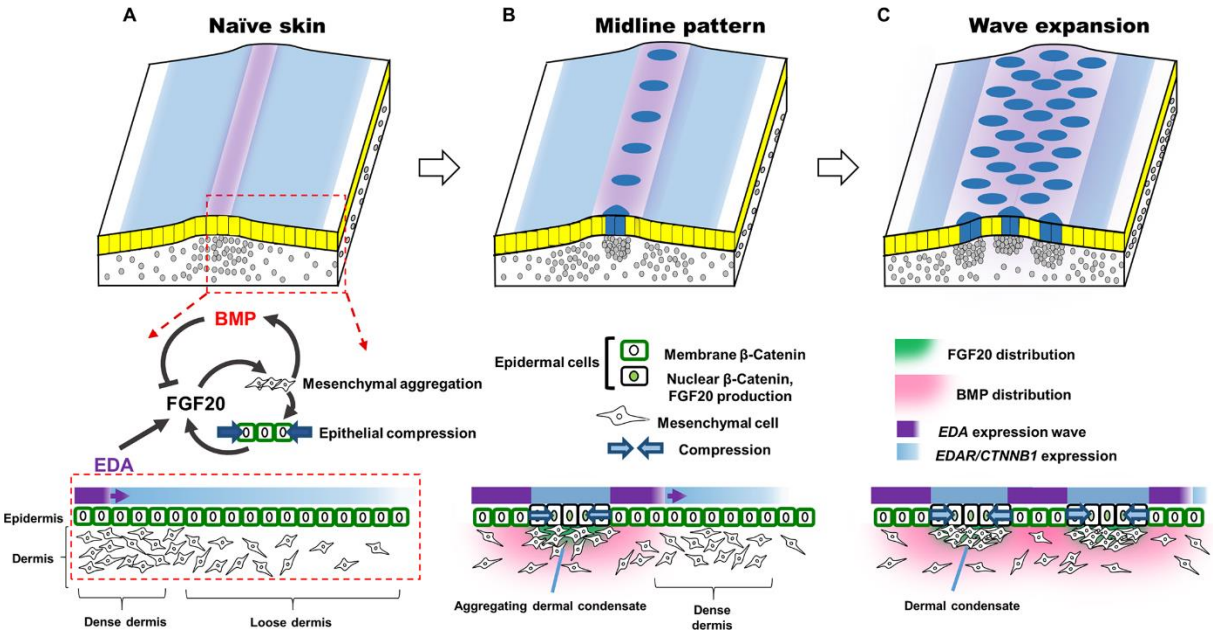

Figure 6: Schematic of the feather patterning mechanism.

(A) A competent epidermis overlies a mesenchyme displaying high mesenchymal cell density on the midline (dense dermis) and gradually decreasing to the sides (loose dermis). (B) A travelling wave of EDA signaling stimulates the epidermal production of FGF20, which induces chemotaxis of mesenchymal cells and thus formation of a dermal condensate. As the condensate forms, *FGF20* expression is further stimulated, thereby reinforcing production of this attractant. The clustering of cells also stimulates the production and secretion of BMP to inhibit *FGF20* production, limiting the size of the incipient primordium and preventing fusions between neighboring primordia. Meanwhile, the previously loose dermis increases in density to reach the threshold density that permits condensate formation. (C) As the EDA signaling wave sweeps across the skin, the reaction-diffusion-taxis system is repeated until the wave terminates at the edge of the tracts. BMP, bone morphogenetic protein; EDA, Ectodysplasin A; FGF20, fibroblast growth factor 20 (from Ho et al 2019).

1.2.1.2. Short range tissue communication

In the 1950's-80's, most studies on pattern formation which followed Turing's model focused on long range signalling resulting from morphogen diffusion (Gierer & Meinhardt, 1972). However, local short-range communication systems were pointed out as a way to organize regular pattern (Inomata, 2017). Such communications termed lateral inhibition and lateral induction can control cell-fate adoption in a negative or positive manner (Gierer & Meinhardt, 1972; Sjöqvist & Andersson, 2019).

- ***Salt and pepper pattern establishment through lateral inhibition.***

The adult body of *Drosophila* is covered by an array of mechanosensory bristles arranged in a strictly defined pattern (Held, 1991). The basic unit of this structure is composed of four different cells types: a hair cell, a socket cell, a sheath cell and a neuron. These cells derive from a single precursor cell called the sensory organ precursor and are distributed in a tightly regulated manner. Sensory organ precursors are derived from epidermal cells in a way that each fated sensory organ precursor is singled out from epithelial cells that cover the fly body (Wigglesworth, 1953; Corson et al., 2017).

In the 1940s Wigglesworth proposed a model in which the differentiation into a bristle apparatus occurs randomly among the epithelial cells, and once a cell starts differentiation it prevents neighbouring cells from doing the same (Wigglesworth, 1940). In this model, specification requires a certain threshold level of "chaetogen", a freely diffusive inducer produced by imaginal cells. This mechanism corresponds to a long-range signalling of positional information with inductive effects but is not enough to drive the final spaced pattern of the bristles. Induced cells must inhibit the same fating in direct neighbouring cells through the expression of an inhibitor (Figure 7) (Richelle & Ghysen, 1979; Ghysen & Richelle, 1979). This model is now well characterized, and it has been termed "lateral inhibition" (Gierer & Meinhardt, 1972). Interestingly, it not only reproduces the pattern of bristles of *Drosophila* and other insects but also the hair pattern found in various mammals such as sheep (Claxton, 1964). In this section we will focus on the mechanism of lateral inhibition.

The regular spacing of *Drosophila* sensory organ precursors through lateral inhibition is controlled by the Delta Notch signalling pathway (reviewed in Sjöqvist and Anderson, 2019). This is a relatively simple signalling system allowing communication between directly neighbouring cells (Figure 7) This signalling pathway is ideally suited to mediate precise patterning cues along tissues as both receptors and ligands are membrane-bound and can thus act as a precise switch to toggle cell fates on or off. Notch is a single-pass transmembrane receptor presented at the cell membrane as a dimer. Its ligand, Delta, is also a single-pass transmembrane protein.

The interaction with Delta induces the proteolytic cleavage of the Notch molecule into a Notch Extracellular Domain (NECD) and Notch Intracellular Domain (NICD) (Sjöqvist and Anderson, 2019). The release of NICD into the cell cytoplasm activates a signalling pathway (Artavanis-Tsakonas et al., 1995) (Figure 7.A). After cleavage, NICD is translocated to the nucleus where it interacts with the transcription factor CSL ("CBF-1" or "RBP-Jκ" in mammals, "Suppressor of Hairless" on *Drosophila* and "LAG-2"). The interaction between NICD and CSL induces the recruitment of co-activators and the subsequent transcriptional regulation of target genes (Figure 7.A). The strength of Notch signalling is dose-dependent since each single Notch receptor activation event generates one signalling molecule, without further signal amplification. Also, many interacting factors modulate the Notch pathway (Andersson et al., 2011; Bray, 2016).

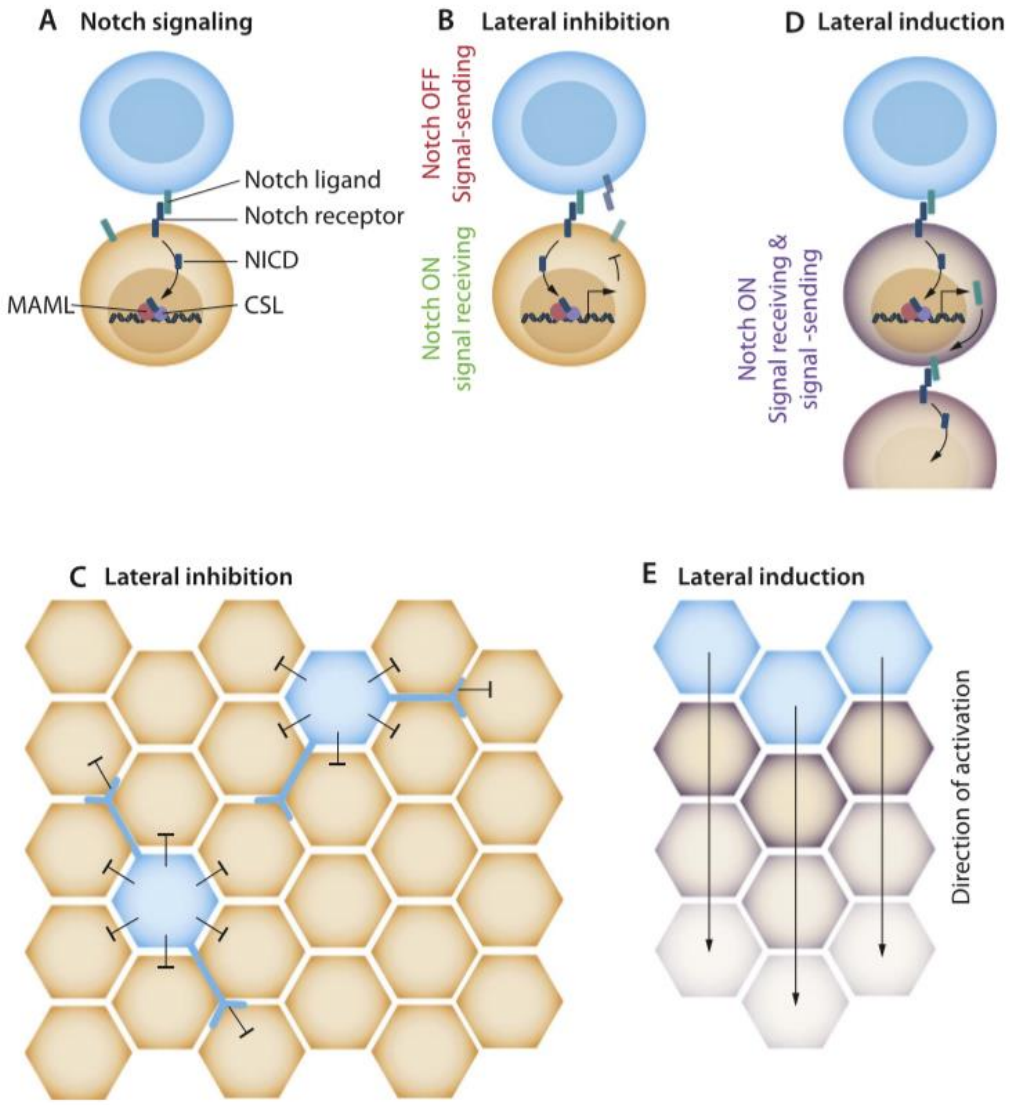

Figure 7: Notch signaling mediates lateral inhibition and lateral induction.
(A) Notch signaling is initiated when a Notch ligand on a signal-sending cell (blue) binds to a Notch receptor on a contacting signal-receiving cell (orange). Binding results in proteolytic processing of the Notch reccptor, releasing the Notch intracellular domain (NICD) which translocates to the nucleus to activate signaling together with the transcription factor CSL (CBF-1/Su(H)/LAG1-1; aka RPJκ) and co-activator Mastermind-like (MAML). (B) Lateral inhibition is a process by which Notch signaling inhibits neighbors in a pool of initially equivalent cells from taking on a default cell state. Notch receptor activation results in downregulation of ligand activation potential, either through decreased ligand expression or through Fringe modification. This mechanism amplifies stochastic differences in ligand or receptor expression, such that one cell becomes signal-sending and one is signal-receiving. (C) This typically results in patterns of cells with signal sending (blue) cells inhibiting several neighbors (orange) from adopting a default cell state. The range of inhibition may be increased by filopodia extensions. (C) Lateral induction is a process by which Notch signaling induces neighbors in a pool of initially equivalent cells to adapt a common fate. Notch receptor activation directly upregulates ligand expression in signal-receiving cells (purple), which can then activate Notch receptors in further contacting cells (purple). (D,E) Lateral induction results in a wave of cells being induced to adapt the same fate. (adapted from Sjöqvist et Anderson 2019)

As mentioned above, the fact that Notch signalling depends on the direct contact between neighbour cells makes it ideally suited to establish different cellular identities. Depending on the developmental context, Notch signal activation can either repress the expression of Notch ligands in signal-receiving cells (Figure. 7B), resulting in lateral inhibition (Figure. 7C) or induce the expression of Notch ligands in signal-receiving cells (Figure. 7D), resulting in lateral induction (See next section) (Figure. 7E)(Sjöqvist & Andersson, 2019).

The mechanism of lateral inhibition resides in the fact that both neighbouring cells express ligand and receptor. The activation of Notch in one cell represses the expression of Delta, and the decreased expression of Delta will in turn reduce Notch activation in contacting cells. In addition to interaction between cells, *cis*-regulation processes occur where Delta and Notch can interact within the same cell, resulting in functionally neutralized Notch receptor, a process called *cis*-inhibition. As the result of *cis*-inhibition, cells where Delta level is higher will turn into signal-sending cells and cannot receive signal via Notch (Sprinzak et al., 2010, 2011). Combination of *cis*- and *trans*-regulation will turn the population into signal sending and signal receiving cells.

Thus, Delta/Notch-mediated lateral inhibition can result in the emergence of a regular pattern of cell distribution. The initial population is composed of identical cells, some of which stochastically express slightly higher levels of Delta ligand in response to minor fluctuations. In the case of lateral inhibition, the direct neighbour cells will answer to Delta increase by stronger activation of Notch receptor. Negative feedback from Notch activation will in turn downregulate Delta expression in these cells, preventing them from inducing Notch in their own neighbours in turn. Moreover, differences in the levels of receptor and ligand concentrations are amplified by negative feedback when a Delta-expressing cell instructs contacting cells to downregulate Notch. The process is also amplified by *cis*-inhibition. This will propagate alternation between Delta-expressing cells surrounded by Notch-expressing cells, resulting in a salt and pepper pattern where Notch-expressing cells adopt a different cell fate from Delta-expressing cells leading to their regular spacing throughout the tissue.

It is possible that cells not only mediate lateral inhibition through close contact but also through filopodia-mediated ligand presentation. Filopodia have been described to increase the range of Notch ligand presentation in *Drosophila* (Cohen et al., 2010; de Joussineau et al., 2003) and in zebra fish (Hamada et al., 2014). However, more recent studies suggest that the inhibitory signal mediated by Delta extends only to the adjacent cell during sensory organs precursor selection (Troost et al., 2015).

- ***Stripe pattern establishment through lateral induction.***

As previously mentioned, depending on the biological context, Notch signalling can transduce inhibition to drive the formation of salt and pepper pattern or reversely, produce longer-range coherence in neighbouring cells through lateral induction (Owen et al., 2000; Petrovic et al., 2014; Liao & Oates, 2017; Sjöqvist & Andersson, 2019). During lateral induction, the ligand binding upregulates the expression of both ligand and

receptor in receiving cells rather than inhibiting the ligand expression. This creates a positive feedback loop followed by a cascade of Notch activation from one cell to the next. Therefore, a cell can induce the neighbouring cells to adopt the same fate (Figure 7 D-E).

The precise establishment of sensory organ precursors has been modelled *in silico.* The model suggests that signalling by Notch can mediate both proneural patterning and sensory organ precursor selection via a single logical operation deployed in time and space to robustly produce a complex stereotyped pattern (Corson et al, 2017).

In the early steps of the sensory organ precursors formation, Notch is required for lateral induction rather than lateral inhibition (Henrique & Schweisguth, 2019). Indeed, before sensory organ precursors are selected through lateral inhibition, a regular pattern of Notch activity precedes the formation of stripes throughout the neuroepithelium. Two parallel bands of high Notch expression form and become flanked by the proneural stripes where Notch is low. Subsequently, the proneural domains that emerge from the stripes give rise to the sensory organ precursors through restriction in space via lateral inhibition. In this tissue, the pattern of Notch activity dynamically evolves from instructing to inhibiting. Besides, these oscillations between induction and inhibition present striking analogies with the reaction-diffusion model in their way to establish the pattern of proneural stripes (Corson et al, 2017)

Interestingly, Notch signalling has also been shown to regulate segmentation in vertebrates during somitogenesis, another case of regular pattern formation (reviewed in Liao and Oates, 2017). In this model, Notch lateral induction (called 'synchronization' in this context) produces long-range coherence in the neighbouring cell states (Liao and Oates, 2017) and Notch mutants produce defective segment boundaries.

The skin of zebrafish presents pigment patterns formed by stripes of three pigmented cell types (xantophores, melanophores and iridophores). The Delta/Notch signalling pathway has been shown to contribute to this pattern generation (Hamada et al., 2014). Members of the Notch ligand family where shown to be expressed in xantophores but not in melanophores, while reversely Notch receptor expression is restricted to melanophores (Hamada et al., 2014). In this context xantophores regulate melanophore survival through Notch signalling mediated by long projection contact. It was suggested that Delta/Notch synergize with other signalling pathway among which the Scf/Kit signalling pathway (Hamada et al., 2014). Interestingly, this signalling pathway has been shown to regulate various processes among which cell survival and cell migration in various developmental context, some of them associated with the generation of regular patterns (see later section).

1.2.2. Spacing pattern by controlled cell and tissue remodelling

During development, many tissues and organs undergo morphogenetic events with drastic remodelling such as cell migration, cell rearrangement and cell shape changes (the

concepts of morphogenesis and the underlying mechanisms will be developed in Chapter 2). In such changing environment, it is obvious that the emergence of regular patterns cannot always depend on the initial positioning of cells. Rather, cell positioning will depend on molecular guidance, cell migration and coordinated cell shape changes, but stochastic event can also be their motor.

In the previous section, we have seen that feather buds form periodic pattern of rows through mesenchymal cell aggregation. However, even if such a developmental process requires cell migration, it is accompanied by patterning cues to determine the sites of aggregation.

In this section, I will present three examples of cells fated in an unordered spatial fashion that become organized in regular patterns through self-organization. The illustrated patterns result from collective and single cell movements based on cell repulsion rather than cell aggregation as shown for feather buds. These examples concern developmental processes in which a precise cell organization is required for the tissue function as well as cases where cells must respect distance to spread through the organism even if their position is not static over time.

- ***Cajal-Retzius cells regular spacing requires contact-repulsion***

During neuronal cortex development, neuronal migration is an essential process to position post-mitotic neurones from their birthplace toward their target position. The cerebral cortex presents a unique pattern of connectivity made from complex structures of distinct layers of neurons. Cajal-Retzius (CR) cells play a crucial role in mammalian cerebral cortex development, by regulating the migration of pyramidal cells to form the cortical layers (reviewed in Barber & Pierani, 2016). The entire cortical surface is indeed covered by CR cells before emergence of the cortical plate, where newborn pyramidal cells form cortical layers. The cortex is colonized by CR cells that migrate tangentially from discrete regions of the pallium, where they are born. The function of CR cells is critically dependent on their distribution into a regular spacing pattern throughout the surface of the mammalian cerebral cortex. This regular spacing pattern results from the combination of random walk migration and contact repulsion between CR (Figure 8) (Villar-Cerviño et al., 2013; Barber et al., 2015; Kaddour et al., 2020). Migrating CR cells spread by following divergent trajectories and frequent changes of direction based on contact-repulsion. As for most contact-repulsion events, it was shown that the mechanisms are dependent on the Eph/ephrin interaction (Villar-Cerviño et al., 2013). The Eph/ephrin signalling induces the repolarization of the cell cytoskeleton upon cell-cell contact and the following separation of contacting cells (Abercrombie & Heaysman, 1954). Interestingly, CR cells homotypic contact-repulsion represents a stochastic example of self-organizing pattern that not relies on exogenous patterning cues (Barber & Pierani, 2016). This process will be detailed in Chapter 2.

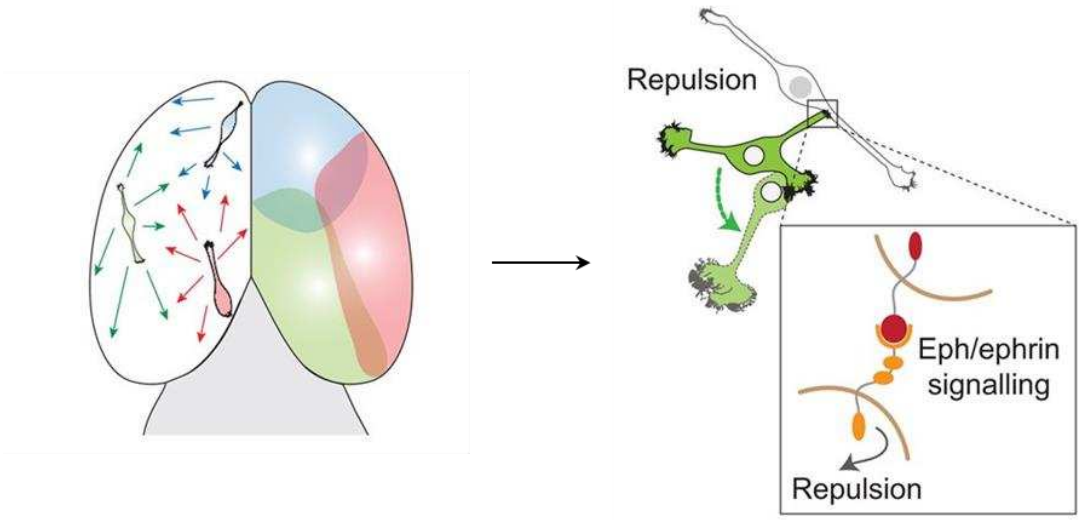

Figure 8: Contact repulsion promote Cajal-Retzius cell regular spacing.

Cajal-Retzius cells in the E12.5 mouse telencephalon spread tangentially from the cortical hem (red), pallial septum (blue) and ventral pallium (green) to distribute along the marginal zone of the developing neocortex. Cajal-Retzius cells form highly dynamic membrane processes that retract or are repulsed upon cell-cell contact, after which cells repolarise and move away from the cell-cell contact zone. Cell repulsion is mediated by Ephrin/Eph bidirectional signalling in Cajal-Retzius cells. (adapted from Reig et al., 2014))

Moreover, the marginal zone of the developing cortex contains several populations of neurons (CR cells, GABAergic interneurons, and nonsubplate pioneer neurons). This marginal zone is organized into sublaminae, adjacent but not overlapping, each of them occupied by a distinct neuronal population. The most superficial one is occupied by CR cells which organize the cortical lamination of the migrating interneurons, located immediately below (Barber & Pierani, 2016). The segregation of CR cells and interneurons into distinct non-overlapping sublaminae of the marginal zone suggests that CR cells and interneurons may also undergo cell-cell repulsive interactions. Together this suggests that cortical development into complex and dynamic patterns of cellular mosaics relies on contact-inhibition of locomotion through homotypic and heterotypic mutual cell-repulsion (Villar-Cerviño et al., 2013).

- ***The mosaic-like architecture of the retina requires homotypic repulsion***

The central nervous system presents a modular architecture with a specific regular distribution pattern of neurons. One of the most striking examples of regular spatial arrangements is the vertebrate retina, which is composed of only seven cell types and forms a thin neuronal sheet in the back of eye. Despite its complex physiological function, it is a deceptively simple structure, where each distinct type of neuron is found within a specific layer (Masland, 1996; Wässle and Boycott, 1991) (Figure 9). The architecture of the retina is so modular in non-random arrays of 'like' neurons, that it is referred to as "mosaic" (Cook & Chalupa, 2000; Wässle et al., 1978). However, the different mosaics observed in the retina are independent from each other: neurones from one subtype

exclude other 'like 'neurones but there is no restriction on their spatial relationship to neighbouring neurones of other subtypes ('non-like') (Rockhill et al., 2000).

The regular distribution of 'like' neurons in the retina is an early process of development that is evolutionary conserved from fish to mammals. Cone photoreceptors, horizontal and amacrine cells have been shown to arrange in spatial order before the generation of all the layers of the retina and before all cells forming the mature arrays migrate to their layer. Furthermore, at the level of individual cell bodies (and dendrites), most retinal cell types have been confirmed to arrange in nonrandom regular spacing (Figure 10 A)(Eglen, 2006; Galli-Resta et al., 2002; Wässle et al., 1978; Wassle & Boycott, 1991; Cook & Chalupa, 2000) .

Many parameters could contribute to their regular spacing, such as homotypic lateral inhibition or apoptosis (Eglen, 2006), but these cells move in their environment and can share contact. For example, migrating amacrine cells have been shown to move side-by-side before getting spaced (Galli-Resta et al., 1997). It was then concluded that in the early retina development, mosaics arise from cell movement and that the minimal spacing results from exclusion rules between 'like' cells (Poché & Reese, 2009). Studies on cholinergic and horizontal cells have shown that their regular mosaic arrays form by continuous repositioning of the cells, in a typical sequence of events: (1) Retinal thickness is not precisely defined in layers of cells and neurons take position independently of one another without forming precise layers. (2) Upon cell movement, 'like' neurons gradually establish a minimal spacing, but they remain located at different depths. (3) Finally, they form monolayers. Moreover, during this process, each mosaic could develop independently of other neuronal types in the retina (Cook & Chalupa, 2000; Galli-Resta et al., 2002).

Contrary to examples shown in previous section, the regular array of neurons does not depend on long-range morphogen gradients, nor on cell fate reversal through lateral inhibition. Here, the progressive spacing distribution is driven by the remodelling of neuronal shape following homotypic cell recognition though short-range interaction. Indeed, the dynamic nature of the dendritic trees is an excellent tool for neurons to explore their environment. Neurons relocalize their cell body to reduce their dendritic overlap, thus organizing themselves in regular arrays. It has been shown that dendrites reorganize their shape by remodelling of the microtubule cytoskeleton and that cholinergic neurons require Microtubule Associated Protein 2 (MAP2) to form regular arrays (Galli-Resta et al., 2002). Further studies have increased our knowledge of mosaic formation through morphological changes of neurites and dendrites in homotypic repulsive interactions (Raven et al., 2005; Huckfeldt et al., 2009), but the molecular cues that drive cell repositioning only start to be revealed (Grueber & Sagasti, 2010; Han et al., 2012; Kay et al., 2012). Furthermore, it has been shown that the retinal Müller glial cells also present a spacing pattern which depends on repulsive homotypic interactions (Figure 10 B) (MacDonald et al., 2017). Together these results suggest that the developmental process of self-avoidance and tiling in retinal cells relies on homotypic contact inhibition of locomotion.

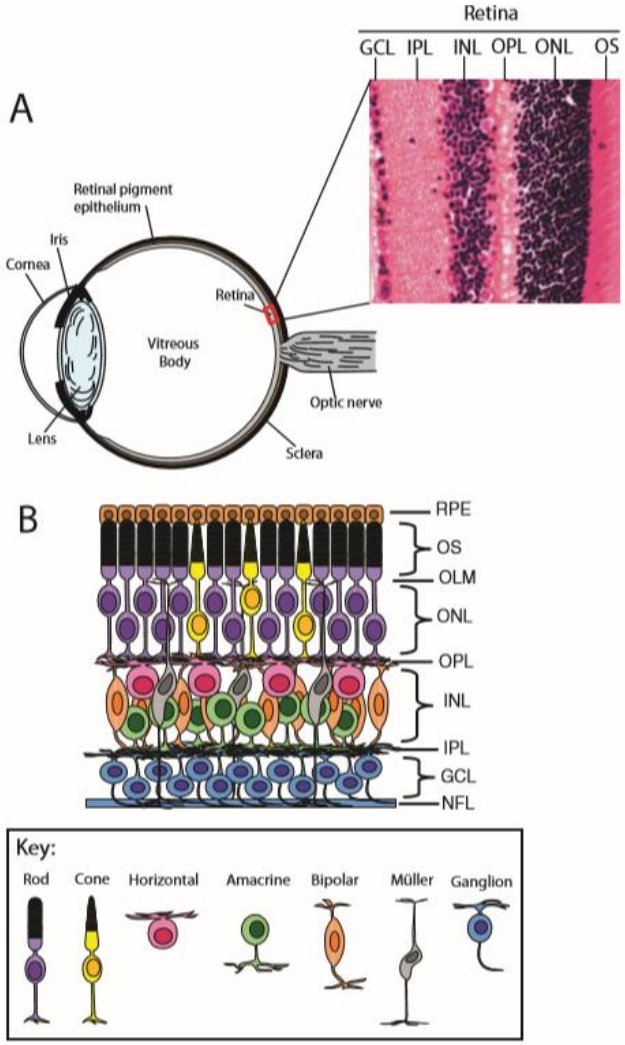

Figure 9: Retinal architecture.

In contrast to the thousands of neuronal cell types in the mature brain, the retina is composed of only six neuronal cell types and one glial cell type, which are derived from a common progenitor cell population and precisely organized into a discrete laminar structure at the back of the eye (A,B). The light-sensing photoreceptors (PR), the rods and cones, are localized to the outer nuclear layer (ONL), the outermost region of the neural retina adjacent to the retinal pigment epithelium (RPE). They form specialized apical extensions at the outer limiting membrane (OLM) of the retina, the outer segments (OS), which contain the light-sensitive photopigments and the visual transduction machinery that enable the PRs to generate a neural signal in response to light. This signal is then transferred to retinal neurons residing within the inner nuclear layer (INL). Bipolar cells transmit this signal radially from the outer retina to the ganglion cell layer (GCL). Signaling from the PRs to the bipolar cells is modulated within the outer plexiform layer (OPL) by inhibitory interneurons positioned within the INL, the horizontal cells. Within the inner retina, the bipolar cells make synapses with the amacrine cells and the ganglion cells. There is a variety of different amacrine cell types, each modulating retinal function through unique circuitry and signaling mechanisms within the inner plexiform layer (IPL). Visual information converges upon the dendrites of different retinal ganglion cell types and is transmitted to the visual centers in the brain via their axons, which initially course beneath the inner surface of the retina in the nerve fiber layer (NFL), collecting at the optic nerve head to form the optic nerve. The primary glial cell population of the retina, the Müller glia, extend across the entire thickness of the retina and provide essential structural and functional support to the neuronal population. For illustrative purposes, a schematic of the human eye is shown in A, but the Hematoxylin and Eosin staining to the right illustrates the cytoarchitecture of an adult mouse retina. (from Poché et al 2009)

- ***Self-distance maintenance of immune cells***

Immune cells such as the macrophages are highly motile and spread throughout the organism to ensure their function of pathogen recognition. During *Drosophila* development, hemocytes disperse evenly throughout the embryo, taking stereotypical migratory routes. One of these routes is along the ventral surface of the embryo, where a three-line cellular pattern is formed (Figure. 11) (Davis et al., 2012). *Drosophila* haemocytes are highly amenable to live imaging, making it easy to analyse their developmental movements *in vivo* (Davis et al., 2012; Stramer et al., 2010). It was shown that the even distribution of haemocytes within the animal requires contact repulsion mechanisms (Davis et al., 2012; Stramer et al., 2010). While the mechanism of mutual repulsion for neurones seems to be stochastic, in the context of hemocytes contact inhibition of locomotion is not and instructs migratory route through precise cell repolarization upon cell-cell contact. The process requires choreographed movement with a stereotyped sequence of kinematic stages and coordinated changes in actin and microtubule dynamics (Davis et al., 2015).

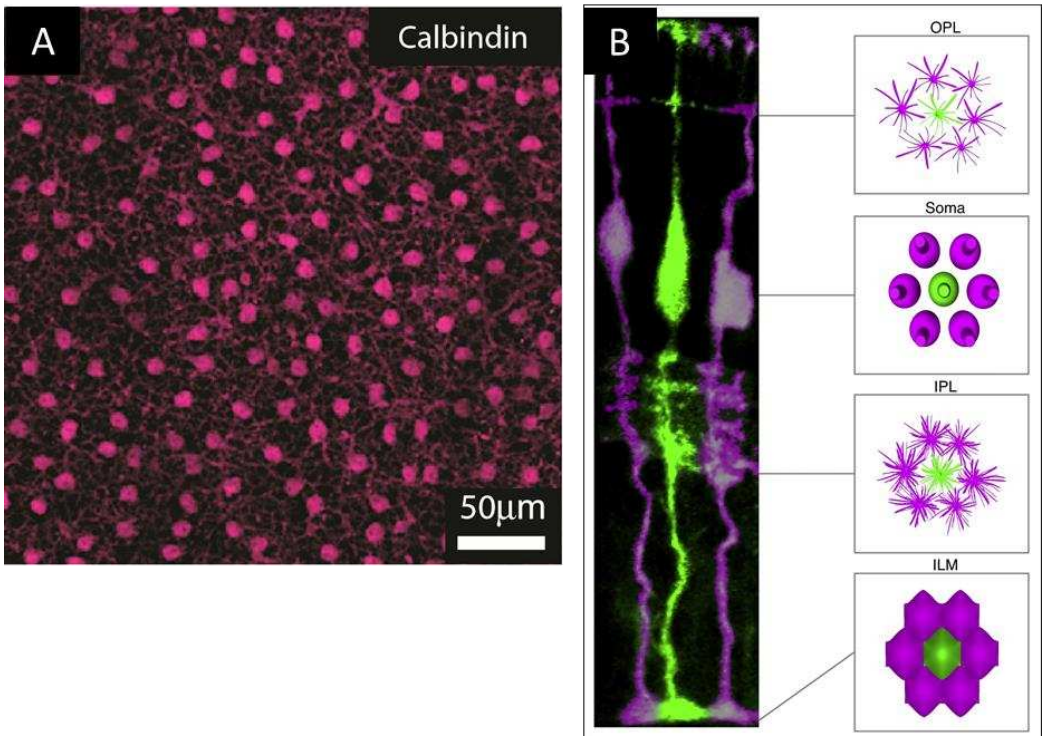

Fig. 10. regular spacing of retinal cells
(A) A retinal flat-mount labeled with an antibody against calbindin, to show the horizontal cell (HC) somata and processes. HCs are non-randomly distributed of across the retina (Poché et al 2009)
(B) The pattern and morphology of Müller glial cells in the retina. One of the most obvious features of Müller glia cells is their even spacing within the retina. Müller glia 'tile' to form a, extensive glial network. Müller glial cells (green) have their own unique special domains with little to no overlap of glial process around the surrounding neurons (purple) This lack of overlap is visible at four distinct domains: the outer plexiform layer (OPL), the somata, the inner plexiform layer (IPL), and the inner limiting membrane (ILM). (Adapted from MacDonald et al, 2017)

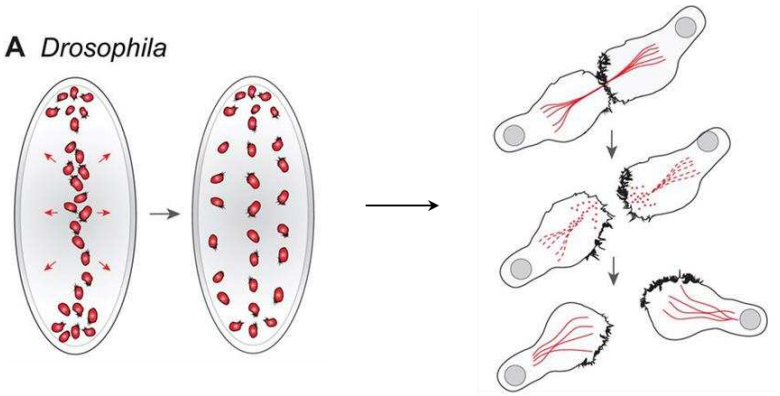

Figure 11: Contact inhibition of cell locomotion promote hemocytes spacing.

left panel: Haemocytes use contact inhibition of locomotion to disperse from the ventral midline to form a 'three-lined' organisation in the *Drosophila* embryo.

right panel: In haemocytes, contact inhibition of locomotion involves a collision of lamellae containing conspicuous arms of microtubule bundles (red lines) that disassemble upon cell-cell contact to enable cell repulsion and turning. (adapted from Reig et al., 2014)

This last example concludes the broad description of the mechanisms involved in pattern generation. Tissue remodelling mechanisms such as radial intercalation and mutual repulsion were at the heart of my work. Therefore, to go deeper in these processes, the next chapter will be dedicated to the cellular mechanisms underlying morphogenesis, including cytoskeleton remodelling and contact inhibition of locomotion as a motor of pattern generation through cell movement.

2. Pattern morphogenesis through cell movement: actors and mechanisms

As described in the previous chapter, regular cellular patterns can arise from cell movements that reorganize cell populations in such a way that each cell occupies a specific position with respect to its neighbours. The purpose of this second chapter is to introduce basic notions about cellular motility and the molecular mechanisms that underlie and control it, before presenting the mechanisms of cell repulsion by which regular pattern arise.

2.1. The cytoskeleton

Cell shape, movements and spatial organization largely depend on a complex and dynamic fibrous component of the cytoplasm, the cytoskeleton (Figure 12 A).

The cytoskeleton is a complex structure made of small molecular bricks that self-assemble into complex fibrous networks to build specific cell architectures (e.g. neurons with elongated axons and dendritic ramifications). Although, the term "skeleton" refers to a static system, the cell cytoskeleton is rather a dynamic system constantly remodeled to trigger cell division, cell shape changes and cellular movements, which together participate to the reorganization of the tissues. The cytoskeleton is comprised of several types of filamentous networks that coexist and interact within cells, participating to their architecture and mechanical properties. Three types of filaments have been described (Figure 12) (reviewed in Hohmann & Dehghani, 2019):

A. Intermediate filament
B. Microtubules
C. Actin filament (also called microfilaments or actin fibers)

Each filament type is composed of assembled monomers and the filament length evolves through monomer polymerization/depolymerization events. The growth/shrinking ratio of each type of fibers as well as their organization is dependent on specific proteins.

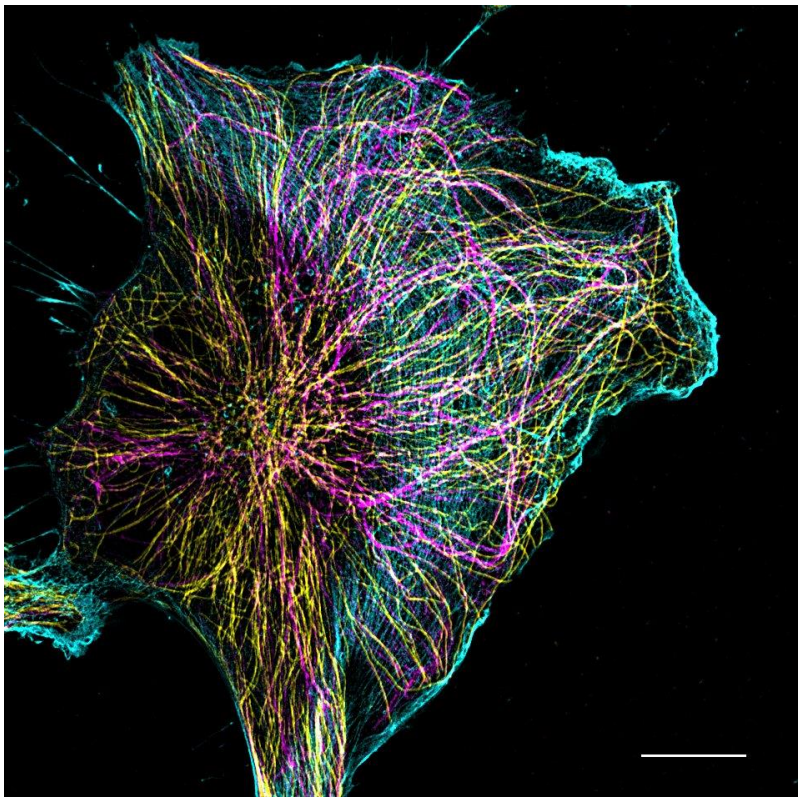

Figure 12: The cytoskeleton shapes the cell

Structured Illumination Microscopy image of a migrating glioma cell showing the actin filaments (cyan), microtubules (yellow) and the intermediate filaments (magenta) (Image from institut Pasteur website, team Cécile Leduc)

Together, these filamentous networks define and control the shape of the cell, its resistance to applied forces exerted by the surrounding environment, the intracellular transport of organelles and material, the interaction with the extracellular matrix, the cell division, the cell migration as well as the maintenance of the cell polarity.

In response to chemical and mechanical sensing, the cytoskeleton structures show extreme dynamic remodeling. However, the microtubules, intermediate filaments and actin filaments cannot be described as separates entities of the cytoskeleton, since intense functional crosstalk has been described (reviewed in Dogterom & Koenderink, 2019). Indeed, the three subsystems directly interact with each other either physically, through steric hindrance, direct binding and cross-linker-mediated binding or chemically, by communication between distinct filament types via interconnected signaling pathways and GRNs (reviewed in Huber et al., 2015). There is plenty of evidence of actin-intermediate filament and actin-microtubule direct binding such that changing the state of one structure will change in turn the state of the others. For example, the growth of microtubules can in turn stimulate the polymerization of actin in lamellipodial protrusions (Basu & Chang, 2007). Also, the crosslinking of intermediate filaments to microfilaments allows the establishment and maintenance of polarity in the migrating cell, showing the importance of cross-talk between the different cytoskeleton fibers (Etienne-Manneville, 2013; Dogterom & Koenderink, 2019).

In the following sections, I will introduce the three different cytoskeleton structures and their mechanical properties, as well as their functions in cellular and developmental processes. A particular attention will be devoted to the actin microfilaments, whose contribution to cell motility is best understood.

2.1.1. Intermediate filaments

Intermediate filaments are so called due to their diameter of 12nm, intermediate between that of microtubules (25nm) and actin filaments (8nm). Their nature is heterogeneous, consisting of heteropolymers of diverse proteins (e.g. keratin, nestin, vimentin) (Leduc & Etienne-Manneville, 2015). Although the composition of the intermediate filaments varies according to the different cell types, their primary structure is very conserved. For all cytoplasmic intermediate filaments, the monomer structure consists of a central α-helix (rod domain) with a non-helical structure at both ends, (called the head domain and the tail domain). The rod domains from two monomers wrap in a spiral around each other, forming a so-called "coiled-coil" dimer. Two dimers associate antiparallel to each other through their rod domain forming apolar tetramers. Eight tetramers form a cylindrical unit-filament and the final intermediate filament is formed by the longitudinal assembly of multiple unit filaments (Figure 13) (Hohmann & Dehghani, 2019). Intermediate filaments are dynamic structures that can shorten, elongate, and rearrange but, contrarily to actin filament and microtubules that are dynamic structures, they are extremely stable, non-polar and do not bind molecular motors so they cannot generate mechanical forces. They are however extremely elastic and can withstand large deformations, a mechanical characteristic absents in microtubules and microfilaments. Their stable structure and their ability to spread through the entire cell cytoplasm suggest that their main functions are to structurally reinforce cells and to organize them into tissues. They connect the external microenvironment to intracellular organelles, absorb the forces exerted on the cell by its environment and transduce mechanical forces generated by the other cytoskeleton components (Wagner et al., 2007).

Among all cytoskeleton components involved in cell migration, so far, intermediate filaments have been the least characterized. As they spread throughout the cytoplasm, their main function is to connect complexes in charge of cell-cell adhesion (desmosomes) and cell-extracellular matrix adhesion (hemi-desmosomes and focal adhesions) (Figure 14). 'Cytoskeletal organizers' from the plakin family play key roles in the maintenance of these adhesive structures and anchor them to intermediate filaments, microtubules and actin microfilaments. In epithelia, cell-cell and cell-substrate contacts are ensured by cadherin-family members, which interact with keratin filaments through proteins of the plakin family: desmoplakin at desmosomes and plectin at hemidesmosomes (Chung et al., 2013). When migration is initiated, cells reorganize the intermediate filament system and remodel adhesion complexes to promote cell migration. In collective migrating cells, local tensons are transmitend between adjacent cells. The mechanoresponse of plakoglobin binding to plasmodesmal cadherins at cell-cell adhesion sites induce the assembly of the

keratin cytoskeleton network at the rear of collective migrating cells while at the front, it orients the protrusive behavior. (Weber et al., 2012). In collective migration, cells must turnover desmosomes to weaken cell-cell contacts, a mechanism allowed by the downregulation of keratin and the increase of vimentin recruitment at focal adhesions, a characteristic of epithelial-to-mesenchymal transition (Chung et al., 2013).

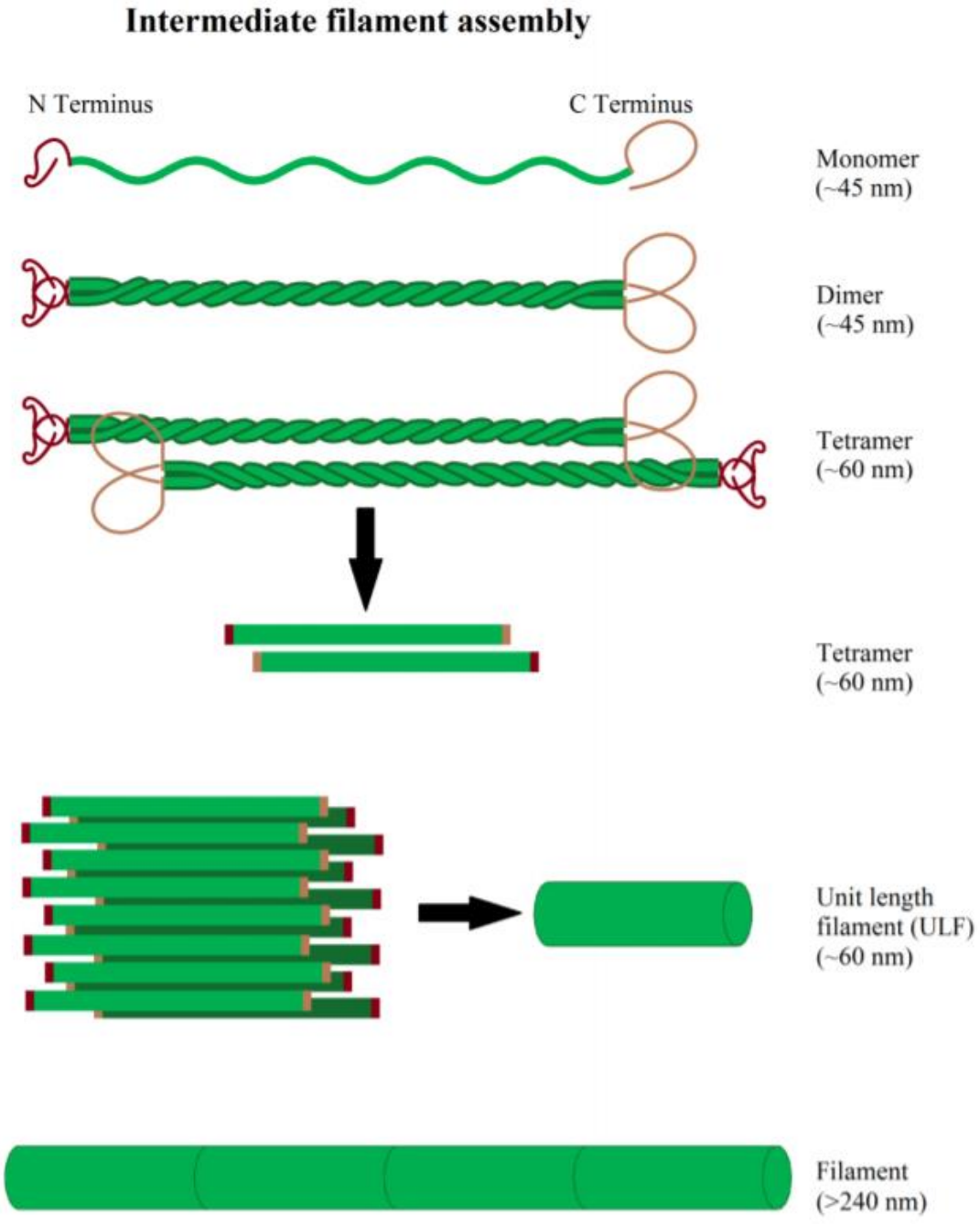

Figure 13: Illustration of intermediate filament assembly.
Intermediate filaments arise from the monomers spiraling around each other to form dimers. Two dimers aggregate to a tetramer and eight tetramers to a unit length filament. Unit filaments form the final filament via end-to-end aggregation. Notably, this process is independent of ATP or GTP (Taken from Hohmann & Dehghani 2019)

In single cell migration, intermediate filaments participate to the formation of the focal adhesions that anchor cells to the substrate. For example, vimentin binds actin via plectin and integrin α2β1 to promote the strengthening of focal adhesions ((Hohmann & Dehghani, 2019). This facilitates mechanical interactions with the surrounding environment and transduces forces through the cell.

Considering that the composition of intermediate filaments varies from one cell type to the other, and the fact that they have not been the focus of my experimental work, detailing their contribution to the mechanisms of cell motility goes beyond the scope of this introduction. Therefore, I will not go deeper in the underlying mechanisms described in several reviews (B.-M. Chung et al., 2013; Etienne-Manneville, 2018).

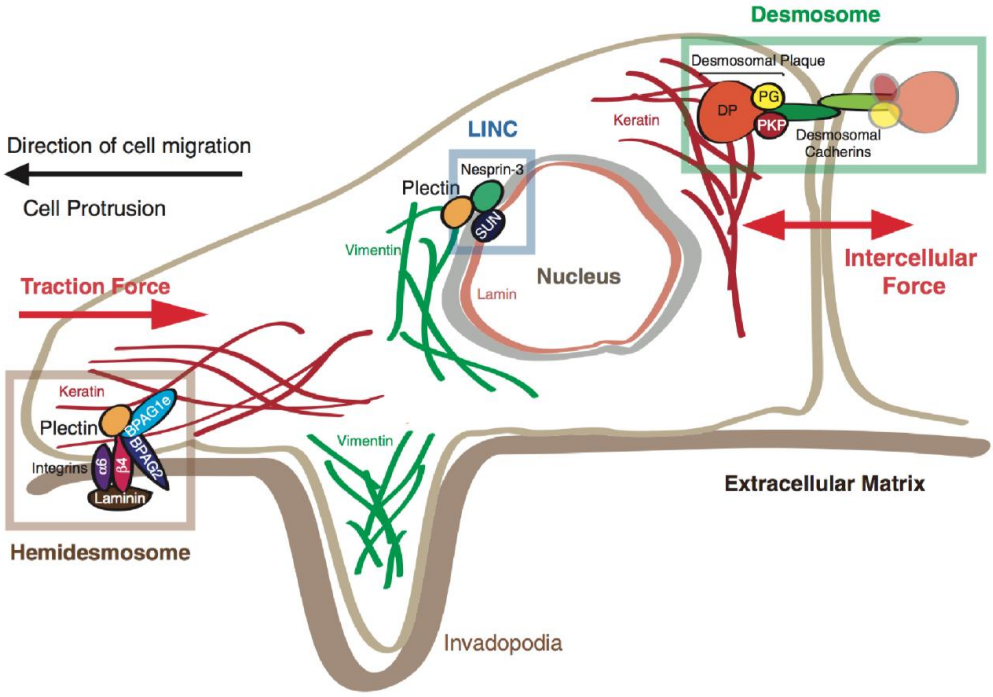

Figure 14: The role of intermediate filaments during cell migration.
The schematic representation shows how intermediate filaments and distinct signaling and structural proteins colocalize within desmosomes and hemidesmosomes. Hence, IFs are involved in facilitating mechanical cell-cell and cell-substrate interactions in order to transmit intercellular or traction forces, respectively. (Taken from Chung et al.,2013)

2.1.2. Microtubules

Microtubules are structural components of the cytoskeleton that participate in cell division, transport of material across the cytoplasm and cell motility. Each microtubule is a hollow rod-like cylinder composed of heterodimers of α- and β-tubulin (reviewed in Akhmanova & Steinmetz, 2008). Upon binding of GTP, the α- and β-tubulin subunits dimerize and the polymerization of α-β-tubulin dimers in a head-to-tail fashion forms polarized protofilaments (Figure 15a). Thirteen protofilaments assemble parallel to each other with the same polarity in a stiff hollow tube: the microtubule filament (Figure 15b). Microtubules polymerize upon addition of new α-β-tubulin GTP-bound dimers to the

growing end of the preexisting microtubule. However, soon after their binding, α-β-tubulin dimers hydrolyze GTP into GDP and become more susceptible to depolymerization. The two ends of microtubules show different kinetics of polymerization with the exposed β-tubulin ends (called 'plus' (+) ends) growing fast and the exposed α-tubulin ends (called 'minus' (-) ends) growing slowly (Figure 15c).

In cells, microtubule orientation is tightly controlled. The microtubule formation (called microtubule nucleation) starts near the nucleus from a specific organelle called the microtubule-organizing center (MTOC) and moves towards the periphery of the cell. The microtubule (-) ends are associated with the MTOC, therefore assembly and disassembly can only occur on the filament (+) ends. Microtubules show dynamic behavior, rapidly switching between shrinkage (catastrophe) and growth (rescue) via the subtraction or addition of tubulin on their free ends, a process termed "dynamic instability" (Figure 15c). When the two ends of a microtubule are free, the (+) end grows while the (-) end shrinks, a process called treadmilling (see section below).

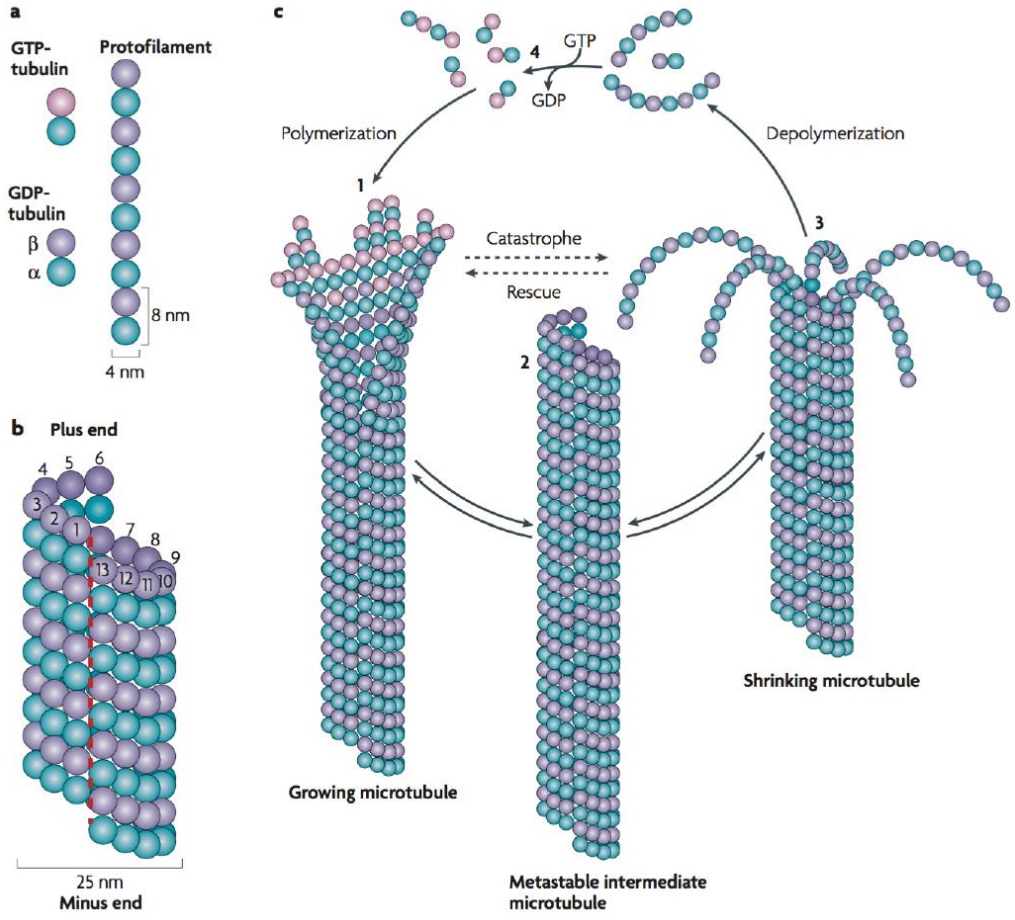

Figure 15: Microtubule structure and dynamics.
a) α- and β-tubulin heterodimers assemble into protofilaments. b) Thirteen protofilaments form a cylindrical, polar microtubule filament. c) The dynamic instability describes the filament's polymerization and depolymerization and its ability to rapidly switch between the two states (catastrophe or rescue, respectively). (Figure taken from: Akhmanova & Steinmetz, 2008)

The dynamics and organization of microtubule network in space and time are mediated by microtubule-associated proteins (MAPs) (Etienne-Manneville, 2013). The (+) end tracking proteins (+TIPs) target non polymerized soluble α- and β-tubulin subunits and regulate the dynamic (+) ends while other MAPs control the microtubule lattice by regulating the alternation between catastrophe and rescue events (Akhmanova & Steinmetz, 2008; Etienne-Manneville, 2013). Additional MAPs pull, slide, anchor or guide the microtubules (Akhmanova & Steinmetz, 2008). They participate to the cell architecture by controlling microtubule dynamics, their response to forces and their interaction with cellular structures and signaling factors (Akhmanova & Steinmetz, 2008). Molecular motors use microtubules as railways and hydrolyze ATP to transport vesicles, proteins, or mRNA from the cell center to the periphery (kinesin) or in the opposite direction (dynein).

Microtubules and their associated motor/non-motor proteins play an essential role in cell migration. They are required to establish and maintain front-to-rear polarity in the migrating cell by crosslinking to intermediate filaments and microfilaments (Etienne-Manneville, 2013; Dogterom & Koenderink, 2019) (figure 16a). Motor proteins also contribute to cell migration by addressing vesicles to the leading edge of the cell and participate to the cell extension at the migration front (figure 16b) (see filopodia/lamellipodia in actin cytoskeleton section). Moreover, microtubules participate to the cell signaling and response to external cues (Figure 16c). For example, microtubule growth locally regulates the activity of RhoGTPases, which in turn stimulate actin polymerization at the migration front(Dogterom & Koenderink, 2019). Furthermore, microtubules and the associated proteins participate to the formation, maturation and disassembly of focal adhesion complexes characteristic of the migrating cell (Figure 17) (reviewed in Etienne-Manneville, 2013). The vesicular traffic of integrins, which play a crucial role in focal adhesion, is dependent on microtubules and the associated motor proteins: after dissociation of focal adhesions, integrin-containing vesicles are addressed to the front of the cell. The polarized recruitment of microtubule-associated motors allows the establishment of a polarized traffic between sites of endocytosis and exocytosis and between the trans-Golgi network and the leading edge of the migrating cell.

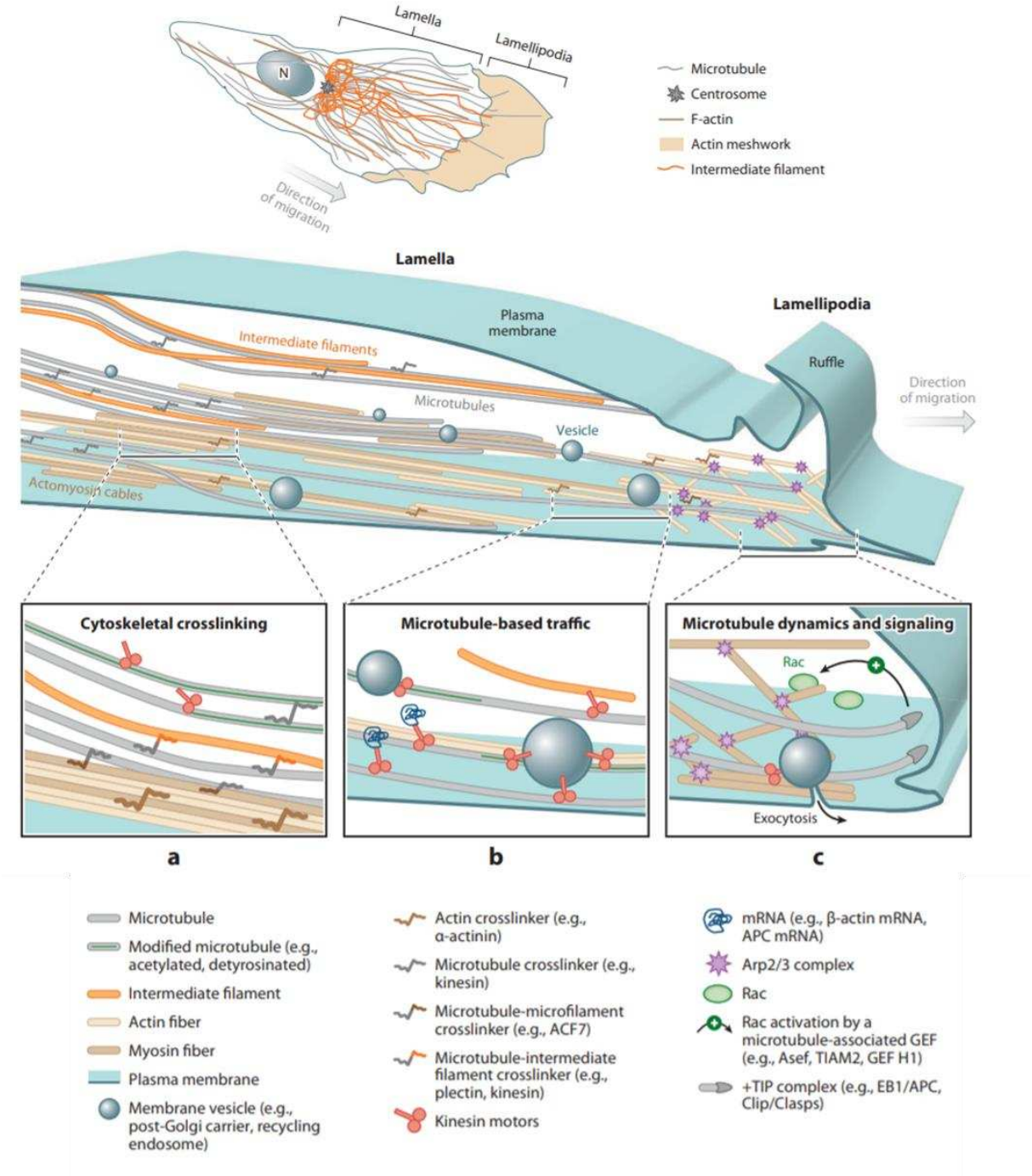

Figure 16: Microtubules participate to cell migration

(a) By crosslinking with actin fibers and intermediate filament, they participate to the protrusion structure and correct microtubule orientation is essential to the front-to-rear polarity of the cell.
(b) The microtubule-based traffic is essential to address vesicles to the leading edge of the cell through (-) to (+) Kinesin motor proteins.
(c) Addressed vesicles furnish the front with material and contribute to the cell extension. In the other hand, microtubules participate to the cell signaling and response to external cues

Abbreviations: APC, adenomatous polyposis coli; EB, end-binding protein; GEF, guanine nucleotide exchange factor; N, nucleus; +TIP, plus-end tracking protein. (Taken from Etienne-Manneville; 2013)

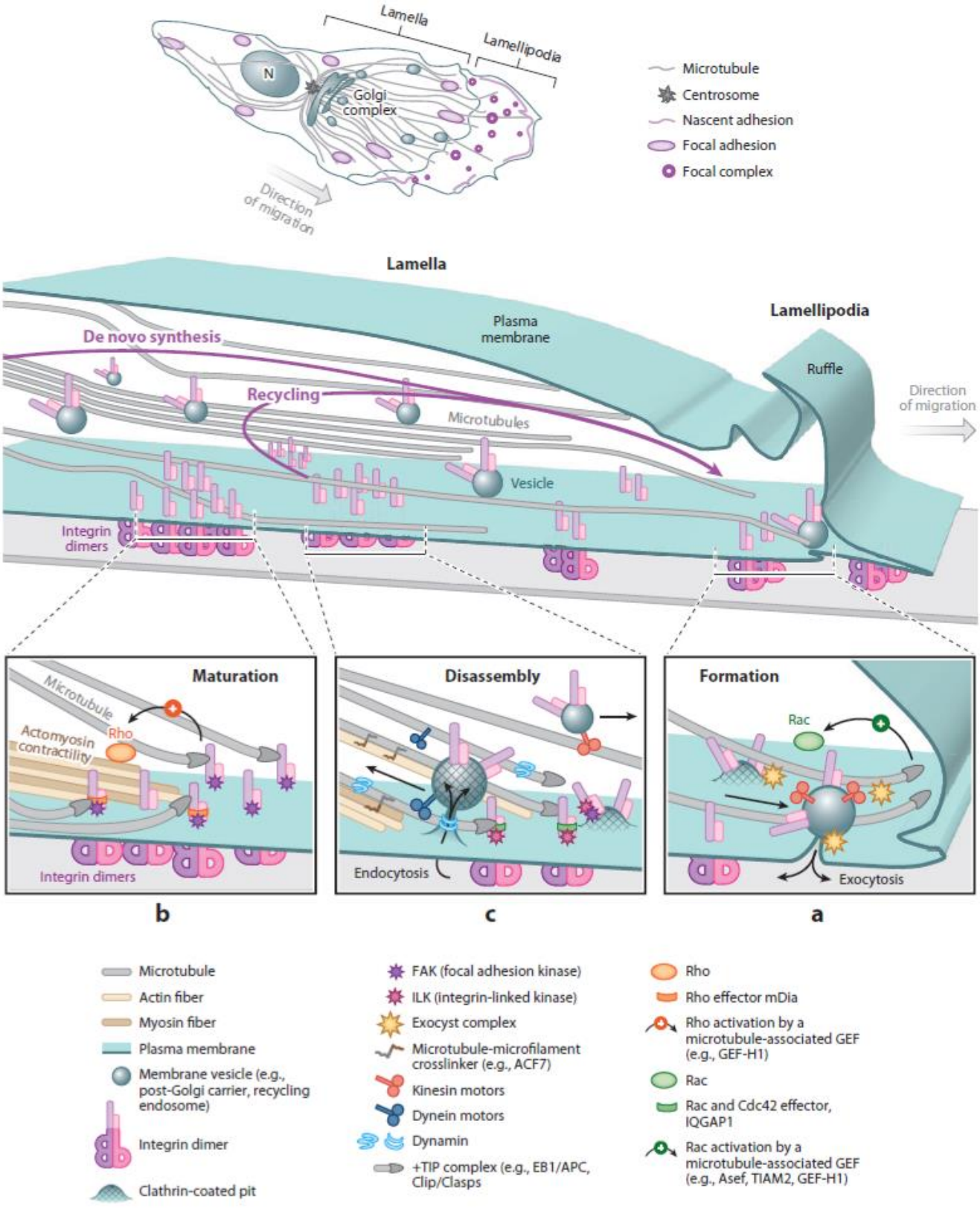

Figure 17: Microtubule-dependent regulation of focal adhesions in migrating cells.
Abbreviations: APC, adenomatous polyposis coli; EB, end-binding protein; GEF, guanine nucleotide exchange factor; N, nucleus. (Taken from Etienne-Manneville; 2013)

2.1.3. Actin filaments

Actin fibers are composed of globular actin (G-actin) monomers, which polymerize and assemble into a double stranded, right-handed helical filament (F-actin) (Figure 18a). Upon binding of ATP (activation) G-actin monomers form dimers, trimers and stable oligomers (nucleation) that will assembly into filaments. Like microtubules, actin fibers are polarized, possessing two ends with distinct kinetics: the barbed end (also called "+ end") which grows fast and the pointed end (or "- end") with slow growth (Figure 18b). With fast growth, the barbed end is mostly composed of ATP-coupled actin monomers while at the pointed end the hydrolysis of ATP to ADP leads to the release of ADP-coupled actin and filament disassembly. At both ends, the rate of polymerization /depolymerization depends on the monomer concentration. At intermediate concentration of monomers (when G-actin and F-actin are at equilibrium), barbed ends grow while pointed ends shorten simultaneously (treadmilling) (Figure 18b).

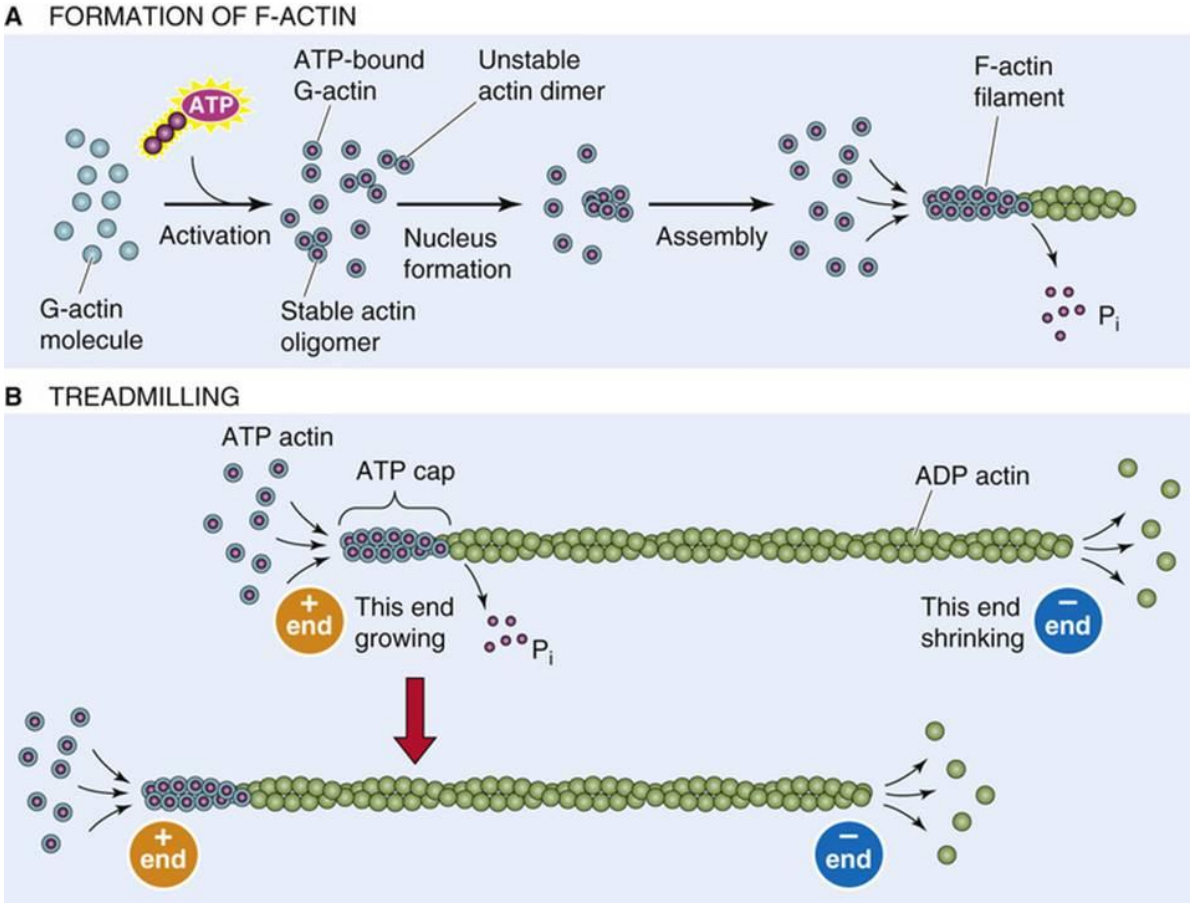

Figure 18: Actin filaments.
A, Single molecules of G-actin form F-actin filaments. **B,** F-actin can grow at the plus end while shrinking at the minus end, with no change in length. P_i, inorganic phosphate. (Taken from Medical Physiology, 3rd Edition - Cellular Organelles and the Cytoskeleton)

Contrary to intermediate filament and microtubules, actin filaments present several types of organization, which together form specific structures within the cell (see section below). The rate of assembly/disassembly, as well as the diverse fiber network architectures, depend on the actin binding proteins that shape the network. Profilin binds actin monomers and regulates ADP/ATP exchange, prevents spontaneous nucleation, and collaborates with nucleation factors to enhance actin polymerization (Hohmann & Dehghani, 2019). On the other hand, capping proteins attach to the barbed end of microfilaments to restrict actin elongation, while actin binding proteins from the ADF/cofilin family are capable of disassembling and fragmenting actin filaments. The non-muscle Myosin II belongs to the molecular motor class of actin binding proteins which bind different actin fibers and make them move to generate forces, whereas crosslinking proteins bind different actin fibers to shape them with different architectures (Blanchoin et al., 2014; Munjal & Lecuit, 2014; Svitkina, 2018; Hohmann & Dehghani, 2019).

The diverse function of these actin binding proteins as well as the function of actin within the migrating cell will be summarized in the following sections.

2.1.3.1. The modular architecture of the actin cytoskeleton in migrating cells.

Within the migrating cells, actin fibers present several modes of organization, reviewed in Blanchoin et al.,2014 (Figure 19):

A. Branched F-actin networks

A branched actin network is based on a primary actin fiber on which several steps of ramification (or branching) occur. Like the branches of a tree, actin branching consists in adding a new nucleation site on a preexisting growing actin filament from which a secondary branch will start its growth. After several steps of branching, a network will result from multiple actin-polymerizing fibers branched together (Figure 19 a). This specific architecture is initiated by nucleation from a complex made of seven proteins: the Arp2/3 complex (for actin related protein 2/actin related protein 3). The Arp2/3 complex, associated with nucleating-promoting factors (NPFs) binds to primary fibers and promotes the formation of new polymerizing actin fibers with a 70° angle to the primary fibers.

Branched actin networks play a role in a variety of cellular processes, including clathrin-mediated endocytosis, meiotic spindle positioning and force generation and shape changes at the leading edge of the migrating cell. In the following sections, I will focus on this latter function.

To generate efficient forces, branched actin networks need to be restricted in space and time to avoid the formation of arrays of parallel bundles growing away from the nucleation sites. This restriction is ensured by capping proteins which avoid the growth of long filaments and, together with Arp2/3 mediated nucleation, lead to the formation of a dense branched actin network composed of subnetworks, each formed by several branched and capped primary fibers. Together, the entanglement of all primary fibers and their sustained branched network act in force generation. Indeed, the push of an individual subnetwork toward the neighboring one creates a repulsive effect resulting in force generation that is independent of motor proteins (Figure 19 a).

B. Cross-linked meshworks

As mentioned in Blanchoin et al 2014, to avoid any confusion, crosslinked meshworks will be defined as arrangements of actin filaments interconnected by proteins that bridge actin filaments together, excluding the branched actin networks described above. Such meshworks result from the crosslinking of independent, pre-polymerized actin filaments with various orientations (Figure 19b) (reviewed in Blanchoin et al., 2014). The distance between filaments depends on the crosslinker proteins that compose the network resulting in a complex macroscopic organization (Winkelman et al., 2016). Among these, the best characterized are α-actinin and filamin for long-distance bridging, and fimbrin and fascin for short-distance bridging. Short-range crosslinkers tightly pack actin filaments into bundles in which actin filaments can be oriented in a parallel, antiparallel, or mixed polarity orientation, depending on the crosslinker. Conversely, long range crosslinkers give rise to either bundles or networks depending on their concentrations (Blanchoin et al., 2014; Winkelman et al., 2016; Hohmann & Dehghani, 2019).

Crosslinked networks play roles in defining the shape and ensuring the mechanical integrity of the cell. As crosslinking proteins bind already existing actin fibers, they play little or no role during actin assembly and in the organization of the network. In this, they stand apart from the Arp2/3 complex, which is involved both in the initiation of actin assembly and in the organization of the network.

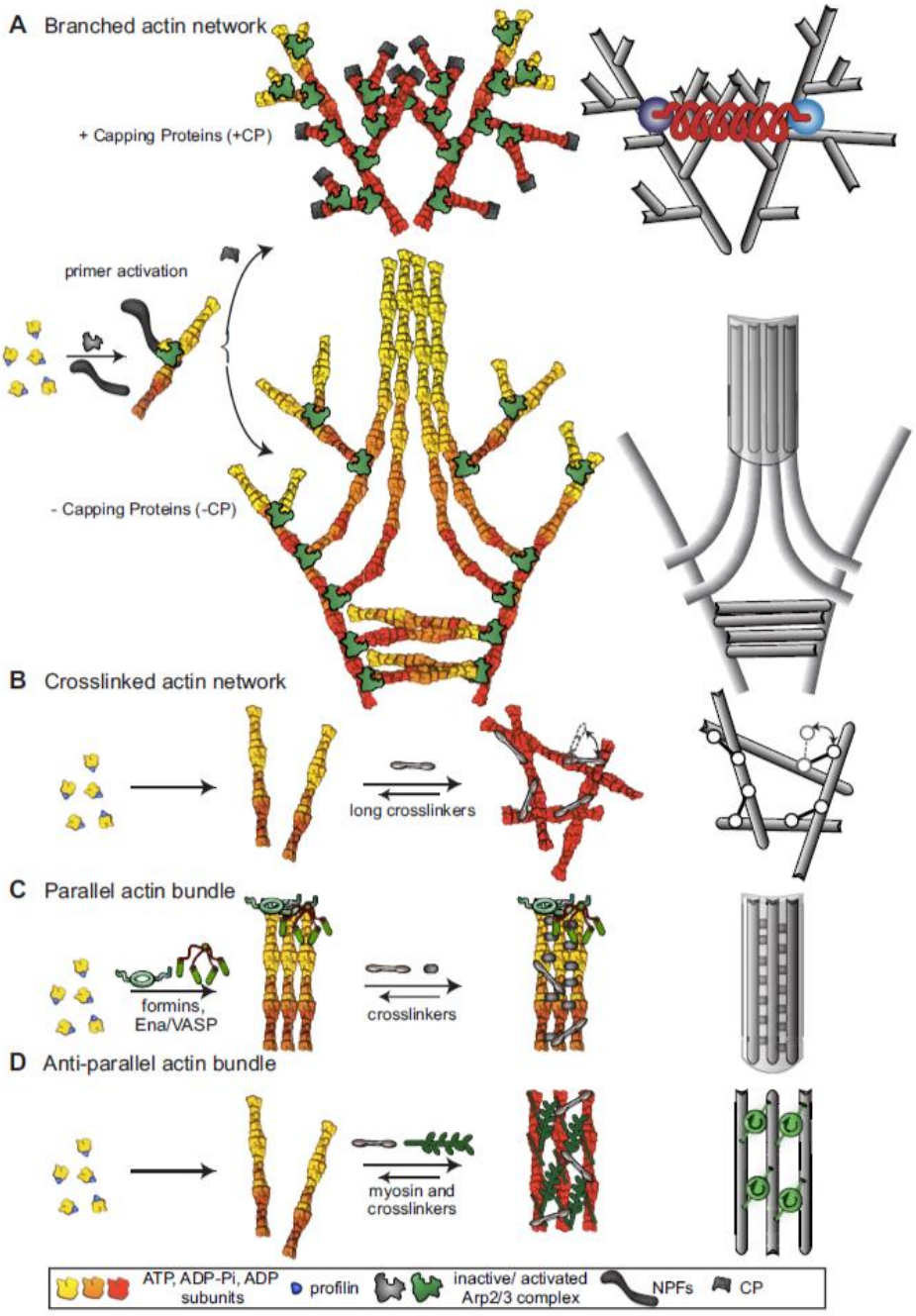

Figure 19: Distinct actin filament organizations and their mechanical description.

A: a branched actin network results from the autocatalytic branching activity of the Arp2/3 complex. Activated by nucleation promoting factors, NPFs, the Arp2/3 complex generates a branched network from the side of a preexisting actin filament, called a "primer." In the presence of capping proteins (+CP), branches are shorter. This yields dense and rigid subnetwork that evolve into an entangled meshwork. The entanglement of filament subnetworks leads to mechanical interactions that are represented by a spring (in red) connecting barycenters (spheres) of adjacent subnetworks. In the absence of capping proteins (-CP), actin filaments grow longer and can either align into an antiparallel organization or bend and coalesce into a parallel bundle. These parallel filaments form stable filopodia-like bundles that act as a solid body. **B**: long crosslinkers organize actin filaments into networks. These bonds act as rigid links and control the global elasticity of the actin network depending on their binding kinetics and concentration. **C**: short crosslinkers tightly pack unbranched filaments, such as those generated by formins or Ena/VASP proteins, into stiff, straight bundles. **D**: molecular motors, myosins, are dynamic links that gather antiparallel filaments into a contractile unit. They act as active springs. On the right, gray diagrams represent mechanical analogs of each molecular structure. (From Blanchoin et al, 2014)

C. Parallel F-actin bundles

As mentioned in the previous paragraph, actin filaments can organize in bundles upon binding of crosslinking proteins including α-actinin, fimbrin, and fascin, resulting in tightly-packed, stiff structures. Most of the times, filaments are arranged in a parallel orientation, with their barbed end facing the cell membrane (Figure 19 D).

Proteins of the Formin and Ena/VASP family are major regulators of actin bundle formations by enhancing actin monomer recruitment at the tips of growing microfilaments (*Drosophila* Enable (Ena) and Vasodilator-Stimulated Phosphoprotein (VASP) are the founding members which gave the name to the family (Krause et al., 2003). Formins and Ena/VASP often cap the barbed end of parallel F-actin bundles, enhancing their elongation in structures like filopodia (see section below) but they also contribute to the bundle structure itself. Indeed, some formins also position to the side of the actin bundles, where they play the role of crosslinkers, while Ena/VASP contributes to the bundle rigidity by magnifying the effect of fascin (Blanchoin et al., 2014; Hohmann & Dehghani, 2019).

In a similar way to branched actin networks, elongating actin bundles can exert pushing forces by their growth. Their elongated structure is found in many cellular contexts including filopodia, microvilli, and hair cells stereocilia (Mattila & Lappalainen, 2008; Blanchoin et al., 2014; Svitkina, 2018).

D. Anti-parallel stress fiber bundles

Anti-parallel actin bundles consist of actin fibers crosslinked by fimbrin and α-actinin. Within these bundles, actin fibers are not all oriented in the same way, resulting in antiparallel organization of actin fibers (Figure 19 D). Also, they are generally less dense than parallel actin bundles since crosslinking bridges act at longer range. These bundles are called stress fibers because upon the binding of the motor protein myosin, antiparallel actin fibers slide in opposite direction resulting in a contraction that generates mechanical forces (Figure 19 D).

This myosin-induced contraction plays crucial roles in cell processes such as cytokinesis and contractility during cell migration. This particular function will be detailed in the following section.

2.1.3.2. Actin-based structures involved in cell motility

As mentioned above, the different actin cytoskeleton structures have specific subcellular localizations. The adherent migrating cell is a good example to illustrate the different structures and the related cytoskeleton organization (Figure 20) (based on reviews from Blanchoin et al., 2013; Svitkina, 2018).

The lamellipodia.

Lamellipodia are large flattened structures observed at the front side of the migrating cells. They are formed by membrane protrusions caused by the mechanical pushing of branched actin fibers. The actin nucleator Arp2/3 mediates the formation of characteristic actin-branched structures. The Arp2/3 complex itself needs the activation of a specific nucleation promoting factor, the Wave complex, while the fast growth of actin fibers is promoted by elongators such as formins (Krause & Gautreau, 2014). Additional cross-linking proteins (e.g. spectrin, filamin or α-actinin) can enrich the network by physically connecting the already assembled actin filaments. Interestingly, all branched actin fibers orient their polymerization with the barbed ends towards the membrane at the leading edge of the cell but with different angles. The large lamellipodia protrusion is the result of large pushing forces exerted by the growing networked filaments (Murrell et al., 2015; Bernhard Wehrle-Haller & Imhof, 2003).

Interestingly, both the Arp2/3 complex and formins are constitutively inactive. Within the cell, they are activated in space and time upon reception of extracellular signals (Higashida et al., 2013) by PIP_2 and RHO-GTPases such as RhoA, CDC42 and RAC (Figure 21. 1-4). The repetitive branching and the local activation of nucleation-promoting factors allow the cell to generate forces on the plasma membrane exactly where it is needed. According to the signals received, the network can easily expand or reorient itself by simply adjusting the rates and sites of nucleation and capping (Figure 21. 5-7).

While polymerizing actin pushes the membrane forward at the leading edge, actin fibers depolymerize at the back of the lamellipodia, ensuring the F/G-actin turnover. The release of actin monomers is a consequence of the ADF/cofilin-mediated cleavage of actin fibers and of the disassembly of branched filament. Also, myosin motors are enriched at the rear of lamellipodia and the tension they generate favors mechanical fragmentation. The global treadmilling, resulting from the continuous nucleation of new “daughter” filaments on the preexisting ones at the front and from the retrograde flow of released actin monomer at the back, thus leads to the forward displacement of the cell (Figure 21. 8-12).

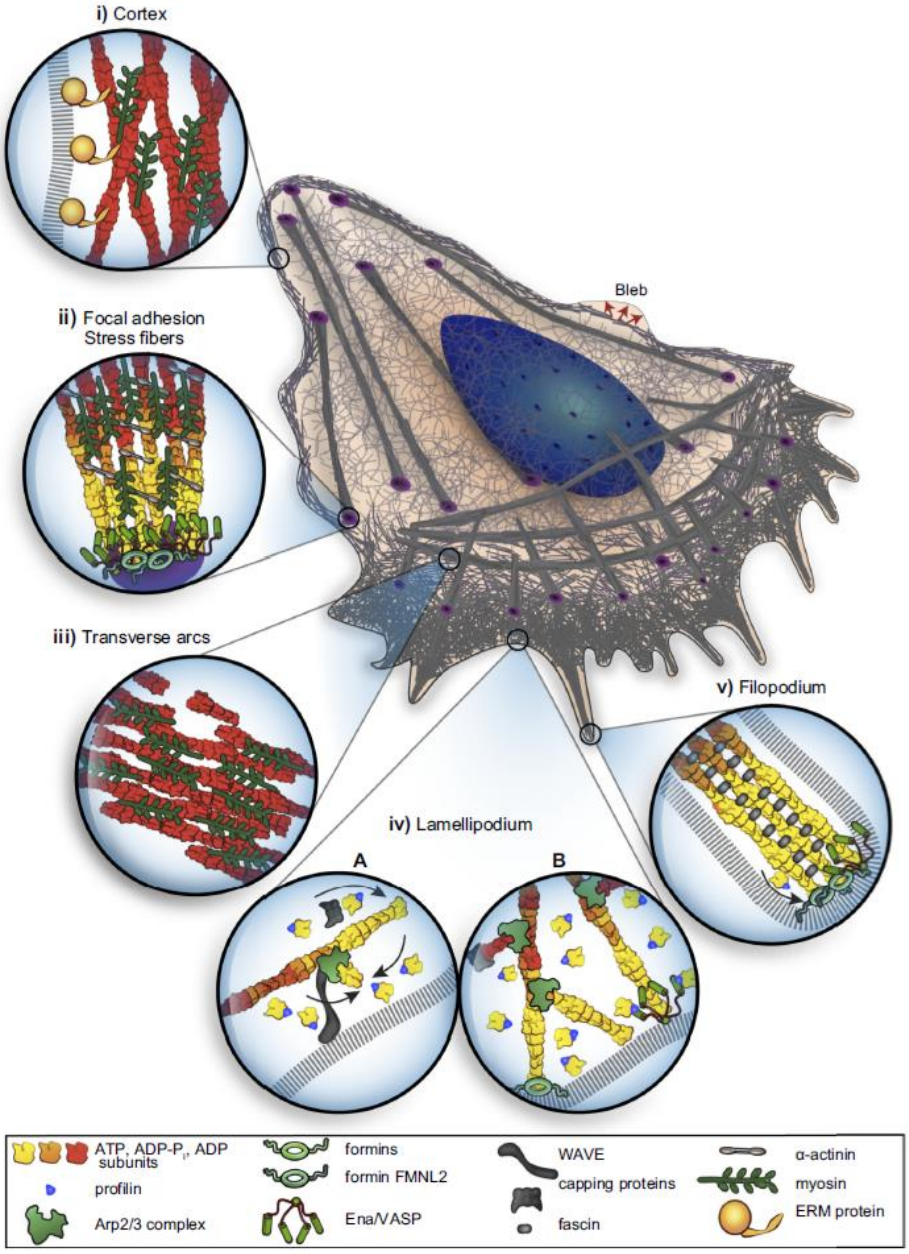

Figure 20: Specialized actin organizations in vivo.

Motile cells have distinct actin organizations in different locations in the cell, specialized for precise functions. i) The actin cortex is anchored to the plasma membrane through ERM proteins and is contractile via myosin activity. ii) One category of contractile bundles, the stress fibers, are found spanning the cell body, usually oriented parallel to the direction of movement. They are attached to focal adhesions and involve a specific set of regulatory intracellular factors, among them formins, Ena/VASP proteins, actinin, and myosin. iii) Transverse arcs are specific antiparallel actin filament formations found at the back of the lamellipodium. They are contractile through myosin activity. iv) The motor organelle, the lamellipodium, hosts rapid, massive, and localized polymerization of branched actin networks. A: initiation of this dendritic network occurs via the concerted activity of locally activated Arp2/3 complex binding to the side of an actin filament "primer" and by interaction with members of the WAVE family of proteins. Elongation of the network occurs by addition of the profilin/actin complex (black arrows) to the barbed ends of actin filament in close contact with the plasma membrane. B: Ena/VASP proteins, the formin FMNL2 and capping proteins control the elongation of the network by modulating the dynamics at filament barbed ends (right zoom inset). Ena/VASP and FMNL2 favor barbed end elongation whereas capping protein blocks it. v) The sensors organelles, filopodia, are filled with parallel actin bundles elongated by the actin polymerases, Ena/VASP and formins, and tightly packed by the short bundler fascin. Another type of leading-edge protrusion are blebs, initially formed as cytoskeleton-free membrane bulges driven by the internal pressure of the cell (brown arrows). (from blanchoin et al 2014)

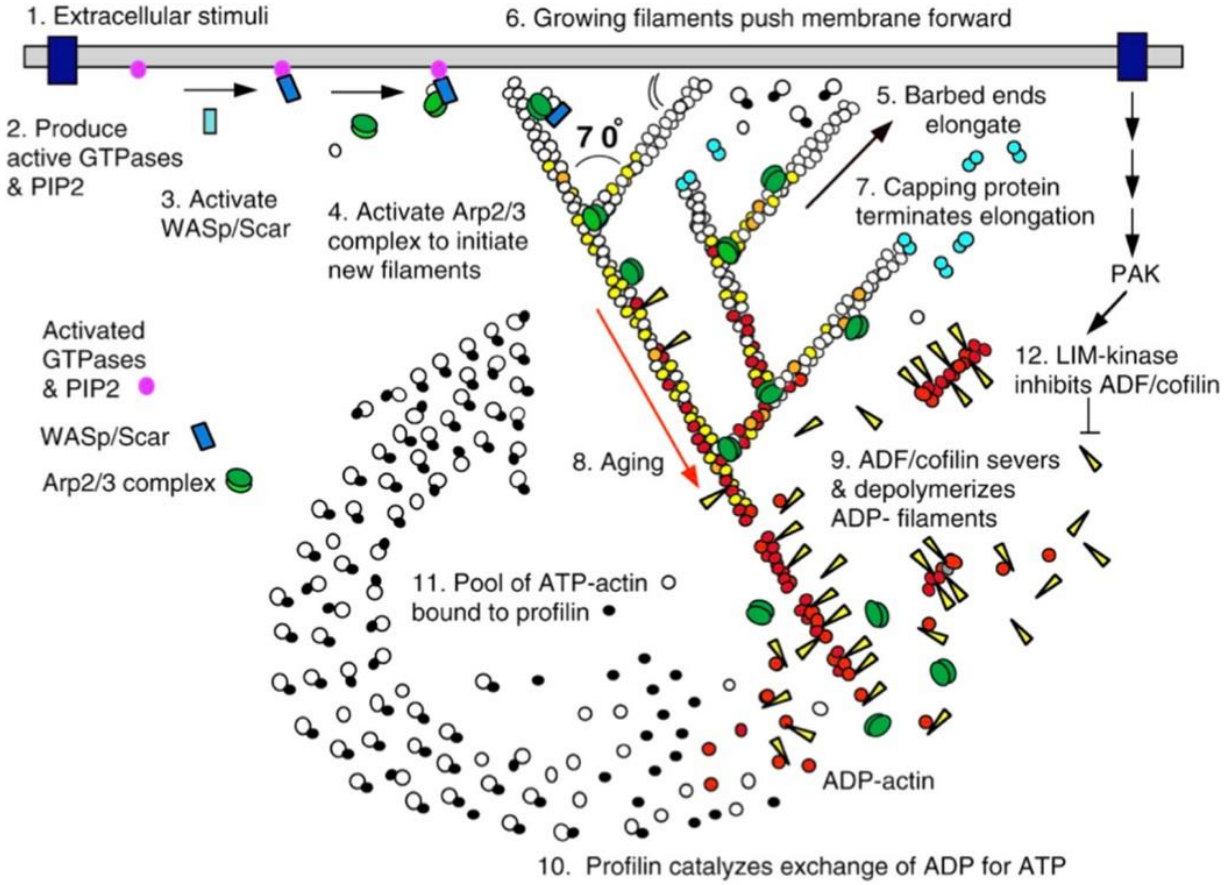

Figure 21: The Dendritic Nucleation/Array Treadmilling Model for Protrusion of the Leading Edge. Based on the original model from Pollard et al., 2000).
(1) Extracellular signals activate receptors. (2) The associated signal transduction pathways produce active Rho-family GTPases and PIP2 that (3) activate WASp/Scar proteins. (4) WASp/Scar proteins bring together Arp2/3 complex and an actin monomer on the side of a preexisting filament to form a branch. (5) Rapid growth at the barbed end of the new branch (6) pushes the membrane forward. (7) Capping protein terminates growth within a second or two. (8) Filaments age by hydrolysis of ATP bound to each actin subunit (white subunits turn yellow) followed by dissociation of the γ phosphate (subunits turn red). (9) ADF/cofilin promotes phosphate dissociation, severs ADP-actin filaments and promotes dissociation of ADP-actin from filament ends. (10) Profilin catalyzes the exchange of ADP for ATP (turning the subunits white), returning subunits to (11) the pool of ATP-actin bound to profilin, ready to elongate barbed ends as they become available. (12) Rho-family GTPases also activate PAK and LIM kinase, which phosphorylates ADF/cofilin. This tends to slow down the turnover of the filaments. (Taken from Higgs, 2018).

The Filopodia

In addition to the large lamellipodia structures presented above, characteristic fingerlike protrusions called filopodia also appear at the migration front of a cell (reviewed in Mattila & Lappalainen, 2008). Filopodia emerge from the branched actin network of lamellipodia to form long and thin protrusions composed of strong actin bundles. In the absence of capping proteins to terminate fiber elongation from branched actin network, formins (e.g. mDia) and Ena/VASP continuously elongate actin fibers that bend and organize in parallel bundles, reinforced by fascin-mediated crosslinking (Figure 19 A and C; Figure 20v). Unconventional Myosin X favors filopodia elongation by continuously furnishing actin monomers to the elongation sites (Svitkina, 2018).

All tight cross-linked fibers are oriented in parallel with their barbed ends towards the membrane, such that their oriented polymerization pushes it to form thin protrusion. Also, actin filaments laterally bind to the cell membrane through proteins of the ERM family (Ezrin, radixin, moesin) (Figure 22)

Filopodia are enriched for various membrane associated receptors and adhesion molecules that allow the cells to reach, sense and grab their environment. The probing of

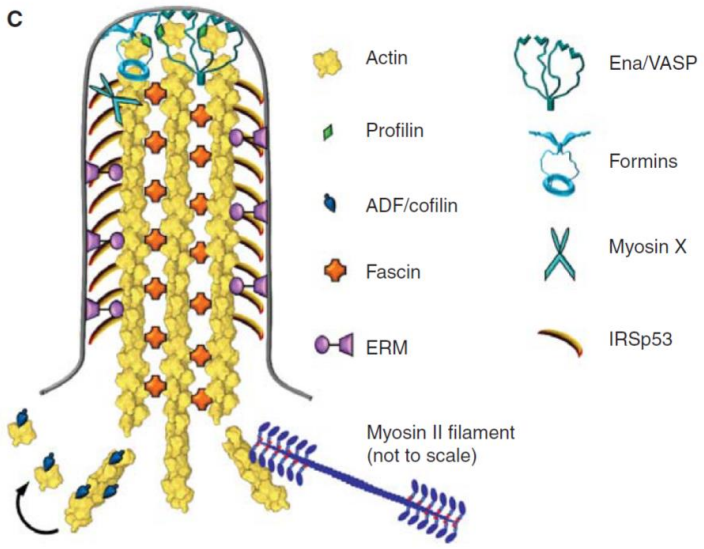

Figure 22: The molecular organization of filopodia.
Actin filaments are oriented with their barbed ends toward the filopodial tip. They are cross-linked into a bundle by fascin and laterally attached to the plasma membrane by ezrin-radixin-moesin (ERM) proteins. Formin and Ena/VASP (vasodilator-stimulated phosphoprotein) proteins associate with the actin filament barbed ends, anchor them to the membrane at the filopodial tip, and promote their elongation by protecting them from capping and recruiting actin–profilin complexes. Unconventional myosin X moves along actin filaments and accumulates at the filopodial tips. I-BAR-domain-containing proteins, such as IRSp53, help to maintain the tubular shape of the filopodial plasma membrane. Actin-depolymerizing factor (ADF)/cofilin and myosin II sever actin filaments at the filopodial base to stimulate actin filament depolymerization and monomer recycling. (from Svitkina 2019)

the substratum by filopodia allows the cell to estimate it stiffness, form focal adhesion with extracellular matrix, and respond to chemotropic cues to direct cell migration or change its direction. To ensure their function, filopodia must constantly reorganize, continuously shifting their actin filament components between polymerized and unpolymerized status, depending on the ERK1/2 signaling pathway (Blanchoin et al., 2014).

Actin cortex

The actin cortex consists of a thin dense interconnected acto-myosin contractile network in close contact with the inner face of the plasma membrane. This interconnected structure is a mix of actin fibers bundled in straight filaments by formins and weaved in a lattice-like network by cross-linker proteins such as actinin, filamin and fimbrin (Figure 20i) (Blanchoin et al., 2014; Chugh & Paluch, 2018).

Contrarily to filopodia and lamellipodia, cortical actin fibers are not uniformly polarized, and can be found in opposite orientations. Moreover, all fibers are attached to the plasma membrane by proteins of the ERM family. This attachment allows the transfer of forces induced by actomyosin contractility to the cell membrane and thus leads to cell shape changes and cell movements. Cortical contractility increases the intracellular hydrostatic pressure, driving the formation of blebs (Figure 20). Blebs are balloon-like membrane bulges that are dynamically extruded at the cell surface in correspondence of holes within the actin cortex or of local detachment of the cortex from the cell membrane. Blebs have been shown to be the motor of cell migration in what is called "amoeboid motility". In this mechanism, the cortical actin network, together with Myosin II contraction, brings forward the cell body upon formation of blebs. At the migration front, the cell forms blebs that are filled with polymerizing actin and myosin II, adheres to the extracellular cell matrix and then moves toward the blebbing sites. Ameboid migration is often observed in constrained environment and replaces or acts together with lamellipodia-filopodia to move on the cell.

The contractile fibers

Also called stress fibers, as their name indicates, contractile fibers are actin filament capable of contractility. They are present all over the cell except within lamellipodia/filopodia. (Figure 20ii-iii). They are formed by unbranched actin bundles in antiparallel orientation, and associate with the non-muscle myosin II that ensures the fiber contractility. Stress fibers can be oriented parallel to the direction of movement and linked to focal adhesion sites (Figure 20ii) or transverse, parallel to the advancing leading edge, just behind the dendritic network of the lamellipodium and not anchored to focal adhesions (Figure 20iii). Stress fiber contractility is required for cell migration and morphogenesis but also involved in cell-cell adhesion and cell-ECM interactions, since they are necessary for adherent junction, tight junction and focal adhesion assembly.

As the cell moves forward, it interacts with the extracellular matrix to which it anchors via focal adhesions. At both ends, proteins of the ERM family anchor stress fibers to the plasma membrane, and through the plasma membrane, to the extracellular matrix at focal adhesion. Also, combinations of adaptor proteins (e.g. talin, vinculin, α-actinin) link the actin stress fiber to ECM-anchored integrin or to adherent junctions (e.g. α-catenin and β-catenin). Stress fibers are not capped and can continuously grow towards the front of the cell where they attach to the newborn focal adhesions. Since they span the whole cell, stress fibers can be interconnected and interact with other actin networks and bundles.

Thus, stress fibers participate to the maintenance of the cell shape as well as to cell shape changes via Myosin II-mediated contraction. During migration, they also contribute to the retraction of the cell back-end and maintain the pulling forces required for efficient migration.

2.2. Morphogenetic processes that shape tissue

2.2.1. The Acto-Myosin contractility generates cell shape changes and cell movement.

As presented in the previous sections, the actin cytoskeleton, together with its associated proteins, is the main actor of cell movement and cell shape changes. On one hand, actin polymerization provides the mechanical push that deforms the cell membrane, a process particularly present in lamellipodia of migrating cells. On the other hand, actin fibers in antiparallel orientation can slide on one another, as in muscle sarcomere contraction, thus generating pulling forces. These contractile forces depend on motor proteins belonging to the Myosin superfamily, which exploit the energy provided by ATP hydrolysis to move along actin filament. This causes the contraction of actin fibers of different actin structures and is responsible for the deformations of muscle and non-muscle cells, cell migration and cytokinesis. Cell migration involves the non-muscle Myosin II class (reviewed in Svitkina, 2018; Wu & Priya, 2019).

The myosin II motor protein is structured by two heads, each containing actin-binding domains and an ATPase motor domain. The two heads are connected by a tail consisting of a coiled-coil rod domain. At the basis of each head, a neck is formed by the essential light chain and the regulatory light chain (Figure 23a). Through their tails, several Myosin molecules associate antiparallel to each other and form short bipolar filaments with a high number of actin-binding heads (Figure 23b)

The hydrolysis of ATP induces conformational changes of the actin-bound myosin II heads. Since actin filaments are polarized polymers, the conformational changes of myosin II induce the translocation of one head towards the barbed ends of the actin filament (Figure 23a). Myosin filaments are associated to antiparallel crosslinked actin fibers that will slide on one another resulting in the contraction or extension of the whole structure, (Figure 23b) depending on the localization of myosin II (Murrell et al., 2015). However, at the whole-cell scale, myosin is generally associated to actin contraction (e.g. stress fibers). Bipolar filaments of myosin II can be easily disassembled allowing the cell to form contractile actomyosin networks at the required place and time. Indeed, upon dephosphorylation of its regulatory light chain, Myosin II folds into an inactive conformation, which cannot polymerize or bind to actin filaments (Figure 23a).

The following sections will introduce a few examples of morphogenetic events in which acto-myosin tension regulates cell shape changes, cell movement and cell migration to organize a developing tissue. Such examples will be chosen to give an overview of the morphogenetic processes involved in the phenomena on which my work was focused.

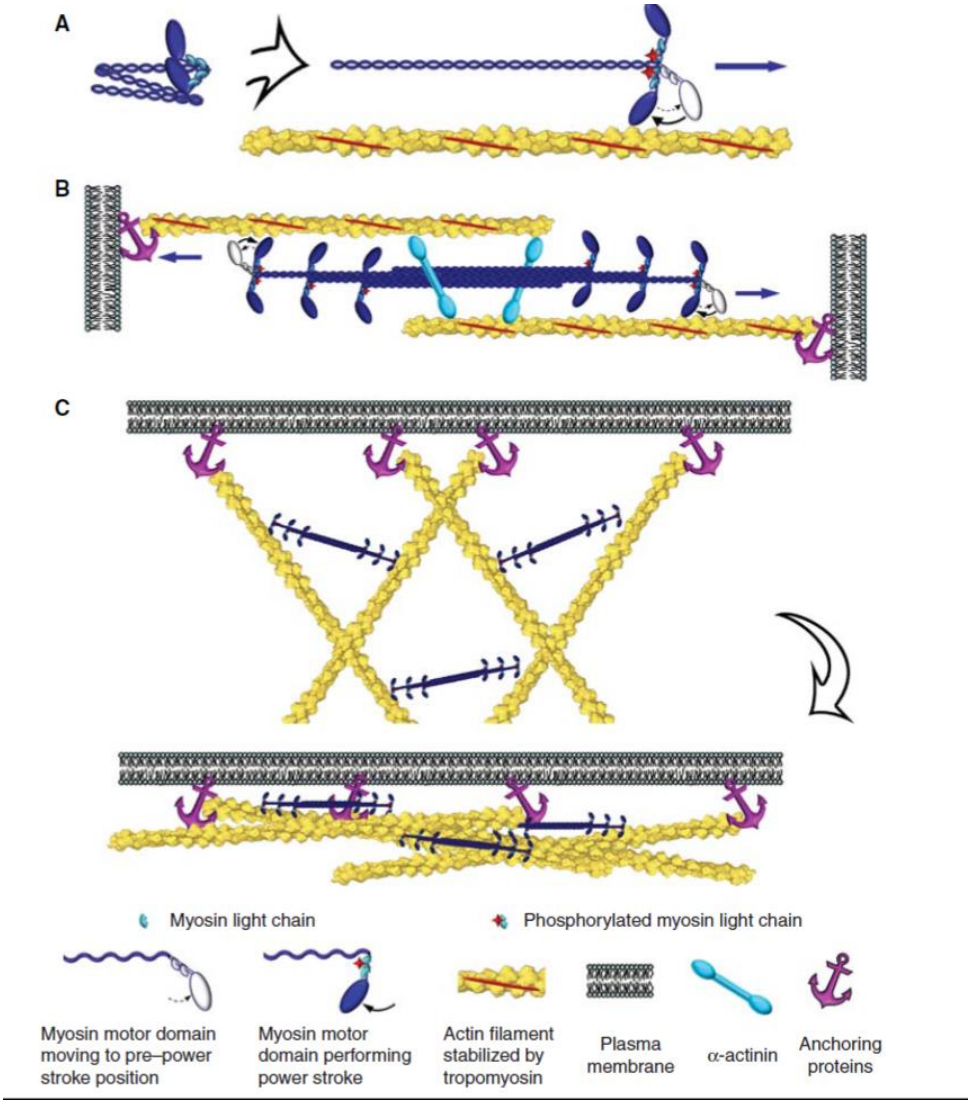

Figure 23: Contractile activity of nonmuscle myosin II.
(A) A hexameric molecule of nonmuscle myosin II has a folded conformation in an inactive state (left). Phosphorylation of the myosin regulatory light chain causes unfolding of the myosin II molecule and restoration of motor activity; this activated myosin II can move toward the barbed end of the actin filament by swinging its motor domain in an ATP-dependent manner (right). Contraction of actin–myosin-II bundles (B) or networks (C) is mediated by bipolar filaments of myosin II that move along oppositely oriented (B) or nonaligned (C) actin filaments anchored at their barbed ends to the plasma membrane or other cellular structures. (from Svitkina 2019).

2.2.2. Epithelium remodeling through cell shape changes and movements.

Because it has been first described *in vitro*, the main cell migration stereotype is an isolated cell crawling on the 2D substrate of a Petri dish. However, *in vivo* cell migration is much more complex as cells evolve in a 3D environment. The range and type of migratory behaviors vary a lot from the highly motile macrophages that easily move among cells to track pathogens to the very restricted motility displayed by ultra-densely packed epithelial cells.

Mono- or multi-layered epithelial sheets are composed of tightly packed adherent epithelial cells held together by intercellular junctions. These are constituted of adhesion molecules organized in clusters or belts that stitch cells together. Adhaerens junctions, formed by the *cis*- and *trans*- homophilic interactions of E-cadherin, are connected to cytoplasmic actin filaments via molecules of the catenin family such as β-catenin and α-catenin, vinculin, and other proteins (Guillot & Lecuit, 2013; Lecuit & Yap, 2015). Despite their structural stability, epithelia can display fluid behaviors since they are subjected to frequent remodeling during embryogenesis, wound healing or self-renewal. Changes of cell shape such as volume fluctuation (e.g. metabolic growth or osmotic swelling), elongation and flattening, allow strong tissue remodeling when coordinated at the tissue level (Figure 24a). Also, even if they cannot migrate individually, epithelial cells can exchange neighbors following coordinated and polarized shape changes (Figure 24b).

This phenomenon is called cell intercalation, and constitutes a fundamental morphogenetic process observed from the early steps of gastrulation to the latest steps of organogenesis in various models (reviewed in Walck-Shannon & Hardin, 2014). Depending on its orientation, the process is called *radial intercalation* (cells exchange place across the thickness of a multilayered tissue) or *planar intercalation* (cells exchange position within the plane of the epithelium, also called medio-lateral intercalation) (Figure 24b)(Walck-Shannon & Hardin, 2014).

Planar intercalation is the driver of convergence-extension, a morphogenetic movement involved in oriented issue elongation. Coordinated narrowing (convergence) and elongation (extension) can lengthen a tissue as in the chick forebrain, *C. elegans* hypodermis, *Drosophila* germband and renal tube of *Xenopus* and mice (reviewed in (Walck-Shannon & Hardin, 2014; Sutherland et al., 2020).

The germband elongation during gastrulation in *Drosophila melanogaster* has emerged as a powerful model to unravel the mechanisms that coordinately control cellular rearrangement (Figure 25) (Bertet et al., 2004). During this process, convergent extension driven by planar intercalation allows the germband to elongate along its anterior-posterior axis and double its length (Figure 25 A, B). The process is tightly polarized through the plane of the tissue. First, intercellular junctions shrink along the dorsal-ventral axis and vanish. The shrinking junction brings four or more cells together at a new vertex resulting from the merging of two opposite sides of the lost junction (convergence). The newly formed vertices are transient and are followed by formation of new junctions in the antero-posterior axis, perpendicular to the dorsal-ventral shortened junctions. This second step draws away cells that where originally in contact (extension). As the result of this coordinated and polarized process, cells shift position: cells originally separated become neighbors, while neighboring cells become separated (Figure 25 C, D). At the whole-embryo scale, this results in the tissue thinning and elongation (Figure 25 A, B).

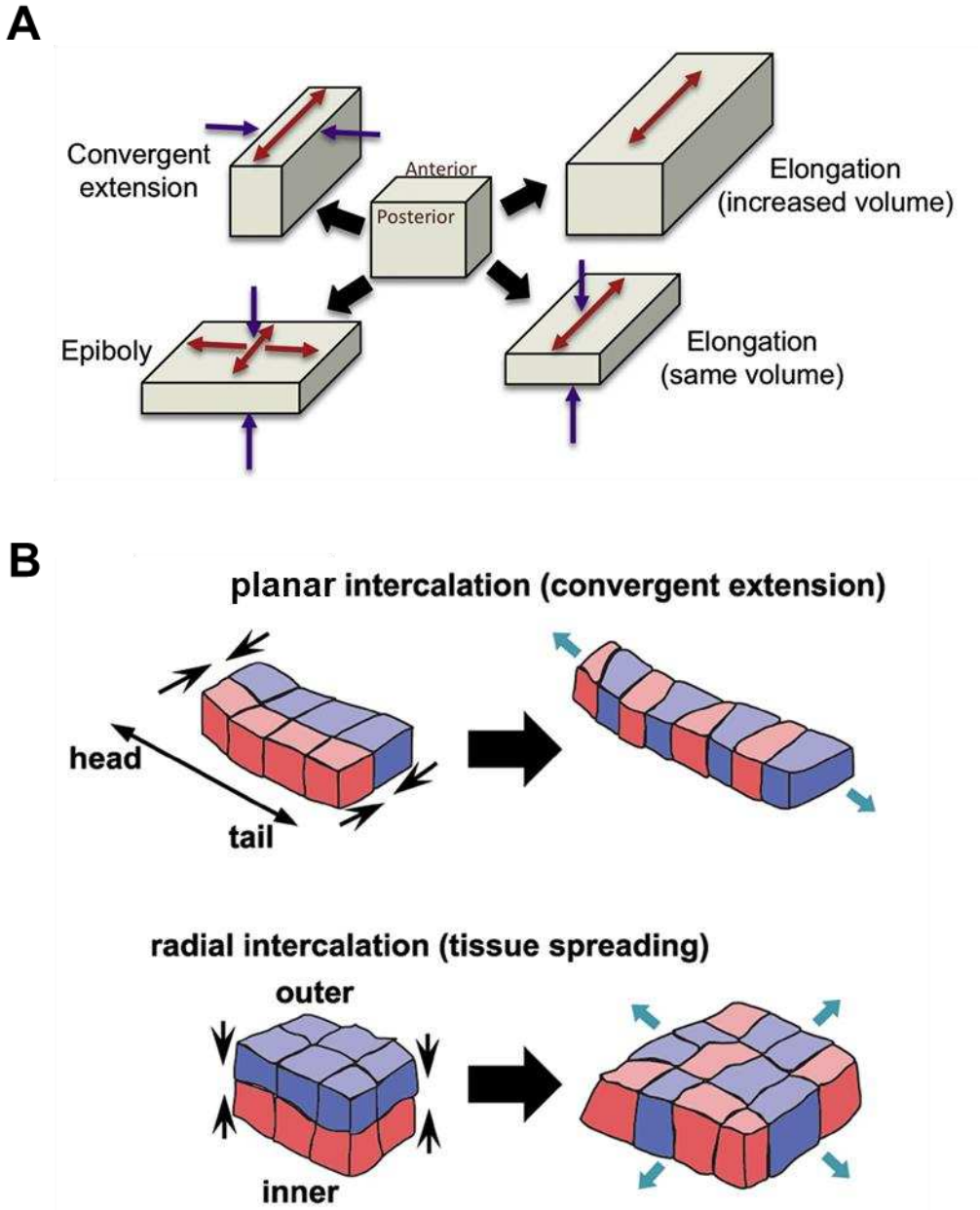

Figure 24. Schematic illustration of tissue shape changes mechanisms.

A) Ways in which a tissue can change shape without change in cell number nor position. Coordinated cell shape can make the tissue longer and narrower (convergent extension), wider and flatter (epiboly) or longer and flatter (elongation) with constant or increasing cell volume. Arrows indicated the direction of tissue shape change (red=expansion; purple=narrowing or thinning). (Adapted from Sutherland et al, 2020).

B) Ways in which a tissue can change shape though cell neighbor exchange. During intercalation process, cells move and exchange their positions with one another on the same plane (planar intercalation, upper illustration) or between superposed plane (radial intercalation, lower illustration). Black arrows indicate the direction of cell movement. Planar intercalation results in tissue lengthening and narrowing, whereas radial intercalation results in tissue spreading as the number of layers are reduced (indicated solid green arrows). (Adapted from Komiya et al., 2017).

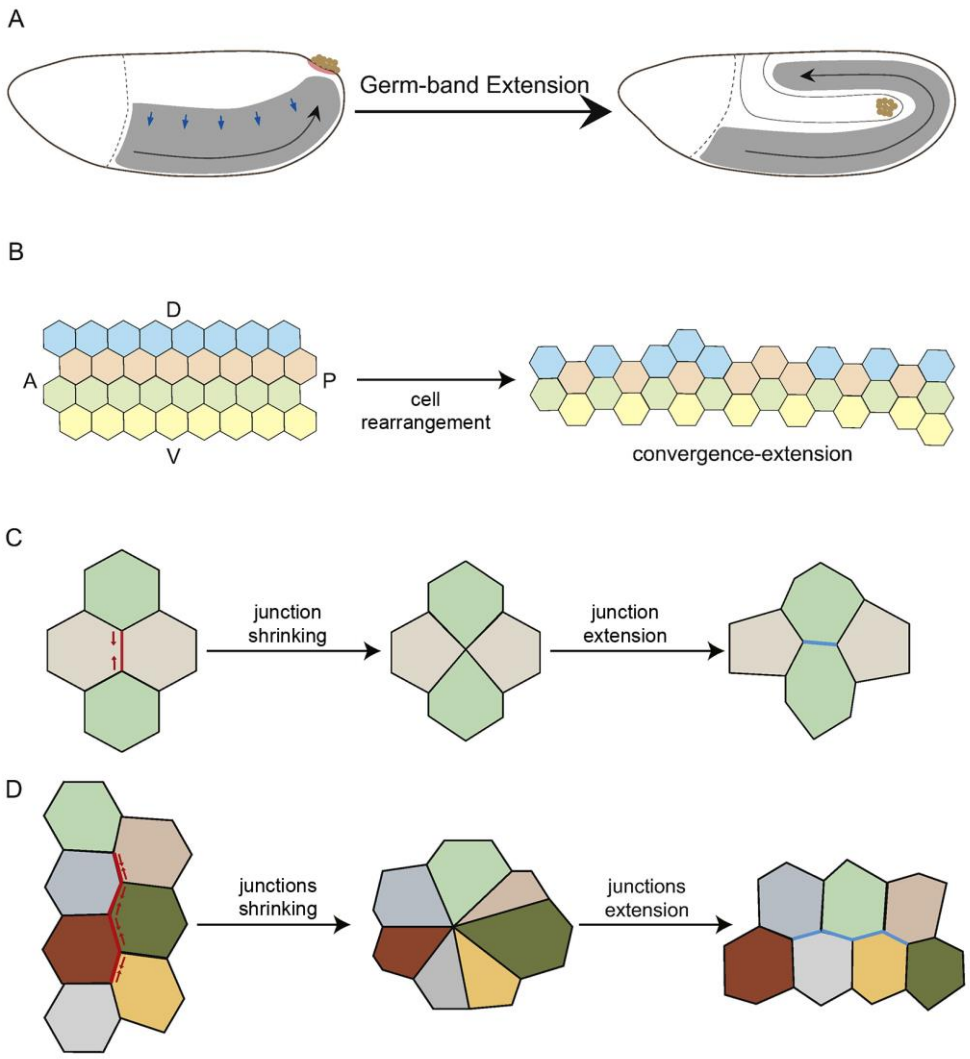

Figure 25. Germ band extension is driven by cell intercalation.

(A) Convergence-extension of lateral epidermis during germ-band extension. (B) Forces directing the lateral epithelial tissue deformation during germ-band extension. Tensile force from posterior midgut invagination induces cell rearrangement in A-P direction. Convergence and extension are driven by cell intercalation. (C-D) The key to neighbor exchanges in germ band is junction dynamics. Single (C) or multiple junction(s) (D) shrink in dorsal-ventral orientation (vertical, in red) and forms a 4x vertex (C) or a multiple cell vertex (D). Then the single (C) or multiple (D) new junction(s) (blue) forms perpendicular in the anterior-posterior orientation. Intrinsic forces are indicated by red arrows in C and D.

(adapted fromKong et al., 2017)

Convergence extension has been shown to require intense crosstalk between cortical tension, promoted by the actomyosin contractile network, and the E-cadherin-based cell-cell adhesion (Guillot & Lecuit, 2013; Lecuit & Yap, 2015).

Pulsatile actin-myosin flow has been observed at the apex of epithelial cells during germband elongation. A centripetal flow locally accumulates actomyosin fibers at the apical cortex of the cells while an anisotropic flow orientates actomyosin fibers along the dorsal-ventral junction (Figure 26A). Upon accumulation of myosin II along the dorsal-ventral axis, actomyosin contraction causes junction shortening. This oriented

accumulation of myosin is coupled to the decrease of cell adhesion between the two cells of the shrinking junction. These adhesions weaken because they contain fewer and smaller E-cadherin clusters. The stress imposed along dorsal-ventral junctions by acto-myosin contraction appears to upregulate E-Cadherin endocytosis (Levayer et al., 2011).

The process of junction elongation remains elusive and it is unclear whether the mechanisms that govern it depend on active or passive contribution (Guillot & Lecuit, 2013). Interestingly, while new vertices are stabilized by myosin II, the elongation of new antero-posterior junctions has been correlated to the decrease of myosin II levels (Bardet et al., 2013). Moreover, a passive contribution to tissue elongation provided by external tensile forces generated by endoderm invagination has been shown to help junction lengthening. Local factors such as pulling forces applied by anterior and posterior cell contraction also contribute to junction elongation, while dorsal and ventral cell constrictions are important to maintain junction elongation.

In other contexts, planar intercalation relies on basolateral protrusion, mostly for mesodermal cells, such as for the ascidian and zebrafish notochord and the frog chordamesoderm convergence extension. These processes are generally under the control of planar polarity cues that regulate typical mechanisms of cell migration. Intercalating cells extend highly polarized basolateral protrusion oriented toward the convergence side. Diverse signals such as Rac and WAVE locally activate the protrusive activity through Arp2/3 dependent actin polymerization (Figure 26 B). Here, rather than mediating junction shrinkage, myosin II is required to generate traction forces leading to cell migration.

In multilayered tissues, radial cell intercalation also plays a role in the spread of tissues by modulating their thickness. The process has been observed in both epidermal and mesodermal cells during gastrulation and in epiboly in fish and frog, during post-gastrulation skin thinning in frog, as well as during thinning of *Drosophila* ventral mesoderm (Walck-Shannon & Hardin, 2014). Since the radial intercalation of *Xenopus* multiciliated cells has been a major focus on my work, the whole process will be developed in a later section.

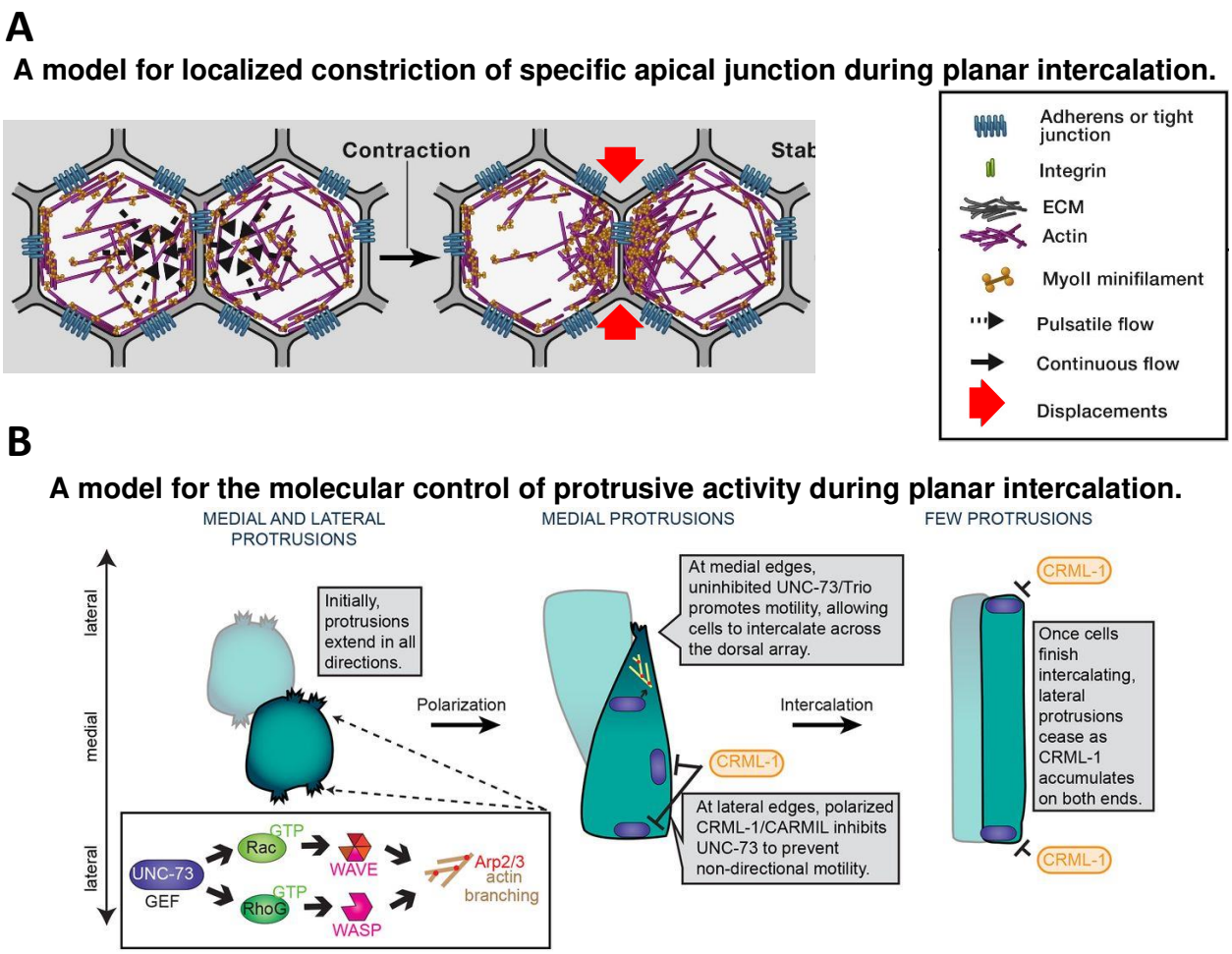

Figure 26: The different mechanisms of force generation during planar cell intercalation

(A) During convergence-extension of the lateral epidermis during germ-band extension in *Drosophila* embryo, cells move by localized junctions remodeling which mostly dependent on cortical tension on the apical surface of the cells. Pulsatile anisotropic flow induces junction shortening during cell intercalation. Resultant enrichment of actin-myosin at the junction stabilizes junction length reduction which make cells exchanges neighbor and moves without needs of basolateral protrusions (adapted from Heisenberg and Bellaïche, 2013).

(B) In the dorsal embryonic epidermis of *Caenorhabditis elegans, dorsal* planar cell intercalation relies on basolateral protrusive activity. Early, as intercalating cells begin to adopt a polarized, wedge-shaped morphology, protrusive activity is broadly distributed at the cell periphery. As intercalation proceeds, protrusions focus medially and basolaterally to produce a single, extending tip. As cell bodies translocate, cells migrate past one another and intercalation completes. The GEF UNC-73, which is broadly distributed, activates CED-10 and MIG-2, but only in regions devoid of CRML-1, which inhibits UNC-73 at lateral edges. Accumulation of CRML-1 at the contralateral edges of intercalating cells may promote protrusive downregulation as intercalation completes. (Taken from Walck-Shannon et al., 2015)

2.2.3. Cell migration

The ability to move is a fundamental property of cells that shape a developing embryo. This ability depends on the cell type and ranges from the restricted cell shape changes

and small cell movements of epithelial cells presented in the previous section to cells that, individually or collectively, migrate along large distances (e.g. some neurons, immune system cells, primordial germ cells, neural crest cells and tumor metastatic cells).

Single cell movements in two-dimensional contexts are powered by repetitive cycles of the following sequence of events: (1) Cells become polarized and organize a migration front with intense protrusive activity constituted of lamellipodia and filopodia that push the cell membrane forward, thus establishing the leading edge of the cell. (2) Cells attach to the extracellular matrix through formation of focal adhesions at the migration front. (3) The cell rear end detaches by removal of focal adhesion and retracts following the contraction of stress fibers. This model is over simplistic since *in vivo* cells evolve in a complex tree-dimensional context, whose chemical composition and physical parameters change and therefore must constantly adapt their mode of migration (Dogterom & Koenderink, 2019). However, one can assume that mesenchymal cells *in vivo* behave in close similarity to the crawling 2D model of cell migration but with a more elongated shape, where flat lamellipodia are replaced by long pseudopodia supported by microtubules (Jayatilaka et al., 2018; Dogterom & Koenderink, 2019). When cells migrate in a highly confined environment with low adhesion, they switch to ameboid motion powered by actin flows on blebs.

In several developmental and physiological contexts (e.g. organogenesis or wound healing) cells migrate collectively. To do so, they must communicate as they move and the underlying mechanisms depend on cell type(s), number and cohesiveness as well as on the guidance cues that control the movement (Mishra et al., 2019). The interactions are not restricted to cells of the migrating cohort since cells interact with their microenvironment (Mishra et al., 2019). In this section, I will discuss a few remarkable examples of cell migration in different developmental contexts and present the underlying molecular mechanisms.

Primordial germ cell migration

Primordial Germ Cells (PGCs) are the first precursors of gametes (spermatozoa and oocytes). A common feature of PGCs in most organisms is that their specification site is far from the future gonad and thus they have to perform a long-range migration through the embryo. Although PGC migrate as a group and present features of collective migration such as homotypic and heterotypic interactions, this cannot be described as a collective migration *stricto sensu* since the cells are not tightly adherent to one another (Mishra et al., 2019). The migration routes differ from one organism to another, but the process shows several shared principles (Figure 27) (Richardson & Lehmann, 2010; Barton et al., 2016; Mishra et al., 2019). The migration route followed by PGCs is dependent on attractive and repulsive guidance cues provided by somatic cells along the path (Richardson & Lehmann, 2010). Here, I will introduce some general concepts and present the signaling pathways that regulate PGC migration (as reviewed in Richardson &

Lehmann, 2010; Mishra et al., 2019), but I will not develop the mechanisms of specification of the PGCs nor their specific migration route.

Once PGCs are specified, they lose adhesive properties and acquire motility and directional cue-dependent polarization to orient their migration (Richardson & Lehmann, 2010). In *Drosophila,* this behavior is regulated through the rhodopsin family G protein-coupled receptor TRE1 which activates small protein G and the GTPase RHO1 to promote cell polarization, downregulation of E-cadherins and migration. As a consequence, cells are polarized in a head to tail fashion with actin-rich protrusions at the front. In several organisms, PGC motility and survival are tightly connected since the signaling pathways in charge of promoting cell migration also favor cell survival. Good examples in mice are SDF1 (Stromal cell Derived Factor 1, also known as CXCL12) (Molyneaux et al., 2003) and Stem Cell Factor (SCF, also known as Steel Factor, Mastocyte Growth Factor or Kit Ligand) (Gu et al., 2009). They act as signaling cues that activate transmembrane receptors: the GPCR (G-protein-coupled-receptor) CXCR4 and the tyrosine-kinase receptor Kit, respectively. SDF1 is a chemokine that through binding of CXCR4 promote filopodia and bleb formation as directional cues in a gradient-dependent manner(Goudarzi et al., 2012; Mishra et al., 2019).

Although the mechanistic details of SCF/Kit pathway will be reviewed in Chapter 4, it is worth presenting briefly here its involvement in PGC migration. The Kit receptor is expressed by PGCs where the SCF/Kit signal regulates survival, proliferation and motility (Gu et al., 2009). In mice, SCF is expressed by both the PGCs and the somatic cells along their migration path. This continuous exposure of PGCs to SCF represent a ‘‘traveling niche’’ in which short-range signaling controls the different aspects of PGC behavior. However, exposure to SCF during migration promotes motility and survival rather than guidance (Gu et al., 2009). PGCs also express a membrane-bound isoform of SCF together with the KIT receptor, thus allowin their homotypic interaction (De Felici, 2005; Gu et al., 2009).

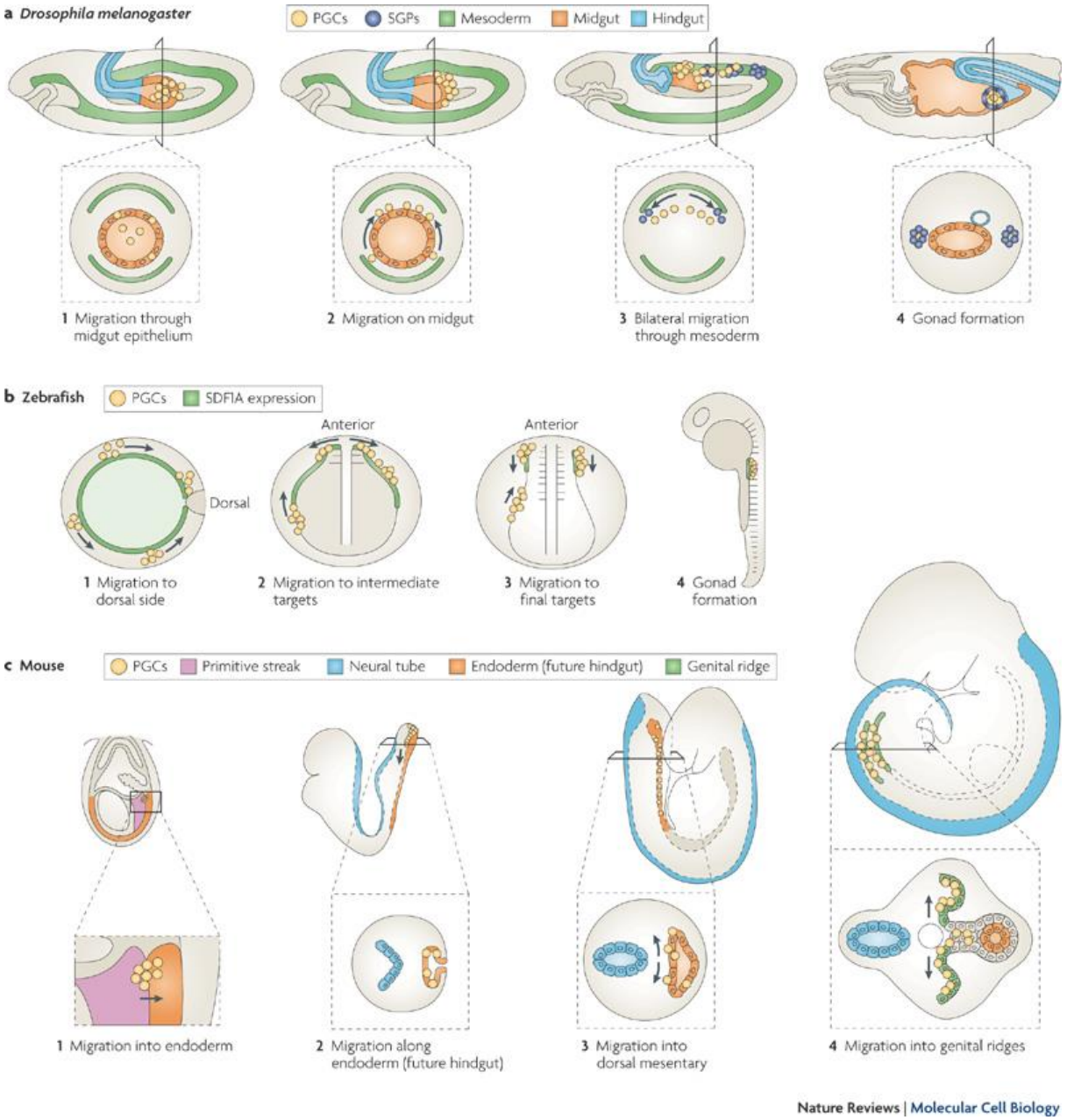

Figure 27: Stages of primordial germ cell migration.

a | Lateral views (top panels) and transverse sections (bottom panels) showing primordial germ cell (PGC) migration in Drosophila melanogaster. After specification, PGCs are carried into the embryo by the midgut primordium. PGCs polarize and migrate through the midgut epithelium at stages 9–10 (~4.5 hours after egg laying (~4.5 hAEL); step 1). PGCs reorient on the midgut towards the mesoderm at stage 10 (~5 h 10 m AEL; step 2). PGCs migrate bilaterally towards the somatic gonadal precursors (SGPs) at stage 11 (~7 hAEL; step 3). PGCs associate with the SGPs and coalesce to form the embryonic gonad (step 4). b | Following specification at four random locations, PGCs in zebrafish migrate dorsally (step 1; animal pole view — the animal pole refers to the portion of the blastula embryo that differentiates into mesoderm and ectoderm). At gastrulation, 4.5 hours' post-fertilization (4.5 hpf), PGCs follow the expression of stromal-derived factor 1a (SDF1A) and at 10.5 hpf somites 1–3 act as intermediate targets (step 2; lateral view, left side). PGCs migrate towards the final target tissue at somites 8–10 at 13 hpf (step 3; frontal view). At 24 hpf, PGCs coalesce with the somatic cells of the gonad (step 4; lateral view, left side). c | PGCs in mice, specified in the proximal epiblast, migrate from the primitive streak to the endoderm (future hindgut) at embryonic day 7.5 (E7.5; step 1). A close-up is shown in the bottom panel. At E8, PGCs migrate along the endoderm (step 2). At E9.5, PGCs migrate bilaterally towards the dorsal body wall (step 3). At E10.5, PGCs reach the genital ridges to form the embryonic gonad (step 4). Lateral views (top panels) and transverse sections (bottom panels) are shown

(from Richardson & Lehmann, 2010).

Neural crest cells

The neural crest is a cohort of multipotent cells, precursors of a large diversity of cellular types including neurons of the peripheral nervous system, smooth muscles, glia, bone, cartilage and melanocytes (Shellard & Mayor, 2019b; Simões-Costa & Bronner, 2015; Szabó & Mayor, 2018) .

In vertebrates, Neural Crest Cells (NCCs) are induced between late gastrula and early neurula stages at the interface between neural and non-neural ectoderm (Figure 28). The entire anteroposterior axis of the neural plate border is able to generate NCCs, except for the most anterior neural ridge which gives rise to the olfactory placode (reviewed in(Theveneau & Mayor, 2012b). Cells from the neural plate border undergo a process called epithelial to mesenchymal transition (EMT), characterized by a switch in the expression of adhesion molecules, a loss of apicobasal polarity and a gain of migratory function (Figure 28c). Induced NCCs thus delaminate from the neuroepithelium (Theveneau & Mayor, 2012b). NCCs are characterized by their long migration range and the tight communication among themselves, as well as with the surrounding tissues (Theveneau & Mayor, 2011, 2012a). According to their position along the antero-posterior axis, NCCs organize in distinct streams with diverse migration routes and modes from individual cells to chains, groups or sheets (Figure 29). (Theveneau & Mayor, 2011, 2012b; Szabó & Mayor, 2018). However, NCCs act mostly as a group and constitute a prime example of collective cell migration (Theveneau & Mayor, 2011). Indeed, NCC migration requires intense cooperation and coordination (reviewed in Shellard & Mayor, 2019a). To properly migrate collectively, groups of NCCs must polarize in the same way, a property referred to as 'supracellular polarity' (Mayor & Etienne-Manneville, 2016; Shellard & Mayor, 2019a).

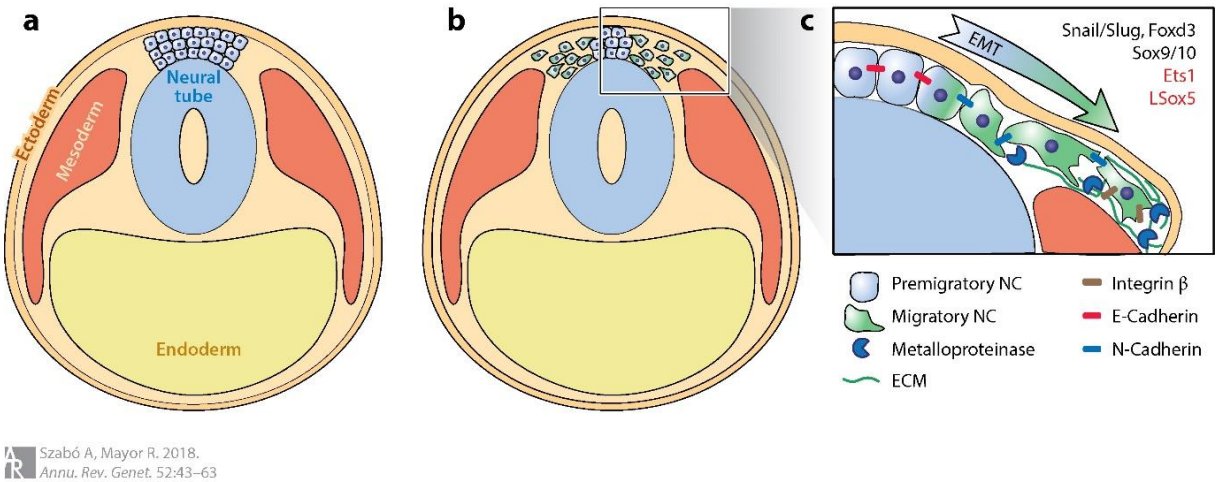

Figure 28: Typical cellular changes during NC delamination.
(a) Before and (b) during NC delamination. (c) Cells weaken their adhesion, lose their apical–basal polarity, and acquire polarized motility. Although these phenotypic changes are shared across species, their genetic control varies. The most common transcription factors inducing EMT are Snail/Slug, Foxd3, and Sox9/10 and, in the cephalic regions, Ets1 and LSox5. Abbreviations: ECM, extracellular matrix; EMT, epithelial-to-mesenchymal transition; NC, neural crest. (taken from Szabo & Mayo, 2018)

Once NCCs become motile, they must follow specific paths, according to their position along the anterior-posterior axis (Figure 29). The surrounding tissues play a major role in the confinement of migrating NCC along these paths (Figure 30a).

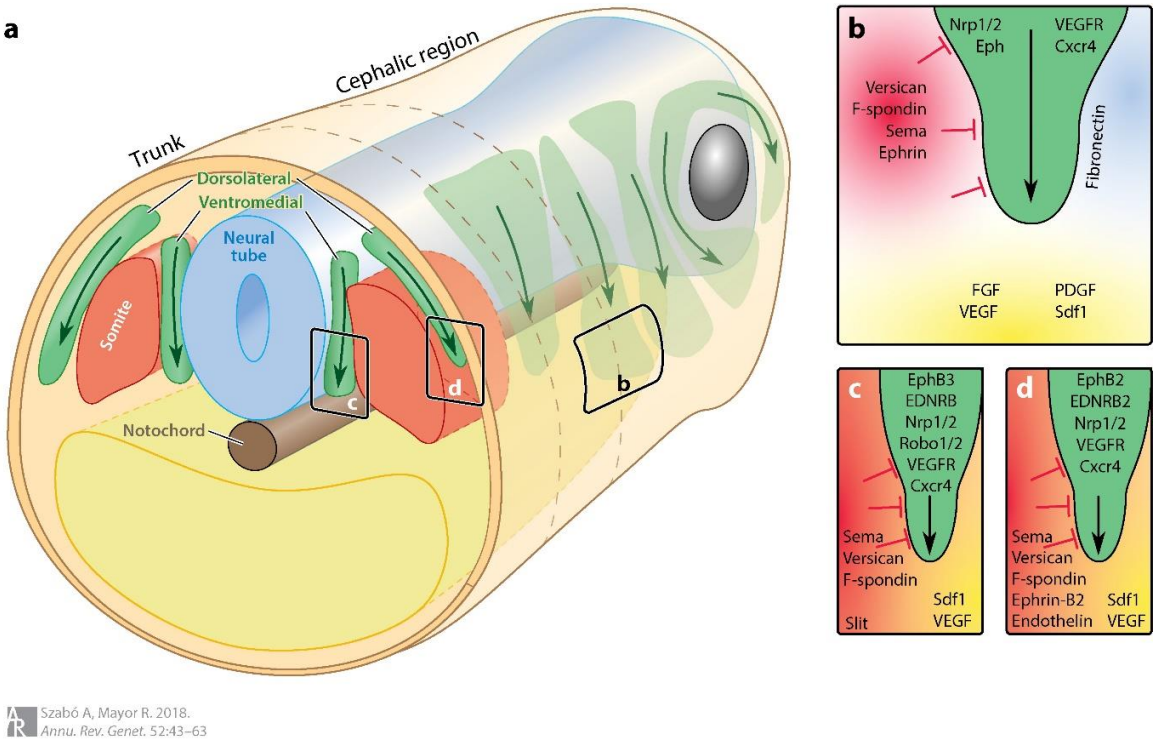

Figure 29: Paths of NC migration are shaped by external positive and negative signals.
(a) Characteristic NC paths in the cephalic and trunk regions. Arrows indicate the cephalic, ventromedial trunk, and dorsolateral trunk migratory paths corresponding, respectively, to panels b–d. (b–d) Main external signals inhibiting (red), promoting (yellow), or allowing (blue) NC migration along the (b) cephalic, (c) ventromedial trunk, and (d) dorsolateral trunk streams. Abbreviations: EDNRB, endothelin receptor B; FGF, fibroblast growth factor; NC, neural crest; Nrp1/2, neuropilins 1 and 2; PDGF, platelet-derived growth factor; Sdf1, stromal cell–derived factor 1; Sema, semaphorin; VEGF, vascular endothelial growth factor; VEGFR, vascular endothelial growth factor receptor.
(taken from Szabo and Mayo, 2018)

Transmembrane receptors such as receptor tyrosine kinase transduce signals from the extracellular environment to the cytoplasm upon binding their ligand. Eph/Ephrins interaction transduces a bi-directional signal in both Eph and Ephrin expressing cells (Klein, 2012; Pasquale, 2008). Eph receptors are classical receptors tyrosine kinase which transduce a phosphorylation-dependent signaling cascade through their intracellular catalytic domains. In contrast, Ephrins on the other hand are anchored to the membrane through a glycosylphosphatidylinositol (GPI) (Ephrin-As) anchor or through a transmembrane domain (Ephrin-B). Both Ephrin As and Bs can signal upon the binding to Eph receptors:

Ephrin As reverse signaling requires coupling to co-receptors while Ephrin Bs intracellular domain is activated by cytoplasmic kinases. An important role played by the Eph/Ephrin signaling pathway is to induce the collapse of cell protrusions, preventing cells to follow wrong paths and favoring their segregation into distinct streams (reviewed

in Szabo and Mayor, 2018). The expression of the different Eph/Ephrins in the various NCC populations and surrounding tissues ensures the specificity of migration of each stream (Figure 29). Besides Ephs and Ephrins, many other molecules influence NCC migration, by providing both attractive and repulsive clues. Endothelins specifically attract the NCCs which express the endothelin receptor B2 (EDNRB2) while repelling those expressing other endothelin receptors such as EDNRB (Pla et al., 2005; Szabó & Mayor, 2018). The semaphorin signaling system can also switch from inhibition to promotion of migration, as illustrated by Sema3C, a well-known regulator of axonal guidance that also regulates cardiac NCC migration (Castellani et al., 2000; Toyofuku et al., 2008).

Chemoattractant/repellant cues from the surrounding cells are not the only regulator of NCC migration. Indeed, NCCs are strongly affected by the extracellular matrix. One of its main components, fibronectin, favors NCC migration while others such as F-spondin and versican inhibit it.

Beside its molecular influence, the physical confinement provided by the environment also plays a critical role in NCC migration by favoring their directional persistence and improving the efficiency of their migration. Indeed, confinement increases NCC density, thus favoring homotypic cell contact, required for optimal migration.

Homotypic cell interactions occur through adhesion molecules such as N-cadherin, homogeneously expressed by NCCs. Upon contact, NCCs undergo contact inhibition of locomotion, a process by which two cells entering in contact cease migration on the side of cell contact and repolarize in different directions to finally move away from each other (Figure 30b). The concept of contact inhibition of locomotion will be presented in next section and here I will only focus on how this mechanism favors NCC migration. One of the main consequences of contact inhibition of locomotion is cell spreading, an opposite process to cellular confinement. After delamination, contact inhibition of locomotion favors cell dissemination away from their origin and along the paths allowed by the surrounding environment. Contact inhibition of locomotion, combined to chemotactic responsiveness, polarizes the motility of NCCs, thus improving the directionality of their migration.

Most experimental evidence supports the idea that collective migration and supracellular polarity are dependent on contact inhibition of locomotion (Stramer and Mayer 2017) but cell separation *per se* cannot account for collective migration. Despite mutual repulsion, NCCs strongly interact together and maintain integrity through attractive interactions to counter the effect of contact inhibition. This attraction depends on chemotaxis through which both the environment and NCCs themselves dictate the collective migration orientation. Indeed, as presented above, the surrounding tissues can dictate the route of NCCs, but these can also attract each other, a process called co-attraction (Figure 30c). For example, NCCs both secrete the complement component factor C3a, a known chemoattractant molecule, and express its receptor C3aR on their surface thus ensuring co-attraction. These mechanisms avoid excessive isolation and scattering of the NCCs induced by contact inhibition of locomotion and provide further evidence of the intense cooperation between both mechanisms.

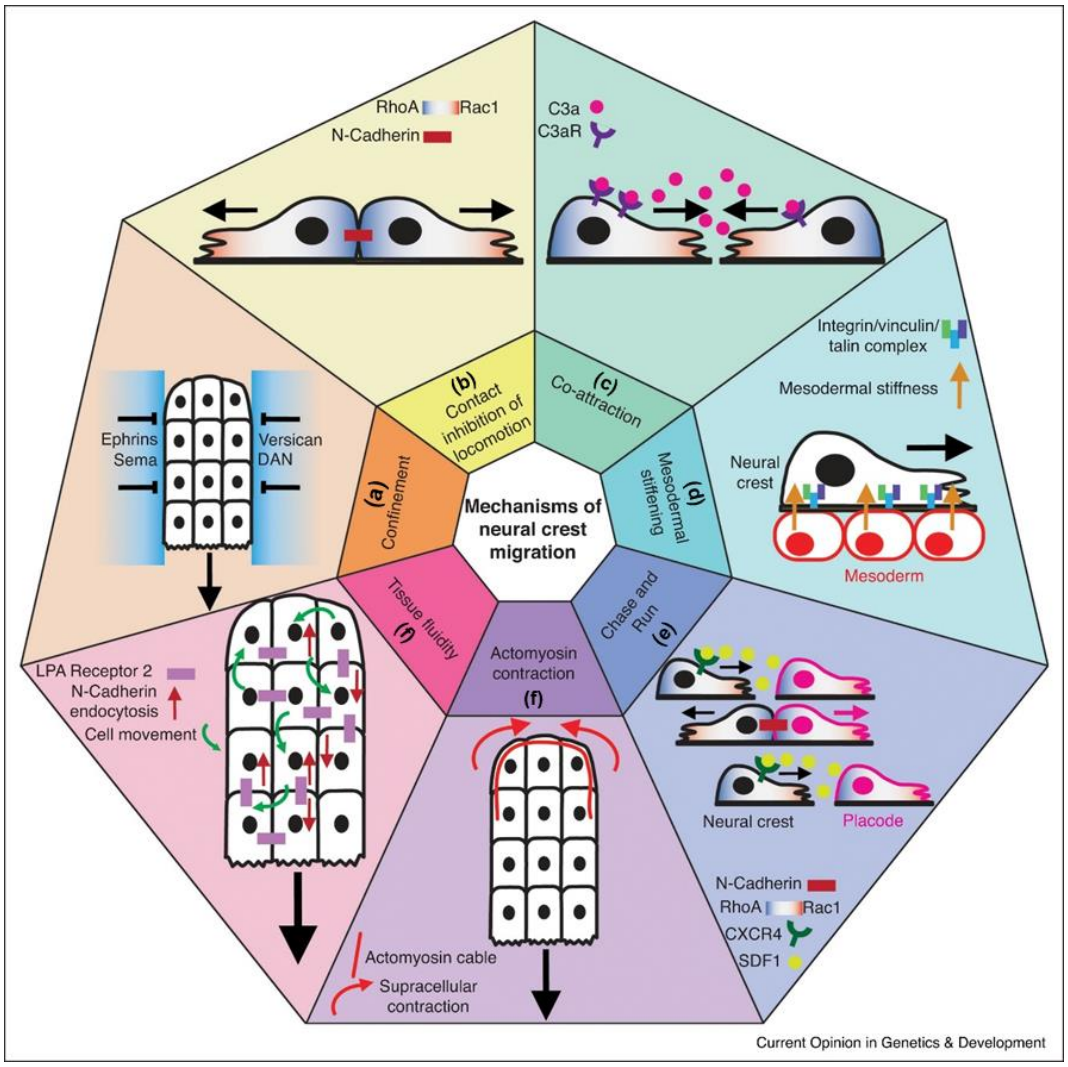

Figure 30. The many mechanisms of cranial neural crest cell migration.

(a) Confinement. Extracellular signalling factors, such as ephrins, semaphorins and DAN, and extracellular matrix components, such as versican, provide inhibitory signals between the neural crest streams to the neural crest, which repels them from entering this environment. (b) Contact inhibition of locomotion (CIL) between neural crest cells. Upon collision of neural crest cells, a molecular cascade of signals including N-Cadherin, non-canonical Wnt/PCP signalling, EphrinB2, TBC1d24, ephrinB2, Src and FAK cause RhoA to become recruited to the contact, Rac1 to be recruited to the opposite edge and a redistribution of forces that causes the cells to repolarise and move away from each other (black arrows). In the context of a cell cluster, this means protrusions and forces are at the free-edge. (c) Co-attraction between neural crest cells. Neural crest cells produce the ligand C3a and its receptor C3aR, meaning cells undergo short-range chemotaxis to each other, helping to maintain the collective. (d) Mesodermal stiffening. Increased density of the mesoderm causes it to stiffen, which is sensed by an integrin/vinculin/talin complex in neural crest cells. This causes an upregulation in N-Cadherin and downregulation in E-Cadherin that triggers neural crest migration. (e) 'Chase and run'. Neural crest cells express the CXCR4, the cognate receptor for the chemokine SDF1, which is produced by the placodal cells. Neural crest therefore 'chase' placodal cells by chemotaxis. Upon engagement of the two cell types, N-Cadherin, non-canonical Wnt/PCP, EphB4, EphrinB2 and TBC1d24 signalling triggers heterotypic CIL between the clusters that redistributes Rac1 and RhoA such that the neural crest 'run' away from the placode. 'Chase and run' results in the co-migration of neural crest and placodal cells. (f) Rear actomyosin contraction. Edge cells of the neural crest cluster have a continuous actomyosin cable. During chemotaxis, SDF1 inhibits actomyosin contraction at the front of the cluster but not at the rear. Rear contraction causes cells to intercalate that ultimately drives the cluster forward. (g) Tissue fluidity. LPAR2-dependent endocytosis of N-Cadherin ensures adhesions and causes constant remodelling of cell junctions, allowing cells to exchange positions. This makes the cluster to behave like a fluid. (adapted from Shellard et Mayor., 2019b)

Mechanical responses to the surrounding tissues also affect NCCs migration (Figure 30d). While NCCs pursue their migration, the density of the underlying mesodermal tissues increases, thus providing a stiffer environment. These changes are sensed by NCCs through the Integrin-Vinculin-Talin complex and favor the E- to N-cadherin switch which in turn induces EMT and migration of NCCs (Barriga et al., 2018).

Many other secreted factors stimulate NCC migration including Vascular Endothelial Growth Factor (VEGF), SDF-1, Fibroblast Growth Factor (FGF), and Platelet-Derived Growth Factor (PDGF). Some of these are specific to individual NCC streams while others are more ubiquitously expressed. VEGF is an example of migration stimulating-factor present all along the NCC migration route. However, as the NCCs move toward its source they sequester it from the environment such that leader cells are exposed to more VEGF than the following ones. This sequestration provides an example a "self-generated gradient" (McLennan et al., 2012). This chemokine gradient may lead to directional migration inducing a leader-follower behavior in the NCC population: "leader cells" respond to chemokine gradient and orient the collective migration of the rest of the cells (the "followers"). SDF-1 has been shown to induce contact-dependent chemotactic response in NCCs (Theveneau et al., 2010) by stabilizing the protrusions extended toward its own source. Interestingly, SDF-1 is secreted by placodal cells localized at the front of the NCCs (Figure 30e). Moreover, placodal cells interact with NCCs and move forward in response to these heterotypic interactions (Theveneau et al., 2013). Thus, placodal cell attract NCCs through SDF-1, and this in turn stimulates placodal cell movement. As for NCCs, placodal cells express N-cadherin which, upon contact with NCCs, induces heterotypic contact-dependent inhibition of locomotion, a process termed as 'chase and run' (Figure 30e) (Theveneau et al., 2013). The run phase of placodal cells also depends on Eph/Ephrin signaling (Yoon et al., 2018). NCCs express on their surface the ligand ephrin B2, which in turn induces contact-dependent inhibition in placodal cells through binding to the EphB4 receptor.

NCCs adopt different behaviors depending on where they are within the stream. The front cells show a dynamic alternation of contact-dependent inhibition and co-attraction, while the rear cells are more cohesive and form ubiquitous tensile actin cables (Figure 30f). In addition to the effect on individual cells presented earlier, SDF-1 contributes to the front-rear polarity of NCCs at the population scale by regulating collective chemotaxis. At the back of NCC stream, supracellular actin-myosin contraction events respond to the SDF-1 gradient and collective contraction of rear cells efficiently moves them forward. Beside supracellular polarity with distinct organization at the front and the rear, NCCs also show fluid-like behaviors (Figure 30g). The collective contraction requires a perfect coordination among cells in the group and, to adapt to the changing architecture of the environment, NCCs show constant remodeling of their cytoskeleton and extensive neighbor exchange events including mediolateral cell intercalation. This fluid-like behavior requires the constant remodeling of adhesion complexes such as endocytosis of N-cadherin controlled by lysophosphatidic acid (LPA) receptor 2 (Kuriyama et al., 2014).

In conclusion, NCC collective migration is the integration of several inputs that endow the NCC cohort with polarized organization, a motile behavior with constant reorganization, allowing them to follow specific routes. These specific behaviors are molecularly controlled at different levels such as:

- Adhesion molecules: the cadherin switch allows EMT, giving to NCCs their migratory behavior and contact inhibition of locomotion and homotypic/heterotypic interactions.
- Small GTPases Cdc42, RhoA and Rac1, which control the polarized organization of actin protrusive activity and contractility (their function will be developed in the context of contact inhibition of locomotion in later section)
- Various transmembrane receptors (e.g. Ephs, CXCR4, VEGFR, PDGFR…), which regulate RhoGTPase activity and then cell direction.

This is of course not an exhaustive list of the mechanisms that dictate collective migration, many of which are described more in depth in other reviews (Friedl & Gilmour, 2009; Mayor & Etienne-Manneville, 2016; Scarpa & Mayor, 2016; Shellard & Mayor, 2019a; Mishra et al., 2019)

Melanocytes

In mice, the NCC-derived melanoblasts (precursors of the hair and skin melanocytes) migrate through the developing dermis to colonize all body regions (Figure 31A), then colonize hair follicles or remain within the epidermis in glabrous skin (Figure 31B). Many factors contribute to their survival, proliferation and migration. The tyrosine kinase receptor KIT starts being expressed when melanoblasts leave the neural tube as premigratory NCCs. In addition to its role in melanogenic fate (Wilson et al., 2004), the SCF/Kit signaling pathway is required for the initiation of melanoblast migration, their survival and proliferation (Wehrle-Haller & Weston, 1995; Mackenzie et al., 1997). Later, the Kit receptor is also required for melanoblast movement from the dermis to the epidermis and their subsequent localization to hair follicles (Nishikawa et al., 1991). Further studies have shown that, although SCF stimulates the random migration of melanoblast and their migration into hair follicle, it does not act as a chemotactic factor but rather as a chemokinetic factor (Jordan & Jackson, 2000). Explant culture experiments showed that the melanoblasts initially distribute randomly, then progressively scatter into the hair follicles (Jordan & Jackson, 2000). It seems that Kit stimulates migration while other factors attract the melanoblasts toward the hair follicles (Thomas & Erickson, 2008). It has also been hypothesized that soluble forms of the SCF ligand stimulate migration while its transmembrane forms result in the homing of melanoblasts to follicles

(Jordan & Jackson, 2000). Indeed, soluble and membrane bound forms of SCF play distinct roles in melanocyte precursor dispersal and survival along the lateral neural crest migration pathway (Wehrle-Haller & Weston, 1995). Furthermore, Kit is expressed in melanophores, one of the three pigment-cell types in zebrafish, and regulates their survival and migration (Parichy et al., 1999; Rawls & Johnson, 2003). Interestingly, the pigmentation disorder piebaldism results from altered mesodermal melanocyte migration (Funkhouser et al., 2019), and this condition has been linked to mutations in the *KIT* gene(Oiso et al., 2013; R A Spritz et al., 1992; Richard A. Spritz et al., 1992).

The fact that SCF acts only as chemokinetic factor implies that other chemoattractant factors required to direct cells toward the hair follicles remain to be identified. In zebrafish, pigments cells organize into a regular pattern of stripes, and it has been suggested that this results from the local accumulation of chemoattractant molecules. One of these could be SDF-1, whose involvement in PGC and NCC migration has been already discussed. However, its known receptor Cxcl4 is not detectably expressed in zebrafish melanophores, (Kelsh, 2004).

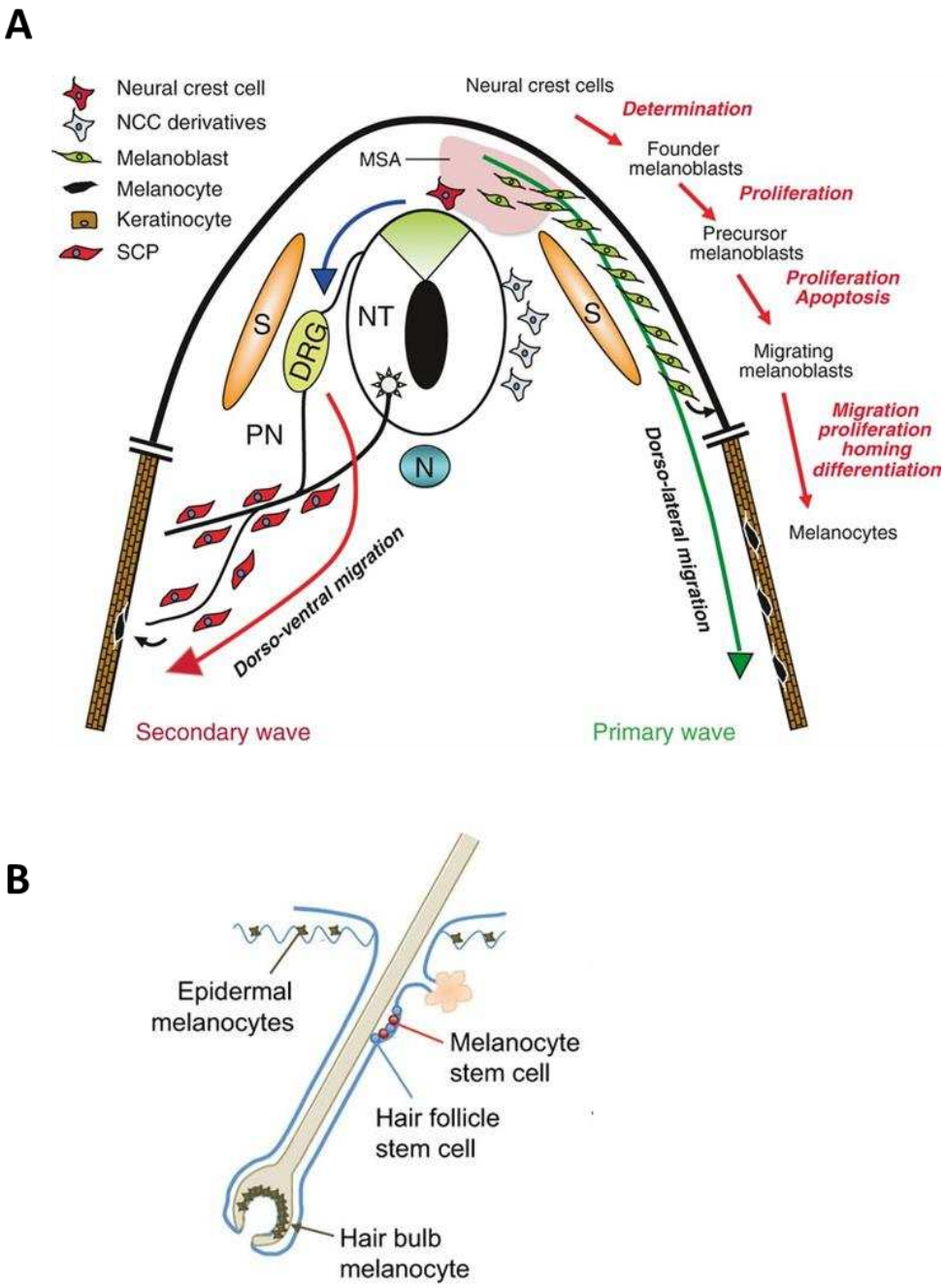

Figure 31: Cellular and molecular mechanisms controlling the migration of melanocytes

(A) Melanocyte specification from neural crest cells. In the trunk region, early migrating neural crest cells (NCCs) move through the dorso-ventral pathway (blue arrow) in between the somites (S) and the neural tube (NT). These cells will give rise among others to neurons of the dorsal root ganglia (DRG). Before migrating along the dorso-lateral pathway (green arrow), melanoblast precursors stall in the migration staging area (MSA), then move between the somites (S) and the ectoderm to ultimately give rise to melanocytes of the first wave. A second wave of melanocytes (red arrow) arises from the Schwann cell precursors (SCPs) associated with the peripheral nerves (PN). Melanocytes are found near the nerve endings. N = notochord. (taken from Bonaventure et al., 2013).

(B) Structure of the mature hair follicles. Melanocyte stem cells (MSCs; pink circles) associated with the hair follicle provide pigmented cells to the growing hair. These follicular MSCs reside in the bulge region of the hair follicle and are supported in a niche by hair follicle stem cells (blue). Differentiated melanocytes (black) reside at the bulb to pigment the growing hair. (Mort et al., 2015).

2.3. Avoiding one's neighbors: the mechanisms of cell repulsion

Along the previous paragraphs we have seen that homotypic interactions and contact inhibition of locomotion favor cell dispersion. These phenomena improve cell dissemination efficiency, increase migration range in NCCs and participate to pattern generation in zebrafish pigment cells. Because this mechanism was also central to the pattern generation studied during my thesis work, I will conclude the present chapter by a description of its underlying cellular and molecular mechanisms.

2.3.1. Contact inhibition of locomotion

In the 50's, pioneer works from Abercrombie on explanted chick heart embryonic fibroblasts revealed a complex behavior in which cell speed and direction of movement change upon cell-cell contact (Abercrombie & Heaysman, 1953). *In vitro*, individual fibroblasts show a reverse correlation between their velocity and the amount of contacts made with other cells. On the other hand, cell-cell contacts are followed by a transient increase of velocity immediately after collision (Abercrombie & Heaysman, 1953) (based on the review from Roycroft & Mayor, 2018). Following work showed that cell-cell contact leads to a decrease of velocity and inhibition of movement in the pre-contact direction, a process later called 'contact inhibition of locomotion' (Abercrombie & Heaysman, 1954). This phenomenon was defined as 'the prohibition, when contact between cells occurred, of continued movement such as would carry one cell over the surface of another' (Abercrombie, 1970).

Contact inhibition is a multistep process (Roycroft & Mayor, 2016):

(1) initially, a contact is formed between the cells;

(2) protrusive activity is inhibited at the site of contact;

(3) the cells repolarize and new protrusions form away from the contact site;

(4) the cells separate and migrate away from each other (Figure 32

As presented earlier, contact inhibition of locomotion can occur between cells of the same type (homotypic context), as shown in chick heart embryonic fibroblast (Abercrombie & Heaysman, 1954), NCCs (Carmona-Fontaine et al., 2008), *Drosophila* hemocytes (Davis et al., 2012), mammalian CR neurons (Villar-Cerviño et al., 2013). It has been suggested in other system such as melanoblasts, pigment cells in zebrafish (Inaba et al., 2012; Yamanaka & Kondo, 2014) and retinal horizontal cells (Poché & Reese, 2009), and many more instances may remain unknown. Moreover, contact-dependent inhibition of locomotion also exist in heterotypic contexts such as NCCs vs placode cells (Theveneau et al., 2013).

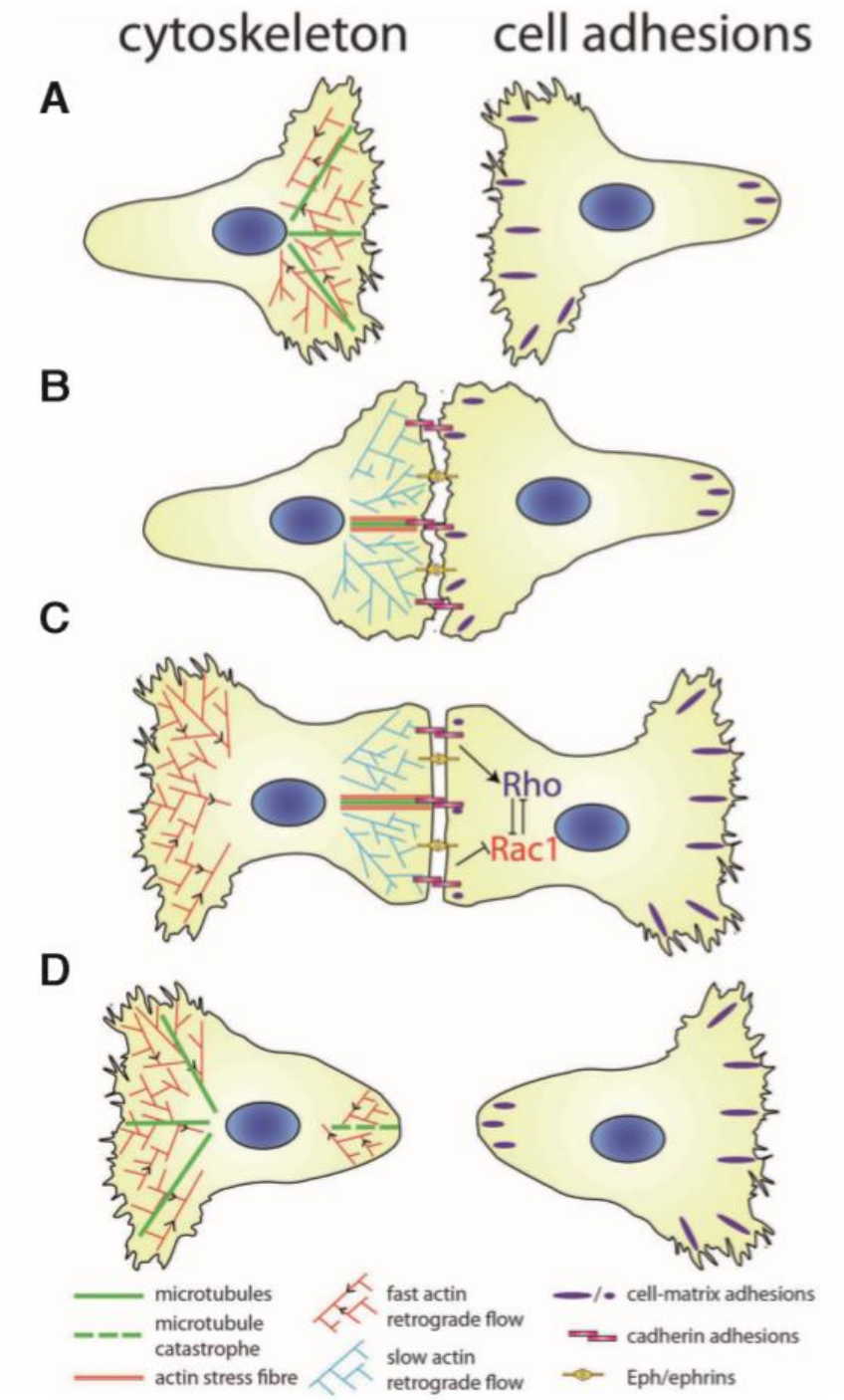

Figure 32. Role of cytoskeleton and cell-cell adhesions in contact inhibition of locomotion.

Illustration of the stages of contact inhibition of locomotion. Cytoskeleton rearrangements are illustrated in the left-hand cell whilst the adhesions involved and how they change is illustrated in the right-hand cell. (A) Freely migrating cells show actin driven protrusions stabilised by microtubules. Cells have large cell-matrix adhesions in their leading edge. (B) Upon a collision cadherin-based adhesions form between cells. Eph receptors bind to ephrin from the colliding cell partner and protrusions start to collapse. Actin flow is reduced and an actin stress fibre and microtubule bundles form, these are aligned between colliding cells. Cell-matrix adhesions begin to disassembly near to the cell-cell contact. (C) Eph/ephrin signalling and cadherin-based adhesions lead to Rho activation and Rac inhibition at the cell-cell contact. Protrusions towards the contact completely collapse. Actin based protrusions develop away from the contact as the cells repolarise. Cell-matrix adhesions begin to enlarge in these new protrusions. (D) The cells eventually separate thanks to the disassembly of large cell-matrix adhesions near the contact, the actin stress fibre and microtubule catastrophe events. Microtubules form in the new leading-edge stabilising protrusions. (From Roycroft & Mayor.,2018)

The molecular mechanisms of contact-dependent inhibition of locomotion have been well characterized and correspond to intense communication between:

1. Adhesion molecules and membrane bound receptors, which recognize cell-cell contact and transduce signaling cascades
2. The cytoskeleton, which is the motor of cell directional motility.
3. Signaling molecules that induce changes in cell velocity and direction upon cell-cell contact.

In the following paragraphs, I will develop the different factors contributing to contact-dependent inhibition of locomotion and their roles in its four main steps.

Colliding cells form cell-cell adhesion

Contact-dependent inhibition of locomotion starts by the formation of cell-cell contact (Abercrombie & Ambrose, 1958). Upon contact, tension is generated in the lamellae of the two colliding cells and adhesion complexes are formed (Figure 32b). Interestingly, adhesion molecules vary according to cell types and the underlying mechanisms will change as well. E- and N-cadherins are among the better-studied adhesion molecules involved in contact inhibition of locomotion. Cadherins can directly interact with actin cytoskeleton causing lamellae to freeze and protrusions to collapse upon cell-cell contact (Figure 32c). p120-catenin, a cytosolic activator of Rac (see next paragraph), is sequestered at cell-cell adhesion complexes through binding to N-cadherin, thus preventing Rac activation at contact sites. These adhesions are transient and break apart when repolarized cells move away from each other (Scarpa et al., 2015).

Rho GTPases control cytoskeleton dynamics and remodeling upon contact-dependent inhibition of locomotion

The Rho GTPase family has been shown as a major player of cytoskeletal remodeling in contact-dependent inhibition of locomotion. In migrating cells, RhoA and Rac/Cdc42 localize at opposite side of the cell, dictating its polarity: Rac1 and Cdc42 are active at the front where they promotes lamellipodia and filopodia respectively (Ridley et al., 1992; Gupton et al., 2007), while RhoA controls ROCK, promoting actomyosin contractions at the back of the cell (Chrzanowska-Wodnicka & Burridge, 1996).

Once cells enter in contact, the first step of contact-dependent inhibition of locomotion is to inhibit the protrusive activity at the colliding site. Upon collision, RhoA and Rac1/Cdc42 activities are swapped. Rac1 and Cdc42 inhibition prevents actin polymerization while RhoA favors cell contractility through ROCK, which contributes to the collapse of protrusions (reviewed in Roycroft & Mayor 2016). Moreover, RhoA and Rac1 show mutual antagonism and the activation of one inactivate the other (Shoval & Kalcheim, 2012). As a consequence of blocking protrusion activity at the contact site, cells cease migration.

To promote cell-separation, cells must then switch their front-rear polarity: each cell must repolarize and form new protrusions on its free edge to move away from the contacted cell (Figure 32d). To do so, Rho GTPases must reverse their functions compared to the colliding site: they should now form a new leading edge away from the contact, where Rac1 is active and RhoA inactive. Once a cell undergoes repolarization, Rac1 will favor actin polymerization on its free edge and cell protrusions will drive cell separation (Scarpa et al., 2015). This shows that cell separation upon contact-dependent inhibition of locomotion only requires efficient protrusive activity away from the contact site. Moreover, RhoA activation at the contact site contributes to actomyosin contraction, favoring the new polarity of the separating cells.

Contribution of cell-matrix adhesion to contact-dependent inhibition of locomotion

During contact-dependent inhibition of locomotion cells also interact with the extracellular cell matrix (reviewed in Roycroft & Mayor, 2018)

It has been suggested that the cell-matrix interaction contributes to lamellae freezing upon cell collision through the action of several effectors such as FAK and paxilin, the effector of α5-integrin and β1-integrin signalling. This is also the case for syndecan-4, a transmembrane heparin sulfate proteoglycan that connects actin to the extracellular matrix through the adapter protein α-actinin. Moreover, syndecan-4 can contribute to Rac1 activity inhibition at the contact site.

Besides, prior to cell separation, cell-matrix adhesion must disassembly at cell-cell contact points, as suggested by the study of NCC contact-dependent inhibition of locomotion (Scarpa et al, 2015). On the other hand, after repolarization, cell-matrix anchoring will be required to generate efficient traction forces.

Transmembrane receptors

In addition to adhesion molecules, transmembrane receptors can also trigger contact-dependent inhibition of locomotion, as exemplified by Eph/ephrin signaling.

The Eph/ephrin signaling system has been widely involved in developmental processes, including axonal guidance, cell migration and formation of tissular/segmental boundaries (reviewed in Klein, 2012; Kania & Klein, 2016). As already mention in Section 2.2.3, the specificity of this signaling system is its ability to signal bidirectionally (Klein, 2012; Pasquale, 2008).

Eph/ephrin signaling is often associated with repulsive responses as in boundary formation, where it regulates cell segregation and border-sharpening between heterotypic cell populations (Taylor et al., 2017) or in homo- and heterotypic contact-dependent inhibition of locomotion as illustrated in several examples throughout this chapter. EphA receptors have been linked to cell protrusion retraction via RhoGTPases. Upon cell-cell contact, EphAs-ephrinAs are recruited to adhesion site and contribute to RhoA/ROCK local activation through GEF-Vav2 recruitment downstream of EphA, contributing then to protrusion collapse (Batson et al., 2014).

Planar cell polarity and non-canonical Wnt pathway regulate Rho GTPase at cell-cell contacts.

The non-canonical Wnt signaling pathway and Planar Cell Polarity (PCP) contribute to a plethora of biological processes including contact-dependent inhibition of locomotion, notably in the context of NCC migration (Mayor & Theveneau, 2014). I will present here a simplified version of this signaling pathway and its contribution to contact-dependent inhibition of locomotion based on the review from Mayor & Theveneau., 2014).

In NCC migration, directional cell movements require a well-established front to-rear cytoskeletal polarization, dependent on coordinated Rho GTPase activity. In migrating cells, the polarized regulation of Rho GTPases has been linked to PCP.

The non–canonical Wnt pathway is transduced either via regulation of the intracellular calcium levels, which in turn affect diverse biological processes, or through small G-proteins such as Rho/Rac, which control planar cell polarity via actin cytoskeleton remodeling. PCP signaling relies on an asymmetrical accumulation of proteins at the opposite poles of the cell, thus contributing to its polarization. Upon cell collision, PCP components are recruited to the contact site to contribute to the local inactivation of Rac and activation of Rho. p120-catenin is known to modulate Rho GTPases downstream of Wnt signaling. N-caherin also inhibits Rac1 activity at adhesion sites and recruit the Src and FAK kinases, which contribute to focal adhesion disassembly and facilitate cell separation.

I non-exhaustively reviewed here how adhesion molecules, together with membrane-bound receptors and PCP proteins coordinate actin polymerization through RhoA/Rac1 balance, leading to cessation of migration upon collision between two cells and to their subsequent repolarization and separation.

Other actors such as the adhesion molecule zyxin have been shown to localize at cell-cell contacts in contact-dependent inhibition of locomotion, but their functions remain unclear (Davis et al., 2015).

Microtubules contribute to cell polarity and contact-dependent inhibition of locomotion

In migrating cells, microtubules (MTs) contribute to cell directionality through the regulation of cell polarization (reviewed in Etienne-Manneville, 2013). As introduced earlier, MTs are stabilized toward the leading edge, promoting membrane ruffling and lamellipodia formation and preventing cell contractility by inhibiting stress fibers and the formation of focal adhesions.

In *Drosophila* heaemocytes, MTs have been shown to contribute to contact-dependent inhibition of locomotion (Stramer et al., 2010; Davis et al., 2015). Bundled microtubules stabilize the leading edge of the cell and, upon intercellular contact, align across the two

colliding cells and inhibit their forward movement. Moreover, microtubules might favor the formation of adhesion complexes known to regulate contact-dependent inhibition of locomotion.

Microtubules also contribute to cell repolarization after collision. Indeed, cell collision induces microtubule collapse through catastrophe and changes in their rate of shrinking/ growth. MTs subsequently stabilize in the orientation opposite to the contact side, favoring new polarization towards the contact-free edge (Roycroft & Mayor, 2016).

To conclude, cell repulsion, by itself or in combination with other cellular behaviors such as attraction, is one of the main drivers of patterning by cellular movements in developmental contexts. While this has been shown in models such as zebrafish melanocytes, *Drosophila* haemocytes (Stramer et al., 2010; Davis et al., 2015), retinal horizontal cells and Cajal-Retzius neurons in mammals (Galli-Resta et al., 2002; Villar-Cerviño et al., 2013), one can expect that many other instances of developmental patterning by cell repulsion remain unknown. The continuous development of live-imaging techniques will likely lead to a rapid increase of our knowledge in this field.

3.Multiciliated cells in *Xenopus laevis* embryonic epidermis: a model of regular cell distribution pattern

Since almost a century, the amphibian *Xenopus laevis* (here called Xenopus for simplicity) has appeared as an attractive vertebrate experimental model system, mainly because it is robust, cheap and easy to maintain in laboratory conditions (Gurdon & Hopwood, 2000; Werner & Mitchell, 2012; Blum & Ott, 2018). Upon injections of Chorionic Gonadotropin hormone, the females spawn up to hundreds of eggs, which after *in vitro* fertilization, develop synchronously and relatively fast (Figure 33). Moreover, the relatively large size of eggs and embryos (>1mm) and their external development, allow their easy observation and manipulation in Petri dishes (Sive et al., 2000). Since the genome of *Xenopus laevis* has been sequenced (Session et al., 2016), many molecular and genetic tools are available. Antisense Morpholino-modified oligonucleotides (MOs) can be injected for loss-of-function assays (Heasman, 2002).

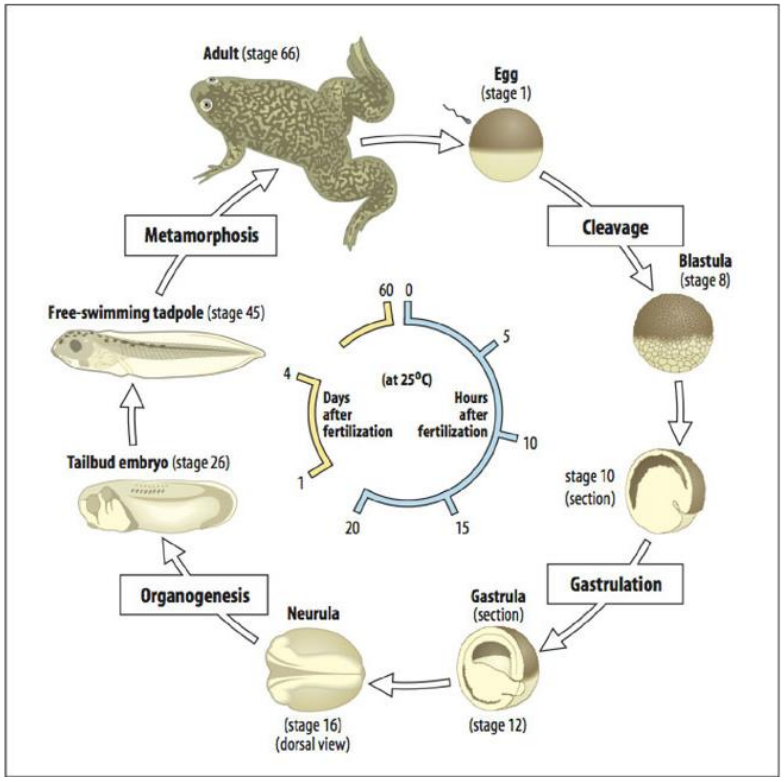

Figure 33: Basics steps of *Xenopus laevis* development

The stages of development of *Xenopus laevis* are defined by the Nieuwkoop and Faber tables. The embryonic development of the *Xenopus laevis* is subdivided into different phases defined on the basis of morphological criteria: fertilization, cleavage, gastrulation, neurulation and organogenesis. After the period of organogenesis, one to two months pass before the tadpole begins its metamorphosis to form an adult *Xenopus*. The adult *Xenopus* is sexually mature at one-year-old.

The precise fate maps currently available allow targeting of specific tissues by injection into their precursor blastomere(s) (Mills et al., 1999; Moody, 1987a, 1987b). More recently, genome editing by CRISPR/Cas9 techniques has been developed (Wang et al., 2015; DeLay et al., 2018) and several transgenic lines are available. Labs have also developed large panel of experiments such as skin transplantation, organoid culture from animal caps explant culture(Sive et al., 2000), immunohistochemistry, colorimetric and fluorescent *in situ* hybridization, confocal and transmission microscopy, live imaging and electron microscopy.

The epidermis of many amphibian embryos and tadpoles is a bilayered mucociliary epithelium where Multiciliated Cells (MCCs), carrying multiple motile cilia are distributed among mucus-producing goblet cells, in a strict spacing pattern (Deblandre et al., 1999; Nokhbatolfoghahai et al., 2005, 2006) (Figure 34 A-C). This tissue constitutes a valuable model system to study several fundamental processes and functions such as radial intercalation (Sedzinski et al., 2016; Jennifer L. Stubbs et al., 2006; Sedzinski et al., 2017), ciliogenesis, cilia polarity and ciliary beating (Ibañez-Tallon et al., 2003; Boutin & Kodjabachian, 2019), but also the cell-cell interaction within mucociliary epithelium (Dubaissi & Papalopulu, 2011). In addition, it is also an interesting biomedical model for the investigation of human diseases (Blum & Ott, 2018).

Because of its accessibility and amenability to live imaging and molecular manipulations the Xenopus larval skin presents exceptional advantages to study mucociliary epithelium (Stubbs et al., 2006; Werner & Mitchell, 2012).

3.1. Mucociliary epithelium

Epithelia are composed of tightly-bound cells organized in mono or multi-layers. They cover the animal body surfaces and act mainly as physical barriers that separate the animal from its environment and protect the underlying tissues from harmful physical and biological factors. Epithelia are commonly classified according to the number of cell-layers that composed them and the morphology of their cells. We can distinguish the squamous, cuboidal, columnar, simple, stratified and transitional epithelium (Van Lommel, 2003).

While maintaining the body integrity is a fundamental function shared by all epithelia, some of them fulfill additional functions that require specialized characteristics. This is the case of the mucosal epithelia of the gut, the secretory epithelia of the kidney and the mucociliary epithelia of the lungs. I will focus here on mucociliary epithelia, which exert varying functions according to the tissue and organism where they are found.

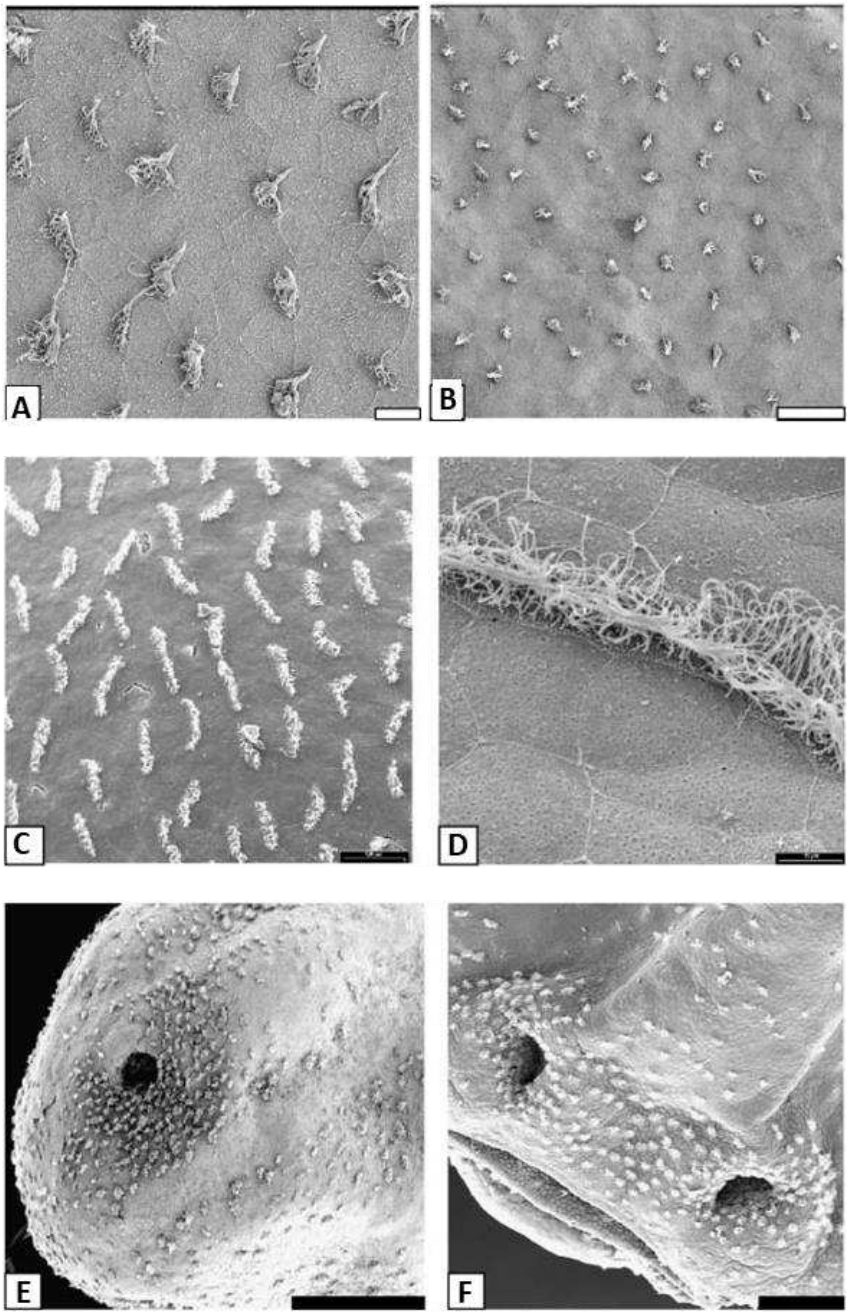

Figure 34: Ciliated cell patterns and shape on different regions in some anuran tadpoles.

A-C: examples of regular ciliated cell patterns: (**A**) H. microcephala, Stage 21, midpart of tail. (**B**) H. minuta, Stage 32, proximal part of tail, (**C**) P. trinitatis, stage 20, lateral side of the trunk. (**D**) Elongated ciliated cells in B. viridis, stage 22, ventral side of the trunk. **E-F**: Examples of irregular ciliated cell patterns around the nostrils. (**E**) B. viridis, stage 25; (**F**) X. laevis, stage 23/24. Scale bars: 20 µm (A;B); 120 µm (C); 15 µm (D). 500 µm (E); 250 µm (F)
(A-B are taken from Nokhbatolfoghahai 2006 and C-F are taken from Nokhbatolfoghahai 2005).

Mucociliary epithelia (MCEs) are pseudostratified epithelia defined by the presence of mucus-secreting goblet cells and multi-ciliated cells (MCCs) carrying dozens to hundreds of motile cilia. MCEs are found in many metazoans and perform different physiological functions (Werner & Mitchell, 2012; Brooks & Wallingford, 2014). In the vertebrate

respiratory tract, the production of mucus allows the capture of inhaled particles and pathogens, which are then removed by ciliary beating-dependent mucus evacuation (mucociliary clearance) (Wanner et al., 1996). In the Fallopian tubes, mucociliary generated flow ensures the migration of the embryo to its site of implantation in the uterus (Hagiwara et al., 1992; Lyons et al., 2006). In Platyhelminthes, MCCs located on the ventral surface of the body allow the animal to move by sliding (Rompolas et al., 2009). In all these examples, MCCs generate robust polarized hydrodynamic forces through the coordinated beating of their motile cilia (Boutin & Kodjabachian., 2019).

The mucociliary epithelium covering the mammalian upper respiratory tract shows histological and cytological similarities with the Xenopus embryonic epidermis. Both tissues present similar mucus-secreting and multiciliated cells (Billett & Gould, 1971; Dubaissi & Papalopulu, 2011). Therefore, the Xenopus MCE can be used to explore the physiology and pathophysiology of human airways (Deblandre et al., 1999; Hayes et al., 2007; Walentek & Quigley, 2017).

3.1.1. The composition of Xenopus MCE

The precise physiological functions of the Xenopus MCE are still incompletely characterized. It has been proposed that the coordinated ciliary movements of the MCCs mobilize mucus or water and that their regular distribution and synchronous beating are required to generate a coordinated fluid flow around the embryo. This could in turn facilitate oxygen exchange between the environment and the epidermis which represent the major tissue for gas exchange before the development of grills and lungs. MCC ciliary movements could also distribute secreted products or play a role in maintaining the epidermis free from infectious agents such as bacteria or fungi (Dubaissi et al., 2014).

3.1.1.1. Mucus producing cells

Mucus secreting cells (also called goblet cells because of their shape) represent the largest cell population of the embryonic Xenopus MCE (Figure 35). As their name suggests it, the main function of mucus-producing cells is the production and secretion of the mucus covering the surface of the embryo. Although its chemical composition is not yet fully characterized, the released mucus is likely to function as an antibacterial barrier as demonstrated by the presence of anti-bacterial factors in goblet cells secretion (Dubaissi et al., 2014; Lang et al., 2016). The Xenopus genome contains 26 genes coding for the gel-forming glycoproteins mucins and several mucins have been detected in the goblet cells secretory vesicles (Dubaissi & Papalopulu, 2011; Dubaissi et al., 2014, 2018; Sim et al., 2018) The mucus also contains lectins, proteins involved in the recognition of pathogen-associated glycans (Nagata et al., 2003), in intracellular protein trafficking, cell adhesion and communication (Nagata, 2005). The secretory activity of the mucus-secreting cells and the mechanisms by which the secreted component interact to build a physical barrier and promote host defense remain poorly understood (Cibois et al., 2014; Dubaissi et al., 2018).

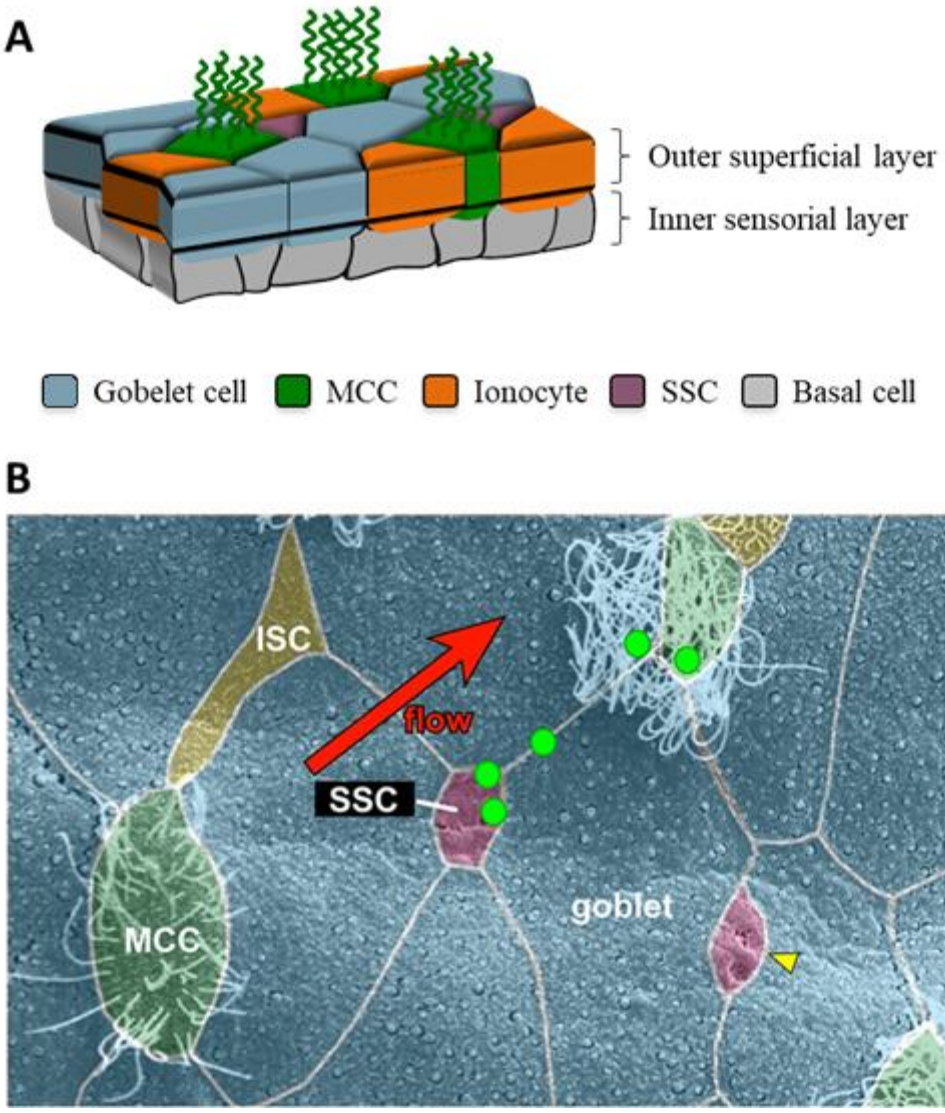

Figure 35: The *Xenopus* embryonic skin

(A) 3D schematic view of the cells that compose the mature embryonic skin of *Xenopus* embryos. The outer superficial layer is composed of mucus producing goblet cells (blue) Multiciliated Cells (MCCs in green), ionocytes (orange), and the Small Secreting Cells (SCCs in purple)

(B) Model of the cell types present in the mucociliary epithelium of the Xenopus laevis tadpole skin. Ionocytes are called ion-secreting cells (ISCs) in this paper. NB: yellow arrow head point toward a SSC intercalated between two goblet cells at a bicellular junction (adapted from Walentek et al, 2014)

3.1.1.2. Multiciliated cells (MCCs)

Multiciliated Cells (MCCs), are defined by the few dozens to hundreds of motile cilia that cover their apical surface (Stubbs et al., 2006; Werner et al., 2011; Cibois et al., 2014; Brooks & Wallingford, 2014; Spassky & Meunier, 2017; Boutin & Kodjabachian, 2019). In Xenopus, MCCs are born in the inner epidermal layer and become fated at the early stages of the embryo development (late gastrula ~st.11-12) (Deblandre et al., 1999). The immature MCC in the inner layer are easily distinguished from other cell types by *in situ* hybridization or immunostaining against α-tubulin, a major component of microtubules

highly enriched in cilia. On the other hand, mature MCCs can be distinguished from the other cells by immunostaining with acetylated-tubulin, a modified form of tubulin presents in mature cilia.

During their maturation, MCCs produce cilia through the process of ciliogenesis. Each cilium is extended from a basal body, an organelle derived from a modified centriole. Each basal body harbors two asymmetric appendages, the rootlet and the basal foot, whose orientation dictates the orientation of the ciliary beating. MCCs must be planary polarized to achieve the tissue-wide alignment of basal bodies required for the coordinated beating of motile cilia and thus the generation of a directional fluid flow along the anterior-posterior axis of the embryo (Boutin & Kodjabachian, 2019). The MCCs are individually scattered across the epidermis and never found adjacent to one another. However, exceptions exist: MCCs are absent from the neural plate and cement glands, while they are present at high density over the head and in mutual contact around the cloacal opening (Figure 34 E-F) (Deblandre et al., 1999; Nokhbatolfoghahai et al., 2005, 2006; Jennifer L. Stubbs et al., 2006).
Interestingly, MCCs are present in the Xenopus epidermis only at embryonic and early larval stages, and transdifferentiate into goblet cells at later developmental stages (st. 43) (Kessel et al., 1974; Cibois et al., 2014). The mechanisms controlling this transition are completely unknown, but it is interesting to note that massive conversion of ciliated cells into goblet cells (mucous metaplasia) is a feature of some human respiratory diseases (Curran & Cohn, 2010; Cibois et al., 2014).

3.1.1.3. Ionocytes

Previously called intercalating non-ciliated cells (Stubbs et al., 2006), ionocytes are small cells scattered within the Xenopus skin. Ionocytes are born in the inner layer and subsequently intercalate into outer-layer where they are often found adjacent to MCCs. Most of the time, direct contact with a single MCC is made by one or two ionocytes (Dubaissi & Papalopulu, 2011). In contrast to MCCs, ionocytes are not evenly dispersed and small groups of two to four can be observed.

Ionocytes have been characterized as proton-secreting cells involved in controlling the pH and the osmotic balance of the developing embryo (Dubaissi & Papalopulu, 2011; Quigley et al., 2011)., They strongly express ion channels and transporters such as vacuolar proton pumps (v-ATPase), chloride ion exchangers (pendrin/slc26a4) proton exchangers such as monocarboxylate transporter 4 which exchanges lactate for protons and carbonic anhydrase 12 (ca12).

Ionocytes also contribute to the development of other cells within MCE (Dubaissi & Papalopulu, 2011). It has been shown that the acidification by V-ATPase is necessary for the activation of signaling pathways, including Wnt, Notch and PCP, which play major role during MCE development (Vaccari et al., 2010; Cruciat et al., 2010; Raymond et al., 2013; Kobia et al., 2014). Finally, ionocytes participate to the regulation of the cilia growth and

ciliary beating, and to the secretion of mucus by goblet cells (Dubaissi & Papalopulu, 2011). Since ionocytes develop often in close physical contact with MCCs, these regulations could be indirectly dependent on pH and osmotic balance regulation or direct via contact-dependent interaction (Dubaissi & Papalopulu, 2011).

The study of frog ionocytes is relevant to the investigation of their function in other tissues such as the mammalian kidney (Dubaissi & Papalopulu, 2011; Quigley et al, 2011). Furthermore, the existence of ionocytes in mammal airways, including those of humans, has been recently reported (Montoro et al., 2018; Plasschaert et al., 2018), thus strengthening the analogy between mammalian airway and amphibian epidermal MCEs.

3.1.1.4. Small secretory cells

The last identified cell-type within the *Xenopus* MCE, the small secretory cells (SSCs), are a third category of secreting cells. They were first observed in 2007 when small cells containing large apical secretory vesicles where described based upon their ultrastructural morphology (Hayes et al., 2007) and later defined according to their specification by Foxa1 (Dubaissi et al., 2014). As MCCs and ionocytes, the SSCs are born within the inner layer and intercalate into the outer layer, although later than the two previous cell types. SSCs are found scattered throughout the epidermis in a non-regular pattern. They are the last cell type to differentiate, much later than the ionocytes and MCCs, at the early tadpole stages (Walentek et al., 2014).

SSCs have been characterized thanks to the presence of vesicles on their apical side, some of them particularly enriched in serotonin (Walentek et al., 2014). Interestingly, it was shown that SSCs contribute to the regulation of cilia beating of the surrounding MCCs (Walentek et al., 2014). SSCs often localize adjacent to MCCs and the serotonin contained in vesicle-like structures is secreted and transported towards the MCCs through cilia-generated flow. (Walentek et al., 2014) As it was previously shown for other systems, also in Xenopus serotonin regulates the ciliary beating frequency (Walentek et al., 2014).

The SSCs also secrete mucus components such as lectins and mucins. It was suggested that serotonin controls the production, composition and secretion of mucus (Walentek et al., 2014; Dubaissi et al., 2014). The regulatory effect of serotonin on mucus secretion could be either autocrine on SSCs or paracrine on goblet cells (Walentek et al, 2014). Since the cilia-generated flow has been suggested to controls mucus clearance, SCCs regulate immune defense in two ways: indirectly through regulation of the cilia-driven fluid flow from neighboring-cells and directly, by participating themselves to the production of the mucus barrier and to antimicrobial defense. Considering that SSCs are a newly discovered cell type, which has been the object of a limited number of studies, further investigations of their development and function are required.

3.1.1.5. Basal cells

Basal cells are a p63 expressing population of cells which are born along with precursors of MCCs, ionocytes and SSCs within the inner layer. They remain inside the inner layer during the embryonic life in a progenitor state and will constitute the proliferating precursors of the multilayered adult epidermis in the course of metamorphosis(Cibois et al., 2014). Since they are the less explored cell type of my thesis work and no much is known about them during the tadpole life, I will not develop it more.

3.2. The development of Xenopus mucociliary epithelium: a multistep process

As already mentioned, MCCs are found at the surface of the embryonic epidermis of most anurans (Figure 34) (Nokhbatolfoghahai et al., 2005, 2006). Despite significant variations among species, one common feature is their remarkable spacing and regular distribution pattern. However, the underlying mechanisms and forces controlling this patterning remain elusive.

In the following sections, I will describe the ontogeny of Xenopus mucociliary epithelium, focusing my attention on MCC specification and intercalation into the outer layer, and introducing the currently available notions on their pattern establishment.

The ontogeny of Xenopus mucociliary epidermis can be schematically subdivided in four successive steps as reviewed in Cibois et al 2014 (Figure 36): (1) ectodermal layer segregation, (2) cell fate specification, (3) radial cell intercalation and (4) cell differentiation. The entire process requires about three days at 23°C.

3.2.1. Ectodermal layer segregation

The Xenopus embryonic skin is derived from the non-neural ectoderm. Starting from the 64 cell-stage, through cleavage and up to the blastula stage, apico-basally oriented asymmetric divisions of the ectodermal cells split the ectoderm into two distinct cell layers: the inner (or sensorial) layer, and the outer (or superficial) layer. The outer layer consists of large cells, which are tightly adherent to each other, while the inner layer is made of smaller and loosely adherent cells (Deblandre et al., 1999).

The apico-basal orientation of cell division depends on the ectodermal cell shape and results in the formation of outer polarized cells, and inner non-polarized cells (Chalmers et al., 2003; Cibois et al., 2014). Indeed, ectodermal cells present an apical-basal polarity with asymmetrical localization of several proteins. Atypical protein kinase C (aPKC), which is enriched apically, is inherited by the outer layer daughter cells; LGL2 and PAR1

are basally localized and inherited by the inner layer cells (Chalmers et al., 2003, 2005; Ossipova et al., 2007; Cibois et al., 2014). Interestingly, aPKC is enriched apically while PAR1 and LGL2 localize to the basolateral region. Their mutual antagonism prevents the co-localization of apical and basolateral enriched groups of proteins (Chalmers et al., 2005; Ossipova et al., 2007). Consequently, the outer layer cells maintain apico-basal polarization acquired from their mother cells and form a true epithelium with tight junctions, while the inner layer cells remain loosely adherent. Based on the results from functional assays it has been suggested that PAR1 is necessary and sufficient for the adoption of MCC fate, whereas aPKC has the opposite effect (Figure 36) (Ossipova et al., 2007). Recently, other asymmetrically localized proteins have been shown to regulate the fate of the two cell layers, and to take part to the MCCs fate specification. The Wnt receptor Lrp6, basally localized in the mother ectodermal cells, preferentially sorts to sensorial ectodermal cells (Huang & Niehrs, 2014).

3.2.2. Cell fate specification

Following ectodermal cell segregation into outer and inner layers, successive steps of cell specification occur in both layers. During gastrulation, cell fate determination occurs and identifies the progenitors of MCCs, ionocytes and SSCs within the inner layer while outer layer cells only commit to goblet cells. In the inner layer, a crucial point is the regulation of the proportion of each cell type (Deblandre et al., 1999; Stubs et al., 2006)

In this layer, all known cell fate determination events are linked to the Notch signaling pathway and lateral inhibition (Deblandre et al., 1999; Bray, 2006). Indeed, Notch signaling regulates the activation of transcription factors upstream of the cell fate specification regulatory networks for the different inner-layer cell types (Kurrle et al., 2020), such as FoxJ1 in MCCs (Jennifer L. Stubbs et al., 2008), FoxI1e in ionocytes (Dubaissi & Papalopulu, 2011), and FoxA1 in SSCs (Dubaissi et al., 2014)

In MCCs, Notch inhibition activates a specific GRN whose key regulators are Gemc1 (Gmnc), Mcidas (Multicilin), Myb, FoxJ1 and Rfx2/3 (Spassky & Meunier, 2017; Boutin & Kodjabachian, 2019) (Figure 37)

The Notch pathway activation also contributes to the specification of other inner-layer cells. In basal cells, Notch activates the transcription of α-Dystroglycan and p63. Interestingly, αDystroglycan is a component of the basal lamina and is required for skin morphogenesis, including MCC radial intercalation (see later section) (Sirour et al., 2011). Another target of Notch signalling in basal cells is p63, a transcription factor required for epidermal development (Sirour et al., 2011). It is likely that additional signaling pathways might be involved in the cell fate choices, among which the BMP pathway, activated in the non-neural ectoderm after cell fate specification (Schohl & Fagotto, 2002; Cibois et al., 2015).

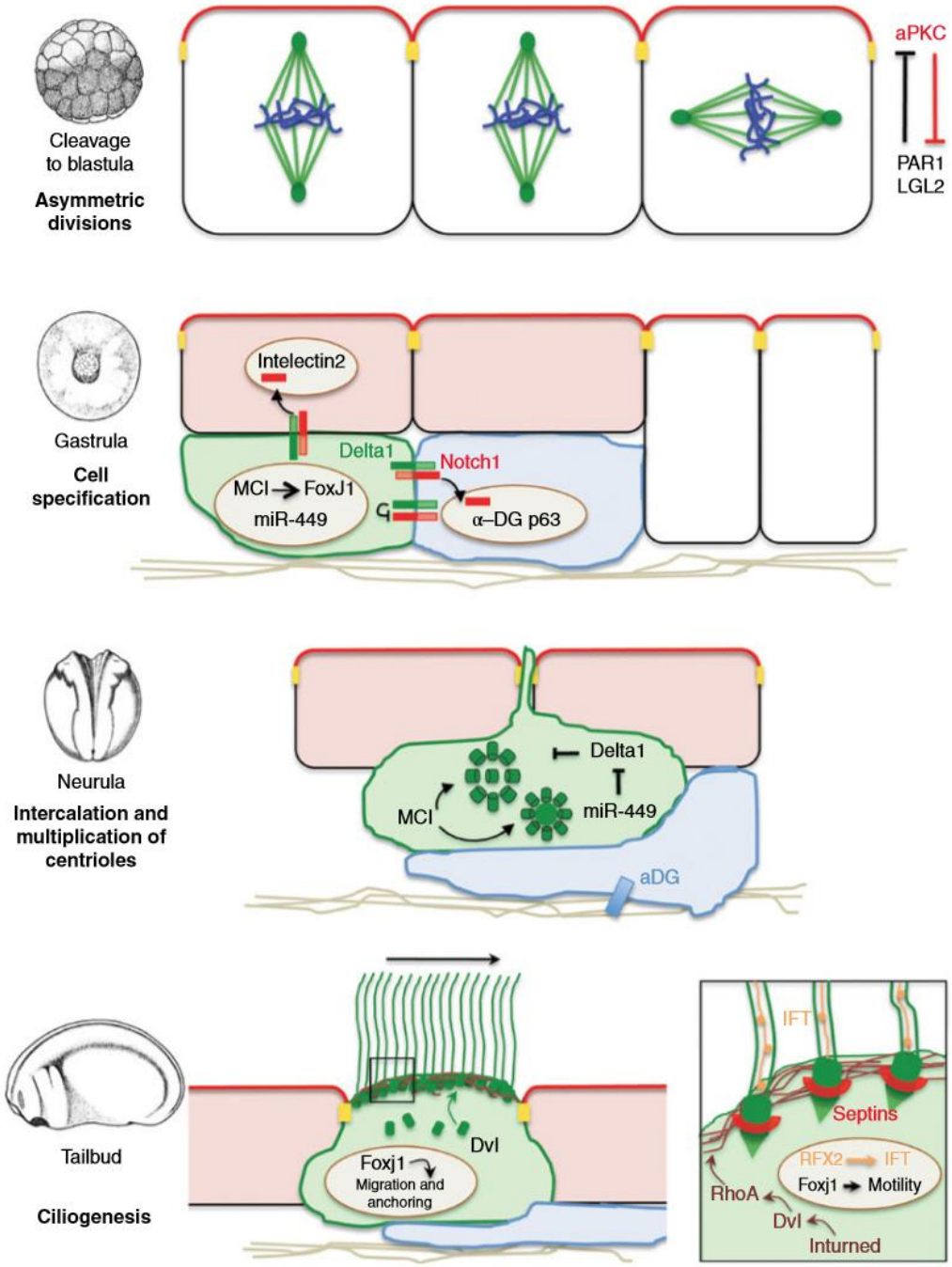

Figure 36: The four steps of MCC biogenesis.

Step 1. From cleavage to blastula stages, divisions along the apical– basal axis generate distinct daughter cells, through asymmetric segregation of maternal determinants; outer cells inherit the apical protein aPKC, which opposes basolateral factors PAR1 and LGL2 to position tight junctions; inner cells do not inherit aPKC and remain loosely packed. Step 2. During gastrulation, MCCs are born in the inner epidermal layer. They express Delta1, which activates the Notch1 receptor both in neighboring inner cells that go on to express the markers α-DG and P63 and in outer cells that in turn express the goblet marker Intelectin2. MCCs express the transcription factors MCI and FoxJ1, as well as the microRNA miR-449. Note that in MCCs, Delta1 appears to inhibit Notch1 in cis. Step 3. During neurulation, MCCs go through two key events, radial intercalation and centrioles multiplication. Intercalation involves two steps: first, MCCs wedge in between the basal domain of outer cells and send protrusions apically. Second, MCCs migrate apically through vertices formed between three or more outer cells. Centriole multiplication is required to produce dozens of BBs necessary for ciliary growth.

Two pathways may be mobilized downstream of MCI: the centriole-dependent duplication pathway and the acentriolar pathway that implicates deuterosomes. This early step of CCP differentiation requires inhibition of Delta1 expression by miR-449. Note that non-intercalating cells make contact with the basal lamina that supports the bilayered epidermis, which allows the interaction of α-DG with extracellular matrix components. Step 4. At tail bud stages, ciliogenesis proceeds through the migration and anchoring of BBs at the apical cortex of the cell, a process under the control of FoxJ1 and PCP components, such as Dvl. PCP factors are also important for the assembly of a cortical actin web necessary for BB anchoring. Finally, cilium elongation can occur through the control of IFT machinery by RFX2, while FoxJ1 controls the expression of motility factors, such as Dynein arms. Septins act as gatekeepers to control the flow of molecules towards the base of the cilium. Rostrocaudal ciliary beating is coordinated between independent MCCs and within each MCC by PCP signaling that fine-tunes the rotation of BBs. Only a selection of the known key players is represented for simplicity. Please refer to the text for a more complete description.

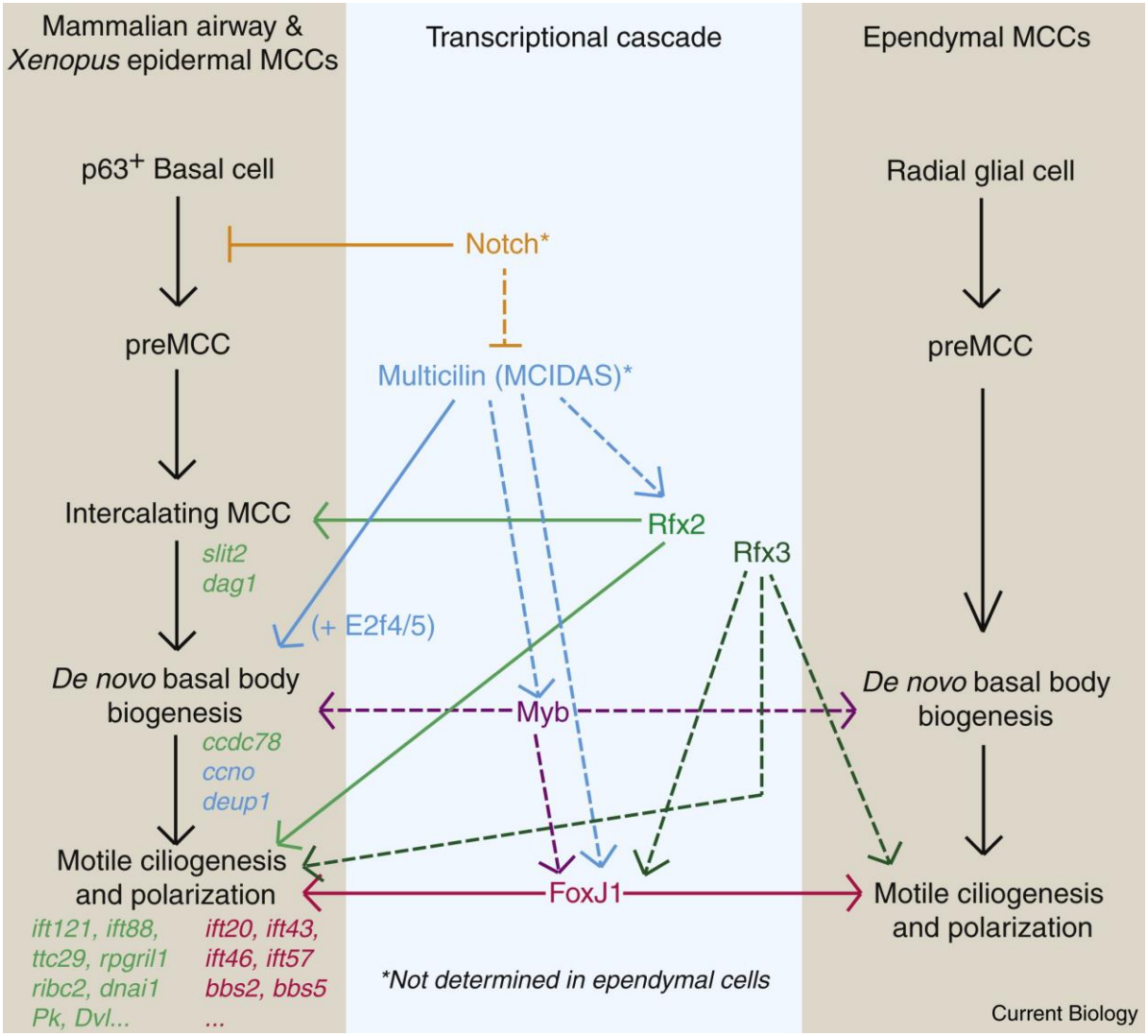

Figure 37: Transcriptional controls of multiciliogenesis.

The transcriptional cascade leading to the generation of multiciliated cell axonemal tufts is outlined for mucociliary multiciliated cells (i.e. the mammalian airway and the Xenopus epidermis) and for ependymal multiciliated cells. Solid lines represent direct interactions, dashed lines represent indirect (or unknown) interactions. Selected known target genes are written in italics and labeled with the color of the transcription factor controlling them. Asterisk indicates that connection is only known for mucociliary cells. (from Brooks & Wallingford., 2014)

3.2.3. Cell intercalation

In 1992 Drysdale and Elinson showed that in neurula stage Xenopus embryos, cells originating from the inner epidermal layer emerge among outer layer goblet cells. At the time, radial cell intercalation was demonstrated through raw experiments in which a portion of control outer layer was grafted onto an inner layer labeled with fluorescein-dextran-amine. This allowed the first visualization of fluorescent intercalating cells among non labelled outer layer cells (Drysdale & Elinson, 1992). It was shown that almost half of the intercalating cells correspond to MCC precursors, while another half correspond to non-ciliated cells (Drysdale & Elinson, 1992; Deblandre et al., 1999). Further technical improvements such as identification of cell type-specific promoters to drive fluorescent protein expression (Stubbs et al., 2006) and colorimetric or fluorescent *in-situ* hybridization allowed a better characterization of the intercalating cells identity. Non-ciliated cells were then shown to correspond to two distinct cell populations: the ionocytes (Dubaissi & Papalopulou, 2011) and SSCs (Dubaissi et al., 2014; Walentek et al., 2014). The three intercalating cell types migrate apically in separate waves (Cibois et al, 2014) starting with MCCs, followed by ionocytes and finally SCCs (Walentek et al., 2014; Collins et al., 2020).

So far, intercalation has been mostly addressed in MCCs, which represent one of the strongest models for radial intercalation (Walck-Shannon & Hardin, 2014; Sedzinski et al., 2016, 2017). MCCs specifically intercalate at junctions formed by at least three outer layer cells, commonly called 'vertices' (Jennifer L. Stubbs et al., 2006).

The intercalation of MCCs from the inner into the outer layer is a multistep process (Figure 38):

(1) The first step of radial cell intercalation is the acquisition of an apico-basal polarity through asymmetric localization of proteins between the apical pole, oriented toward the outer layer, and the basal pole.
(2) Polarized MCCs emit apical protrusions to probe the gaps between outer layer cells and find vertices.
(3) Once a MCC is robustly anchored to a single vertex, rearrangement of outer layer intercellular junctions occurs to separate the basolateral surfaces of outer layer cells and allow insertion of the MCC.
(4) When intercalating into vertices, MCCs adopt a pyramidal cell shape and insert among outer layer cells to reach the surface of epidermis and form adherent junctions with outer layer cells to ensure barrier function (Stubbs et al, 2006).
(5) After reaching the surface, MCCs adopt a more columnar cell shape and expand their apical surface (Chung et al., 2014; Sedzinski et al., 2016, 2017).

Interestingly, MCCs intercalate as individual cells, whereas ionocytes and SSCs can emerge to the surface in small groups of two or three cells. These differences can be explained by the fact that ionocytes and SSCs can reside next to each other, but also that they are smaller than MCCs. It is also known that the MCCs intercalate before non-ciliated cells (Stubbs et al., 2006). Furthermore, it was shown that both ionocytes and SSCs often

associate in direct contact with MCCs. Therefore, it is possible that non-ciliated cells can indirectly contribute to the MCCs spacing by physically separating MCCs at the time of their intercalation. However, the mechanisms underlying the regular spacing of MCCs have been poorly addressed (Deblandre et al., 1999; Jennifer L. Stubbs et al., 2006) and will be developed further at the end of this chapter.

On the contrary, the MCCs insertion among outer layer cells has been well studied and several biochemical factors and physical parameters that control this process have been described over the past decade. As we will see throughout this section, MCC intercalation seems to be a mostly cell-autonomous process (Kim et al., 2012; Chung et al., 2014; Werner et al., 2014; Sedzinski et al., 2016, 2017).

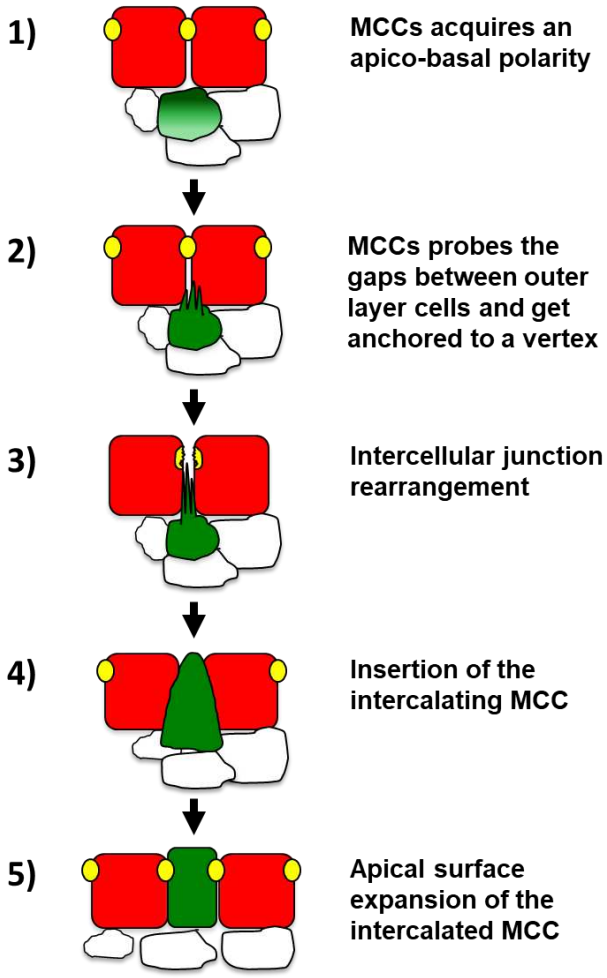

Figure 38: The steps of MCCs radial intercalation

Schematic representation of the epidermis with the outer layer (red) made of adherent epithelial cells (adhesion complex in yellow) and the inner layer made of mesenchymal cells where MCCs (green) and other cells (white) are born. (1) MCCs acquires an apico-basal polarity through asymmetric localization of proteins between the *de-novo* apical pole, oriented toward outer layer cells and basal pole (represented by a dark green to light green gradient). (2) Then polarized MCCs emit apical protrusions to probe the gaps between outer layer cells and find vertices. (3) When an MCC is robustly anchored to a single vertex, the intercalation starts with rearrangement of intercellular junctions to separate the basolateral surfaces of outer layer cells and allow insertion of the MCC. (4) When intercalating into vertices, MCCs adopt a pyramidal cell shape and insert among outer layer cells to reach the surface of epidermis and form adherent junctions with outer layer cells to ensure barrier function. (5) After reaching the surface, MCCs adopt a more columnar cell shape and expand their apical surface. (This scheme summarize the description made by Chung et al, 2014 and Sedzinski et al, 2016)

- ***The contribution of extracellular matrix: the role of α-Dystroglycan (α-DG)***

The dystroglycan complex is a major component of basement membrane and favors interaction between cells and extracellular matrix (ECM). α-Dystroglycan contains an extracellular subunit, which favor cell-ECM interactions by acting as a laminin receptor. The β-DG transmembrane subunit on the other hand, interacts with the cell cytoskeleton through an actin-binding domain (Winder, 1997).

In Xenopus, α-DG is one of the known regulators of MCC intercalation (Sirour et al., 2011). Futhermore, α-DG is a direct target of Rfx2 transcription factor (Chung et al., 2014). The contribution of α-DG to MCCs intercalation seems to be indirect since no expression of α-DG was observed in intercalating cells. However, α-DG inhibition significantly affects ectoderm through the reduction of laminin and fibronectin in ECM, a general loss of cell-cell contact caused by decreased levels of E-cadherin at cell-cell adhesion complexes and more general defects such as reduced flattening of the sensorial layer and blocked cell intercalation (Sirour et al., 2011).

However, the mechanism of action of α-DG in MCC intercalation remains unclear (Sirour et al., 2011). Interestingly the Slit/Robo signaling pathway, which functionally interact with α-DG is also a transcription target of Rfx2 (Chung et al., 2014). Thus inhibition of Rfx2 impairs MCCs insertion among outer layer cells and their apical surface extension in a similar way to α-DG (Chung et al., 2014; Sirour et al., 2011)

- ***MCCs requires proper apical-basal polarity establishment to intercalate***

Several apicobasal polarity markers and factors involved in cytoskeletal apicobasal polarization have been identified in MCCs (Park et al., 2008; Kim et al., 2012; Werner et al., 2014; Ossipova et al., 2015; Collins et al., 2020) and shown to be involved in the intercalation process.

Apical localization of Rab11, a member of the small GTPase family involved in vesicular trafficking and required for both the establishment of the apical-basal polarity and cell-junction formation, is required for MCC intercalation (Roeth et al., 2009; Kim et al., 2012) Interestingly, Rab11 becomes apically polarized before the cells intercalate (Kim et al., 2012). MCCs lacking Rab11 still establish an apical-basal polarity but this is randomly oriented with respect to the epidermal surface and MCCs with incorrect orientation remain trapped within the ectodermal inner layer (Kim et al., 2012). The function of Rab11 in cell intercalation seems to be specific of MCCs since ionocytes were not affected (Kim et al., 2012)

The Par complex is a common regulator of diverse cellular processes among which the establishment of apical-basal polarity. The Par complex also controls adherent junction formation and directed cell migration (Werner et al., 2014). During MCC intercalation, the Par complex localizes at their apical aspect where it associates to apical membrane (Werner et al., 2014) and its inhibition impairs intercalation and apical surface expansion. Interestingly, the inhibition of the Par complex also impairs the correct apical distribution of centrioles in intercalating MCCs (Werner et al., 2014). Indeed, the centriole marker

centrin was shown to polarize apically prior to intercalation of MCCs (Kim et al., 2012). Centrin is a component of the centrosome and contributes to microtubule network polarization, suggesting the implication of microtubule network in the apically polarized migration of intercalating cells.

Centrioles represent a central element in the cilia formation process in MCCs. Within MCCs, centrioles multiply to generate large numbers of basal bodies, each of which will provide the seed for the biogenesis of a cilium. Interestingly, centriole amplification occurs when MCCs are not yet intercalated and the newly formed centrioles cluster at the level of the nucleus (Klos Dehring et al., 2013). The centriole cluster moves apically before MMCs initiate intercalation (Figure 39) (Werner et al., 2014). In migrating cells, the centrioles contribute to the microtubules network polarization by localizing between the nucleus and the leading edge of the cell. In intercalating MCCs the leading edge correspond to the apical side of the cell. Interestingly, pharmacological inhibition of microtubules by Nocodazole impairs MCC intercalation and apical surface expansion (Werner et al., 2014)

The apical-basal polarity complex Par also contributes to the polarization of microtubules. Inhibition of CLAMP, a microtubule binding protein and an interactor of the Par complex, impairs intercalation of both MCCs and non-ciliated cells (Werner et al., 2014). During intercalation, the Par complex drives apical basal polarization of cells, as well as the recruitment of centrioles and CLAMP to the apical side of the cells.

The apical recruitment of centrioles and microtubule-binding proteins to the cell apical side contributes to the assembly of the microtubule network required for intercalation (Figure 39) (Werner et al., 2014). Indeed, microtubule nucleation on the apical side of intercalating cells independently of their orientation is sufficient to provide the structural rigidity required by the intercalating cells to break through the epithelial barrier made by outer layer cells (Collins et al., 2020).

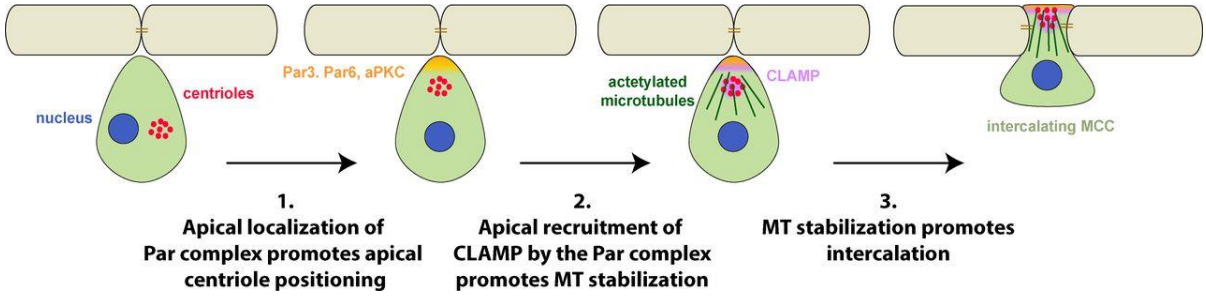

Figure 39: Model for the steps involved in regulating MT stability during radial intercalation.

We propose that the Par complex mediates both apical positioning of centrioles (1) and asymmetric accumulation of CLAMP (2). CLAMP asymmetry leads to asymmetric stabilization of MTs (2) along the axis of migration that promotes intercalation (3). (Werner et al, 2014)

The MCCs contain a larger number of centrioles than ionocytes and SSCs and intercalate first while specification of the three cell types takes place during the same time window (Takahashi et al., 2015; Kurrle et al., 2020). A correlation between the number of

centrioles per cells and the timing of intercalation has been proposed (Collins et al., 2020). Indeed, reducing the number of centrioles in MCCs delays their intercalation without blocking it completely. On the other hand, increasing the number of centrioles in MCCs leads to a more precocious intercalation (Collins et al., 2020). Artificially increasing centriole amplification in ionocytes speeds up their intercalation. This suggests that the sequential intercalation between MCCs and ionocytes might be caused by the difference in their centriole contents and the resulting faster assembly of the microtubule network in MCCs (Collins et al., 2020).

The core PCP components Vangl2, Prickle3 (Pk3) and Disheveled have been shown to regulate MCC radial intercalation (Ossipova et al., 2015). Indeed, Disheveled (Park et al., 2008), Vangl2 and Pk3 accumulate at the apical side of intercalating MCCs (Ossipova et al., 2015). Depletion of core PCP proteins and interference with PCP signaling impairs the orientation of MCCs toward the ectoderm surface and their intercalation (Ossipova et al, 2015). Moreover, KIF13B, a microtubule motor kinesin that physically interacts with Disheveled, promotes PCP signaling and regulates MCC intercalation. Together with the previously described role of Rab11, this suggests a role of microtubule-dependent trafficking in MCC radial intercalation (Kim et al., 2012, Ossipova et al., 2015). The role of PCP signaling in radial intercalation seems not to be restricted to MCCs, since its inhibition also affects the deep layer ectoderm radial intercalation during epiboly (Ossipova et al., 2015).

- ***The actin cytoskeleton generates pushing forces for the apical emergence of intercalating MCCs***

In this last section, I will introduce the role of actin, a major driver of MCC radial intercalation (Vladar & Axelrod, 2008; Walck-Shannon & Hardin, 2014; Sedzinski et al., 2016, 2017; Kulkarni et al., 2018)

Mature MCCs present a dense apical actin network required for basal body anchoring and orientation. However, this dense network of actin fibers establishes early during the step of radial intercalation (Sedzinski et al., 2016). As presented in Chapter 2, actin polymerization and actomyosin fibers are major contributors to force generation in cell-shape changes and cell movement and migration (Guillot & Lecuit, 2013; Heisenberg & Bellaïche, 2013) and are thus likely to play a role in MCC intercalation.

MCC apical emergence and apical surface expansion require pushing forces generated by Formin1-dependent actin polymerization (Sedzinski et al., 2016). As MCCs intercalate, there is no cell shape change in their basal and medial region, but rather an increase of cell volume and apical actin enrichment that precede their apical surface expansion (Sedzinski et al., 2016). Neither myosin nor E-cadherin is required for apical surface expansion. Interestingly, Formin1 was shown to be a direct target of Rfx2 and to accumulate on the apical side of intercalating MCCs. Formins are direct effectors of RhoA GTPase. Inhibition of RhoA activity impairs Formin1 apical localization, thus decreasing apical actin polymerization and the following apical surface expansion (Sedzinski et al., 2017).

- ***The contribution of outer layer cells***

While the molecular mechanisms of MCC intercalation are now relatively well understood, the possible contribution of outer layer cells to this process has been poorly characterized. Outer layer cells have been described as a relative static structure that rearranges locally to accommodate the insertion of intercalating cells (Stubbs et al., 2006). It was then proposed that outer layer cells limit the total number of intercalation events by restricting it to vertices formed by at least three outer layer cells (Stubbs et al., 2006). Interestingly, the supernumerary MCCs generated upon Notch inhibition saturate all the available outer layer vertices, many MCCs remaining trapped within the inner layer (Deblandre et al., 1999; Stubbs et al, 2006). However, the restriction of intercalation appears more severe for MCCs than for the other classes of intercalating cells. The fact that MCC intercalation is restricted at vertices was explained by differences in cell size (MCCs are twice as large as non-ciliated cells). It was also proposed that intercellular adhesion might be weaker at vertices and/or that they provide more space to the intercalating cells to insert. (Stubbs et al, 2006). Indeed, vertices represent interruptions of the conventional bi-cellular adherent junctions and take a specialized form called tri-cellular junction. These structures contain a bigger intercellular gap than bi-cellular junctions and are much more complicated to seal (Ikenouchi et al., 2005; Higashi & Miller, 2017) (Figure 40). However, the restriction of intercalation at vertices has been mostly described for MCCs and we cannot exclude that ionocytes and SSCs can intercalate at bi-cellular junction (Figure 35B, yellow arrow head) (Walentek et al., 2014)

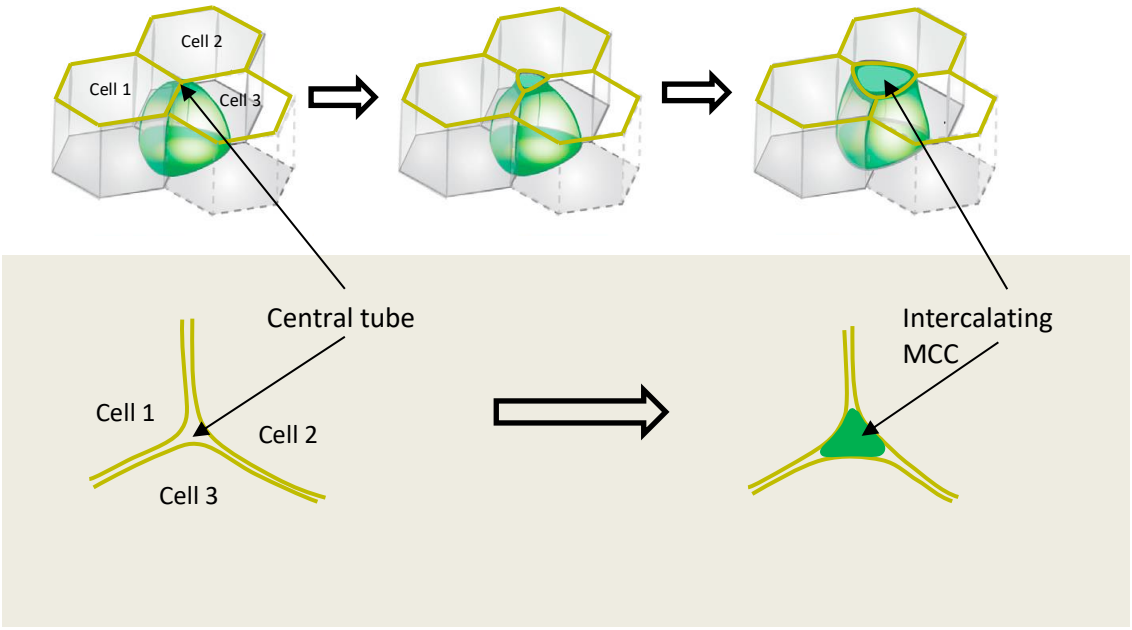

Figure 40: MCCs intercalate at tri-cellular contacts.
At the junction between three cells, cell-cell junctions take on a specialized organization called tri-cellular tight junction (tTJs). tTJs are found apically of Tjs. tTJs form a central tube that cannot be completely sealed (adapted from Sedzinski et al., 2016 by M. Zilliox)

Outer layer cells also contribute to intercalation regulation. For example, RhoA expression levels in outer layer cells directly adjacent an intercalating MCC regulate the outer layer rigidity and affect the intercalating rate (Sedzinski et al., 2016). Also, no proof of molecular communication between outer layer cells and the intercalating cells have been shown so far. Most studies on radial cell intercalation focused on the process from the intercalating cells perspective while outer layer was considered as permissive. The only exception is provided by Stubbs and colleagues' discussion of the potential mechanisms played by outer layer cells in restricting MCCs intercalation as single cells (Stubbs et al 2006). However, the involvement of outer layer cells remains speculative and its function remains to be address.

3.2.4. Cell differentiation

Once intercalating inner layer cells have completed their radial intercalation, the final step is their differentiation. Here, I will shortly present the differentiation of MCCs on which my work was focused but I will not develop the other cell types.

The last step of cell differentiation is called ciliogenesis (reviewed in Cibois et al, 2014; Spassky and Meunier, 2017; Boutin and Kodjabachian, 2019). It consists in the construction of multiple motile cilia each originating from a basal body. This step is schematized as following radial intercalation as cilia are not made before the cell emerge but some crucial steps of ciliogenesis are concomitant to radial intercalation.

As mentioned earlier, MCC specification relies on a gene regulatory network at the end of which centriole amplification is triggered by Gemc1 and Mcidas activation, while FoxJ1 and Rfx 2/3 coordinately control the genesis of motile cilia (Spassky and Meunier, 2017; Boutin and Kodjabachian, 2019).

Once hundreds of centrioles are made, they are addressed to the apical aspect of intercalated MCCs and converted into basal bodies that will be template for motile cilia (Boutin and Kodjabachian, 2019). Basal bodies are docked into an apical cortex made of a dense actin meshwork.

Basal bodies characterized by two appendages, the rootlet and the basal foot, required to determine the correct orientation of the basal body and thus of the ciliary beating. Insertion in the subapical actin network ensures the regular spacing of basal bodies while microtubules connect basal bodies to each other and ensure their proper alignment and orientation.

Once cilia start beating, planar polarization ensures the orientation of MCCs and the beating of their cilia across the plane of the tissue to generate an anteroposterior fluid-flow (Werner and Mitchell, 2012).

3.3. MCC patterning.

Despite the large interest for the regular spacing pattern of MCCs, shared among anurans (Nokohbztolfoghahai et al, 2005) and the extensive study of Xenopus MCE, the mechanisms underlying the establishment of this pattern remain unclear (Deblandre., 1999; Stubbs., 2006). Although the functional signification of this patter is unclear, its presence in many amphibians suggests that it represents an evolutionarily conserved advantage. Over almost thirty years MCC radial intercalation has been the focus of research activity, but only two publications have addressed the question of their regular spacing.

The first one shows the involvement of Delta/Notch signaling pathway in the control of MCC numbers (Deblandre et al., 1999). This pioneering study proposed that the scattered pattern of MCCs is pre-established within the inner layer and results from Notch-mediated lateral inhibition. The well-known effect of Notch mediated lateral inhibition in many systems led to the assumption of a "pre-printed" scattered pattern of MCCs before their intercalation. However, at the time of this publication the spatial resolution provided by colorimetric *in-situ* hybridization was insufficient to clearly analyze the initial distribution of MCCs within the inner layer.

It was later proposed that radial intercalation acts as a second step to constrain the insertion of MCCs only at vertices and to refine the spacing pattern (Deblandre et al., 1999; Stubbs et al., 2006). Indeed, it was shown that the outer layer can accommodate twice as many MCCs upon Notch inhibition, with no violation of the non-contiguity rule, suggesting that MCCs spacing stems from the limited availability of intercalation sites rather than from lateral inhibition *per se* (Stubbs et al., 2006; reviewed in Werner & Mitchel., 2012). However, no one ever formulated the possibility that MCCs drastically change their distribution from their birth to their intercalation. Only small-scale cell displacements or shape changes were proposed (Stubbs et al., 2006)

As we have seen in the section devoted to intercalation, the regular spacing is a unique property of MCCs (Stubbs et al, 2006). The cell size argument was convincing enough to explain why MCCs intercalate individually and only at vertices while ionocytes and SSC can intercalate in pairs or small groups. Moreover, although this aspect has never been properly and quantitatively addressed, ionocytes and SSC can intercalate at bi-cellular junctions (Figure 35B). This shows sthat during intercalation, MCCs do not experience the same constraints from outer layer cells as SSCs and ionocytes and could explain why MCCs intercalate individually while the other cell types are able to do so in groups.

Stubbs et al hypothesize that outer-layer cells topologically act as a bottleneck, which restricts intercalation in several ways. The first one would be the physical difficulty of establishing apical junctions with outer cells, which occurs only at the apical vertex. Because of their size, MCCs are restricted in their intercalation. The second would be inhibitory interactions among intercalating cells, which may influence the patterns of intercalation for MCCs and non-ciliated cells. We know now that all cell types do not

intercalate at the same time (Collins et al, 2020) making unlikely the fact that non-ciliated cells influence the intercalation of MCCs. A third possibility is that inhibitory interactions occur among MCCs. Once a given MCC is engaged in a vertex, it prevents other MCCs from accessing to it.

The development of live-imaging techniques has allowed a better investigation of the mechanisms underlying radial intercalation but also of those controlling the establishment of the MCC pattern, as I did during my thesis. Also, the possibility that signaling pathways specific to MCCs might explain their regular spacing relative to the other intercalating cell type has never been addressed. In the next chapter, I will present the Scf/Kit signaling pathway, which my work revealed as a major player in establishing the regular spacing of MCCs.

4. The SCF/Kit signaling pathway in cell migration and cell repulsion

In vertebrates, the Scf/Kit signaling pathway regulates various functions and developmental processes such as hematopoiesis, fertility, pigmentation, gut movement and nervous system development (Lennartsson & Rönnstrand, 2012). Also, mutations of the Kit receptor have been linked to pathologies including several malignancies, such as acute myeloid leukemia, mastocytosis, gastrointestinal stromal tumors and melanoma (Abbaspour Babaei et al., 2016). At the cellular level, the Scf/Kit signaling pathway was shown to regulate many processes including cell survival, cell proliferation, cell differentiation, cytoskeletal rearrangement, chemotaxis and cell migration (Lennartsson & Rönnstrand, 2012; Meininger et al., 1992; Runyan et al., 2006; Samayawardhena et al., 2007; Bernhard Wehrle-Haller et al., 2001; Zuo et al., 2016).

The Scf/Kit signaling pathway has been extensively studied over the last 30 years but, because of its link to malignancies, most information came from clinical trials and from studies on mice or human cell lines. Also, because of its important role in stem cell regulation, most of the literature is focused on its role in cell survival and proliferation but other functions in several developmental contexts remain largely unexplored.

During my thesis, I characterized the Scf/Kit function in a hitherto unexplored developmental context. My work was mostly focused on the cellular responses of perturbation of the SCF/Kit signal, without attempting a detailed characterization of the underlying signaling mechanism(s). Therefore, in this chapter, I will not attempt a complete review of the downstream cascade(s) triggered by SCF/Kit.

4.1. The Stem Cell Factor (SCF) ligand

The Kit ligand (KitL) has been attributed many different names depending on the biological context where it was characterized. These include Stem Cell Factor (SCF), Mast cell Growth Factor (MGF) or Steel factor (SLF, which came from the *steel* locus where the gene is encoded).

SCF is a single pass transmembrane protein with an extracellular domain, a transmembrane domain, and a small intracellular region (Figure 41A). In mammals, two isoforms, soluble or membrane-bound exist. They result from alternative splicing events, resulting in *Scf* mRNAs containing or lacking the exon 6. The extracytoplasmic aminoacid stretch encoded by exon 6 contains a consensus site for endopeptidase cleavage. The SCF cleavage requires proteases such as Matrix metalloprotease-9, chymase-1 and members

of the ADAMs family including ADAM17 and ADAM33 (reviewed in Lenartsson & Ronstrand., 2012). Proteolytic cleavage at this site leads to the release of a 165-aa soluble portion of the molecule. In contrast, the isoform lacking exon 6 is not cleaved and mostly retained as a 220-aa membrane-bound molecule (Figure 41A ch4) (Anderson et al., 1991). The Xenopus genome contains, two *scf* genes, *scf-S* and *scf-L* (S and L refer to the chromosome they are present) reportedly expressed throughout the developing non-neural ectoderm (Goldman et al., 2006; Martin & Harland, 2004). Only the exon 6-containing splice form of *scf* has been reported but the proteolytic cleavage of the coded protein remains to be proved since the exon 6-coded aa stretch present low similarity with mammals and does not contains obvious proteolytic consensus sites (Hultman et al., 2007).

SCF has been first characterized as a growth factor, a function ensured by its extracellular domain that specifically binds to the Kit receptor. Both soluble and membrane-bound isoforms assemble into homodimers and are able to activate the Kit receptor. However, the signaling pathways that they trigger differ in terms of kinetics and downstream effectors (Miyazawa et al., 1995). These differences will be developed later in this chapter.

While SCF has been well characterized as the only known ligand that can activate the Kit receptor, it has recently emerged that SCF-Kit interaction also transduce a signal within the Scf-expressing cells (Buono et al., 2018). Interestingly, the membrane-bound SCF present a small intracellular domain whose function remains largely unexplored. It was then shown in-vitro that Scf-Kit interactions trigger a bi-directional signaling (Buono et al., 2018).

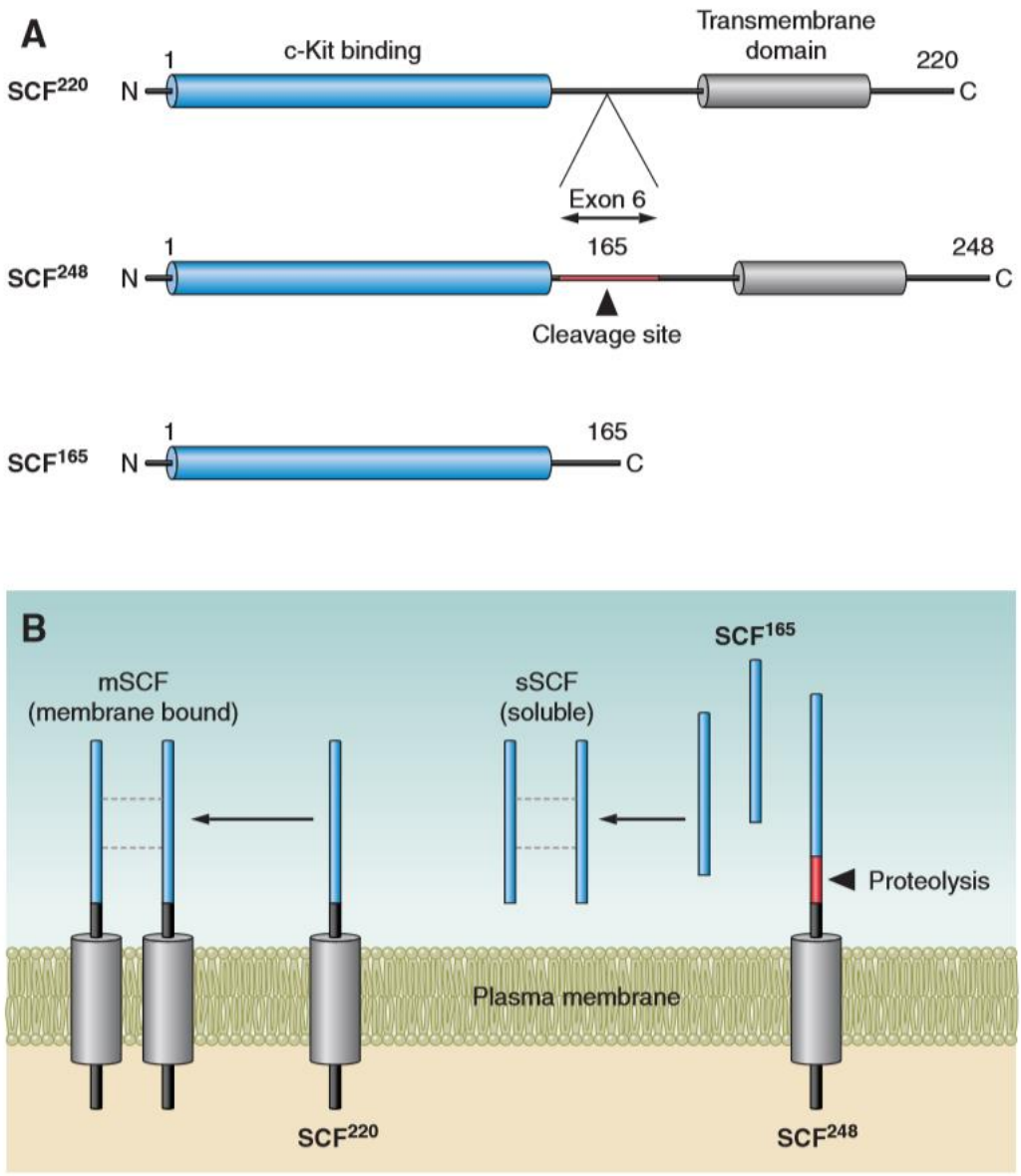

Figure 41 Schematic representation of stem cell factor (SCF) splice forms and protein processing.

A: SCF protein is produced as two transmembrane forms due to alternative splicing of exon 6, SCF220, and SCF248. In SCF248, exon 6 is kept and encodes a proteolytic cleavage site, generating the soluble SCF165. B: SCF220, lacking the cleavage site, forms membrane-bound SCF dimers (mSCF), and SCF248 is processed to SCF165 that forms soluble SCF(sSCF). Dashed lines indicate that the SCF dimers are held together by non-covalent interactions. (from (Lennartsson & Rönnstrand, 2012).

4.2. The tyrosine kinase receptor KIT

The Kit receptor belongs to the type III receptor tyrosine kinase family, characterized by the presence of five immunoglobulin-like domains in its extracellular portion, a single-pass transmembrane domain, a split intracellular kinase domain, the two portions of

which are separated by an insert region, and the COOH-terminal tail (Figure 42A). The ligand binding induces a rapid dimerization of the receptor and conformational change in the receptor dimer (Figure 42B). Finally, conformational changes bring the two kinase domains closer, and induce their auto-transphosphorylation on intracellular tyrosine residues localized in the juxtamembrane region, the kinase insert, the kinase domain and the COOH-tail (Figure 42C).

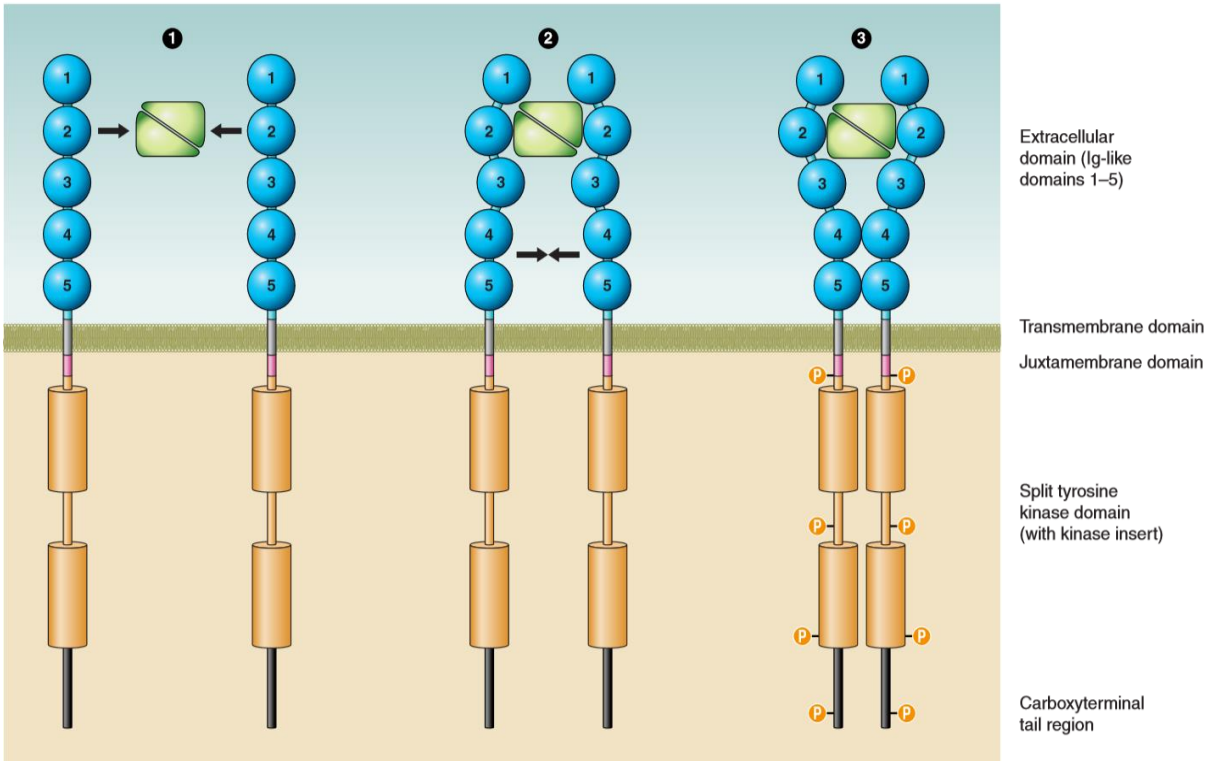

Figure 42. Schematic representation of SCF-induced c-Kit activation.

1) The ligand for c-Kit, SCF, is a bivalent protein that drives formation of c-Kit homodimers by interaction with Ig-like domain1–3. 2) SCF brings two c-Kit monomers in close proximity of each other, allowing for interactions between Ig-like doman 4 and 5 in adjacent c-Kit molecules. 3) The homodimeric state of c-Kit brought about by the SCF and further stabilized by interactionsbetweenIg-likedomain4/5 allows for efficient trans-phosphorylation in the juxtamembrane region (Tyr568 and 570), kinase insert region (Tyr703, 721, 730, and 747), kinase domain (Tyr823 and 900) (by Src kinases), and COOH-terminal tail (Tyr936). (from Lenartsson & Ronstrand, 2012).

In mice, complete loss of Kit receptor expression leads to death *in utero*, probably because of severe anemia, while heterozygote animals present anemia, pigmentation defects and reduced fertility. The severity of the observed phenotype is correlated to the tyrosine kinase activity of the receptor (Rönnstrand, 2004).

As for other receptor tyrosine kinases, Kit is downregulated to adapt the signaling strength to the biological needs. There are at least three levels of c-Kit downregulation that function in concert: 1) removal from the cell surface and intracellular degradation, 2) inactivation of the kinase domain by serine phosphorylation, and 3) tyrosine dephosphorylation. These regulatory strategies vary according to the presence of soluble or membrane-bound ligand (Lennartsson & Rönnstrand, 2012).

4.3. The SCF/c-KIT signaling pathway controls cell adhesion, migration and cytoskeletal reorganization.

The signal transduction downstream of c-Kit involves many effectors among which PI3-kinase, Src family kinases, mitogen-activated protein kinases, and phospholipases are the best characterized (reviewed in Lenartsson & Ronstrand, 2012). The effectors of the SCF/Kit signaling cascade highly depend on the cellular context and they often function as complex integrated signaling circuits. In the following section, I will focus my attention on examples where SCF/Kit signaling pathway regulates cell migration, cytoskeletal remodeling and adhesion, biological processes which are closer to my work, without attempting a detailed characterization of the involved downstream pathways.

Although SCF/Kit plays a role in cell adhesion, migration and cytoskeletal reorganization in several biological systems, these aspects of Kit biology have remained largely underinvestigated compared to its function in cell survival, cell proliferation and cell differentiation (Lennartsson & Rönnstrand, 2012; Rönnstrand, 2004). Nevertheless, the SCF/Kit signaling is essential for these processes as exemplified by primordial germ cells and melanoblasts (see chapter 2) but also hematopoietic cells (Okumura et al., 1996; Okayama & Kawakami, 2006), dental pulp progenitors (Pan et al., 2013) and neural cells (Sun et al., 2004). In the brain, neuronal stem/progenitor cell (NSPC) are recruited to sites of injury, a process for which Kit signaling is required (Sun et al, 2004). Furthermore, the SCF/Kit signaling pathway has been shown to regulate other aspect of cell motility than migration, such as axonal extension, which directly depends on actin cytoskeleton (Gore

et al., 2008). In bone marrow-derived mast cells, Kit stimulation by SCF recruits Wiskott-Aldrich Syndrome Protein (WASP) resulting in the phosphorylation and activation of Rho GTPase Cdc42 and the Arp2/3 complex and the following fillopodia formation (Mani et al., 2009).

While cell migration is dependent on dynamic cytoskeletal changes, cell adhesion requires specific cytoskeletal organization to favor stable cell-cell interactions (Samayawardhena et al., 2007; Tabone-Eglinger et al., 2014).

Differences in Kit signaling following interaction with soluble vs membrane-bound SCF are a key point in the control of the two opposite processes of cell adhesion and cell migration. As mentioned earlier, soluble and membrane-bound forms of SCF can trigger different effects (Miyazawa et al., 1995). Usually, the stimulation with soluble SCF leads to a rapid but transient activation of the Kit receptor tyrosine kinase activity, as well as to its fast degradation. On the other hand, stimulation with the membrane-associated isoform can drive opposite effects depending on the cellular context. Many reports show a more sustained activation of Kit by membrane-bound SCF than by it soluble form (Miyazawa et al., 1995). It also appears that the pathway triggered by membrane-bound SCF is not dependent on the intrinsic tyrosine-kinase activity of Kit (Gough et al., 2015; Tabone-Eglinger et al., 2012; Tabone-Eglinger et al., 2014; Koma et al., 2005). Also, no report has addressed how membrane-bound SCF signaling might be affected by cell type-specific co-factors. However, it has been shown that the Kit receptor response can be modulated by specific modifications. For example, in response to SCF stimulation, Protein kinase C (PKC) mediates phosphorylation of the Kit receptor on its serine residues, which in turn inhibits Kit autophosphorylation on tyrosine residues. Thus, despite the fact that Kit is engaged in an interaction with SCF, its kinase activity dependent-signal is blocked. In this context, independently of the Kit tyrosine kinase activity, SCF stimulation of Kit induces a motility response including actin reorganization and chemotaxis. Here, PKC is suggested to participate to a negative feedback loop which regulates the Kit receptor and determines whether the effect of Kit will be preferentially mitogenic or motogenic (Blume-Jensen et al., 1993). PKC inhibition abolished cell motility and allows Kit receptor induces mitogenic effect under SCF stimulation.

The differences in strength between soluble and membrane-bound SCF can be easily explained as the consequence of anchoring the ligand to the membrane and thus preventing internalization of the receptor-ligand complex (Kurosawa et al., 1996). Indeed, compared to the soluble ligand, membrane-bound SCF induces a more persistent activation of Erk1/2 and p38 mitogen-activated protein kinase (MAPK) (Kapur et al., 2002). Qualitative differences in the downstream effectors have also been noted, such as the specific recruitment of PLCγ upon stimulation with membrane-bound SCF (Gommerman et al., 2000). However, the effect of KIT signaling largely depends on the cellular context.

Other studies have shown that interaction of Kit with SCF stimulates cell-cell adhesion. Long-lived complexes between Kit and membrane-bound SCF can themselves function as adhesive complexes. This has been shown in the case of melanocytes, which are anchored to intraepithelial niches by the interaction between Kit and membrane-bound SCF, in collaboration with integrins (Tabone-Eglinger et al., 2012; Tabone-Eglinger et al., 2014). Furthermore, it was shown that membrane-bound Scf-Kit clusters ensure adhesion but also mechanical anchorage of cells (Tabone-Eglinger et al., 2014). *In vitro* experiments show that membrane-bound SCF-mediated resistance to physiological shear stress is only an order of magnitude less than that due to integrin-mediated adhesion.

Similar results were observed with mast cells, native immune cells from bone marrow hematopoietic progenitors, which migrate to peripheral tissues after circulating in the blood vessels as immature progenitors (Kirshenbaum et al., 1999; Metcalfe et al., 1997; Lennartsson & Rönnstrand, 2012). Mast cells express the Kit receptor and their migration is largely regulated by SCF produced by adjacent cells. Apart from its role in mast cell migration, SCF/Kit signaling is also important for mast cell survival and its attachment to the submucosa, the so-called tissue homing process. In this process, membrane-bound SCF is expressed by target tissues such as endothelial cells (Mierke et al., 2000), fibroblasts of the conjunctive tissue (Koma et al., 2005) and airway epithelia (Gough et al., 2015). As a third example, Scf-Kit behavior as an adhesive complex was also demonstrated between primordial germ cells (PGCs) and somatic cells (Pesce et al., 1997). In this last example *in vitro* experiments showed that the PGCs only adhere to somatic cells when these express the membrane-bound form of SCF, but not the soluble form. Moreover, increasing the concentration of soluble SCF inhibit cell adhesion (Pesce et al.,

1997). A common point between the Kit adhesive properties in melanocytes, mast cells and PGCs is that this function does not requires the downstream phosphorylation cascade. In all three systems, adhesion was suppressed by antibodies that inhibit the Scf-Kit interaction but not by function-blocking antibodies that inhibit the Kit kinase-dependent signaling. Similarly, pharmacological inhibitors of the Kit tyrosine kinase activity and kinase-dead mutant forms of Kit do not impair adhesion. Together this demonstrates that KIT and SCF can display adhesive function independently of the Kit kinase-dependent signaling.

Interestingly even if Scf-Kit interaction in cell-cell adhesion does not require Kit kinase activation, it triggers other cellular responses in the Kit expressing cells (Tabone-Eglinger et al., 2014). For example, it was shown that membrane-bound SCF/Kit clusters induce F-actin polymerization. Interestingly, actin polymerization is affected by mutations on the juxtamembrane domain and within the PI3K recruitment site but not by mutations of the kinase domain (Tabone-Eglinger et al., 2014).

Soluble SCF was described as a chemokine and has been characterized as a chemoattractant and/or chemotactic factor able to stimulate cell migration and cytoskeletal reorganization in different developmental contexts. For example, soluble SCF has been described as a homing factor for dental pulp progenitors. During regeneration, their migration to their niche requires Rho-mediated cytoskeletal rearrangements and is dependent on the KIT pathway and its downstream effectors PI3K/Akt and MEK/ERK (Pan et al., 2013). Scf is the principal factor produced within tissue that can induce mast cells chemotaxis, dependent on Kit-mediated actin reorganization (Blume-Jensen et al., 1991; Halova et al., 2012). The SCf/Kit signal also affects other actin-dependent aspects of mast cell biology. This is a case of degranulation, where SCF synergize with other parameter to promote actin remodeling and the following release of vesicles (Smrž et al., 2013).

Melanocyte recruitment to the hair follicle, illustrated in Chapter 2, summarizes well the importance of the two soluble and membrane-bound forms of SCF: first, soluble SCF stimulate the migration of melanocytes, which are subsequently anchored to the hair follicle by the membrane bound SCF expressed by hair follicles cells (Jordan & Jackson, 2000; Wehrle-Haller & Weston, 1995).

5. Aim of my work

The team of Laurent Kodjabachian in the Institute of Developmental Biology of Marseille (IBDM) is focused on the biology of ciliated epithelia. The team is studying the development of the embryonic epidermis of the amphibian *Xenopus laevis* to explore the cellular and molecular mechanisms in charge of controlling the development of mucociliary epithelia. As presented in chapter three, the embryonic epidermis of *Xenopus* develops in four successive steps. My thesis work was focused on elucidating the mechanisms that generate a regular pattern of distribution of the multiciliated cells (MCCs).

Interestingly, preliminary results showed that MCCs precursors are not regularly distributed at birth, which suggest that the mechanisms of pattern generation are distinct from other mechanisms than control cell specification in space and time with respect to the final distribution pattern.

Moreover, preliminary data from the team showed that impaired Scf/Kit signaling leads to an abnormal distribution of MCCs, which are found aggregated in clusters rather than isolated. MCCs express KIT shortly after their specification within the inner epithelial layer, while SCF is preferentially expressed by the outer layer cells. From these observations we hypothesized that the SCF/KIT signaling pathway acts as a guidance system controlling the transition from a disordered to a regular distribution of MCCs.

The aim of my work was to characterize the behavior of MCCs before the intercalation phase and to understand the role played by the SCF/KIT pathway in establishing their regular spacing pattern.

In the first step of my work, I developed live imaging techniques to record the behavior of MCCs *in vivo* through the depth of two epidermal layers in a growing embryo. This represented a technical challenge since this technique was not available in the host team and had actually has never been applied before to *Xenopus*. After developing this technique, I focused my work on characterizing the mechanisms that generate the regular pattern of MCCs distribution.

6. Results

6.1. Manuscript under revision at Dev Cell

The SCF/KIT pathway implements self-organised epithelial patterning by cell movement.

Alexandre Chuyen[1], Charlotte Rulquin[1], Virginie Thomé[1], Raphaël Clément[1], Laurent Kodjabachian[1,2,3*] and Andrea Pasini[1,3*]

1. Aix-Marseille Univ, CNRS, IBDM, Marseille, France

* Correspondence : andrea.pasini@univ-amu.fr; laurent.kodjabachian@univ-amu.fr

2. Lead contact

3. Co-senior authors

Highlights

- Immature multiciliated cells transit from a disordered to an ordered pattern
- The transition is a self-organising process based on repulsive and affinity movements
- ARP2/3-dependent actin remodelling is required for pattern emergence
- The SCF/KIT pathway promotes both repulsion and affinity movements

eTOC blurb

In developing *Xenopus* epidermis, immature multiciliated cells (MCCs), initially chaotically distributed within an inner layer, emerge in an orderly pattern among cells of the outer layer. This process involves MCC mutual repulsion and affinity towards outer-layer intercellular junctions. The SCF/KIT signalling pathway promotes both properties to allow regular MCC distribution.

SUMMARY

How individual cell behaviours lead to the emergence of global patterns is poorly understood. In the *Xenopus* embryonic epidermis, multiciliated cells (MCCs) are born in a random pattern within an inner mesenchymal layer, and subsequently intercalate at regular intervals into an outer epithelial layer. Using both experiments and mathematical modelling, we show that this transition from chaotic to ordered distribution relies on mutual repulsion among motile immature MCCs, and affinity towards outer-layer intercellular junctions. Consistently, ARP2/3-mediated actin remodelling is required for MCC pattern emergence. Using multiple functional approaches, we show that the Kit tyrosine kinase receptor, expressed in MCCs, and its ligand Scf, expressed in outer-layer cells, are both required for regular MCC distribution. While Scf behaves as a potent adhesive cue for MCCs, Kit expression is sufficient to confer order to a disordered heterologous cell population. Our work reveals how a single signalling system can implement self-organised large-scale patterning.

Keywords:

SCF/KIT, pattern formation, self-organisation, *Xenopus*, ciliated epithelium, cell motility, cell-cell repulsion, adhesion, actin cytoskeleton.

INTRODUCTION

Orderly cellular patterns have always captured the attention of scientists, and understanding the mechanisms and forces that control their establishment is one of the long-standing aims of developmental biology. In the past decades, classical and molecular genetics approaches have led to the identification of robust Gene Regulatory Networks (GRNs) that generate patterns by concomitantly specifying cellular identity and position within developing embryos (Briscoe and Small, 2015; Davidson, 2010). However, patterns of regular cell distribution can also emerge when the stochastic movements of motile cell populations are partially restricted, for example by mutual repulsion. Such phenomena have been described in rat retina (Galli-Resta et al., 2002), mouse cerebral cortex (Villar-Cervino et al., 2013), zebrafish epidermal pigmented cells (Walderich et al., 2016) and *Drosophila* haemocytes (Davis et al., 2012) but the underlying molecular mechanisms are only starting to be unravelled.

In vertebrates, one striking example of ordered cellular pattern is provided by the embryonic epidermis of the amphibian *Xenopus*, where hundreds of cells carrying multiple motile cilia (Multiciliated Cells or MCCs) are found distributed among mucus-producing goblet cells, according to a regular spacing pattern (Deblandre et al., 1999). The ontogeny of this mucociliary epithelium occurs through a multistep process (Cibois, 2014). At cleavage stages, asymmetric cell divisions partition the embryonic non-neural ectoderm into an outer epithelial and an inner mesenchymal layer. At gastrula stages, the outer layer gives rise to a sealed epithelium containing only goblet cells, while MCCs are born within the inner layer, together with osmoregulatory ionocytes, serotonin-secreting Small Secretory Cells (SSCs) and basal cells. The BMP and Delta/Notch pathways have been shown to control the number of MCCs, ionocytes and SSCs born within the inner layer (Deblandre et al., 1999) (Stubbs et al., 2006) (Hayes et al., 2007) (Quigley et al., 2011) (Cibois et al., 2015). Starting at neurula stages, the MCCs, ionocytes and SSCs migrate apically in separate waves to radially intercalate into the outer layer, where they will complete their differentiation (Cibois, 2014). Strikingly, however, only MCCs display a regular pattern of distribution in the mature epithelium. Although the precise physiological function of

Xenopus MCCs remains to be addressed, a regular pattern of distribution may be optimal to homogenize fluid flows powered by beating cilia. MCCs always insert into the outer layer individually and exclusively in correspondence of junctions among at least three outer-layer goblet cells (vertices) (Chung et al., 2014; Deblandre et al., 1999; Stubbs et al., 2006). Radial intercalation involves a first phase in which immature MCCs in the inner layer emit apically-polarized protrusions to probe outer-layer vertices, followed by a phase of apical expansion, when their apical aspect actually emerges at the surface of the outer layer and progressively expands in its plane to allow for cilia assembly (Chung et al., 2014; Stubbs et al., 2006)(Sedzinski et al., 2016). While multiple studies have addressed the cellular and molecular mechanisms of radial MCC intercalation (Sirour et al., 2011)(Kim et al., 2012)(Chung et al., 2014)(Werner et al., 2014)(Sedzinski et al., 2016, 2017), how the regularly dispersed pattern of mature MCCs is generated remains to be resolved. It has been suggested that MCC pattern formation may result from an interplay between the mechanisms that define the numbers of committed immature MCCs and the number and distribution of outer-layer vertices available for intercalation (Deblandre et al., 1999; Stubbs et al., 2006; Werner and Mitchell, 2012). While these two parameters are indisputably involved, it is unclear whether they are sufficient to explain pattern emergence. Here, we hypothesize that MCC movement may be another key ingredient, which has never been evaluated. Using transient transgenesis, we could record the movements of immature MCCs in the inner layer, and concluded that MCC spacing pattern was largely established prior to intercalation. Using mathematical modelling, we found that mutual repulsion among MCCs and affinity for outer-layer intercellular junctions are sufficient to account for the final dispersed pattern. These two behaviours were readily apparent from our live recordings. Confirming the importance of MCC movements, inhibition of ARP2/3-mediated actin remodelling impaired lamellipodia-like protrusions in MCCs, homotypic MCC repulsion and MCC spacing pattern, without affecting intercalation. We also uncover a hitherto unknown role of the signalling pathway dependent on the interaction between the transmembrane tyrosine kinase receptor Kit, expressed in MCCs, and its ligand Scf, expressed in outer-layer cells, for MCC pattern emergence. The SCF/KIT signalling

pathway has a well-established role in controlling actin cytoskeleton and cell motility in a variety of vertebrate systems (Lennartsson and Ronnstrand, 2012; Meininger et al., 1992; Runyan et al., 2006; Samayawardhena et al., 2007; Wehrle-Haller et al., 2001; Zuo et al., 2016) and KIT stimulation with SCF was found to result in the phosphorylation and activation of ARP2/3 (Mani et al., 2009). Using a variety of functional assays, we established the capacity of the Scf/Kit system to promote both the repulsive and adhesive interactions predicted *in silico*, and thus identified for the first time a major regulator of the *Xenopus* MCC patterning process. This work illustrates how a large cell population can self-organise to adopt a regular spacing pattern, through semi-random movements constrained by a balance between repulsive and attractive cues.

RESULTS

Emergence of MCC ordered pattern precedes radial intercalation.

Fluorescent In Situ Hybridization (FISH) of *Xenopus* embryos with the MCC marker *α-tubulin* (*α-tub*) revealed that at stage 14 (early neural plate stage), immature MCCs were irregularly distributed within the non-neural ectoderm inner layer (Figure 1A) and very often in direct contact with each other (Figure 1B). Co-staining with an antibody against the tight junction protein ZO-1, to mark outer-layer apical tight junctions, also showed that at this stage *α-tub*-positive MCCs were not positioned in correspondence of outer-layer vertices (Figure 1A, 1C). In the course of development, however, *α-tub*-positive MCCs were increasingly often found as separate cells (Figure 1A, 1B), and progressively localized each in correspondence of an individual vertex (Figure 1A, 1C), into which they finally inserted, thus progressively taking up an apparently more orderly pattern (Figure 1A). To quantify the progression from an irregular to a regular distribution, we developed an order index based on Delaunay triangulation of the centroids of *α-tub*-positive cells. Such an index is inversely proportional to the variation of distances among centroids and would reach its highest value when MCC centroids are perfectly ordered in staggered rows. As

shown in Figure 1D, the order index of the MCC population progressively increased from stage 14 through stage 25, when MCCs are intercalated into the outer layer.

The apparent increase in order may result non-exclusively from selective death or cell fate reversal of misplaced MCCs, or from MCC movements. Fluorescent detection of the apoptotic executioner Caspase 3/7 activity as a proxy of apoptosis failed to reveal dying cells in the ectoderm of control embryos from stage 15 to stage 18, as opposed to cycloheximide-treated embryos (Trindade et al., 2003) (Figure S1A and movie S1). To evaluate the possible contribution of cell-fate reversal, we performed *α-tub* FISH in embryos from a transgenic line expressing RFP under the control of the MCC-specific α-tub promoter (Stubbs et al., 2006). Due to the long RFP half-life (26h), any immature MCC switching its identity to that of a different inner layer cell type should retain RFP fluorescence while losing endogenous *α-tub* transcripts. Such cases were never observed, ruling out MCC fate reversal during normal development (Figure S1B, S1C). In contrast, we noticed that robust *α-tub* signal was occasionally detected in RFP-negative cells, compatible with events of asynchronous MCC specification (Figure S1B, S1C).

The lack of MCC death or fate reversal led us to favour the hypothesis that cell motility might play a major role in the progressive emergence of a regular pattern of MCC distribution.

Time-lapse video microscopy reveals MCC motility

To evaluate whether MCCs are motile, we injected embryos with constructs carrying the fluorescent markers GFP or LifeActGFP (Belin et al., 2014) under the control of the α-tub promoter, and followed the behaviour of labelled MCCs in living embryos. Despite the high degree of mosaicism, which restricted transgene expression to a small percentage of MCCs, fluorescence levels were sufficient to allow live recording starting from stage 14 and for a duration of up to 8 hours. Spinning-disk confocal video microscopy showed that GFP-expressing MCCs indeed moved actively within the plane of the inner layer until they stopped in correspondence of vertices where they began to intercalate (Figure 2A and movie 1). As the F-

actin-binding reporter LifeActGFP allowed for much better visualisation of the whole cell shape and of cellular protrusions, we exploited it for most of our subsequent experiments. We thus found that LifeActGFP-expressing MCCs extended and retracted actin-rich lamellipodia-like processes within the ectoderm inner layer and progressively changed their shape from flat mesenchymal to more compact and pyramidal (Figure 2B and movie 2). These observations suggested that cell motility may indeed be important to establish a regular MCC pattern.

A cell motility-based mathematical model for MCC pattern establishment.

We next built an energy-based mathematical model to identify the minimal ingredients necessary to recapitulate the observed self-organisation of motile MCCs. In this simplified model, MCCs can move in a bi-dimensional plane against a network representing outer-layer junctions (see STAR methods). As homotypic repulsion is often required for homogeneous dispersion of motile cellular populations (Davis et al., 2012; Villar-Cervino et al., 2013), we introduced a first term related to MCC mutual repulsion, such that proximity to another MCC increased energy (see STAR methods). In addition, we reasoned that homing of MCCs to outer-layer vertices must imply a marked affinity for epithelial junctions. Thus, we introduced a second term related to affinity, such that the overlap of MCCs with junctions decreased energy (see STAR methods). The model also included a steric constraint in the form of a hard-core potential, to prevent complete overlap between MCCs. Starting from a random spatial distribution of MCCs, a standard Monte-Carlo scheme was used to allow system evolution. At each step, any given MCC was assigned a random, diffusion-like prospective displacement. A displacement was systematically accepted if it lowered the system total energy. If on the contrary it increased system energy, its acceptance probability decayed exponentially with energy increase (see STAR methods). This eventually led the system towards equilibrium configurations. In an affinity-dominated regime (i.e. when the contribution of mutual repulsion is negligible), MCCs rapidly re-located at nearby vertices, where they could maximise their interaction with outer-layer junctions and minimize their energy. However, this occurred regardless of the position of other MCCs, so that no overall regularity of

distribution was observed (Figure 2C and movie 3). In contrast, in a repulsion-dominated regime, MCCs repelled each other and distributed according to a regular pattern that maximized their mutual distance, regardless of the position of outer-layer vertices (Figure 2D and movie 4). Finally, in an intermediate regime in which the repulsion and affinity terms were commensurate, a trade-off situation was observed, in which MCCs both located at outer-layer vertices and dispersed homogeneously (Figure 2E and movie 5; also see STAR methods). Thus, self-organised MCC distribution can be captured in a simple mathematical model where movements are constrained by homotypic repulsion and affinity for outer-layer junctions.

Mutual repulsion and affinity for outer-layer junctions underlie MCC pattern establishment.

We next explored whether MCC mutual repulsion and affinity for outer-layer junctions predicted to be important in our *in silico* model were indeed detectable *in vivo*. In cases where low mosaicism allowed for visualisation of several neighbouring LifeActGFP-expressing MCCs we found that, whenever in the course of their movements two such cells came into contact, they withdrew from each other (Figure 3A and S2A and movie 6). Overall, the average time of contact between two LifeActGFP-expressing cells was calculated at 12.11+/-18.96 minutes (average +/- SD) (Figure 3F). On the other hand, imaging of embryos simultaneously injected with α-tub::LifeActGFP and with a synthetic mRNA coding for a membrane-localized form of RFP to label outer-layer cells revealed that, while in the inner layer, most MCCs preferentially moved along the junctions among outer-layer cells (92.55% of 94 analysed MCCs closely followed outer-layer junctions over >2hrs) (Figure 3B, 3G and movie 7). These observations confirmed that homotypic repulsion and affinity for outer-layer junctions are likely important for the emergence of a regular MCC pattern.

The actin cytoskeleton appeared to be involved in both MCC mutual repulsion and in their affinity for outer-layer junctions. MCCs often established transient contacts with each other via LifeActGFP-enriched lamellipodia-like structures that were subsequently retracted (Figure 3A and

S2A) and LifeActGFP-rich cellular protrusions were apically extended by MCCs as they crawled along junctions among outer-layer cells (Figure S2B and movie S2).

As a first step towards dissecting the role of the actin cytoskeleton in MCC patterning, we took advantage of well-characterised pharmacological inhibitors of the two main pathways of actin polymerisation: CK-666, an inhibitor of the actin-branching nucleator ARP2/3 (Hetrick et al., 2013) and SMIFH2, an inhibitor of the actin-bundling factor FORMIN (Rizvi et al., 2009). FISH for *α-tub* coupled with ZO-1 IF on embryos treated with 100µM CK-666 from stage 12 and fixed at stage 25 showed that most MCCs had properly emerged at the outer-layer apical surface (Figure S2C), but were irregularly distributed and often in direct contact with one another (Figure 3D, 3H, 3I). Consistent with this observation, spinning-disk confocal video microscopy of α-tub::LifeActGFP- and mRFP-injected embryos treated with CK-666 showed a decrease in mutual repulsion among MCCs (average time of contact +/- SD: 48.54+/-49.10 min) (Figure 3F) and formed small clusters (movie S3). On the other hand, in CK-666-treated embryos, MCCs still moved preferentially along outer-layer junctions (92.31% of 26 analysed MCCs) (Figure 3G). An apparent increase in the occurrence of spiky filopodia-like structures over broader, lamellipodia-like ones (Figure S2D, S2D' and movie S3), reminiscent of what has been described in ArpC3$^{-/-}$ murine fibroblast (Suraneni et al., 2015) was also observed. Interestingly, a fusion protein between the p41 subunit of the actin-branching nucleator ARP2/3 and EGFP, specifically expressed in MCCs by means of the α-tub promoter together with LifeActRFP, accumulated just behind the leading edge of the LifeActRFP-rich protrusions and was quickly relocated when these collapsed and reformed at different cellular locations following MCC contacts (Figure S2E and movie S4).

In contrast to what we observed following CK-666 treatment, in embryos treated from stage 12 with the FORMIN inhibitor SMIFH2 at 50µM, MCCs were properly dispersed and positioned at vertices, but their apical emergence at stage 25 was delayed (Figure 3E, 3H, 3I and Figure S2C), in agreement with published data (Sedzinski et al., 2016). Our results thus reveal the importance of actin cytoskeleton-mediated cell movements in MCC patterning and uncover a possible

functional dichotomy between actin branching, required for MCC mutual repulsion and regular distribution, and actin bundling, involved in the actual intercalation and apical emergence of MCCs.

The Receptor Tyrosine Kinase Kit is expressed in MCCs, its ligand Scf in outer-layer cells.

Next, we searched for a molecular mechanism that could sustain self-organised MCC pattern emergence. We reasoned that both homotypic repulsion and affinity towards outer-layer junctions must involve cell surface molecules. Our attention was drawn to the Receptor Tyrosine Kinase (RTK) Kit, which has been identified as a transcriptional target of the MCC-inducing factor Multicilin/Mcidas in *X. laevis* epidermis (Kim et al., 2018; Ma et al., 2014; Stubbs et al., 2012). In addition, its transcripts have been detected by single-cell transcriptomics in *X. tropicalis* immature and mature MCCs (Briggs et al., 2018) (https://kleintools.hms.harvard.edu/tools/currentDatasetsList_xenopus_v2.html). As the signalling pathway dependent on KIT and its ligand SCF (Stem Cell Factor, also known as KITLG, Mast Cell Growth Factor or Steel Factor) is known to control actin cytoskeleton and cell motility, we hypothesized that it might also be involved in controlling the cellular behaviours that underlie the regular pattern of *Xenopus* MCCs. Whole-mount ISH with an RNA probe recognizing transcripts of both *kit-L* and *kit-S* homeologs detected expression by scattered cells in the non-neural ectoderm starting from early gastrula (stage 10) and persisting through later developmental stages (stage 26) (Figure S3A). FISH on sectioned embryos revealed that in the developing epidermis *kit* transcripts were exclusively co-expressed with the MCC markers *foxj1* and *α-tubulin* (Figure 4A). Conversely, expression throughout the developing non-neural ectoderm has been reported for *scf-L* and, at much lower levels, for *scf-S* (Goldman et al., 2006; Martin and Harland, 2004) (Figure S3B). RT-PCR on total mRNA from animal caps confirmed the expression of *scf-L* from stage 12 to 22, but failed to detect *scf-S* (Figure S3C). FISH revealed that *scf-L* transcripts were prevalently localised in the outer layer, with much lower levels of expression in the inner layer (Figure S3B'). In particular, *scf-L* expression was rarely detected and only at very low levels in *kit*-positive

MCCs (Figure 4B). Accordingly, single-cell transcriptomics revealed that in *X. tropicalis* non-neural ectoderm, expression of *scf* is highest in goblet cells and excluded from MCCs (Briggs et al., 2018) (https://kleintools.hms.harvard.edu/tools/viewTree.html?tree data/final_180213)

In many tetrapods, SCF is synthesised as a transmembrane molecule but alternative splicing of the exon 6 during mRNA maturation can remove a major serine-protease cleavage site. As a result, the exon 6-containing isoform is cleaved to release a soluble peptide, while the exon 6-spliced isoform can only be cleaved at much slower rates at other sites, and thus has a longer half-life as a cell membrane-associated molecule (Brannan et al., 1991; Flanagan et al., 1991; Lennartsson and Ronnstrand, 2012). Both soluble and membrane-anchored isoforms of SCF are able to activate the KIT receptor, albeit with different kinetics and biological outcomes (Gommerman et al., 2000; Lennartsson and Ronnstrand, 2012; Miyazawa et al., 1995; Tabone-Eglinger et al., 2014; Tabone-Eglinger et al., 2012). RT-PCR with primers encompassing exon 6 showed that only the exon 6-containing isoform of *scf-L* was detected in developing *Xenopus* ectoderm (Figure S3C). However, the amino-acid stretches coded by exon 6 in Scf-L and Scf-S have very low similarity to mammalian exon 6 and do not display obvious consensus sites for proteolytic cleavage (Hultman et al., 2007). To address the subcellular localisation of *Xenopus* Scf, we generated a construct coding for a C-terminal EGFP-tagged version of Scf-L (Figure 4C) and expressed it in the embryonic ectoderm alone or together with an RFP-tagged version of the tight junction protein ZO-1 (Higashi et al., 2016). Scf-GFP chimeric protein was primarily detected in the lateral plasma membrane of outer ectodermal cells, just basal to ZO1-RFP (Figure 4D, 4D'). However, Western blotting of lysates of Scf-GFP-injected animal caps with an anti-GFP antibody revealed the presence of a peptide compatible with cleavage at exon 6, together with the uncleaved full-length protein (Figure 4E). We thus assume that both membrane-anchored and soluble forms of Scf-L may be present in the developing *Xenopus* ectoderm.

Perturbations of the Scf/Kit signal disrupt MCC patterning

As a first step towards addressing the possible role of Kit signalling in MCC pattern establishment, we took advantage of the KIT tyrosine-kinase pharmacological inhibitor, axitinib (Hu-Lowe et al., 2008). Spinning-disk confocal video microscopy of α-tub::LifeActGFP- and mRFP-injected embryos treated with 50μM axitinib from stage 12 showed that MCCs displayed strongly decreased mutual repulsion (Figure 5A and movie 8) with a time of contact of 59.20+/-58.15min (average+/-SD) (Figure 5C), but maintained crawling along outer-layer junctions (91.07% of 56 analysed MCCs) (Figure 5C'). An *α-tub* FISH/ZO-1 IF time course on axitinib-treated embryos confirmed that MCCs were largely able to intercalate but did not disperse properly (Figure 5E, 5G-I). As an alternative method to impair Kit activity, we injected a dominant-negative form lacking the TK domain of the receptor (Goldman et al., 2006). Consistently, dn-Kit also caused severe disruption of MCC spacing, although apical emergence and ciliogenesis were largely preserved (Figure S4 and movie S5). Only few Kit-deficient MCCs, often still in direct contact to already inserted ones, were found trapped within the internal layer at stage 25 (Figure S4D').

To further confirm the involvement of Kit in MCC pattern establishment, we designed morpholino-modified antisense oligonucleotides (MOs) to block the translation of *kit-L* and *kit-S* mRNAs (MO-ATG-kit-L and MO-ATG-kit-S), or their splicing at the exon2-intron2 junction (MO-splice-kit-L and MO-splice-kit-S) (Figure S5A, S5B). After validation (Figure S5C, S5D), MOs were injected in the two animal ventral blastomeres of 8-cell embryos as cocktails of either MO-ATG-kit-L+S (10ng/blastomere) or MO-splice-kit-L+S (15ng/blastomere). Similar to axitinib-treated and dn-Kit-injected embryos, *α-tub* FISH and ZO-1 IF at stage 25 showed that *kit* MO-injected MCCs were properly intercalated but irregularly distributed and present in small clusters (Figure 5F-I). Co-injection of *kit* MOs with an mRNA coding for full-length Kit-S and carrying seven silent mutations rescued MCC dispersion, thus confirming that this phenotype could be specifically attributed to Kit inactivation (Figure S5E, S5E'). As splicing- and translation-blocking *kit* MOs yielded the same results (Figure S5F, S5F'), all subsequent

experiments were performed with the latter ones. Thus, spinning-disk confocal video microscopy of embryos injected with α-tub::LifeActGFP and 10ng/blastomere *kit* MO revealed that MCCs failed to separate from each other (average time of contact +/- SD: 58.48+/-53.31 min) and were compromised in their ability to follow outer-layer intercellular junctions (67.14% of 70 analysed MCCs followed junctions) (Figure 5B-C' and movie 9). Remarkably, *kit* MO-injected MCCs appeared to emit more filopodia-like than lamellipodia-like structures, similar to CK-666 treatment (Figure 5B' and movie 9).

As Kit function is likely to reflect interaction with its cognate ligand Scf, we then proceeded to address the effect of Scf knockdown on MCC pattern. MOs were designed to block the translation of both *scf-L* and *scf-S* mRNAs (MO-ATG-scf-L/S) (Goldman et al., 2006), or the exon2-intron2 splicing of the *scf-L* mRNA (MO-splice-scf-L) (Figure S6A, S6B). After validation (Figure S6C, S6D), 10ng/blastomere of MO-ATG-scf-L/S was injected in epidermal precursor blastomeres at 8-cell stage. *α-tub* FISH and ZO-1 IF at stage 25 showed defects in MCC dispersion (Figure 6A-D), while insertion into the outer layer appeared largely normal (Figure S6F). Injection of 10ng/blastomere of MO-splice-scf-L led to the same phenotype as MO-ATG-scf-L/S (Figure S6E, S6E') and this latter MO was used for all subsequent experiments. Spinning-disk confocal video microscopy of embryos injected with α-tub::LifeActGFP and Scf MO showed that MCCs displayed reduced repulsion (average time of contact +/- SD: 40.31+/-20.04 min) (Figure 6E, 6F and movie 10).

Remarkably, when *scf* MO was injected with mRFP at 16-cell stage to increase mosaicism, most MCCs at stage 25 were found at the border of, rather than within, Scf-depleted clones (Figure 6G). Analysis at stage 16 showed that MCCs were initially distributed homogeneously across *scf* MO-injected and uninjected areas, suggesting that the observed terminal distribution was due to migration of MCCs outside regions devoid of Scf. Spinning-disc video microscopy of areas straddling clonal boundaries showed that indeed, MCCs often left Scf-depleted regions and stopped migrating as soon as they encountered an uninjected outer-layer cell. Interestingly, a

majority of MCCs appeared to move across *scf* MO-injected regions without following outer-layer junctions (only 43.55% of 62 analysed MCCs follow junctions) (Figure 6H, 6I and movie 11). Strikingly, *in silico* simulations revealed that MCC accumulation at clonal boundaries could only be recapitulated when both MCC mutual repulsion and affinity towards outer-layer junctions were absent from clones surrounded by normal tissue (Figure 6J and movies 12-14). This suggests that Scf might be able to convey both a repulsive and an adhesive signal.

The Scf/Kit signalling system promotes both adhesive and repulsive functions.

Our data suggest that the Scf/Kit pathway supports both mutual MCC repulsion and MCC affinity for outer-layer junctions. As a first step to test this hypothesis, we ectopically expressed the Scf-GFP chimera in MCCs by means of the α-tub promoter. *α-tub* FISH and GFP IF at stage 25 showed that this resulted in large clusters of non-injected MCCs forming around Scf-GFP-expressing MCCs (Figure 7A-C). This suggests that high-level Scf expression creates a situation where adhesion dominates repulsion. Spinning-disc video microscopy further confirmed that Scf-GFP-expressing MCCs formed closely packed groups that did not dissociate over periods of more than 3h (Figure 7D and movie 15). We conclude from these data that Scf can act as a potent adhesive cue towards Kit-expressing MCCs.

We then tested whether the presence of the Kit receptor was sufficient to help dispersion of non-MCC intercalating cells. To this aim, embryos were injected with an mRNA coding for full-length Kit-S and subjected to FISH with a probe against the ionocyte marker, *v1a* (Quigley et al., 2011). In control embryos, ionocytes displayed an irregular pattern of distribution and were often found in adjacent positions (Figure 7E, 7H, 7I). In contrast, *kit* RNA injection endowed ionocytes with the capacity to disperse and adopt a more regular pattern of distribution (Figure 7F-I). This last set of experiments suggest that the Scf/Kit signalling system is sufficient to promote adhesive and repulsive functions, both necessary to establish a regular pattern of MCC distribution.

DISCUSSION

A cell movement-based view of *Xenopus* MCC patterning

Although *Xenopus* MCCs have been the object of extensive investigation in the past years, most studies have focused on their specification within the inner epidermal layer and their radial intercalation among outer-layer goblet cells. In contrast, much less is known on the mechanisms that control MCC distribution pattern. A pioneering study proposed that the MCC scattered pattern results from Notch-mediated lateral inhibition in the inner layer and the constraint of intercalation at outer-layer vertices (Deblandre et al., 1999). However, it was later shown that the outer layer can accommodate twice as many MCCs upon Notch inhibition, with no violation of the non-contiguity rule (Deblandre et al., 1999; Stubbs et al., 2006). This indicates that in normal condition, vertices are in large excess of incoming MCCs and that MCC spacing is not directly linked to the pattern of distribution of vertices. Our data are the first to unambiguously show that MCCs actively move within the inner layer and that motility is the main driver of their transition from a chaotic distribution, characterized by extensive inter-MCC contacts, to an orderly pattern, where MCCs are present as isolated cells, each localised in correspondence of an outer-layer vertex. In situations of severe actin or Scf/Kit pathway perturbations, we found that regular spacing between MCCs was lost despite proper intercalation. Thus, we can safely conclude that MCC pattern establishment occurs independently of radial intercalation. *In silico* simulation defined two conditions required to evenly distribute a population of internal motile cells below epithelial vertices: 1) motile cells must repel each other, thus minimizing their mutual contacts, 2) they must maximize their contacts with outer-layer junctions, so as to stabilize at vertices, which display the highest local density of junctions. Filming live MCCs in developing embryos allowed us to visualize these two behaviours and to reveal that actin cytoskeleton is involved in both. Immature MCCs in the inner layer extend unpolarized basolateral actin-rich protrusions with which they move and explore the surrounding environment. Whenever two such MCCs come into direct contact, the actin-rich protrusions involved in the contact are retracted, while others are deployed in different regions of the cell body, thus resulting in the two cells moving away from each other. Concomitantly, immature MCCs also emit apically-polarized actin-rich protrusions

towards junctions between outer-layer cells. Despite the fact that both basolaterally- and apically-directed actin protrusions largely coexist within each MCC, a clear temporal shift between the two is observed: over time, the basolateral protrusive activity decreases, while the apically-directed one gains in intensity and stability (see example in Figure 2B and movie 2). This shift correlates with a progressive decrease of MCC motility within the inner layer and enhanced stabilization under individual vertices. Presumably, this transition must be asynchronous among MCCs to allow for fine tuning of the spacing pattern over time. Consistent with this idea, we found evidence that MCC specification itself may be asynchronous (Figure S1). As a result, by early tailbud stage, all MCCs end up finding a free vertex at regular intervals, to which they anchor and through which they subsequently intercalate.

Self-organised generation of a regular cellular pattern by mutual repulsion and homing.

Our data show that within the inner layer of the developing *Xenopus* epidermis, immature MCCs move in a partially random fashion, their free displacements being constrained by mutual repulsion and affinity for outer-layer intercellular junctions, and that these movements are required for the establishment of a regularly-dispersed MCC pattern. This observation prompts analogies with other instances of developmental patterns emerging from the semi-stochastic movements of cell populations. Phenomena of contact-dependent homotypic repulsion in which mutually contacting cells withdraw projections and/or change direction of movement underlie the regular distribution of Cajal-Retzius (CR) neurons (Villar-Cervino et al., 2013) and Retinal Horizontal (RH) cells (Galli-Resta et al., 2002) in mammals, pigment cells in zebrafish (Walderich et al., 2016) and haemocytes in *Drosophila* (Davis et al., 2012). The case of *Xenopus* MCC patterning shows nevertheless some specificities. Most notably, MCCs are already present throughout most of the developing epidermis at the start of the patterning process, such that their scattering relies almost exclusively on short-range "wobbling" random movements, without need for a concomitant long-range directional migration as is the case for CR neurons. As a consequence, MCCs are unpolarised and lack a well-defined leading process. Moreover, unlike

418 *Danio* pigment cells, scattering MCCs are post-mitotic and the patterning system may not need to
419 adjust to variations in absolute cell numbers. Finally, in sharp contrast with *Drosophila*
420 haemocytes, which continue moving and repelling each other at every encounter, even after
421 regular distribution is reached, dispersed MCCs become fixed by anchoring and intercalating into
422 outer-layer vertices. Interestingly, to our knowledge, the only other described case of (semi-)
423 orderly epithelial intercalation of a population of individually dispersed motile cells occurs during
424 the development of the peripheral nervous system in the cephalochordate Amphioxus (Benito-
425 Gutierrez et al., 2005; Kaltenbach et al., 2009), but the underlying mechanisms are unknown.
426 Overall, our work reveals a new instance of self-organised tissue-wide developmental patterning,
427 emerging from the interplay of stochastic short-range repulsive and stabilizing intercellular
428 interactions, rather than relying on tightly controlled GRNs and classical guidance mechanisms.
429 This is probably the most information-parsimonious strategy to optimise the distribution of a cell
430 population whose function requires that its area of dispersion be covered completely but non-
431 redundantly. Our identification of a molecular pathway responsible for controlling MCC
432 dispersion, independently of cell numbers and differentiation, will make it possible to functionally
433 explore the physiological meaning of such a pattern and the possible outcome of its perturbation.
434
435 **Implementation of *Xenopus* MCC patterning by the SCF/KIT pathway.**
436 The molecular mechanisms controlling homotypic repulsion-mediated patterning have been
437 clearly identified in few cases only. The Eph RTKs and their ephrin ligands control the dispersion
438 of CR neurons in the mammalian cortex (Villar-Cervino et al., 2013). Protocadherins and the
439 immunoglobulin-superfamily proteins Dscams have been involved in the homotypic repulsion
440 phenomena underlying mammalian RH cells tiling (Fuerst et al., 2008; Ing-Esteves et al., 2018),
441 while the scattering of zebrafish pigment cells appears to rely on a variety of cell surface
442 molecules, among which connexins and a potassium channel (Irion et al., 2014; Iwashita et al.,
443 2006).

Our data show that the signal triggered by the interaction between the RTK Kit and its ligand Scf is required to establish the regularly dispersed pattern of *Xenopus* MCCs. Although this notoriously pleiotropic signalling pathway has been involved in many instances of cell migration, cell movement, cell adhesion, axonal guidance and cytoskeletal rearrangement, this is the first time that it has been shown to play a role in controlling the tissue-wide regular dispersion of a large cellular population. Remarkably, *kit* appears to be a direct transcriptional target of the multiciliogenesis master controller Multicilin/Mcidas (Kim et al., 2018; Ma et al., 2014; Stubbs et al., 2012). Such integration, through a common regulator, of fate determination and motility behaviour may explain how thousands of individual cells of the same type can self-organise to achieve a global collective pattern.

Our results are also remarkable in showing that the activity of a single receptor/ligand couple can result in the two opposite but temporally coexisting biological outcomes of MCC mutual repulsion and affinity for outer-layer junctions. Although these two phenomena might seem difficult to reconcile, the SCF/KIT signalling system has already been shown to promote apparently contrasting cell behaviours, such as migration and homing/adhesion, for example in melanoblasts (Jordan and Jackson, 2000; Wehrle-Haller and Weston, 1995), Hematopoietic Stem Cells (HSCs) (Heissig et al., 2002; Tajima et al., 1998) and Primordial Germ Cells (PGCs)(Gu et al., 2009; Gu et al., 2011; Runyan et al., 2006). Currently, the simplest and most widely accepted explanation, supported by *in vivo*, *ex vivo* and *in vitro* data, is that the membrane-bound and the soluble forms of the SCF ligand can both bind to and activate the KIT receptor, but with different kinetics, therefore triggering distinct, probably antagonistic signalling pathways and eliciting multiple cellular responses. In relevance to our work, soluble SCF has been shown to lead to transient activation of the KIT intrinsic TK activity, and to promote cell motility (Jordan and Jackson, 2000; Tabone-Eglinger et al., 2014; Tabone-Eglinger et al., 2012). Conversely, membrane-bound or immobilised SCF leads to formation of long-lived adhesive SCF/KIT complexes at the cell surface, independently of KIT TK activity (Tabone-Eglinger et al., 2014; Tabone-Eglinger et al., 2012). Our data show that the transmembrane Scf can be cleaved in *Xenopus* epidermis, thus

raising the possibility that the dichotomy between membrane-associated and soluble Scf-dependent signals also controls the balance between adhesion and repulsion required for correct MCC patterning. It is easy to picture that the basolateral localisation of transmembrane Scf in outer-layer cells might favour/stabilise the interaction of Kit-expressing MCCs with intercellular junctions, and even more so with vertices, where the density of the Scf signal is expected to be highest. This view is supported by our observations that MO-mediated depletion of Scf or Kit altered MCC migration along outer-layer junctions. In contrast, axitinib treatment did not cause the same defect, suggesting that TK activity is dispensable for MCC/outer cell interaction, consistent with published evidence (Tabone-Eglinger et al., 2014). Our ectopic expression assay also clearly demonstrated that full-length Scf can act as a potent adhesive cue towards Kit-expressing MCCs. Incidentally, it also revealed that the patterning system cannot afford Scf to be expressed in MCCs, consistent with our double FISH data, and with transcriptomic analysis suggesting that Mcidas negatively regulates *scf* (Ma et al., 2014).

By contrast, it is less simple to imagine how soluble Scf could promote MCC mutual repulsion. One possible explanation is that soluble Scf permeating the inner layer provides a motogenic signal, as described for example for mouse melanoblasts (Jordan and Jackson, 2000), thus keeping MCCs constantly moving around and dispersing until they are anchored to a free vertex by the strongly adhesive signal of membrane-bound Scf. Alternatively, the interaction between soluble Scf and Kit might initiate a cross-talk with other molecules expressed at the MCC surface and directly responsible for the mutual repulsion response, such as ephrins and Ephs. However, the remarkable finding that the overexpression of wild-type Kit is sufficient to induce the dispersion of ionocytes suggests that the repulsive activity relies largely on the activity of Kit itself, without the need for other, MCC-specific cell surface molecules. It is thus likely that the signalling cascade connecting Kit to the cytoskeletal effectors of cell repulsion and adhesion is a rather direct and short one.

Scf/Kit signalling and MCC actin cytoskeletal dynamics.

Our data from pharmacological inhibition experiments suggest that different modes of actin polymerization, required for the formation of distinct types of cellular protrusions, control separate aspects of MCC behaviour. Following treatment with CK-666, an inhibitor of the actin-branching factor ARP2/3, MCCs present more filopodia-like extensions, show decreased mutual repulsion and major patterning defects, but no intercalation abnormalities. On the other hand, treatment with the actin bundling inhibitor SMIFH2 strongly delays intercalation without affecting patterning. The SCF/KIT pathway has been shown to control ARP2/3 activation (Mani et al., 2009) and in our model system its inhibition indeed results in defects similar to those due to CK-666 treatment: MCCs make filopodia-like protrusions and present patterning defects but are able to insert into the outer layer. Both CK-666 treatment and Scf/Kit pathway inhibition also increase the duration of MCC mutual contacts. Arp2/3 -/- fibroblasts, in which motility only relies on filopodia, show defects in mutual repulsion-dependent collective cell movements, such as those involved in wound healing (Suraneni et al., 2012).

We can thus propose a model in which the main role of the Scf/Kit pathway in *Xenopus* immature MCCs is the promotion of actin-based protrusions: Kit activation by soluble Scf would induce transient basolateral lamellipodia, required for redirecting MCC movements away from each other after mutual contact; membrane bound SCF would stabilize the more persistent apical protrusions required for anchoring MCCs to the vertices. Such a model warrants future validation by cell biological and biochemical approaches.

Conclusions

We show here that, during development, seemingly complex and highly ordered cell patterns can be obtained by the combination of two relatively simple cell behaviours, without need for a highly regulated patterning system. Moreover, deployment of the same signalling system, presumably activated with different kinetics by soluble and membrane-anchored forms of a single ligand, can control both behaviours. This further stresses the importance of self-organising systems in developmental biology.

ACKNOWLEDGMENTS

AC was supported by a doctoral fellowship from the French Ministry for Higher Education, Research and Innovation (MESRI). CR was supported by a postdoctoral fellowship from the Turing Centre for Living Systems (CENTURI). The project leading to this publication has received funding from Excellence Initiative of Aix-Marseille University - A*MIDEX, a French "Investments for the Future" program (Projet 'Pépinière d'Excellence 2017 to AP). The work was also supported by funding from Cancéropôle PACA (Programme Emergence 2017to AP), the Fondation pour la Recherche Médicale (DEQ20141231765, EQU201903007834 to LK), and the Association pour la Recherche contre le Cancer (PJA 20141201815 to LK). Imaging was performed on PiCSL-FBI core facility supported by the French National Research Agency through the "Investments for the Future" program (France-BioImaging, ANR-10-INBS-04). We are indebted to E. Bazellières, J. Christian, R. Harland, C. Kintner, A. Miller, M. Ogawa, O. Rosnet and J-P. Tassan for the gift of plasmids. We thank F. Roguet for *Xenopus* husbandry. We warmly thank Anna Adamiok, Marie Cibois and Marie Zilliox for preliminary experiments, Marc Billaud, Claudio Collinet and Laurence Röder for insights on the project, past and present members of the Kodjabachian laboratory, in particular Camille Boutin and Olivier Rosnet, for discussions, help and technical support, Elsa Bazellières and Vincent Bertrand for insightful comments on the manuscript.

AUTHOR CONTRIBUTIONS

Conceptualisation: AC, LK, AP. Methodology: AC, RC, CR, VT, AP. Software: RC, CR. Formal analysis: AC, RC, CR. Investigation: AC, RC, CR, VT, AP. Validation: AC, CR, VT, RC, LK, AP. Resources: LK. Supervision: LK, AP, RC. Project administration: LK, AP. Funding acquisition: LK, AP, RC. Writing - original draft: AC, AP. Writing - review and editing: LK, AP.

DECLARATION OF INTERESTS

The authors declare no competing interests.

FIGURE LEGENDS

Figure 1. The orderly pattern of mature MCCs results from progressive changes in cell distribution.

A: Fluorescent *In Situ* Hybridization (FISH) was used to reveal *α-tubulin*-positive immature MCCs (green), combined to immunofluorescence against the tight junction protein ZO-1 to reveal outer-layer intercellular junctions (white). In the course of development, MCCs were increasingly found as isolated, regularly-shaped cells, each localised in correspondence of a single outer-layer vertex. Scale bar is 25μm. **B:** Graph showing the percentage of *α-tub*-positive cells directly in contact with varying numbers of other *α-tub*-positive cells (gray-shaded from 0 to to ≥4). **C:** Graph showing the number of ZO-1-positive outer-layer vertices superimposable onto the planar projection of each *α-tub*-positive MCC. **D:** Graph showing the order index calculated from Delaunay tessellation of the centroids of *α-tub*-positive cells. The order index increased during development, reflecting the progressive transition from a chaotic to an orderly MCC distribution.

Figure 2. *In silico* modelling of MCC behaviour reveals that mutual repulsion and affinity for outer-layer junctions are required for proper pattern establishment.

A: Spinning disk confocal video microscopy was used to track α-tub::GFP transgenic MCCs within the inner epidermal layer. Still frames from movie 1 are shown. Asterisks point two MCCs that moved under mRFP-injected outer-layer cells. Blue and orange dots serve as landmarks to appreciate MCC mobility. **B:** Still frames from movie 2. α-tub::LifeActGFP revealed an intense actin-based protrusive activity that progressively shifted from the basolateral to the apical aspect of the cell. **C-E:** Frames from simulation movies 3, 4 and 5, respectively. The black meshwork represents outer-layer intercellular junctions, and red circles the underlying MCCs. The upper row

shows the initial random distribution of MCCs, the bottom row shows the final patterns obtained under the different regimes. **C:** In a regime where MCC affinity for outer-layer junctions dominated, MCCs localised at vertices, but failed to disperse properly. **D:** In a regime where MCC mutual repulsion dominated, MCCs were regularly distributed, but did not localise at vertices. **E:** In a regime where mutual repulsion and affinity for outer-layer junctions were balanced, MCCs were dispersed and positioned at vertices.

Figure 3. MCCs display both behaviours of mutual repulsion and affinity for outer-layer junctions.

A: Frames from movie 6. α-tub::LifeActGFP labelling revealed that whenever MCCs came in contact via actin-based lamellipodia, these subsequently retracted. **B:** Frames from movie 7 showing an α-tub::LifeActGFP-labelled MCC (magenta asterisk) moving along the intercellular junctions among overlying outer-layer cells labelled by mRFP. The blue and the red arrowheads highlight the initial and final position of the labelled MCC. The last panel recapitulated the positions of the observed MCC over 3h. The black dotted line shows the displacement of the MCC centroid. **C-E:** Embryos were treated from stage 12 with 1% DMSO (C), 100μM ARP2/3 inhibitor CK-666 (D), and 50μM FORMIN inhibitor SMIFH2 (E) and analysed at stage 25 by *α-tub* FISH and ZO-1 IF to examine MCC patterning. **D:** Following CK-666 treatment, MCCs intercalated into the outer layer but were irregularly distributed. **E:** Treatment with SMIFH2 led to a normal MCC patterning but impaired apical insertion and expansion. In all cases, scale bar is 20μm. **F:** Graph showing the duration of MCC mutual contacts in control and CK-666 treated embryos. **** p-value < 0.0001 on a student t-test. **G:** Graph showing the proportion of MCCs that followed outer-layer junctions over a period of 2h. **H:** Graph showing MCC order index at stage 25 in CK-666-treated and SMIFH2-treated embryos vs control embryos. **I:** Graph showing the distribution of the number of contacts among MCCs at stage 25 in control, CK-666- and SMIFH2-treated embryos.

Figure 4. Expression of transcripts encoding Kit and its ligand Scf in the developing *Xenopus* epidermis.

A: Double FISH on sectioned embryos with probes against *kit* (green) and the MCC markers *foxJ1* or *α-tubulin* (red) revealed that *kit* was only expressed in MCCs. **B:** Double FISH on sectioned embryos showed that *scf-L* (red) expression was prominent in outer-layer cells and virtually undetectable in *kit*-positive MCCs (green). In **A** and **B**, DAPI (blue) highlights the nuclei. **C:** Schematic drawing of the Scf-GFP chimera, showing the extracellular (EC), transmembrane (TM) and intracellular (IC) domains of Scf-L (light blue), the C-terminal EGFP tag (green), the possible protease cleavage site in exon 6 (red arrowhead), as well as the sizes of the full-length protein and the membrane-retained cleavage product. **D:** Top view of live outer-layer cells from an embryo injected with mRNAs coding for the Scf-GFP (green) and the RFP-ZO-1 (red) fusion proteins. GFP fluorescence was localised at the membrane. Scale bar is 20μm. **D':** Orthogonal view of the intercellular junction within the dashed white box in **D** shows that the Scf-GFP chimera was mainly localised to the basolateral membrane, immediately basal to ZO-1. Scale bar is 5μm. **E:** Lysates from animal caps injected with mRNA coding for either GFP or Scf-GFP were subjected to Western blotting with an anti-GFP antibody. Single and double asterisks point respectively to the 55kDa full-length Scf-GFP and to the 37kDa band corresponding to the membrane-retained product of proteolytic cleavage at exon 6.

Figure 5. Inhibition of Kit activity disrupts MCC patterning.

A: Frames from movie 8. In 50μM axitinib-treated embryos, LifeActGFP-positive MCCs (green, magenta asterisk) failed to properly separate from each other. **B:** Frames from movie 9. In MO-ATG-kit-L+S-injected embryos, LifeActGFP-positive MCCs (green, magenta asterisk) failed to properly separate from each other. In **A** and **B**, mRFP (red) labelled outer-layer cell membranes. **B':** A close-up of the boxed area in **B**, showing highly-branched filopodia-like structures. **C:**

Quantification of MCC mutual contact times in control, axitinib-treated and MO-ATG-kit-L+S-injected embryos. **** p-value < 0.0001 on a student t-test. **C':** Graph showing the proportion of MCCs that followed outer-layer junctions over a period of 2h in control, axitinib-treated, and *kit* MO-injected embryos. **D-F:** *α-tub* FISH (green) and ZO-1 IF (white) showed that compared to control embryos (**D**) MCCs were irregularly distributed in axitinib-treated (**E**) and *kit* MO-injected (**F**) embryos at stage 25. In **F**, mRFP mRNA (red) was used as *kit* MO tracer. In all cases, scale bar is 20µm. **G:** Graph showing the percentage of MCCs intercalated into the outer layer at stages 20, 22 and 25. Intercalation was scored positive when MCCs displayed ZO-1 junctions. Kit inhibition delayed but did not prevent intercalation. **H:** Graph showing the distribution of the number of contacts among MCCs at stage 25 in control, axitinib-treated and *kit* MO–injected embryos The progressive dispersion of *α-tub*-positive MCCs is disrupted in Kit-deficient conditions. **I:** Graph showing MCC order index at stage 25 in axitinib-treated and *kit* MO-injected embryos vs control embryos.

Figure 6. Down-regulation of the Scf signal disrupts MCC patterning.

A, B: *α-tub* FISH (green) and RFP IF (red) revealed that compared to control embryos (**A**) MCCs were irregularly distributed in MO-ATG-scf-L/S–injected embryo (**B**) at stage 25. mRFP mRNA was used as *scf* MO tracer and to outline outer-layer cells. **C:** Quantification of MCC mutual contacts in control and *scf* MO-injected embryos. **D:** Graph showing MCC order index at stage 25 in *scf* MO-injected embryos vs control embryos. **E:** Frames from movie 10. In *scf* MO-injected embryos, LifeActGFP-positive MCCs (green) failed to properly separate from each other. mRFP (red) labelled outer-layer cell membranes. Asterisks label individual MCCs. Dots label two outer-layer cells for reference. **F:** Graph showing the duration of MCC mutual contact in control and *scf* MO-injected embryos. **** p-value < 0.0001 on a student t-test. **G:** *α-tub* FISH (green) and RFP IF (red) of embryos injected with *scf* MO at 16-cell stage and fixed at different developmental times. RFP was used as a MO tracer. MCCs were evenly distributed between MO-positive (red)

and MO-negative areas at stage 16 (left column) and accumulate at the boundary between the two areas at later stages (middle and right columns). **H:** Frames from movie 11, showing a LifeActGFP-positive MCC (yellow asterisk), which left its initial position within the MO-positive area (white arrowhead) and stopped at the boundary with the MO-negative region. In contrast, MCCs outside the MO-positive area did not significantly move. The yellow dotted line shows that the tracked MCC did not follow outer-layer junctions. In all cases, scale bar is 20μm. **I:** Graph showing that a majority of MCCs did not follow outer-layer junctions in *scf* MO-injected embryos compared to control. **J:** Frames from simulation movie 12. Mathematical modelling predicted that motile MCCs tend to accumulate at boundaries between regions devoid of both repulsive and attractive signals and normal regions.

Figure 7. Adhesive and repulsive activities of Scf/Kit signal.

A: *α-tub* FISH and GFP IF on stage 25 embryos injected with α-tub::Scf-GFP showed that non-injected *α-tub*-positive and Scf-GFP-positive MCCs formed aggregates. Scale bar is 50μm. **B:** A higher magnification view shows that non-injected *α-tub*-positive MCCs were tightly packed around Scf-GFP-positive MCCs. Scale bar is 20μm. **C:** Graph showing the distribution of the number of MCC mutual contacts in control and α-tub::Scf-GFP-injected embryos. **D:** Frames from movie 13 showing the stability of Scf-GFP-positive MCC clusters over time. Scale bar is 20μm. **E-G':** Control embryos (E) and embryos injected with 0.1 or 1ng mRNA coding for full length Kit-S, fixed at stage 25 and processed for FISH with the ionocyte marker *v1a*. IF against endogenous ZO-1 (E) or against co-injected mRFP (F, G) highlighted outer-layer junctions. Kit overexpression led to more regular dispersion of ionocytes compared to control. Scale bar is 50μm. **H:** Graph showing that ionocytes established fewer mutual contacts in Kit-S-injected than in control embryos. **I:** Ionocyte order index was increased in Kit-S-injected embryos with respect to control embryos.

STAR METHODS

Ethics statement

All procedures were performed following the Directive 2010/63/EU of the European parliament and of the council of 22 September 2010 on the protection of animals used for scientific purposes. Experiments on *X. laevis* were approved by the 'Direction Départementale de la Protection des Populations, Pôle Alimentation, Santé Animale, Environnement, des Bouches du Rhône' (agreement number F 13 055 21).

Embryo culture and injection

Ovulation was stimulated in *X. laevis* adult females from NASCO (https://www.enasco.com) by injection of (800 units/animal) Human Chorionic Gonadotropin (Chorulon^{R}). On the following day, eggs were recovered by squeezing, fertilized *in vitro* with sperm from NASCO males, de-jellied in 2% cysteine hydrochloride (pH 8.0) and washed, first in water, then in 0.1X MBS (Modified Barth's Saline). Embryos were kept in 0.1X MBS at 13°C, 18°C or 23°C until they reached the stage suitable for injection (8-cell or 16-cell), then transferred in 4% Ficoll in 1X MBS. Injections were performed using needles made from pulled glass capillaries and mounted on a Nanoject II injector (Drummond). Embryos were injected in animal ventral blastomeres to target the non-neural ectoderm. One blastomere (in 8-cell stage embryos) or two contralateral blastomeres (in 16-cell stage embryos) were injected, according to the desired degree of mosaicism.

Plasmids

Plamid name	backbone	linearized with	amount injected/blastomere	Reference
pαTub::GFP	pCS2+	NotI	50-60pg	Stubbs et al.

				2006
pαTub::RFP	pCS2+	NotI	50-60pg	Made in the lab
pαTub::LifeActGFP	pCS2+	NotI	50-60pg	
pαTub::LifeActRFP	pCS2+	NotI	50-60pg	
pαTub::EGFPp41	pCS2+	NotI	30-50pg	
pαTub::Scf-GFP	pCS2+	NotI	50-60pg	
pCS107-Scf-L-GFP	pCS107	NotI	//	
pαTub::MOresKit-S	pCS2+	NotI	//	
pCMV-MOresKit-S	pCMVSport	NotI	//	

All αTubulin promoter-based constructs were generated from pαTub::GFP (a gift from C. Kintner), either with the In-Fusion^{R} HD Cloning Kit (Takara Bio) or by standard restriction enzyme-mediated cloning.

For In-Fusion cloning, the pαTub:: backbone, excluding the GFP ORF, was PCR amplified using the Phusion^{R} High-Fidelity DNA Polymerase (New England BioLabs, #M0530) and the primers pαtubfor:5'-TCTAGAACTATAGTGAGTCGT-3' and pαtubrev:5'-CGACCGGTGGATCTGTTGTTGG-3'.

To generate pαTub::RFP, the RFP ORF was PCR amplified from the pCS2+mRFP plasmid (a gift from O. Rosnet) with the Phusion^{R} High-Fidelity DNA Polymerase and the primers InFuRFPfor:5'-CAGATCCACCGGTCGCATGGCCTCCTCCGAGGACGT-3' and InFuRFPrev:5'-CACTATAGTTCTAGATTAGGCGCCGGTGGAGTGGCG.

To generate pαTub::LifeActGFP, the LifeActGFP ORF was PCR amplified from the pmEGFP-Lifeact-7 plasmid (a gift from E. Bazellières) with the Phusion^{R} High-Fidelity DNA Polymerase and the primers InFuLifeactfor:5'-CAGATCCACCGGTCGTATGGGTGTCGCAGATTTGAT-3' and InFuLifeactGFPrev:5'-CACTATAGTTCTAGATTACTTGTACAGCTCGTCCA-3'.

To generate pαTub::LifeActRFP, the LifeActRFP ORF was PCR amplified from the pmRuby-Lifeact-7 plasmid (a gift from E. Bazellières) with the Phusion^{R} High-Fidelity DNA Polymerase

and the primers InFuLifeactfor:5'-CAGATCCACCGGTCGTATGGGTGTCGCAGATTTGAT-3' and InFuRFPrev:5'-CACTATAGTTCTAGATTAGGCGCCGGTGGAGTGGCG.

To generate pαTub::EGFPp41, the EGFPp41 ORF was PCR amplified from the EGFP-p41-Arc plasmid (a gift from M. Ogawa) with the Phusion^{R} High-Fidelity DNA Polymerase and the primers InFuEGFPfor:5'-CAGATCCACCGGTCGTATGGTGAGCAAGGGCGAGGAG-3' and InFup41rev:5'-CACTATAGTTCTAGATCACTTAATCTTCAGATCTTT-3'.

In all the above cases, the vector and insert PCR products were run on agarose/TAE gel, purified with the Macherey-Nagel^{TM} NucleoSpin^{TM} Gel and PCR Clean-up kit, then recombined using the In-Fusion^{R} HD Cloning Kit according to the manufacturer's instructions.

To make the pCS107-Scf-L-GFP construct, the pCS107-XlSteel1 plasmid (a gift of R. Harland), containing the Xl-Scf-L cDNA, was PCR amplified using the Phusion^{R} High-Fidelity DNA Polymerase and the primers Steel1fus-for:5'-GCCACAAATCCCCCTTGTAAAGT-3' and Scf1-3'endfus-rev:5'-TATAACACCGACATCAGTTGTGG-3', in order to generate a linearized backbone lacking the Scf-L stop codon and 3'UTR. The GFP ORF was PCR amplified from the pαTub::GFP construct using the Phusion^{R} High-Fidelity DNA Polymerase and the primers Scf1-GFPfus-for:5'-GATGTCGGTGTTATAGTGAGCAAGGGCGAGGAGC-3' and GFP3'Scf1fus-rev:AGGGGGATTTGTGGCTTACTTGTACAGCTCGTCACT-3'. Vector and insert PCR products were run on agarose/TAE gel, purified with the Macherey-Nagel^{TM} NucleoSpin^{TM} Gel and PCR Clean-up kit, then recombined using the In-Fusion^{R} HD Cloning Kit according to the manufacturer's instructions.

The pCS107-Scf-L-GFP plasmid was used both as template for making Scf-GFP mRNA and to generate the pαTub::Scf-GFP construct. To this aim, the Scf-L-GFP ORF was PCR amplified from pCS107-Scf-L-GFP using the Phusion^{R} High-Fidelity DNA Polymerase and the primers αtubSCFGFPfor:5-CAGATCCACCGGTCGTATGAAGAAGACAAAAACTTGG-3' and InFuLifeactGFPrev:5'-CACTATAGTTCTAGATTACTTGTACAGCTCGTCCA-3'. The gel-purified PCR product was recombined into the pαTub:: backbone using the In-Fusion^{R} HD Cloning Kit.

To generate the pCMV-MOresKit-S plasmid, the *kit-S* ORF was PCR amplified from the Dharmacon/GE clone 4030854 (*Xenopus laevis kit-b*), using the Phusion^{R} High-Fidelity DNA Polymerase and the primers αtubMOresKitSfor:5-CAGATCCACCGGTCGTGCTACAA**ATG**AG**T**CA**C**AT**C**CC**T**TT**T**CT**G**AC**T**GTCAGG -3' (in bold, the Kit-S start codon, in bold underlined the seven silent mutations introduced to generate mismatches with MO-ATG-kit-S) and αtuBKitSrev:5'-CACTATAGTTCTAGATCAGCCGTCGCTGTTCATCAACAG-3'. The gel-purified PCR product was recombined into the pαTub:: backbone using the In-Fusion^{R} HD Cloning Kit, thus creating the pαTub::MOresKit-S plasmid. This was subsequently cut with AgeI and NotI and the MOresKit-S ORF-containing fragment was ligated into AgeI/NotI cut pCMVSport6.

All constructs were made using the StellarTM Competent Cells (Clontech) transformed and grown according to the manufacturer's instructions. Small- and medium-scale plasmid preparations were performed with Macherey-Nagel^{TM} NucleoSpin^{TM} Plasmid QuickPure^{TM} and NucleoBond^{TM} Extra Midi kits.

mRNA synthesis

Sense mRNAs were synthesized from linearized plasmids with the Ambion mMessage mMachine kit® (Life Technologies) according to the details provided in the table below, then purified with Macherey-Nagel^{TM} NucleoSpin^{TM} RNA Clean-up kit. After determination of the concentration, aliquots were kept at -80°C.

Plasmid name	**Vector**	**Linearised with**	**Transcribed with**	**Amount injected /blastomere**	**Reference**
pCS2+mRFP	pCS2+	NotI	Sp6 RNA pol	0,5 ng	
pCS2+GFPgpi	pCS2+	NotI	Sp6 RNA pol	0,5ng	Chartrain et al., 2003

pCS107-Scf-L-GFP	pCS107	NotI	Sp6 RNA pol	1 ng	Made in the lab
pCS2+RFP-ZO1	pCS2+	NotI	Sp6 RNA pol	1ng	Higashi et al., 2016
pCS2+dnKit	pCS2+	NotI	Sp6 RNA pol	0,5ng	Goldman et al., 2006
pCMV-dnKit-GFP	pCMVSport6	NotI	Sp6 RNA pol	0,5g	Made in the lab
pCMV-MOresKit-S	pCMVSport6	NotI	Sp6 RNA pol	0.1-1ng	Made in the lab

Morpholinos

Morpholinos (MOs) were purchased from GENE TOOLS®. ATG-kit-L-MO and ATG-kit-S-MO were injected together at 10ng/MO/blastomere. kit-S-e2i2spl-MO and kit-L-e2i2spl-MO were injected together at 15ng/MO/blastomere. ATG-scf-L/S-MO was injected at 10ng/blastomere and scf-L-e2i2spl-MO at 20ng/blastomere. The blue-tagged version of ATG-scf-L/S-MO was injected at 20ng/blastomere.

MO name	Sequence
ATG-kit-L-MO	5'-TCGTAAAGGATGGAAAGTGGCTCAT-3'
ATG-kit-S-MO	5'-CCGTAAGGAATGGAATATGGCTCAT-3'
kit-S-e2i2spl-MO	5'-TGTAACCTTATGAATGACTTACCCT-3'
kit-L-e2i2spl-MO	5'-GGAACCCAATGAATGACTTACCCTT-3'
ATG-scf-L/S-MO	5'-GGTAGCTTGTCTATTATCCCCTTAG-3'
scf-L-e2i2spl-MO	5'-TGGCTAGGTAAAACTCTTACCAGTT-3'

Pharmacological inhibitors

Stock solutions of pharmacological inhibitors (all from Sigma-Aldrich®) were prepared in DMSO and added to embryos cultured in MBS 0,1X at the stages and concentrations and for the times shown in the following table. Cycloheximide treatment was perform by incubating embryos at stage 14 in MBS 0,1X containing 300µM cycloheximide two hours before live imaging.

Drugs	Source	Reference	Concentration in 0,1X MBS	Incubation time and stage
Axitinib	Sigma-Aldrich	AG-013736	50µM	From stage 12
CK-666		SML0006	100µM	
SMIFH2		S4826	50µM	
Cycloheximide		C7698	300µM	From stage 14

Apoptosis detection:

The CellEvent™ Caspase-3/7 Green Detection Reagent (Invitrogen™) was dissolved in DMSO and added to stage 14 control or cycloheximide-treated embryos in MBS 0,1x at 20µM final concentration.

***In situ* hybridization and immunostaining**

Whole-mount chromogenic In Situ Hybridization (ISH) and whole-mount Fluorescent In Situ Hybridization (FISH) were performed as previously detailed (Castillo-Briceno and Kodjabachian, 2014; Marchal et al., 2009). Embryos were fixed in MEMFA (0.1 M MOPS pH 7.4, 2 mM MgSO4, 1 mM EGTA, 3.7% v/v formaldehyde) 1h30 at room temperature or overnight at 4 °C then dehydrated o/n in 100% methanol at −20 °C. For FISH on section, embryos were fixed in MEMFA, stored in methanol o/n at −20 °C, rehydrated in PBT (PBS + Tween 0.1% v/v), treated with triethanolamine 100mM and acetic anhydride, incubated in increasing sucrose concentrations,

800 embedded in OCT (VWR Chemicals), cut in 12 µm-thick cryosections and stored at -80°C. Before
801 hybridization, embryos were rehydrated in PBT (PBS+0.1% Tween20), treated with Proteinase K
802 (8 min at 2 µg.ml^{-1}), then, for FISH, the endogenous peroxydase activity was blocked by
803 incubation with H_2O_2 3% in PBS for 20 min. For single staining, RNA probes were labeled with
804 digoxigenin-dUTP (Roche). For double staining, various combinations of digoxigenin/fluorescein-
805 labeled riboprobes were used. For each hybridization, the following amounts of riboprobes were
806 used: *α-tubulin* 1ng; *v1a* 40 ng; *foxj1* 100ng; *kit* 200ng; *scf-L* 100ng to 300ng for embryos at stage
807 11-16 and stage19-20, respectively. Hybridization was performed overnight at 60 °C. After
808 hybridization, the embryos were washed at increasing stringency in SSC/0.1% CHAPS, rinsed
809 extensively in MABX (Maleic Acid Buffered solution +0.1% Triton X), then the digoxigenin-
810 labelled probe was revealed through incubation with a sheep anti-DIG antibody conjugated to HRP
811 (POD) (Roche, 1:500). On the third day, embryos were extensively washed in MABX, then
812 staining was revealed using Tyramide Signal Amplification—TSA TM Plus Cyanine
813 3/5/Fluorescein System (PerkinElmer®). This reaction was then blocked in a bath of 2% H2O2 for
814 20 min.
815 Following FISH labeling, immunostaining was performed by incubating the embryos in MABX-
816 BR2%, 15% FBS with the antibodies listed in the following table. After extensive washes in
817 MABX, embryos were flattened by cutting along the antero-posterior axis and mounted in Mowiol
818 (Sigma-Aldrich) for confocal imaging.

Antibody	**Species**	**Source**	**Dilution**
ZO1-TJP1	Mouse IgG1	Thermo Scientific	1:200
GFP	Chicken	Aves Labs	1:500
RFP	Rat monoclonal IgG2a	Chromotek	1:500
Alexa Fluor 568 anti-rat	Goat	Molecular	1:500

Alexa Fluor 488 anti-chicken	Goat	Probes	1:500
Alexa Fluor 647 anti-mouse IgG1	goat		1:800

Confocal and electron microscopy

To limit the movement of the embryo during live imaging, control or treated stage 14-15 embryos were embedded in 0,8% LMP agar in 0,1X MBS within a small chamber made with two coverslips and silicon grease. Time-lapse imaging was done at 23°C starting at stage 14-15 and for a duration of 2 to 8 hours on a Nikon Roper spinning disc Eclipse Ti inverted microscope using a 20X_objective (for apoptosis recording), or 40X/60X _1.25 N.A water-immersion objective (for all the other experiments). Image acquisition was performed with the Meta-Morph software. 20µm-deep Z sections were acquired every 0,5 to 2min in 0,5 to 0,7µm steps, averaging 2. To compensate for the fluorescence intensity variations across different injected embryos, the laser power was adjusted for each experiment. Excitation wavelengths were 488nm, 561nm and 445nm for GFP- and RFP- tagged protein and for blue-tagged MO, respectively.

Fixed whole embryos and sections were examined on Zeiss LSM 510 and 880 confocal microscopes. Four-color confocal Z-series images were acquired using sequential laser excitation, converted into single plane projection and analysed using ImageJ/FIJI software (see image analysis section).

For Scanning Electron Microscopy (SEM), stage 27 control or treated embryos were fixed for 4h in 3% glutaraldehyde in 0.1 M phosphate buffer pH 7.4 (19 mL monosodium phosphate 0.2 M and 81 mL disodium phosphate 0.2 M), washed in phosphate buffer and filtered bi-distilled water, progressively dehydrated in ethanol at 25%, 50%, and 70% for 30 min each time, then stored in fresh ethanol 70% at 4 °C o/n. Embryos were further dehydrated with vigorous agitation once in 90% ethanol, and twice in 100% ethanol, for 30 min each, then subjected to CO_2 critical point desiccation (CPD030, Balzers) at 40 °C and 75-80 bars. Finally, samples were sputter-coated with

gold (vacuum 1 × 10–12 Torr, beam energy 3–4 keV) and stuck on the support with conductive glue for immediate SEM digital imaging (FEI TENEO) of the skin epidermis.

Image analysis

All images were processed with the imageJ/Fiji free software.

Z-stacks from confocal video microscopy were converted into single plane projection by maximum intensity or sum intensity projection. Each channel was processed separately with the optimized z-section corresponding to the outer/inner layer cell staining. All visible MCCs were manually tracked with the 'manual tracking' plugin. Cell contact events were estimated by counting the time between the first and the last non-ambiguous contact time points. Cell contacts already established at the beginning of filming or persisting beyond its end were excluded from quantification.

To characterize the migratory path of MCCs relative to outer-layer cell junctions the following criteria were applied: MCC emits protrusions in correspondence of outer-layer cells junctions; overlap between MCC shape and outer-layer cells junctions; correlation between direction of MCC migration and orientation of the outer-layer cells junctions. Cells already engaged in radial intercalation with permanent contact with vertices and ambiguous cases were removed from quantification.

Analysis of the apical-basal global cell-shape was done through maximum intensity projections of resliced z-stacks following X,Z and Y,Z orientations with 0,5µm interval from images at the indicated time point. Analysis of Scf-GFP/ZO-1RFP signal localization was done on resliced z-stacks from z-series at 0.2µm intervals, taken along chosen intercellular junctions. 3D-projection of intercalating MCCs probing junctions and vertices was made using the 'clear volume' plugin.

To check for the depletion of Scf-GFP protein by a blue-fluorescent tagged version of ATG-scf-L/S-MO in live we proceeded as follows: mRNAs coding for Scf-GFP and mRFP were co-injected in the two animal ventral blastomeres at stage 8-cell stage, then blue-tagged ATG-scf-L/S-MO was injected in two of the four animal ventral blastomeres at 16-cell stage. GFP, RFP and blue fluorescence were recorded at stage 16.

Images from fixed whole embryos and sections obtained with 510 and 880 LSM confocal microscopes were converted into single plane projection by maximum intensity projections. To calculate MCC and ionocyte mutual contacts and order indexes, as well as the relation of MCCs to vertices and their intercalation, the outlines of individual *α-tubulin*- or *v1a*-positive cells were manually drawn from maximum intensity projections of 20X 450x450µm images using Wacom® Intuos Pro graphic tablet and FIJI 'ROI manager' tool. Mutual contacts and overlapping to ZO-1-positive vertices were manually defined. MCCs were considered intercalated when their apical surface was clearly outlined by a ZO-1 signal. Ambiguous cases were classified as 'non defined' (nd). To calculate the Order Index, cell areas and centroids were defined and the data processed as described in the section 'Mathematical Modelling'.

Western blots

Animal caps were obtained by manual dissection from stage 10 embryo in 1X MBS (Sive et al, 2000) and kept in 0,5X MBS until matched control embryos reached stage 17-18, then snap-frozen in liquid nitrogen and stored at -80°C or immediately lysed by boiling for 5min in 50mM Tris-HCl (pH 7.5), 2% w/v SDS, 1mM DTT. After addition of 5x Bromophenol blue/Glycerol, samples were loaded on Acrylamide PAGE gels and run using the Hoefer™ Mighty Small™ II Mini system with Tris/Glycine/SDS buffer. Transfer to nitrocellulose membranes was performed in Tris/Glycine/Ethanol buffer using the Hoefer™ TE22 Mini Tank Blotting Unit. Membranes were rinsed with water, stained with Ponceau Red, washed three times for 10min each time in TBS-T (20mM Tris-HCl, 150mM NaCl, pH 7.5, 0.05% v/v), blocked for 1h in TBS-T+5% (w/v) non-fat dry milk, then incubated with a rabbit anti-GFP antibody (Torrey Pines Biolabs, TP401, 1:1000 in TBS-T + non-fat dry milk) overnight at 4°C. After 4 washes (15min each) in TBS-T, membranes were incubated for 1h at room temperature with a goat anti-rabbit-HRP-conjugated antibody (Invitrogen, 1:5000 in TBS-T + non-fat dry milk) then washed four times (15min each) in TBS-T. The signal obtained from enhanced chemiluminescence (Western lightning ECL Pro, Perkin Elmer) was detected with MyECL Imager (Life Technologies).

PCR

Whole embryos or animal caps were snap frozen at different stages and stored at −80 °C. Total RNAs were purified with the Qiagen RNeasy kit (Qiagen). RT reactions were carried out using iScript™ Reverse Transcription Supermix (BIO-RAD). PCRs were carried out with GoTaq® G2 Flexi DNA Polymerase (Promega). Amplification of exon6 was performed using the primers scf-L-ex6for: 5'-GGACCTTGTACCATGCCTGC-3 and scf-L-ex6rev : 5'-ATTCCTCTGCCAGGTCTGGA-3 for *scf-L* ; scf-S-ex6for: 5'-TCGGCCTCTTCTTTGTATCG-3' and scf-S-ex6rev: 5'-GTACAGTACAGTGTTAATAG-3' for *scf-S*. To check for the efficiency of kit-S-e2i2spl-MO, the following primers were used: check-splMOkitS1for: 5'-ACCATGAACTGGACTTACCTGTGG-3' and check-splMOkitLSrev: 5'-CTTCAATGTCCCACTCTGATTTCC-3'. To check for the efficiency of kit-L-e2i2spl-MO the following primers were used: check-splMOkitL1for: 5'-TCCTTTACGATCACAATGAGCTGG-3' and check-splMOkitL1rev: 5'-TTACATGAATAGAGAATGTGCTGC-3'.

Statistical analysis

Graphs were done with Graphpad Prism8 software as well as statistical analysis when indicated using student t-test. Time of contact among MCCs was compared using unpaired parametric student t-test and junction following behaviour by Fisher test. The number of samples analysed in all graphs is presented in Table S1.

Mathematical modelling

Geometry

The outer layer, considered as a static canvas that can influence the behaviour of two-dimensional N_{cells} MCCs (red disks), is extracted from the segmented image of a ZO-1 IF of a stage-14 control embryo. The system dynamics were modelled using the effective energies associated with the two mechanisms of MCC mutual repulsion and affinity for outer layer intercellular junctions. The evolution from a random initial state to the final state was guided by an algorithm imposing a progressive decrease of the system total energy. Mathematical expressions for the repulsion and affinity energies were chosen in correspondence with the qualitative behaviours observed in experiments.

Energies

To account for mutual repulsion, a pair-repulsion energy with an exponential decay on a typical length scale equal to the MCC radius r_{cell} was chosen. To prevent the overlap among neighbouring MCCs, the repulsion energy was supplemented with a hard-core corresponding to the minimal allowed distance between two cells. Based on experimental observations showing that MCC overlap does not exceed half their size, the hard core was defined as r_{cell}. To ensure that two nearby MCCs undergo a local energy gradient and to prevent aberrant configurations where two MCCs remain stuck with a distance smaller than r_{cell}, the hard-core energy decreases between $r_{ij} = 0$ and r_{cell}.

Thus, the pair-repulsion energy reads $E_{rep}(r_{ij}) = \begin{cases} k_{rep} e^{-r_{ij}/r_{cell}} & \text{if } r_{ij} \geq r_{cell} \\ A(2 - r_{ij}/r_{cell}) & \text{if } r_{ij} < r_{cell} \end{cases}$, where r_{ij} is the distance between the centers of MCCs *i* and *j*, r_{cell} is the MCC radius and k_{rep} the repulsion constant (positive). The constant *A* of the hard-core energy is chosen large ($A = 100$), so that the probability for a MCC to be at a distance lower than r_{cell} from another MCC is very small ($e^{-100} \simeq 10^{-44}$).

Affinity for junctions was accounted for with a negative energy term proportional to the overlap between MCCs and outer-layer junctions, calculated as the total pixel intensity of the junction network covered by MCCs. The affinity energy of a cell i is then $E_{aff}(i) = -k_{aff} \sum_{(x,y)\in\Omega_i} \sigma_{x,y}$ where k_{aff} is the affinity constant (positive), Ω_i is the set of pixel positions covered by the MCC i and $\sigma_{x,y}$ is the value of the pixel at the position (x, y) of the epithelial canvas. The minus sign ensures that the energy decreases when the total pixel intensity covered by the MCC i increases.

To build the epithelial canvas used to calculate the affinity energy, a Gaussian blur of a size equal to a MCC diameter was applied to the segmented epithelium matrix. This considerably fastens the simulations by directing MCCs towards junctions thanks to an energy gradient, without changing the final state. Note that this could also reflect that regions lining junctions are mechanically more favourable, as the height of the epithelial cells is minimal at junctions.

Dynamics

The total energy of the system is the sum of the repulsion and affinity energies of all the MCCs $E_{tot} = \sum_i E_{aff}(i) + \sum_{i\neq j} E_{rep}(r_{ij})$ where i and j refer to MCCs. Monte-Carlo simulations of the system were performed with a Metropolis algorithm to impose the energy minimization constraint. At each time step of the simulation a random displacement was computed and attributed to each MCC. This displacement corresponds to a diffusive motion with a diffusion constant yielding typical jumps of one-tenth of a cell-radius distance. Moves were accepted or rejected following a Metropolis algorithm depending on the value of $\Delta E_{tot} = E_{tot}(after) - E_{tot}(before)$, the difference between the system total energy after and before each move. If the total energy has decreased ($\Delta E_{tot} < 0$) the move is accepted. If the total energy has increased ($\Delta E_{tot} > 0$) the move is rejected in most cases but has a nonzero probability to be accepted if the increase is of the order of the thermal energy $k_B T$ (k_B is the Boltzmann constant and T the temperature, both set to 1 in our simulations), with a probability given by $\exp(-\Delta E_{tot}/(k_B T))$. The virtual-time of the

simulation is increased by one after N_{cells} such dynamical steps (one Monte-Carlo time step). The simulation was run for a Monte-Carlo time sufficient for the system to reach a stationary final state.

Depending on the respective weight of the energy constants k_{rep} and k_{aff} final states with different qualitative patterning of the MCCs were generated. Let alpha be the ratio between energy constants, $\alpha = k_{rep}/k_{aff}$. When $\alpha \gtrsim 10^7$, the total energy of the system E_{tot} is dominated by the repulsion energy. When $\alpha \lesssim 10^3$, the total energy of the system is dominated by the affinity energy.

Quantification

In order to have a more quantitative description of the system state, two indices were defined, to quantify the MCC spatial order and their localization at junctions, respectively.

The order index I_o was computed from Delaunay tessellation of MCC positions. The position of each MCC is computed as a single point, located at its centroid. Systems with different MCC densities ρ_{cells} (defined as the ratio between the total area occupied by MCCs and the available area of the epithelium) were distinguished, since the number of possible final MCC organisations increases with the available space.

The order index I_o is a measure of the narrowness of the distribution of areas A_{Del} of Delaunay triangles while accounting for the available space via ρ_{cells}: $I_o = (1 - \rho_{cells})\left(1 - \frac{\mathrm{sd}(A_{Del})}{\mathrm{mean}(A_{Del})}\right)$.

I_o is minimal when the standard deviation of Delaunay areas is of the order of its mean and is large when the standard deviation is small compared to the mean. Therefore I_o is maximal when MCCs are perfectly ordered and minimal when they are most disordered. Note that this definition of order was used both for simulations and experimental data.

The covering index I_c, representing the extent of overlapping between outer-layer junctions and MCCs, was computed as the total pixel intensity of the epithelium covered by MCCs, $\sum_i \sum_{(x,y)\in\Omega_i} \sigma_{x,y}$, minus a noise term. This noise term, corresponding to the background value of covered pixels in a purely random configuration of MCCs, was computed by averaging the pixels $\sigma_{x,y}$ of the whole epithelium and multiplying this value by the cell surface $i_c^{noise} = \mathrm{mean}(\sigma_{x,y})\, \pi\, r_{cell}^2$. The covering index was normalized by a term

accounting for the maximal possible extent of overlapping of junctions by one MCC. This was obtained by finding the maximal possible overlapping value for a cell C scanning among all possible positions (x_C, y_C) of its center $i_c^{max} = \max_{(x_C,y_C)} \sum_{(x,y)\in\Omega_C} \sigma_{x,y}$.

Thus the covering index is $I_c = \frac{N_{cells}^{-1} \sum_i \sum_{(x,y)\in\Omega_i} \sigma_{x,y} - i_c^{noise}}{i_c^{max} - i_c^{noise}}$.

The index is thus minimal when the overlap of MCCs with junctions does not exceed the overlap obtained from a random scattering of MCCs. It is maximal when the overlap is the highest possible.

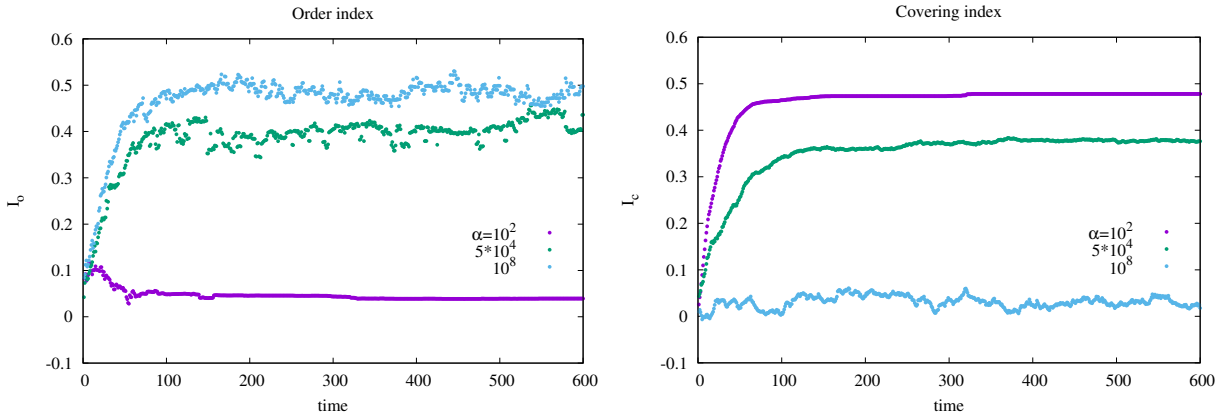

Order and covering index evolution with time for different values of $\alpha = k_{rep}/k_{aff}$.

In the repulsion dominated regime ($\alpha=10^8$) MCCs evolve toward a strict ordering regardless of junctions hence the order index is large while the affinity index is small. In the affinity-dominated regime ($\alpha=10^2$), MCCs finally localize under junctions/vertices regardless of other MCCs, yielding a large affinity index while the order index remains small. In the intermediate regime ($\alpha=5\text{x}10^4$) the two indices take intermediate values.

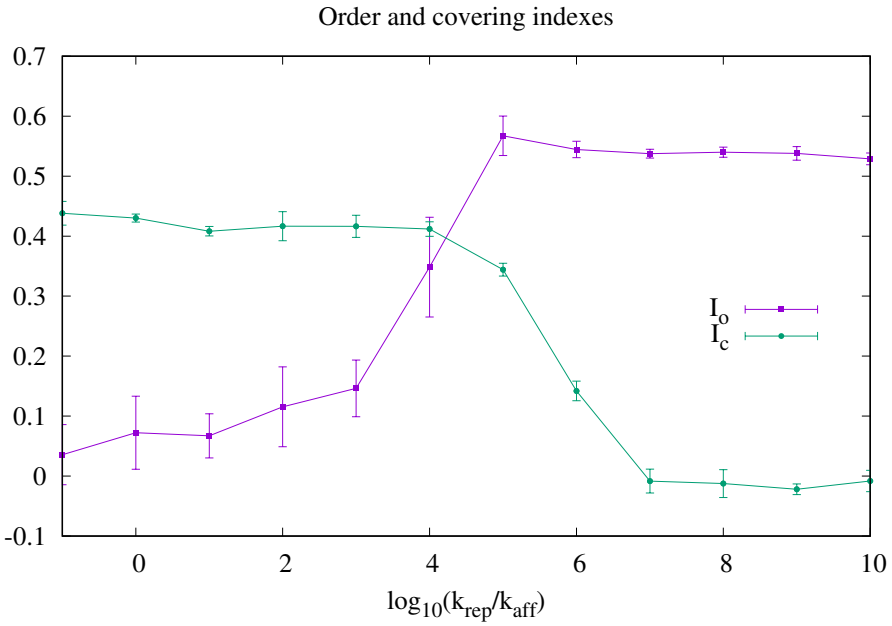

Final values of order and affinity indices for different simulation conditions.

The points represent mean values computed over five simulations and the error-bars represent the standard deviation.

Clonal simulations

In clonal simulations, where patches of the epithelium lack either or both repulsion and affinity, the set of clone regions was called Z, and the new interaction constants k_{rep}^{Z} and k_{aff}^{Z}. The energies depending on the position of the MCCs (inside or outside Z) were thus modified.

The repulsion energy reads

$$E_{rep}(r_{ij}) = \left\{ \begin{array}{c} k_{rep}\ \exp\left(-r_{ij}/r_{cell}\right) \text{ if } (i,j) \notin Z \\ k_{rep}^{Z}\ \exp(-r_{ij}/r_{cell}) \text{ if } (i,j) \in Z \\ \sqrt{k_{rep}\ k_{rep}^{Z}}\ \exp(-r_{ij}/r_{cell}) \text{ if } (i \in Z \text{ and } j \notin Z) \text{ or } (j \in Z \text{ and } i \notin Z) \end{array} \right\}$$

for $r_{ij} \geqslant r_{cell}$ (the hard-core energy of $E_{rep}(r_{ij})$ in section *Energies* is unchanged when $r_{ij} < r_{cell}$), and the affinity energy reads $E_{aff}(i) = -\sum_{(x,y)\in\Omega_i} k_{aff}(x,y)\ \sigma_{x,y}$ with $k_{aff}(x,y) = \left\{ \begin{array}{c} k_{aff} \text{ outside } Z \\ k_{aff}^{Z} \text{ inside } Z \end{array} \right\}$

Movie titles

Movie 1: MCCs move actively within the plane of the ectoderm inner layer.

Movie 2: Dynamic behaviour of the actin cytoskeleton in immature MCCs.

Movie 3: In a simulation dominated by MCC affinity for outer-layer junctions, MCCs home to vertices, but do not disperse properly.

Movie 4: In a simulation dominated by MCC mutual repulsion, MCCs disperse properly, but do not home to vertices.

Movie 5: In a simulation where MCC mutual repulsion and affinity for outer-layer junctions are balanced, MCCs disperse and home correctly to vertices.

Movie 6: When MCCs come into contact via lamellipodia-like structures, they withdraw from each other.

Movie 7: MCCs preferentially move along outer-layer intercellular junctions.

Movie 8: MCC mutual repulsion is strongly decreased in axitinib-treated embryos.

Movie 9: MCC mutual repulsion is strongly decreased in *kit* MO-injected embryos.

Movie 10: MCC mutual repulsion is strongly decreased in *scf* MO-injected embryos.

Movie 11: In *scf* MO mosaic embryos, MCCs leave Scf-depleted regions without following outer-layer intercellular junctions.

Movie 12: Mathematical modelling predicts that MCCs tend to accumulate at boundaries between regions devoid of both repulsion and affinity, and normal regions.

Movie 13: When only repulsion is suppressed in clones surrounded by normal regions, MCCs remain within the clones but do not disperse homogeneously.

Movie 14: When only affinity is suppressed in clones surrounded by normal regions, MCCs disperse homogeneously within the clones but do not preferentially associate to vertices.

Movie 15: MCCs overexpressing Scf-GFP form stable aggregates.

Movie S1: Fluorescent labelling of activated caspases 3 and 7 reveals no apoptotic cell death within the ectoderm.

Movie S2: Tilted 3D projection from movie 7 showing MCC apically-directed protrusions occurring in correspondence of outer-layer intercellular junctions.

Movie S3: MCC mutual repulsion is strongly decreased in CK-666-treated embryos.

Movie S4: A GFP-tagged version of ARP2/3 subunit p41 localizes to lamellipodia-like structures and is lost following their retraction upon MCC mutual contact.

Movie S5: MCC mutual repulsion is strongly decreased in dn-Kit-injected embryos.

REFERENCES

Belin, B.J., Goins, L.M., and Mullins, R.D. (2014). Comparative analysis of tools for live cell imaging of actin network architecture. Bioarchitecture *4*, 189-202.

Benito-Gutierrez, E., Nake, C., Llovera, M., Comella, J.X., and Garcia-Fernandez, J. (2005). The single AmphiTrk receptor highlights increased complexity of neurotrophin signalling in vertebrates and suggests an early role in developing sensory neuroepidermal cells. Development *132*, 2191-2202.

Brannan, C.I., Lyman, S.D., Williams, D.E., Eisenman, J., Anderson, D.M., Cosman, D., Bedell, M.A., Jenkins, N.A., and Copeland, N.G. (1991). Steel-Dickie mutation encodes a c-kit ligand lacking transmembrane and cytoplasmic domains. Proc Natl Acad Sci U S A *88*, 4671-4674.

Briggs, J.A., Weinreb, C., Wagner, D.E., Megason, S., Peshkin, L., Kirschner, M.W., and Klein, A.M. (2018). The dynamics of gene expression in vertebrate embryogenesis at single-cell resolution. Science *360*.

Briscoe, J., and Small, S. (2015). Morphogen rules: design principles of gradient-mediated embryo patterning. Development *142*, 3996-4009.

Castillo-Briceno, P., and Kodjabachian, L. (2014). Xenopus embryonic epidermis as a mucociliary cellular ecosystem to assess the effect of sex hormones in a non-reproductive context. Front Zool *11*, 9.

Chung, M.I., Kwon, T., Tu, F., Brooks, E.R., Gupta, R., Meyer, M., Baker, J.C., Marcotte, E.M., and Wallingford, J.B. (2014). Coordinated genomic control of ciliogenesis and cell movement by RFX2. Elife *3*, e01439.

Cibois, M., Luxardi, G., Chevalier, B., Thome, V., Mercey, O., Zaragosi, L.E., Barbry, P., Pasini, A., Marcet, B., and Kodjabachian, L. (2015). BMP signalling controls the construction of vertebrate mucociliary epithelia. Development *142*, 2352-2363.

Cibois, M., Scerbo, P., Thomé, V., Pasini, A. and Kodjabachian, L. (2014). Induction and Differentiation of the Xenopus Ciliated Embryonic Epidermis. In Xenopus Development, M.K.a.J.Z. Kubiak, ed. (Oxford: John Wiley & Sons, Inc).

Davidson, E.H. (2010). Emerging properties of animal gene regulatory networks. Nature *468*, 911-920.

Davis, J.R., Huang, C.Y., Zanet, J., Harrison, S., Rosten, E., Cox, S., Soong, D.Y., Dunn, G.A., and Stramer, B.M. (2012). Emergence of embryonic pattern through contact inhibition of locomotion. Development *139*, 4555-4560.

Deblandre, G.A., Wettstein, D.A., Koyano-Nakagawa, N., and Kintner, C. (1999). A two-step mechanism generates the spacing pattern of the ciliated cells in the skin of Xenopus embryos. Development *126*, 4715-4728.

Flanagan, J.G., Chan, D.C., and Leder, P. (1991). Transmembrane form of the kit ligand growth factor is determined by alternative splicing and is missing in the Sld mutant. Cell *64*, 1025-1035.

Fuerst, P.G., Koizumi, A., Masland, R.H., and Burgess, R.W. (2008). Neurite arborization and mosaic spacing in the mouse retina require DSCAM. Nature *451*, 470-474.

Galli-Resta, L., Novelli, E., and Viegi, A. (2002). Dynamic microtubule-dependent interactions position homotypic neurones in regular monolayered arrays during retinal development. Development *129*, 3803-3814.

Goldman, D.C., Berg, L.K., Heinrich, M.C., and Christian, J.L. (2006). Ectodermally derived steel/stem cell factor functions non-cell autonomously during primitive erythropoiesis in Xenopus. Blood *107*, 3114-3121.

Gommerman, J.L., Sittaro, D., Klebasz, N.Z., Williams, D.A., and Berger, S.A. (2000). Differential stimulation of c-Kit mutants by membrane-bound and soluble Steel Factor correlates with leukemic potential. Blood *96*, 3734-3742.

Gu, Y., Runyan, C., Shoemaker, A., Surani, A., and Wylie, C. (2009). Steel factor controls primordial germ cell survival and motility from the time of their specification in the allantois, and provides a continuous niche throughout their migration. Development *136*, 1295-1303.

Gu, Y., Runyan, C., Shoemaker, A., Surani, M.A., and Wylie, C. (2011). Membrane-bound steel factor maintains a high local concentration for mouse primordial germ cell motility, and defines the region of their migration. PLoS One *6*, e25984.

Hayes, J.M., Kim, S.K., Abitua, P.B., Park, T.J., Herrington, E.R., Kitayama, A., Grow, M.W., Ueno, N., and Wallingford, J.B. (2007). Identification of novel ciliogenesis factors using a new in vivo model for mucociliary epithelial development. Dev Biol *312*, 115-130.

Heissig, B., Hattori, K., Dias, S., Friedrich, M., Ferris, B., Hackett, N.R., Crystal, R.G., Besmer, P., Lyden, D., Moore, M.A.*, et al.* (2002). Recruitment of stem and progenitor cells from the bone marrow niche requires MMP-9 mediated release of kit-ligand. Cell *109*, 625-637.

Hetrick, B., Han, M.S., Helgeson, L.A., and Nolen, B.J. (2013). Small molecules CK-666 and CK-869 inhibit actin-related protein 2/3 complex by blocking an activating conformational change. Chem Biol *20*, 701-712.

Higashi, T., Arnold, T.R., Stephenson, R.E., Dinshaw, K.M., and Miller, A.L. (2016). Maintenance of the Epithelial Barrier and Remodeling of Cell-Cell Junctions during Cytokinesis. Curr Biol *26*, 1829-1842.

Hu-Lowe, D.D., Zou, H.Y., Grazzini, M.L., Hallin, M.E., Wickman, G.R., Amundson, K., Chen, J.H., Rewolinski, D.A., Yamazaki, S., Wu, E.Y.*, et al.* (2008). Nonclinical antiangiogenesis and antitumor activities of axitinib (AG-013736), an oral, potent, and selective inhibitor of vascular endothelial growth factor receptor tyrosine kinases 1, 2, 3. Clin Cancer Res *14*, 7272-7283.

Hultman, K.A., Bahary, N., Zon, L.I., and Johnson, S.L. (2007). Gene Duplication of the zebrafish kit ligand and partitioning of melanocyte development functions to kit ligand a. PLoS Genet *3*, e17.

Ing-Esteves, S., Kostadinov, D., Marocha, J., Sing, A.D., Joseph, K.S., Laboulaye, M.A., Sanes, J.R., and Lefebvre, J.L. (2018). Combinatorial Effects of Alpha- and Gamma-Protocadherins on Neuronal Survival and Dendritic Self-Avoidance. J Neurosci *38*, 2713-2729.

Irion, U., Frohnhofer, H.G., Krauss, J., Colak Champollion, T., Maischein, H.M., Geiger-Rudolph, S., Weiler, C., and Nusslein-Volhard, C. (2014). Gap junctions composed of connexins 41.8 and 39.4 are essential for colour pattern formation in zebrafish. Elife *3*, e05125.

Iwashita, M., Watanabe, M., Ishii, M., Chen, T., Johnson, S.L., Kurachi, Y., Okada, N., and Kondo, S. (2006). Pigment pattern in jaguar/obelix zebrafish is caused by a Kir7.1 mutation: implications for the regulation of melanosome movement. PLoS Genet *2*, e197.

Jordan, S.A., and Jackson, I.J. (2000). MGF (KIT ligand) is a chemokinetic factor for melanoblast migration into hair follicles. Dev Biol *225*, 424-436.

Kaltenbach, S.L., Yu, J.K., and Holland, N.D. (2009). The origin and migration of the earliest-developing sensory neurons in the peripheral nervous system of amphioxus. Evol Dev *11*, 142-151.

Kim, K., Lake, B.B., Haremaki, T., Weinstein, D.C., and Sokol, S.Y. (2012). Rab11 regulates planar polarity and migratory behavior of multiciliated cells in Xenopus embryonic epidermis. Dev Dyn *241*, 1385-1395.

Kim, S., Ma, L., Shokhirev, M.N., Quigley, I., and Kintner, C. (2018). Multicilin and activated E2f4 induce multiciliated cell differentiation in primary fibroblasts. Sci Rep *8*, 12369.

Lennartsson, J., and Ronnstrand, L. (2012). Stem cell factor receptor/c-Kit: from basic science to clinical implications. Physiol Rev *92*, 1619-1649.

Ma, L., Quigley, I., Omran, H., and Kintner, C. (2014). Multicilin drives centriole biogenesis via E2f proteins. Genes Dev *28*, 1461-1471.

Mani, M., Venkatasubrahmanyam, S., Sanyal, M., Levy, S., Butte, A., Weinberg, K., and Jahn, T. (2009). Wiskott-Aldrich syndrome protein is an effector of Kit signaling. Blood *114*, 2900-2908.

Marchal, L., Luxardi, G., Thome, V., and Kodjabachian, L. (2009). BMP inhibition initiates neural induction via FGF signaling and Zic genes. Proc Natl Acad Sci U S A *106*, 17437-17442.

Martin, B.L., and Harland, R.M. (2004). The developmental expression of two Xenopus laevis steel homologues, Xsl-1 and Xsl-2. Gene Expr Patterns *5*, 239-243.

Meininger, C.J., Yano, H., Rottapel, R., Bernstein, A., Zsebo, K.M., and Zetter, B.R. (1992). The c-kit receptor ligand functions as a mast cell chemoattractant. Blood *79*, 958-963.

Miyazawa, K., Williams, D.A., Gotoh, A., Nishimaki, J., Broxmeyer, H.E., and Toyama, K. (1995). Membrane-bound Steel factor induces more persistent tyrosine kinase activation and longer life span of c-kit gene-encoded protein than its soluble form. Blood *85*, 641-649.

Quigley, I.K., Stubbs, J.L., and Kintner, C. (2011). Specification of ion transport cells in the Xenopus larval skin. Development *138*, 705-714.

Rizvi, S.A., Neidt, E.M., Cui, J., Feiger, Z., Skau, C.T., Gardel, M.L., Kozmin, S.A., and Kovar, D.R. (2009). Identification and characterization of a small molecule inhibitor of formin-mediated actin assembly. Chem Biol *16*, 1158-1168.

Runyan, C., Schaible, K., Molyneaux, K., Wang, Z., Levin, L., and Wylie, C. (2006). Steel factor controls midline cell death of primordial germ cells and is essential for their normal proliferation and migration. Development *133*, 4861-4869.

Samayawardhena, L.A., Kapur, R., and Craig, A.W. (2007). Involvement of Fyn kinase in Kit and integrin-mediated Rac activation, cytoskeletal reorganisation, and chemotaxis of mast cells. Blood *109*, 3679-3686.

Sedzinski, J., Hannezo, E., Tu, F., Biro, M., and Wallingford, J.B. (2016). Emergence of an Apical Epithelial Cell Surface In Vivo. Dev Cell *36*, 24-35.

Sedzinski, J., Hannezo, E., Tu, F., Biro, M., and Wallingford, J.B. (2017). RhoA regulates actin network dynamics during apical surface emergence in multiciliated epithelial cells. J Cell Sci *130*, 420-428.

Sirour, C., Hidalgo, M., Bello, V., Buisson, N., Darribere, T., and Moreau, N. (2011). Dystroglycan is involved in skin morphogenesis downstream of the Notch signaling pathway. Mol Biol Cell *22*, 2957-2969.

Stubbs, J.L., Davidson, L., Keller, R., and Kintner, C. (2006). Radial intercalation of ciliated cells during Xenopus skin development. Development *133*, 2507-2515.

Stubbs, J.L., Vladar, E.K., Axelrod, J.D., and Kintner, C. (2012). Multicilin promotes centriole assembly and ciliogenesis during multiciliate cell differentiation. Nat Cell Biol *14*, 140-147.

Suraneni, P., Fogelson, B., Rubinstein, B., Noguera, P., Volkmann, N., Hanein, D., Mogilner, A., and Li, R. (2015). A mechanism of leading-edge protrusion in the absence of Arp2/3 complex. Mol Biol Cell *26*, 901-912.

Suraneni, P., Rubinstein, B., Unruh, J.R., Durnin, M., Hanein, D., and Li, R. (2012). The Arp2/3 complex is required for lamellipodia extension and directional fibroblast cell migration. J Cell Biol *197*, 239-251.

Tabone-Eglinger, S., Calderin-Sollet, Z., Pinon, P., Aebischer, N., Wehrle-Haller, M., Jacquier, M.C., Boettiger, D., and Wehrle-Haller, B. (2014). Niche anchorage and signaling through membrane-bound Kit-ligand/c-kit receptor are kinase independent and imatinib insensitive. FASEB J *28*, 4441-4456.

Tabone-Eglinger, S., Wehrle-Haller, M., Aebischer, N., Jacquier, M.C., and Wehrle-Haller, B. (2012). Membrane-bound Kit ligand regulates melanocyte adhesion and survival, providing physical interaction with an intraepithelial niche. FASEB J *26*, 3738-3753.

Tajima, Y., Moore, M.A., Soares, V., Ono, M., Kissel, H., and Besmer, P. (1998). Consequences of exclusive expression in vivo of Kit-ligand lacking the major proteolytic cleavage site. Proc Natl Acad Sci U S A *95*, 11903-11908.

Trindade, M., Messenger, N., Papin, C., Grimmer, D., Fairclough, L., Tada, M., and Smith, J.C. (2003). Regulation of apoptosis in theXenopus embryo by Bix3. Development *130*, 4611-4622.

Villar-Cervino, V., Molano-Mazon, M., Catchpole, T., Valdeolmillos, M., Henkemeyer, M., Martinez, L.M., Borrell, V., and Marin, O. (2013). Contact repulsion controls the dispersion and final distribution of Cajal-Retzius cells. Neuron *77*, 457-471.

Walderich, B., Singh, A.P., Mahalwar, P., and Nusslein-Volhard, C. (2016). Homotypic cell competition regulates proliferation and tiling of zebrafish pigment cells during colour pattern formation. Nat Commun *7*, 11462.

Wehrle-Haller, B., Meller, M., and Weston, J.A. (2001). Analysis of melanocyte precursors in Nf1 mutants reveals that MGF/KIT signaling promotes directed cell migration independent of its function in cell survival. Dev Biol *232*, 471-483.

Wehrle-Haller, B., and Weston, J.A. (1995). Soluble and cell-bound forms of steel factor activity play distinct roles in melanocyte precursor dispersal and survival on the lateral neural crest migration pathway. Development *121*, 731-742.

Werner, M.E., and Mitchell, B.J. (2012). Understanding ciliated epithelia: the power of Xenopus. Genesis *50*, 176-185.

Werner, M.E., Mitchell, J.W., Putzbach, W., Bacon, E., Kim, S.K., and Mitchell, B.J. (2014). Radial intercalation is regulated by the Par complex and the microtubule-stabilizing protein CLAMP/Spef1. J Cell Biol *206*, 367-376.

Zuo, K., Kuang, D., Wang, Y., Xia, Y., Tong, W., Wang, X., Chen, Y., Duan, Y., and Wang, G. (2016). SCF/c-kit transactivates CXCR4-serine 339 phosphorylation through G protein-coupled receptor kinase 6 and regulates cardiac stem cell migration. Sci Rep *6*, 26812.

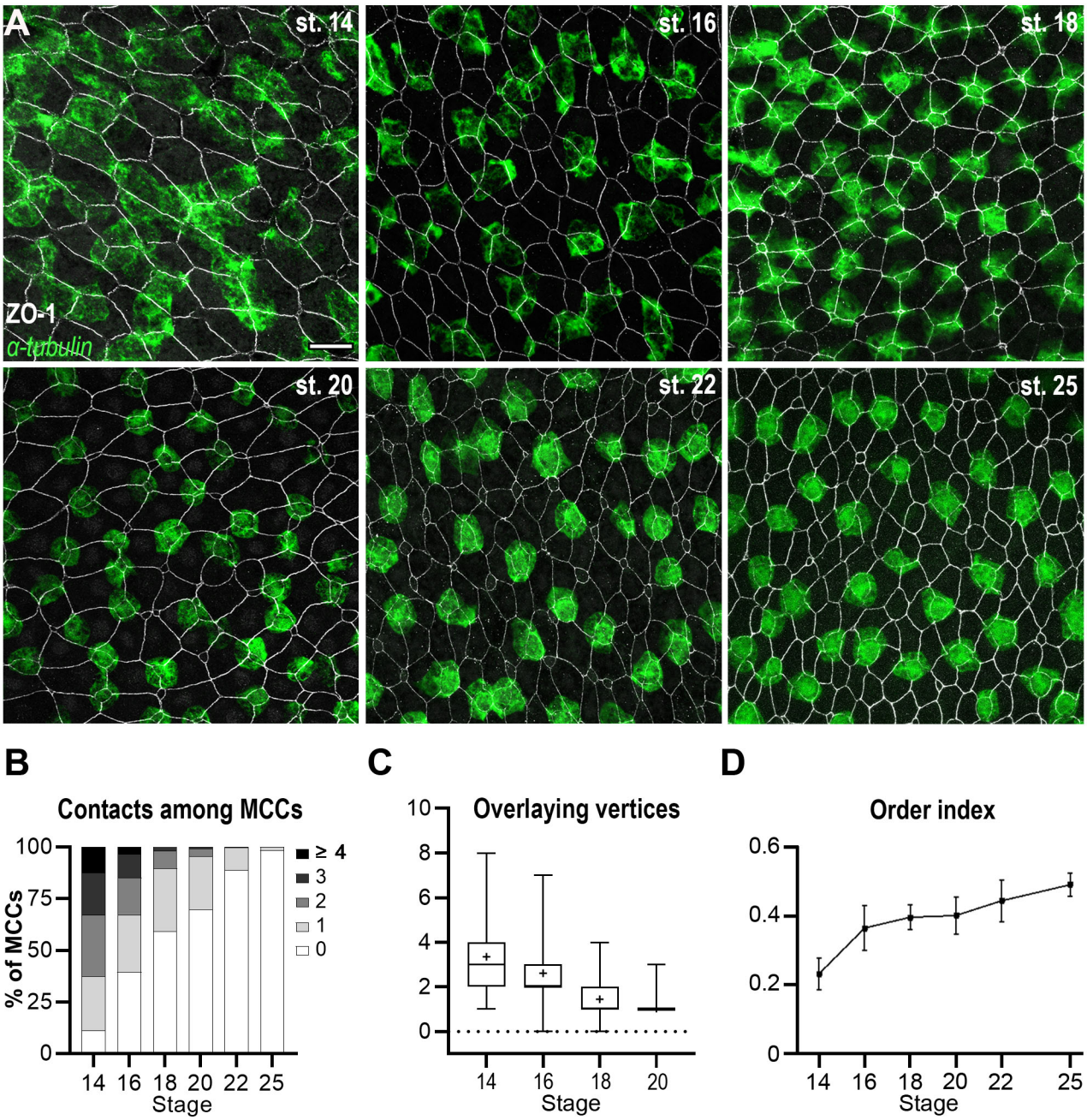
A
st. 14
st. 16
st. 18
st. 20
st. 22
st. 25
ZO-1
α-tubulin
B
Contacts among MCCs
% of MCCs
100
75
50
25
0
≥ 4
3
2
1
0
14 16 18 20 22 25
Stage
C
Overlaying vertices
10
8
6
4
2
0
14 16 18 20
Stage
D
Order index
0.6
0.4
0.2
0
14 16 18 20 22 25
Stage

Figure 1

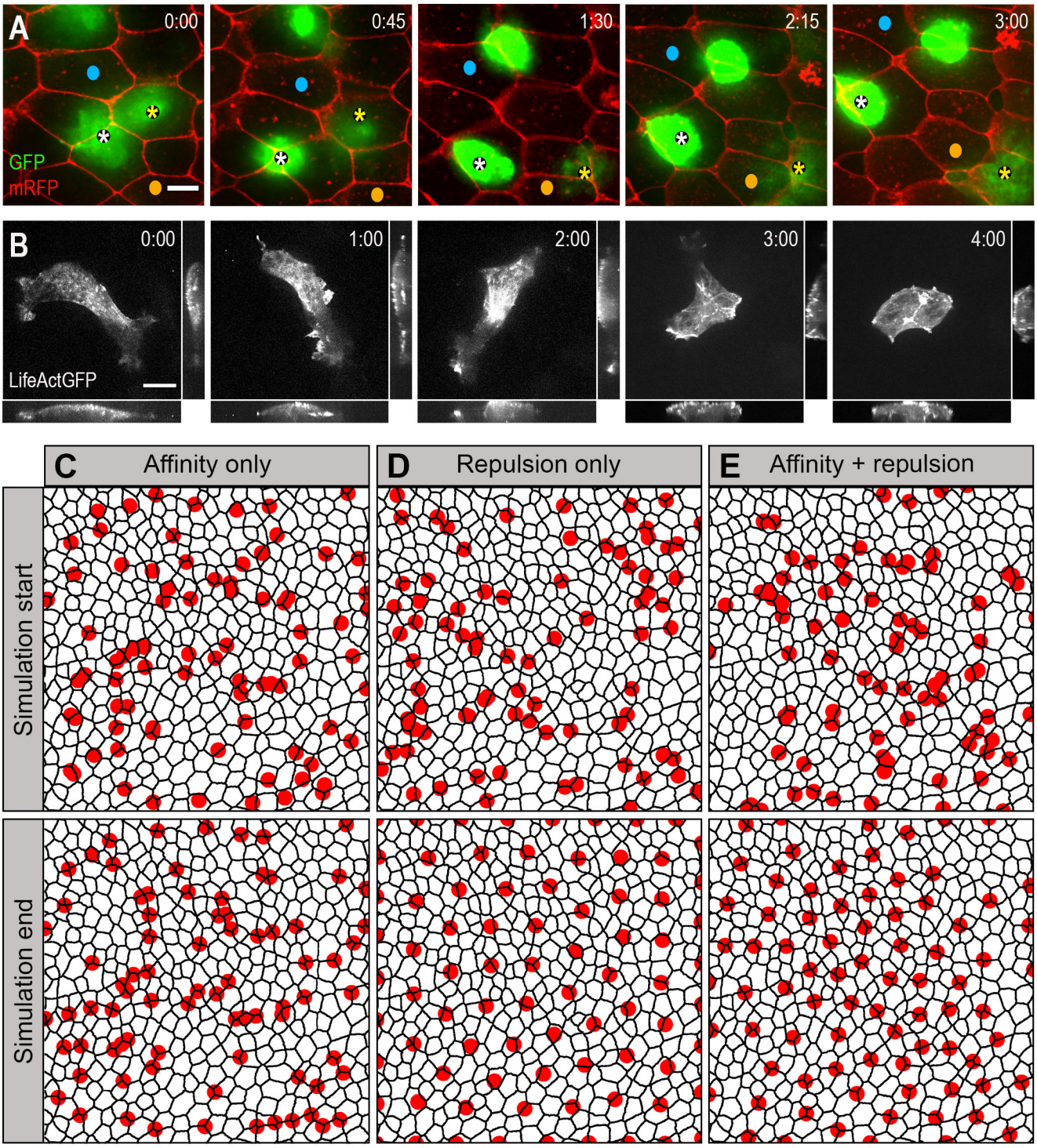
A
0:00
0:45
1:30
2:15
3:00
GFP
mRFP
B
0:00
1:00
2:00
3:00
4:00
LifeActGFP
C Affinity only
D Repulsion only
E Affinity + repulsion
Simulation start
Simulation end

Figure 2

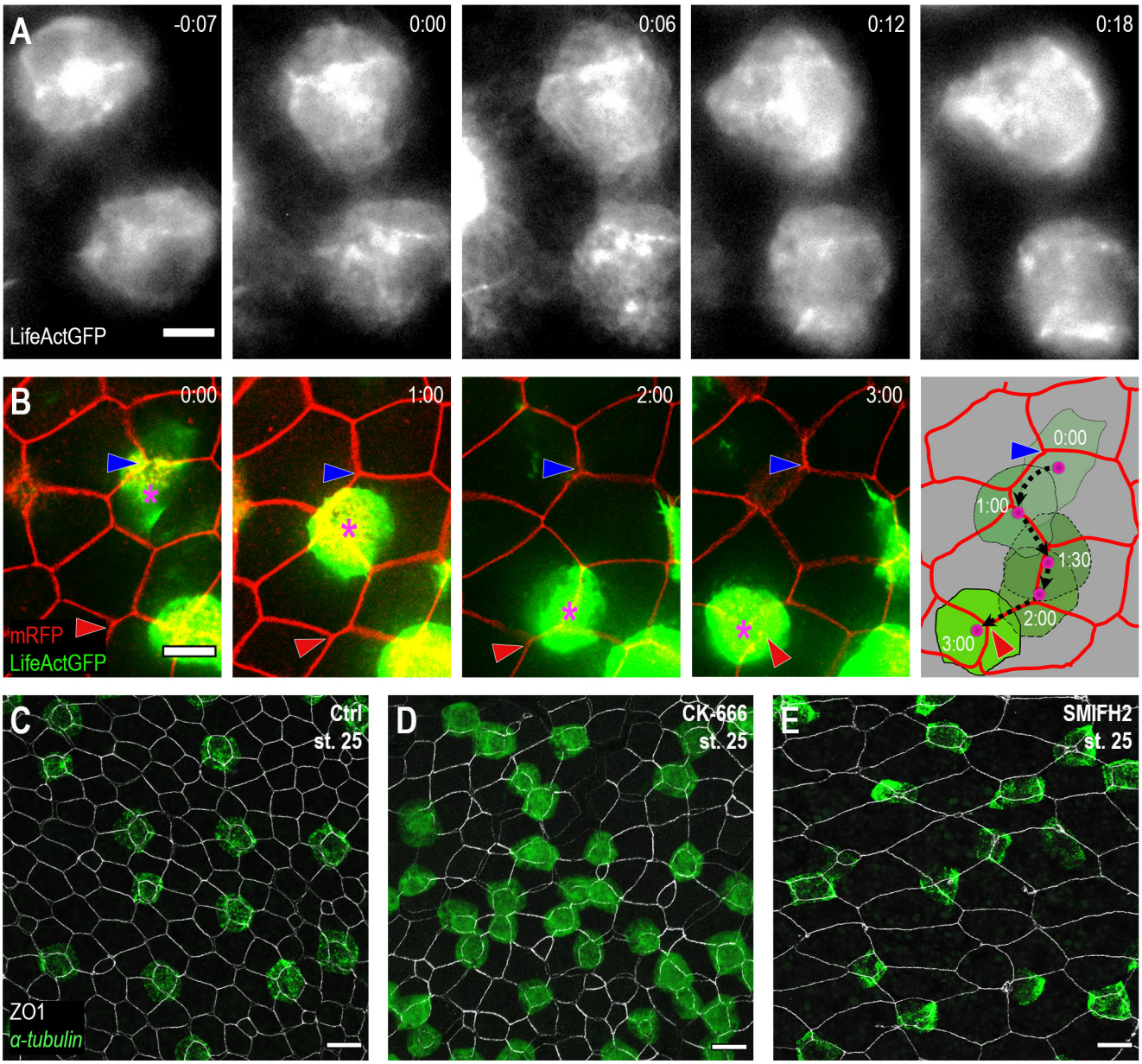
A
-0:07
0:00
0:06
0:12
0:18
LifeActGFP
B
0:00
1:00
2:00
3:00
mRFP
LifeActGFP
0:00
1:00
1:30
2:00
3:00
C
Ctrl
st. 25
D
CK-666
st. 25
E
SMIFH2
st. 25
ZO1
α-tubulin
F
Time of contact
****
Time (min)
250
200
150
100
50
0
Ctrl
CK-666
G
MCCs follow junctions
ns
% of MCCs
100
75
50
25
0
yes
no
Ctrl
CK-666
H
Order index
0.6
0.4
0.2
0
Ctrl
CK-666
SMIFH2
I
Contact among MCCs
% of MCCs
100
75
50
25
0
≥ 4
3
2
1
0
Ctrl
CK-666
SMIFH2

Figure 3

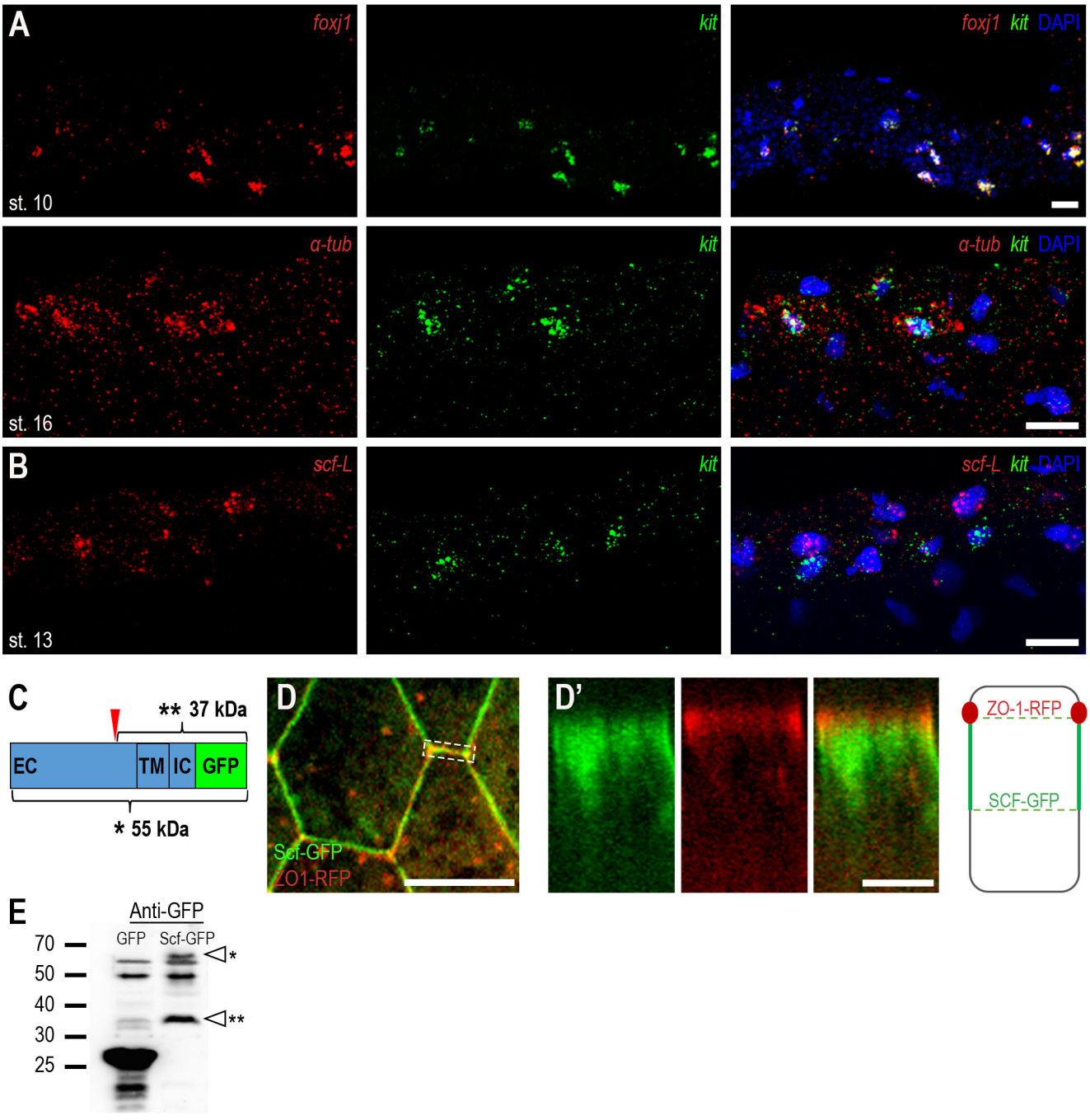
A
foxj1
kit
foxj1 kit DAPI
st. 10
α-tub
kit
α-tub kit DAPI
st. 16
B
scf-L
kit
scf-L kit DAPI
st. 13
C
** 37 kDa
EC
TM
IC
GFP
* 55 kDa
D
Scf-GFP
ZO1-RFP
D'
ZO-1-RFP
SCF-GFP
E
Anti-GFP
GFP
Scf-GFP
70
50
40
30
25
*
**

Figure 4

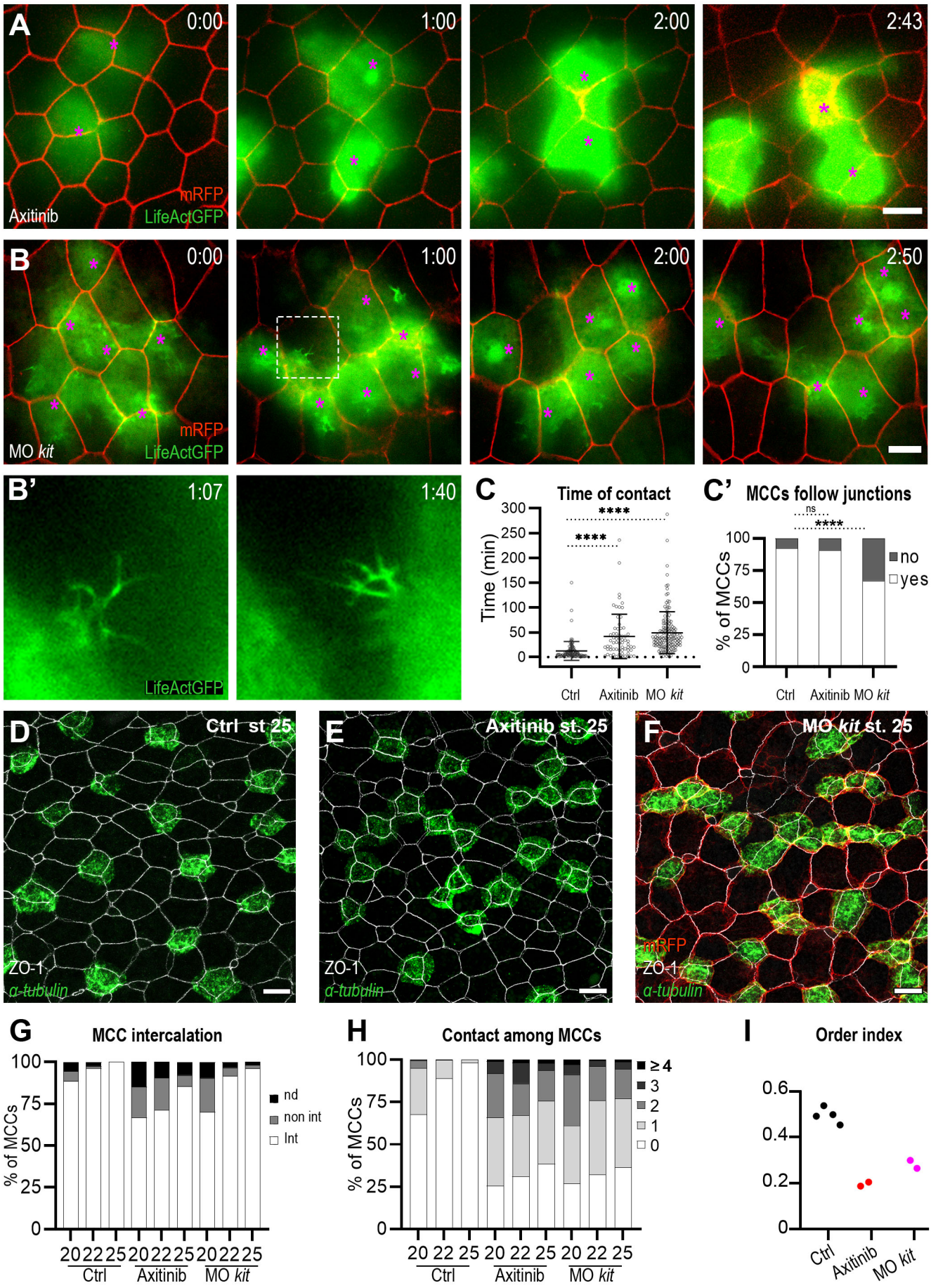
A
0:00
1:00
2:00
2:43
Axitinib
mRFP
LifeActGFP
B
0:00
1:00
2:00
2:50
MO kit
mRFP
LifeActGFP
B'
1:07
1:40
LifeActGFP
C
Time of contact
Time (min)
300
250
200
150
100
50
0
****
****
Ctrl
Axitinib
MO kit
C'
MCCs follow junctions
ns
****
% of MCCs
100
75
50
25
0
no
yes
Ctrl
Axitinib
MO kit
D
Ctrl st 25
ZO-1
α-tubulin
E
Axitinib st. 25
ZO-1
α-tubulin
F
MO kit st. 25
mRFP
ZO-1
α-tubulin
G
MCC intercalation
% of MCCs
100
75
50
25
0
nd
non int
Int
20 22 25 20 22 25 20 22 25
Ctrl
Axitinib
MO kit
H
Contact among MCCs
% of MCCs
100
75
50
25
0
≥4
3
2
1
0
20 22 25 20 22 25 20 22 25
Ctrl
Axitinib
MO kit
I
Order index
0.6
0.4
0.2
0
Ctrl
Axitinib
MO kit

Figure 5

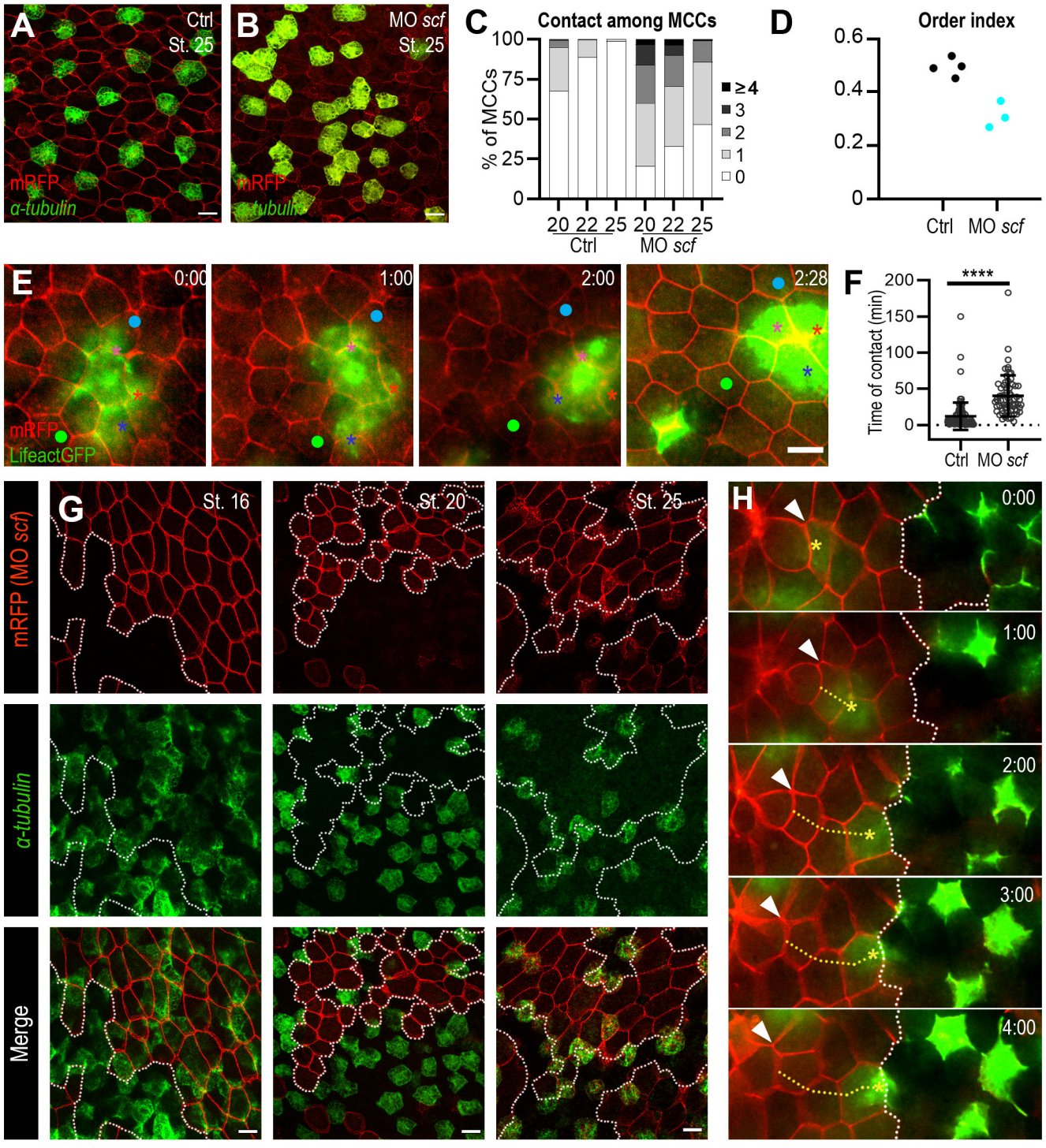
A
Ctrl
St. 25
mRFP
α-tubulin
B
MO scf
St. 25
mRFP
α-tubulin
C
Contact among MCCs
% of MCCs
100
75
50
25
0
≥4
3
2
1
0
20 22 25 20 22 25
Ctrl
MO scf
D
Order index
0.6
0.4
0.2
0
Ctrl
MO scf
E
0:00
1:00
2:00
2:28
mRFP
LifeactGFP
F
****
Time of contact (min)
200
150
100
50
0
Ctrl
MO scf
mRFP (MO scf)
α-tubulin
Merge
G
St. 16
St. 20
St. 25
H
0:00
1:00
2:00
3:00
4:00
I
MCCs follow junctions
****
% of MCCs
100
75
50
25
0
no
yes
Ctrl
MO scf
J
Simulation start
Simulation end
MCCs
Low afffinity
+ low repulsion zones

Figure 6

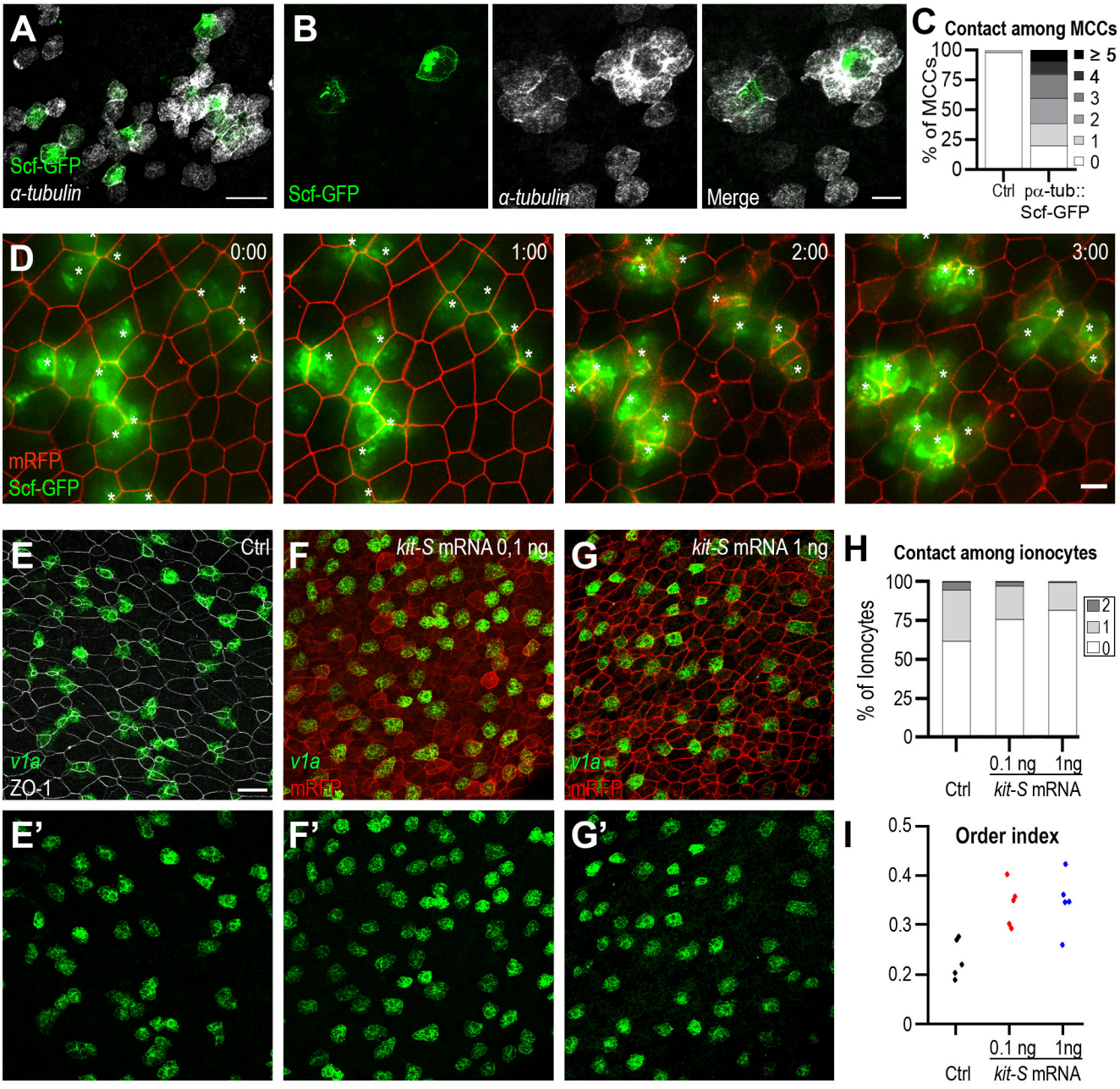
A
Scf-GFP
α-tubulin
B
Scf-GFP
α-tubulin
Merge
C
Contact among MCCs
% of MCCs
100
75
50
25
0
≥ 5
4
3
2
1
0
Ctrl
pα-tub::
Scf-GFP
D
0:00
1:00
2:00
3:00
mRFP
Scf-GFP
E
Ctrl
v1a
ZO-1
F
kit-S mRNA 0,1 ng
v1a
mRFP
G
kit-S mRNA 1 ng
v1a
mRFP
H
Contact among ionocytes
% of Ionocytes
100
75
50
25
0
2
1
0
Ctrl
0.1 ng
1ng
kit-S mRNA
E'
F'
G'
I
Order index
0.5
0.4
0.3
0.2
0
Ctrl
0.1 ng
1ng
kit-S mRNA

Figure 7

SUPPLEMENTARY FIGURES

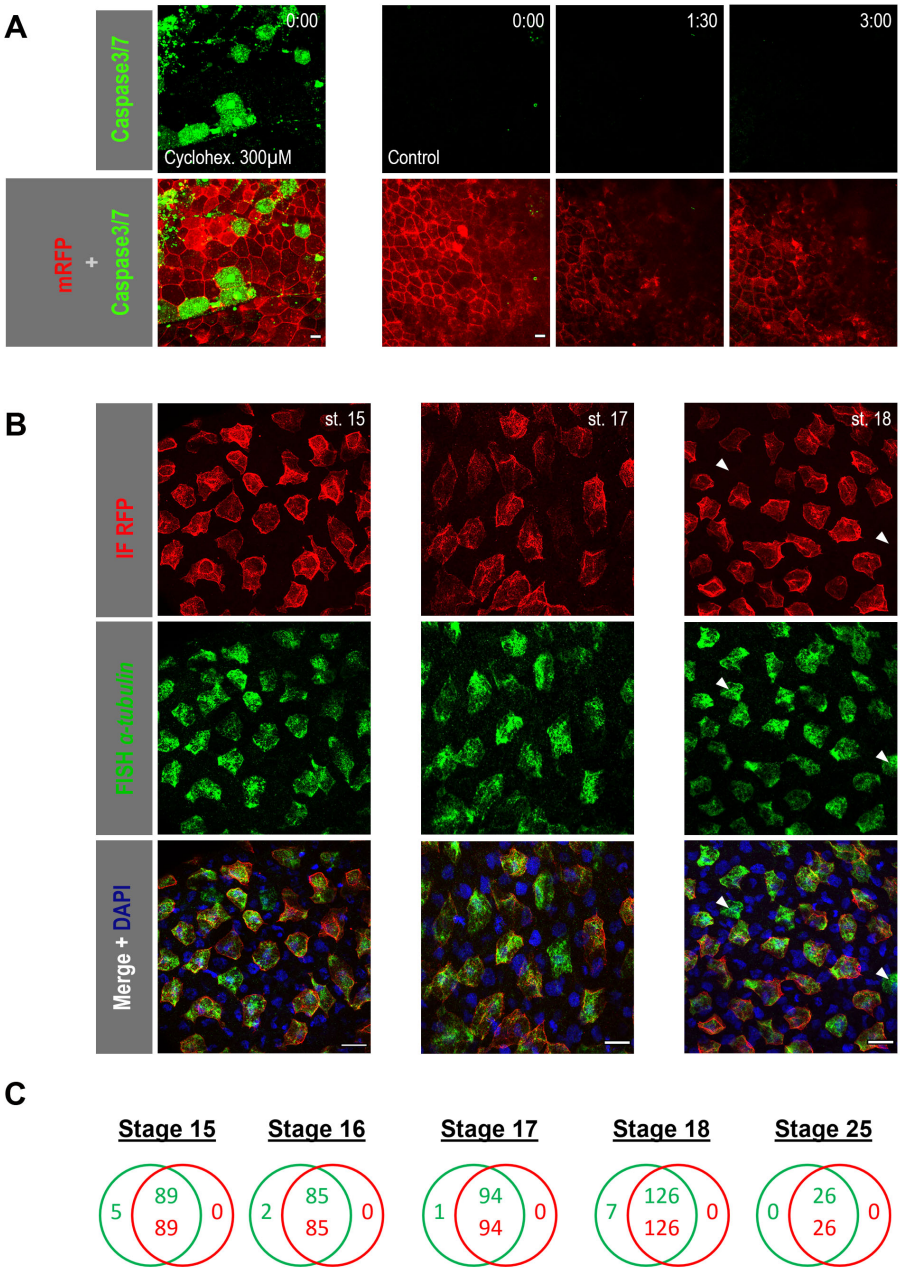

Figure S1

Figure S1. Cell death and cell fate reversal are unlikely to play a major role in establishing the MCC regular pattern.
A: Stage 15 mRFP-injected *Xenopus* embryos were incubated with the CellEvent™ Caspase-3/7 Green Detection Reagent to detect activation of the executioner Caspases 3 and 7 in presence of 300µM cycloheximide as an apoptosis inducer (Trindade et al., Development, 2003) (left) or of 1% (v/v) DMSO as a control and filmed for 3h (right). Apoptotic cells (green) were found in the epidermis of cycloheximide-treated embryos (left), but not in control ones, even after prolonged observation (right). Embryos were injected with mRFP (red) to allow a better visualisation of cell outlines. Scale bar is 20µm. **B:** α-tub::RFP transgenic embryos were fixed at different developmental stages and subjected to IF with an anti-RFP

antibody (red, top row) and FISH against *α-tubulin* (green, middle row). Merging the two channels (bottom row) showed few *α-tub*-positive, RFP-negative cells (white arrowheads), but failed to uncover any RFP-positive, *α-tub*-negative cells. DAPI staining (blue, bottom row) allowed the identification of nuclei. Scale bar is 20μm. **C:** Venn diagrams showing the overlap of the GFP- and RFP-positive cell populations at different developmental stages.

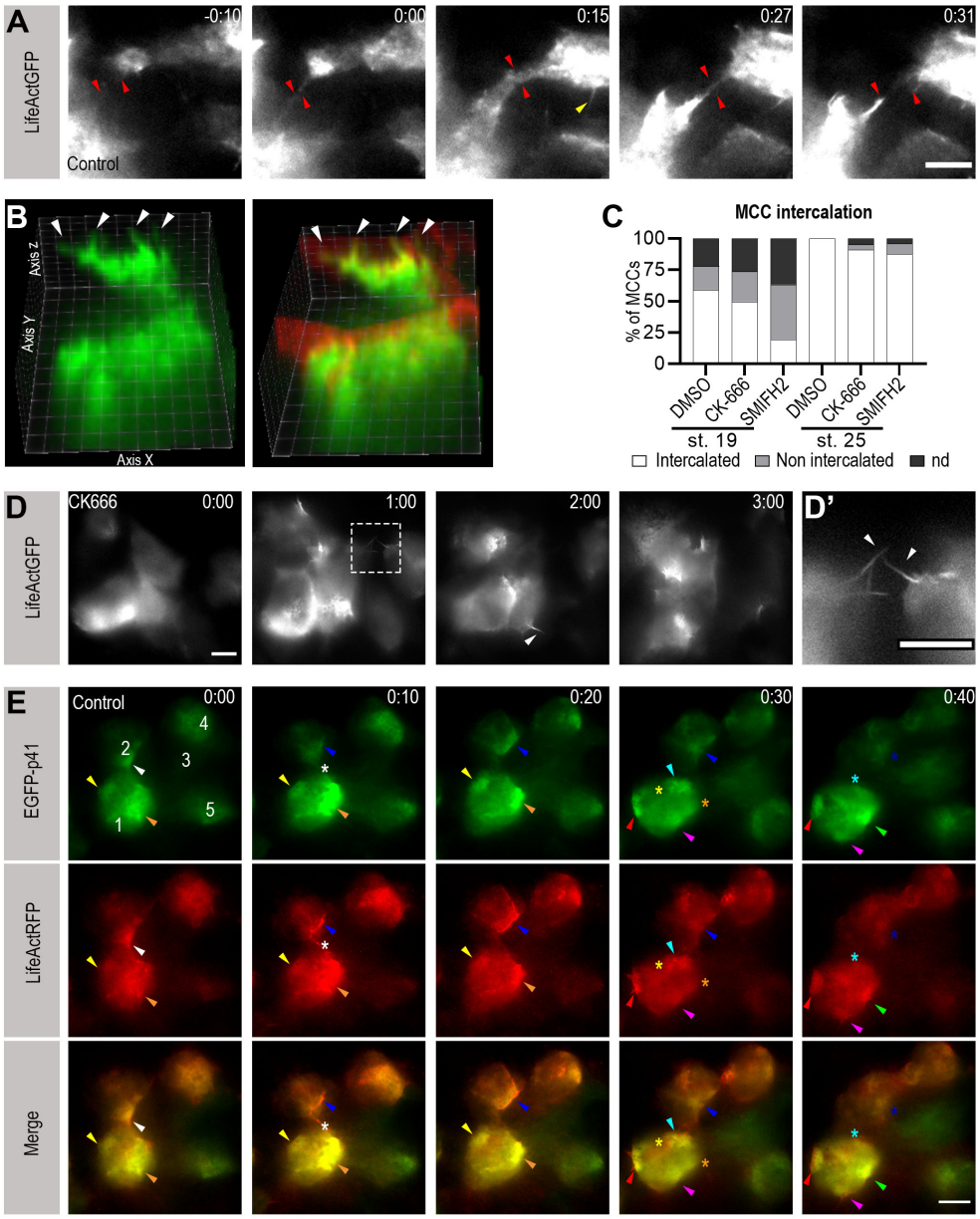

Figure S2

Figure S2. Role of actin cytoskeleton in MCC patterning.
A: Frames from a movie showing LifeActGFP-expressing MCCs establishing transient contact via lamellipodia-like structures (red arrowheads) that were subsequently retracted. The yellow arrowhead points to an example of thinner, filopodia-like structures. Scale bar is 20µm. **B:** A tilted 3D projection from movie S2 showing that apically directed protrusions (white arrowheads) corresponded to outer-layer cell junctions. **C:** Quantification of MCC intercalation at stage 19 and stage 25 in control embryos and embryos treated with CK-666 or SMIFH2. **D, D':** Frames from movie S3 showing that LifeActGFP-expressing MCCs displayed decreased mutual repulsion in CK-666 treated embryos. White arrowheads point to filopodia-like structures. Scale bar is 20µm. **E:** Frames from movie S4 showing that local accumulations of a GFP-tagged version of the branched actin-nucleator ARP2/3 subunit p41 colocalised with the LifeActRFP signal in lamellipodia-like structures (arrowheads), but were lost following MCC mutual contact (asterisks). White numbers show different MCCs. Scale bar is 20µm.

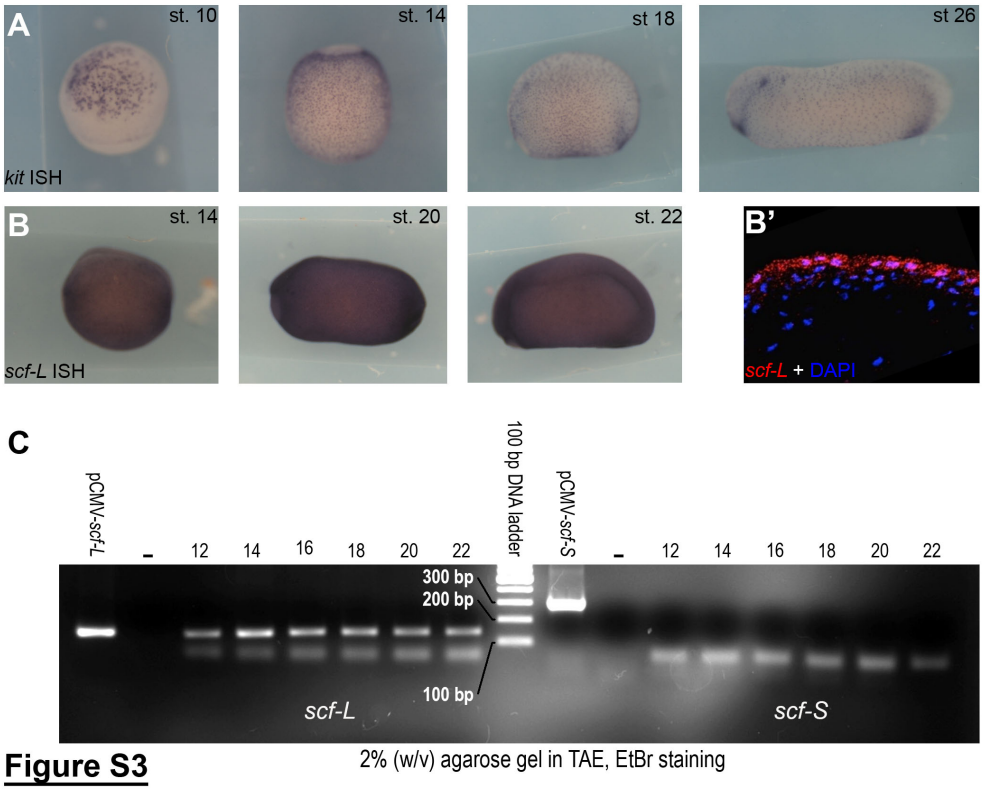

Figure S3

Figure S3. Expression of *kit* and *scf* in *Xenopus* epidermis.
A: Whole-mount ISH with a probe against *kit-L* and *kit-S* revealed expression in scattered non-neural ectoderm cells at stages 12 to 24. Anterior is to the top for stages 12 and 14, to the left for stages 18 and 24. **B:** Whole-mount ISH with a probe against *scf-L* revealed expression throughout the ectoderm from stages 14 to 22. Anterior to the left. **B':** FISH on a sectioned embryo at stage 25 revealed stronger *scf-L* expression (red) in the ectoderm outer layer. DAPI (blue) stained the nuclei. **C:** RT-PCR on total RNA from animal caps at different developmental stages with primers encompassing the exon6 region of *scf-L* (left) or *scf-S* (right) amplified a 141bp band, only for *scf-L*, which was present at all developmental stages analysed. Plasmids containing the full-length cDNA of either *scf-L* (pCMV-Sport6-Scf-L) or *scf-S* (pCMV-Sport6-Scf-S) were used as positive controls for amplification. Molecular weight marker is GeneRuler 100bp Plus DNA Ladder (Thermo Scientific).

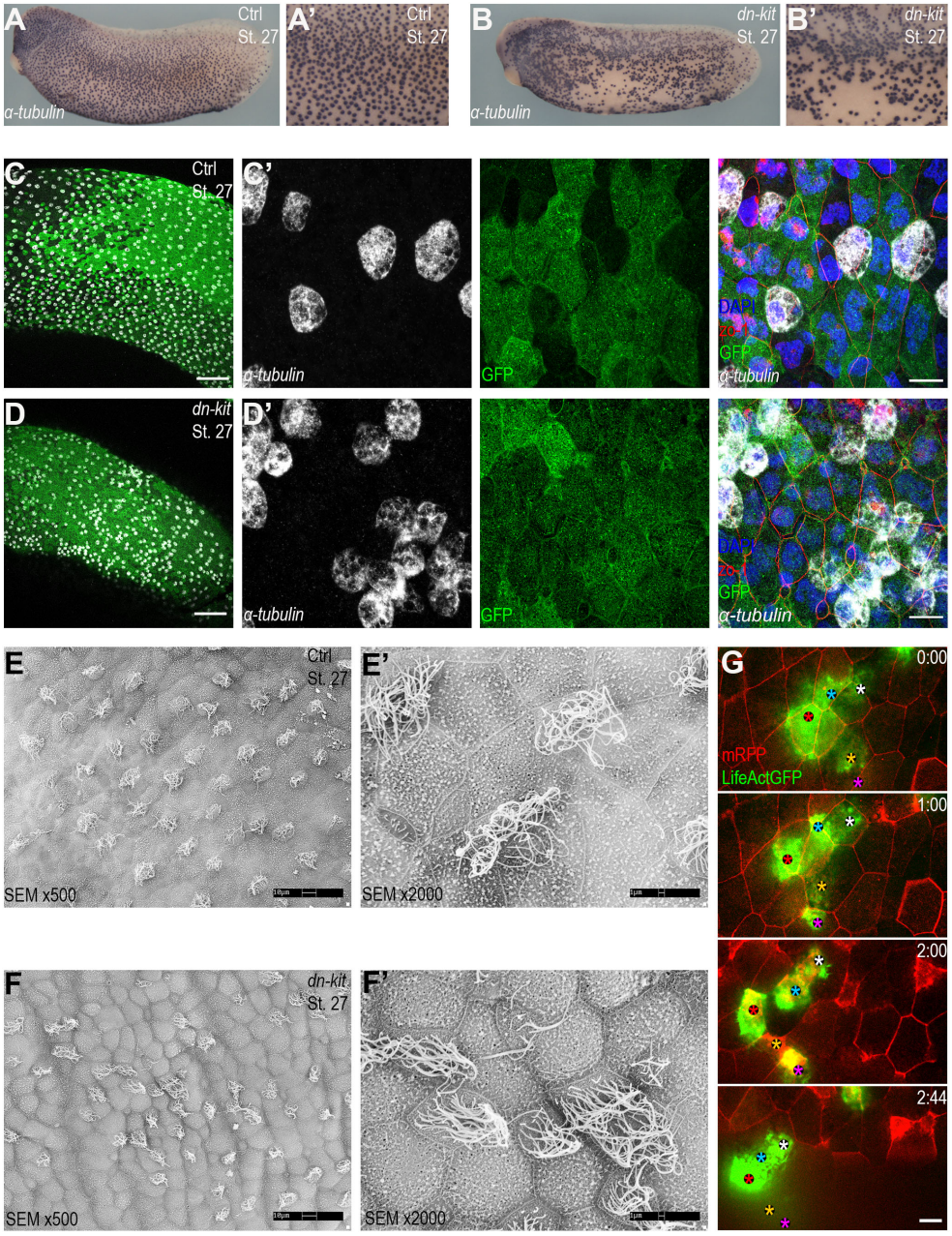

Figue S4

Figure S4. Expression of dominant-negative Kit affects MCC distribution.
A, B: Whole-mount ISH with a probe against *α-tubulin* revealed normal MCC distribution in stage 27 control embryos (A) and patterning irregularities in age-matched *dn-kit* injected embryos (B). **A'** and **B'** are close-ups of A and B respectively. **C, D:** Whole-mount FISH with a probe against *α-tubulin* (white) in control (C) and *dn-kit* injected (D) stage 27 embryos. mRNA coding for GFP (green) was used as a tracer for *dn-kit* mRNA, DAPI (blue) stained nuclei. Scale bar is 200µm. **C'** and **D'** are close-ups of C and D, respectively, showing the irregular clustering of MCCs in *dn-kit* injected embryos. Scale bar is 20µm. **E, F:** scanning electron microscopy images of control (E) and *dn-kit* injected (F) stage 27 embryos. **E'** and **D'** are close-ups of E and D, respectively, showing that MCCs in *dn-kit* injected embryos were irregularly clustered but did produce cilia. **G:** Frames from movie S5, showing that LifeActGFP-positive MCCs failed to separate properly in *dn-kit* injected embryos. mRNA coding for RFP (red) served as tracer for *dn-kit* mRNA. Scale bar is 20µm.

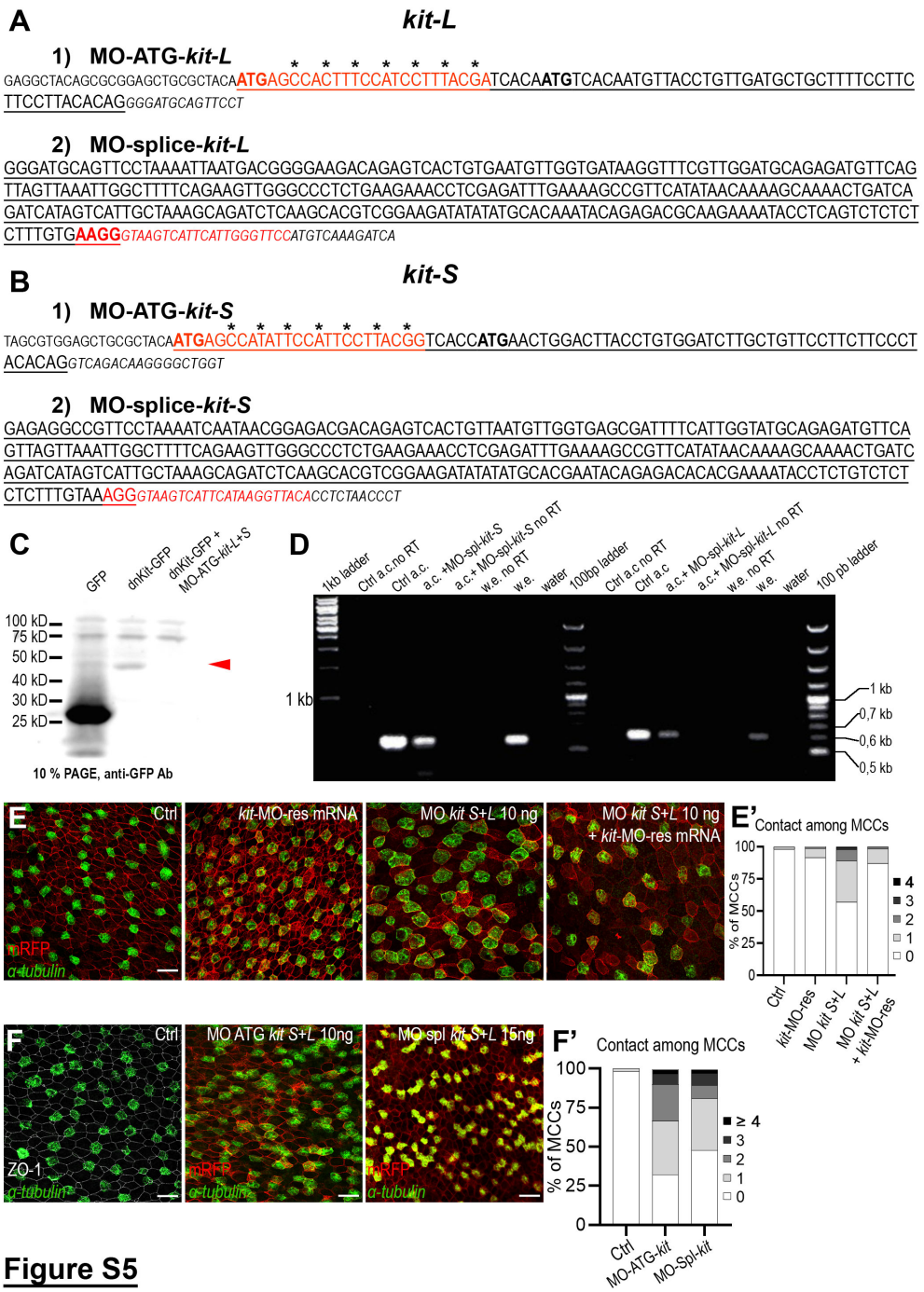

Figure S5

Figure S5. Characterisation of Morpholino Oligos against *kit-L* and *kit-S*.
A: Morpholino Oligos against *kit-L*. **1)** Upper case underlined: *kit-L* exon 1; lower case: 5'UTR; lower case italic: intron 1; in red the stretch targeted by MO-ATG-kit-L. **2)** Upper case underlined: *kit-L* exon 2; lower case italic: intron 2; in red the stretch targeted by MO-splice-kit-L. **B:** Morpholino Oligos against *kit-S*. **1)** Upper case underlined: *kit-S* exon 1; lower case: 5'UTR; lower case italic: intron 1; in red the stretch targeted by MO-ATG-kit-S. The asterisk/arrowheads point to the seven bases mutated to generate MOres-kit-S. **2)** Upper case underlined: *kit-S* exon 2; lower case italic: intron 2; in red the stretch targeted by MO-splice-kit-S. **C:** Lysates from animal caps injected with mRNA coding for GFP and mRNA coding for a C-terminally GFP-tagged dominant-negative form of Kit-S alone or together with MO-

ATG-kit-L+S were subjected to Western blotting with an anti-GFP antibody. The red arrowhead points to a GFP-positive band corresponding to the intracellular fragment generated by proteolytic cleavage of the dn-Kit-GFP protein, which was lost in embryos co-injected with MO-ATG-kit-L+S. **D:** RT-PCR on *kit-L* and *kit-S* to test the action of the splice-blocking MOs; a.c.: animal caps; w.e.: whole embryos; 0.8% agarose/TAE gel. The injection of MO-splice-kit-S or MO-splice-kit-L resulted in a decrease of the levels of *kit-S* and *kit-L* mRNAs, respectively. **E:** *α-tub* FISH (green) and RFP IF (red) on stage 25 embryos showed, from left to right, normal MCC distribution in control embryos and in embryos injected with mRNA coding for morpholino-resistant form MOres-kit-S alone, abnormal MCC clustering in embryos injected with MO-ATG-kit-L+S, and recovery of normal MCC distribution in embryos co-injected with MO-ATG-kit-L+S and MOres-kit-*S* mRNA. In all cases, mRNA for RFP was used as an injection tracer. Scale bar is 20μm. **E':** A quantification of MCC clustering at stage 25 in control embryos, embryos injected with MOres-kit-S mRNA alone, MO-ATG-kit-L+S alone and MO-ATG-kit-L+S together with MOres-kit-S mRNA. **F:** *α-tub* FISH (green) and ZO-1 IF (white) on control embryos (left panel) and embryos injected with either MO-ATG-kit-L+S (middle panel) or MO-splice-kit-L+S (right panel) showed that both ATG- and splice-targeting MOs led to the same phenotype of irregularly distributed and clustered MCCs at stage 25. mRFP mRNA (red) was used as MO tracer. Scale bar is 20μm. The graph in **F'** shows a quantification of the abnormal MCC clustering in MO-ATG-kit-L+S and MO-splice-kit-L+S injected embryos.

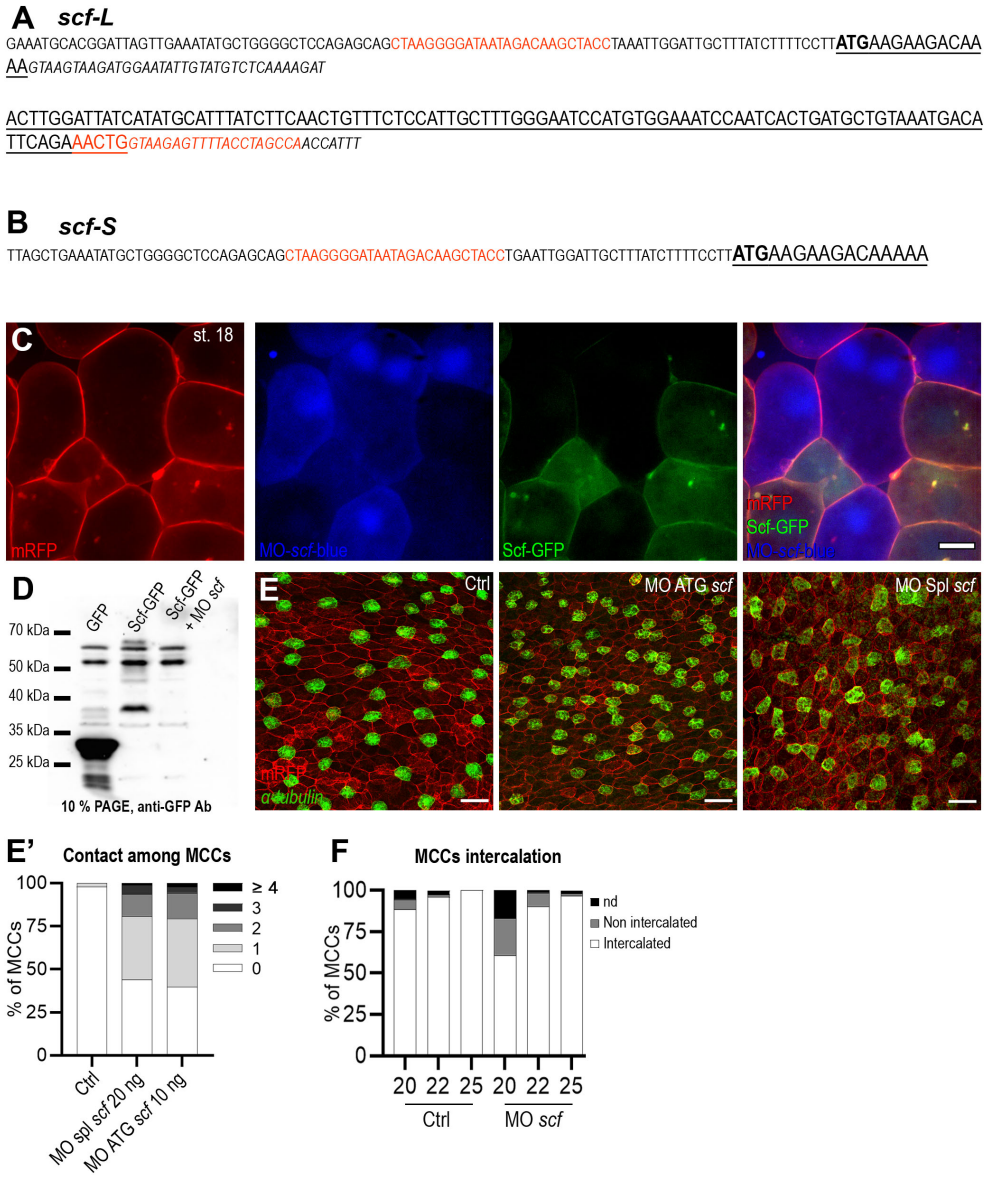

Figure S6

Figure S6. Characterisation of Morpholino Oligos against *scf-L* and *scf-S*.
A: Morpholino Oligos against *scf-L*. **1)** Upper case underlined: *scf-L* exon 1; lower case: 5'UTR; lower case italic: intron 1; in red the stretch targeted by MO-ATG-scf-L/S. **2)** Upper case underlined: *scf-L* exon 2; lower case italic: intron 2; in red the stretch targeted by MO-splice-scf-L. **B:** Morpholino Oligos against *scf-S*. **1)** Upper case underlined: *scf-S* exon 1; lower case: 5'UTR; in red the stretch targeted by MO-ATG-scf-L/S. **C:** Top view of live outer-layer cells from a stage 18 embryo co-injected with mRNAs coding for Scf-GFP (green) and RFP (red), as well as a blue-tagged version of MO-ATG-scf-L/S. The Scf-GFP signal was lost from the MO-receiving cells, while the RFP signal was unchanged. Scale bar is 20µm. **D:** Lysates from animal caps injected with mRNA coding for GFP, Scf-GFP and Scf-GFP together with MO-ATG-scf-L/S were subjected to Western blotting with an anti-GFP antibody. Bands corresponding to the 55kDa full-length Scf-GFP and to the 37kDa exon 6 proteolytic cleavage product were absent from MO-ATG-scf-L/S injected embryos. **E:** *α-tub* FISH (green) and RFP (red) IF on control embryos (left panel) and embryos injected with either MO-ATG-scf-L/S (middle panel) or MO-splice-scf-L (right panel) showed that both ATG- and splice-targeting

MOs led to the same phenotype of irregularly distributed and clustered MCCs at stage 25. mRFP mRNA (red) was used as MO tracer. Scale bar is 20μm. **E'** shows a quantification of the abnormal MCC clustering in MO-splice-scf-L/S and MO-ATG-scf-L/S-injected embryos. **F**: A quantification of the MCC intercalation in control and *scf* MO-injected embryos.

Figure	Stage/ condition	n cells	n embryos	n experiments
1 B	14	456	4	3
	16	591	5	3
	18	408	4	3
	20	761	6	3
	22	572	6	3
	25	450	6	3
1 C	14	422	3	2
	16	587	4	2
	18	306	3	2
	20	331	2	1
1 D	14	440	3	2
	16	490	4	3
	18	306	3	2
	20	331	2	1
	22	384	4	2
	25	227	4	2
3 F	Ctrl	108	4	4
	CK-666	62	5	5
3 G	Ctrl	94	10	10
	CK-666	26	3	3
3H	Ctrl	227	4	4
	CK-666	209	2	2
	SMIFH2	144	2	2
3I	Ctrl	248	4	1
	CK-666	491	6	1
	SMIFH2	457	6	1
5 C	Ctrl	108	4	4
	Axtitinib	64	3	3
	MO *kit*	147	5	5
5 C'	Ctrl	94	10	10
	Axtitinib	56	9	9
	MO *kit*	70	5	5
5 G	Ctrl st 20	683	6	2
	Ctrl st 22	267	4	2
	Ctrl st 25	377	6	4
	Axtitinib st 20	441	5	2
	Axtitinib st 22	625	4	2
	Axtitinib st 25	724	6	3
	MO *kit* st 20	248	2	1
	MO *kit* st 22	370	3	1
	MO *kit* st 25	411	4	2
5 H	Ctrl st 20	761	6	3
	Ctrl st 22	572	6	3
	Ctrl st 25	663	12	4
	Axtitinib st 20	830	8	3
	Axtitinib st 22	753	5	2
	Axtitinib st 25	735	8	2
	MO *kit* st 20	860	5	2
	MO *kit* st 22	998	8	2
	MO *kit* st 25	857	9	3

Figure	Stage/ condition	n cells	n embryos	n experiments
5 I	Ctrl	227	4	4
	Axtitinib	231	2	2
	MO *kit*	219	2	2
6 C	Ctrl st 20	761	6	3
	Ctrl st 22	572	6	3
	Ctrl st 25	518	8	4
	MO *scf* st 20	678	7	4
	MO *scf* st 22	545	6	1
	MO *scf* st 25	768	8	4
6 D	Ctrl	227	4	4
	MO *scf*	220	3	3
6 F	Ctrl	108	4	4
	MO *scf*	64	5	5
6 I	Ctrl	94	10	10
	MO *scf*	62	5	5
7 C	Ctrl	506	8	2
	paTub::Scf-GFP	515	8	2
7 H	Ctrl	1707	16	2
	kit mRNA 0,1 ng	1526	15	2
	kit mRNA 1 ng	1704	17	2
7 I	Ctrl	272	5	2
	kit mRNA 0,1 ng	301	5	2
	kit mRNA 1 ng	299	5	2
S2 C	Ctrl st 19	373	3	1
	CK-666 st 19	288	3	1
	SMIFH2 st 19	386	3	1
	Ctrl st 25	116	2	1
	CK-666 st 25	208	2	1
	SMIFH2 st 25	144	2	1
S5 E'	Ctrl	954	14	2
	kit-MO-Res	837	13	2
	MO *kit*	1049	14	2
	MO *kit* + *kit*-MO-res	894	14	2
S5 F'	Ctrl	558	8	2
	MO *kit* ATG	522	5	2
	MO *kit* spl	592	6	2
S6 E'	Ctrl	602	12	2
	MO Spl *scf* 20 ng	624	10	2
	MO ATG *scf* 10ng	723	7	2
S6 F	Ctrl st 20	683	6	2
	Ctrl st 22	267	4	2
	Ctrl st 25	226	4	2
	MO *scf* st 20	720	7	3
	MO *scf* st 22	408	4	1
	MO *scf* st 25	367	5	2

Table S1: Total number of cells, embryos and repeat experiments for all graphs in all figures

Movie 1

Click here to access/download

Supplemental Videos and Spreadsheets

movie 1.avi

Movie 2

Click here to access/download

Supplemental Videos and Spreadsheets

movie 2.avi

Movie 3

Click here to access/download

Supplemental Videos and Spreadsheets

movie 3.avi

Movie 4

Click here to access/download

Supplemental Videos and Spreadsheets

movie 4.avi

Movie 5

Click here to access/download

Supplemental Videos and Spreadsheets

movie 5.avi

Movie 6

Click here to access/download

Supplemental Videos and Spreadsheets

movie 6.avi

Movie 7

Click here to access/download

Supplemental Videos and Spreadsheets

movie 7.avi

Movie 8

Click here to access/download

Supplemental Videos and Spreadsheets

movie 8.avi

Movie 9

Click here to access/download

Supplemental Videos and Spreadsheets

movie 9.avi

Movie 10

Click here to access/download

Supplemental Videos and Spreadsheets

movie 10.avi

Movie 11

Click here to access/download

Supplemental Videos and Spreadsheets

movie 11.avi

Movie 12

Click here to access/download

Supplemental Videos and Spreadsheets

movie 12.avi

Movie 13

Click here to access/download

Supplemental Videos and Spreadsheets

movie 13.avi

Movie 14

Click here to access/download

Supplemental Videos and Spreadsheets

movie 14.avi

Movie 15

Click here to access/download

Supplemental Videos and Spreadsheets

movie 15.avi

Movie S1

Click here to access/download

Supplemental Videos and Spreadsheets

movie S1.avi

Movie S2

Click here to access/download

Supplemental Videos and Spreadsheets

movie S2.avi

Movie S3

Click here to access/download

Supplemental Videos and Spreadsheets

movie S3.avi

Movie S4

Click here to access/download

Supplemental Videos and Spreadsheets

movie S4.avi

Movie S5

Click here to access/download

Supplemental Videos and Spreadsheets

movie S5.avi

6.2. Experiments required for manuscript revision

6.2.1. The affinity of MCCs for outer layer cell junctions is a non-random behavior

In the submitted manuscript, the live-imaging of embryos co-injected with α-tub::LifeActGFP and with a synthetic mRNA coding for a membrane-localized form of RFP to label outer-layer cells revealed that, while in the inner-layer, most MCCs preferentially moved along the junctions among outer-layer cells (92.55% of 94 analyzed MCCs closely followed outer layer junctions over >2hrs) (Figure 3B, 3G and movie 7). We also analysed the position of the MCCs relative to the outer layer cells by co-staining of embryos for the MCC marker *a-tubulin* (*a-tub*) (Fluorescent In Situ Hybridization-FISH) and the tight junction protein ZO-1 to mark outer-layer apical tight junctions (ImmunoFluorescence-IF) (Figure 1 A). We next quantified the number of outer-layer vertices positioned in correspondence of each MCC (Figure 1 A, C). The graph shows that the size of MCCs relative to the outer layer cells is large enough to observe MCCs positioned in correspondence to up to 8 outer-layer vertices.

While each MCC progressively localizes in correspondence to an individual vertex, the number of vertices and junctions than a single MCC can overlap in the early stage is large enough to suspect that the quantified movement of MCCs relative to the outer layer cells junction might be random. Indeed, the observation that MCCs move within the inner layer by following the outer layer intercellular junctions could result from the large size of MCCs relative to the outer layer cells junction distribution. Therefore, the changes in the direction of MCC movements, that we interpreted as a consequence of their affinity for the outer layer junctions, could just be random. In other words, MCCs are so large that, regardless of the direction they take, they are always associated with outer layer cells junctions.

To test this hypothesis, a negative control was made *in silico* after rotating the outer layer cells mRFP signal by 90° (Figure T1 B, movie T1). In the resulting movie, cells continue to be observed in correspondence to outer cells junctions, but the proportion of cells qualified as “following junctions” is significantly decreased (Figure T1 C). In this artificial condition we often observe MCCs travelling below outer layer cells and ignoring the outer layer cells junctions. This result suggests that MCCs following outer layer cells junctions is a non-random effect in control condition.

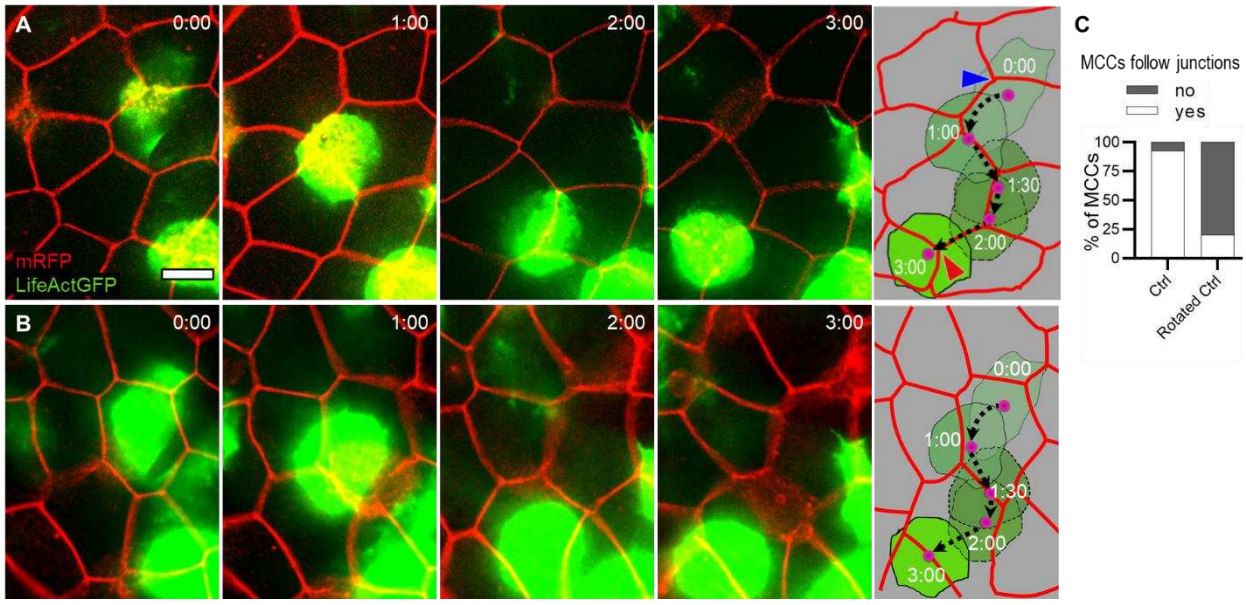

Figure T1: MCCs affinity for outer layer cells junctions is a non-random behavior.

(A) Frames from movie 7 showing an α-tub::LifeActGFP-labelled MCC (magenta asterisk) moving along the intercellular junctions among overlying outer-layer cells labelled by mRFP. The blue and the red arrowheads highlight the initial and final positions of the labelled MCC. The last panel recapitulated the positions of the observed MCC over 3h. The black dotted line shows the displacement of the MCC centroid. **(B)** Frames from movie 7 after rotating *in silico* the mRFP channel by 90° to the left. As shown in the right scheme, the trajectory of the tracked MCC is the same but the movement of the cell doesn't follow any more the outer layer cell junctions. **(C)** Graph showing the proportion of MCCs that followed outer-layer junctions over a period of 2h before and after *in silico* rotation of the outer layer mRFP channel by 90°.

6.2.2. Quantification of cell speed

In the submitted manuscript, we characterized the behavior of MCCs during the phase of pattern establishment preceding their radial intercalation. However, a proper quantification of the cell speed and time delays associated with mutual repulsion was missing. In this section, I will present preliminary result from the ongoing quantifications requiered by the reviewers. Notably, a particular statement in the discussion was challenged: l. 375 'Our data are the first to unambiguously show that MCCs actively move within the inner layer and that motility is the main driver of their transition from a chaotic distribution, characterized by extensive inter-MCC contacts, to an orderly pattern, where MCCs are present as isolated cells, each localised in correspondence of an outer-layer vertex.'; and l. 394: 'This shift correlates with a progressive decrease of MCC motility within the inner layer'.

The measurement of cell speed was challenging because of technical issues due to the tissue growth-induced lateral drift occurring in all our movies. We thus use an *in silico* approach based on a Deep Learning strategy coupled to a Kanade-Lucas algorithm to stabilize our movies and a manual tracking of MCCs centroid over time to extract information about the instantaneous speed of the cells (Figure T2 A). In this graph, we plot the mean instant speed of all recorded MCCs from control conditions and the trending curve to facilitate the analysis of MCC speed evolution over time. The MCC mean instant speed can be subdivided in three steps: acceleration, plateau and deceleration. At the beginning of the movies, the mean cell speed is nearly null and progressivelly increases to reach up to 0,47µm/min after 40min. Then, a plateau phase with minor fluctuations of the mean instant speed lasts for about 90min and is followed by progressive decrease of the instant speed which tends to zero. However the large standard error of the mean shows that the cells are not synchronized: immobile and migrating cells exist simultaneously. These results suggest that the migratory behavior of the MCCs is acquired around stage 14-15, when our live imaging experiments start. During the plateau with 'maximal' cell speed, we can assume that most MCCs separate through mutual repulsion and then the motility progressively decrease as MCCs switch from lateral migration to radial intercalation.

We then analyzed case by case the evolution of instant cell speed relative to mutual repulsion events to test wether the maximal migration phase is associated with mutual repulsion (Figure T3 B, C). When looking closely at individual cells, we noticed that the instant speed oscillates from null to spike migration over time (Figure T3 B). We then looked at MCCs in a region with a high density of LifeactGFP-expressing MCCs and tracked two cells to analyze their trajectories and interactions, both between themselves and with the other neighboring MCCs (Figure T3 C, blue and red dots and lines) as well as the respective instant speed of the tracked MCCs (Figure T3 B). Interestingly, when the red and blue cells enter in contact, both cells freeze and their motility becomes null (Figure T3B dark C, Figure T3C time 25min). Nearly 20 minutes later, the blue and red MCCs have separated, both cells have turned the direction of their movements by nearly

180° and the speed of both cells increase higher than before the collision (Figure T3B dark S). While the red cell remains in a apparently more MCC-dense region and often changes direction upon collision with other cells (Figure T3 B red asterisk), the blue cell moves to an apparently less MCC-dense area and shows a higher speed, together with a more persistent directional migration over a longer distance. Then the blue MCC is stopped again when it collides with two MCCs and changes direction (Figure T3C time 1:55 and 4:00, blue asterisks). After 4 hours, the apparent order of the system is greatly improved with a better dispersion of the MCCs, some of which appear stabilized underneath vertices and ready to intercalate.

It is worth mentioning that the MCC movement directionality often changed upon mutual contact but also correlated with outer layer cells junctions, showing that both elements affect the system, as predicted by our matematical model.

Together, this result strengthened the previous statement of a MCC population getting progressively regularly spaced within the iner layer through mutual repulsion. Besides, as MCCs become regularly spaced and move along the outer layer junctions, they gradually decrease their lateral motility, associate with individual vertices and start the radial intercalation movements. This quantification also reveals a decrease of speed associated with mutual repulsion, followed by an increase in speed when cells separate.

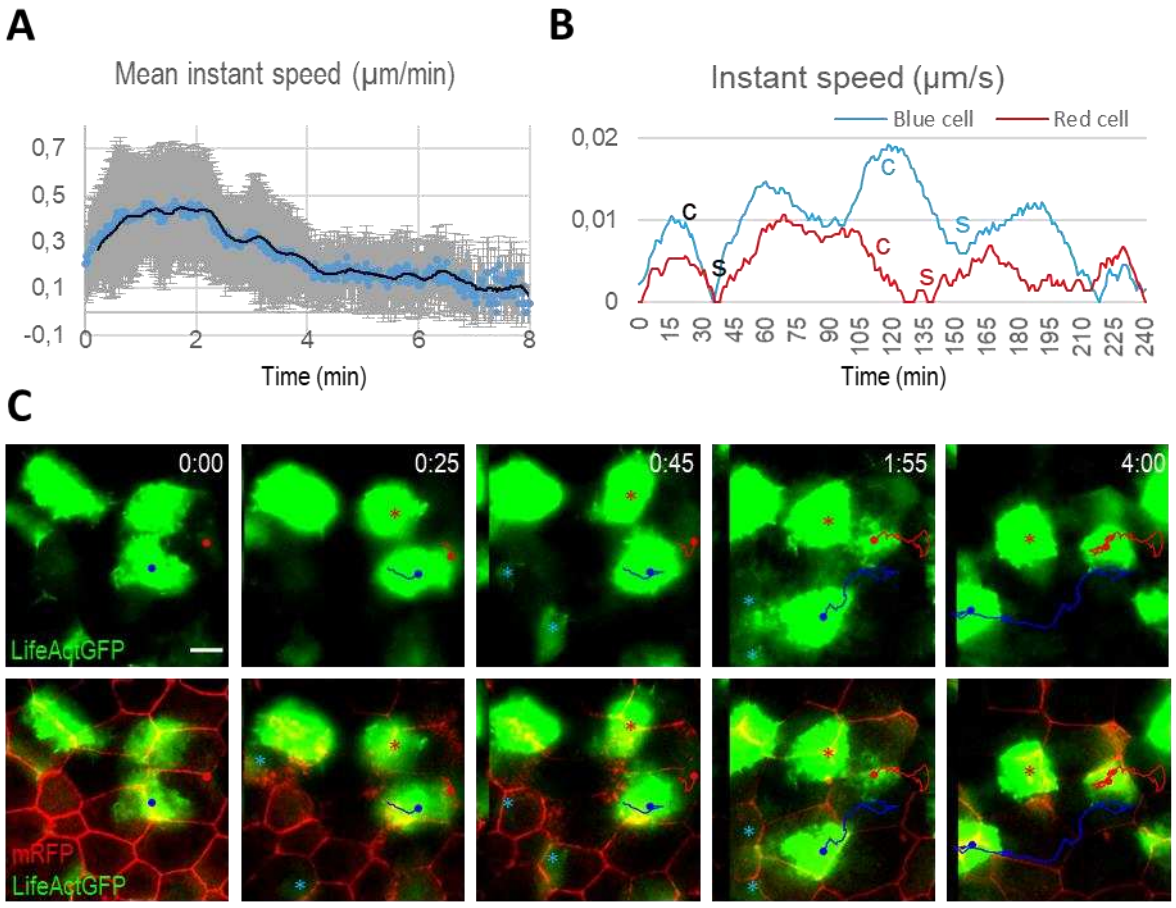

Figure T2: Characterization of cell speed during mutual repulsion.

(**A**) Mean instant speed of all control condition movies (n = 66 cells). Dark line represents the smooth mean with a time period of 15min and gray bars represent the standard error of the mean.

(**B**) Graphical representation of the instant speed of the blue and red tracked cells showing the evolution of their speed upon mutual contact and after separation (dark C and S respectively). Both cells show variation in their instant speed after collision with neighbouring cells (blue and red C and S).

(**C)** Still frames from movie T2 recorded with Spinning disk confocal video microscopy in control condition showing tracked α-tub::LifeActGFP-labelled MCC (upper panel) or merged a-tub::LifeActGFP-labelled MCC and RFP-labeled outer layer cells junctions (lower panel). Dots show the approximate centroids of two tracked MCCs and lines show the trajectories of the cells throughout the movie. After the blue and red cells have collided (25min), the two cells separate by changing direction by approximately 180° as shown by trajectory lines. Blue and red asterisks shows cells that have been impacted by blue and red cells respectively and correlate with the variations of instant speed shown in graph B.

6.2.3. Does the cleaved version of Scf stimulate the mutual dispersion of MCCs?

Several experimental evidences presented in the submitted paper suggest that, as it has been described for other models, soluble and membrane-bound forms of Scf might control distinct aspects of the MCC patterning process, namely, mutual dispersion and that affinity to the outer layer junctions. To corroborate these findings and to reply to the reviewers' criticisms, we performed a series of additional experiments.

We injected embryos with full-length *scf* mRNA, and followed the behavior of labelled MCCs with α-tub::LifeActGFP in mRFP-injected embryos (Figure T3 A, movie). Spinning-disk confocal video microscopy of stage 15 embryos revealed that LifeActGFP-expressing MCCs (labelled with red, pink and white asterisks) do not efficiently separate and show long time of contact. While the pink cell is intercalating, the red one continue to emit protrusion toward the direction of the pink cell and often extend protrusion toward the bottom of one outer layer cells. In the same time, the white cell that was remaining in contact with the pink cell moves away but totally ignores the outer layer cells junctions. Together this suggests that the affinity for the outer-layer cells junctions is impaired by ectopic expression of Scf. Colorimetric α-*tub in situ* on stage 25 embryos injected with full-length *scf* mRNA shows that the distribution of MCCs is severely impaired, with large clusters of MCCs forming (Figure T3B, unpublished data from A.Pasini). Together these results suggest that full-length *scf* expressed throughout the whole epidermis affect both the affinity of MCCs for outer layer cells junctions and the mutual repulsion.

To test the hypothesis that SCF is cleaved (as suggested by Figure 4E of the manuscript) and regulates the mutual repulsion among MCCs, we injected a commercially available mouse recombinant SCF protein (mSCF) in the blastocoel of Xenopus embryos which had been previously depleted of endogenous Scf by MO *scf* injection at stage 8 cells (Figure T3 F)., Embryos injected in the blastocoel with Bovine Serum Albumin (BSA) as a control or with mSCF alone show a regular dispersion of the MCCs at stage 25 (Figure T3 C, D). However, no differences were visible between embryos injected with MO-*scf* alone and those co-injected with MO-*scf* and mSCF (Figure T3 E-F). Since the efficiency of mouse SCF o stimulate Xenopus Kit receptor has not been proven, we cannot conclude from this result.

To pursue the investigation of possible distinct roles of cleaved and membrane anchored Scf forms, we generated a construct coding a tagged, truncated version of Scf. In this construct, a FLAG tag and a STOP codon are introduced immediately upstream to the transmembrane domain of Scf, to generate a truncated, tagged version of the protein, which we expect to be soluble. (Figure T3G). The mRNA generated by this construct is also resistant to the action of MO-Scf, since it lacks the MO recognition sequence. Western Blotting with an anti-FLAG antibody of lysates of animal caps or whole embryos injected with amRNA coding for this truncated protein reveal its correct expression (Figure T3 I).

However, the protein was not detected in the supernatant from injected animal caps or whole embryos, raising doubts about its processing and secretion. Moreover, injection of the mRNA coding for this MO-resistant, truncated and FLAG-tagged protein, alone or in combination with MO-scf, severely impairs the distribution of the MCCs (Figure T3 H,I), making it impossible to draw clear conclusions from this experiment.
We are currently generating other, shorter, versions of the tagged and truncated Scf, where the Stop codon is inserted upstream or immediately downstream of the exon 6.,

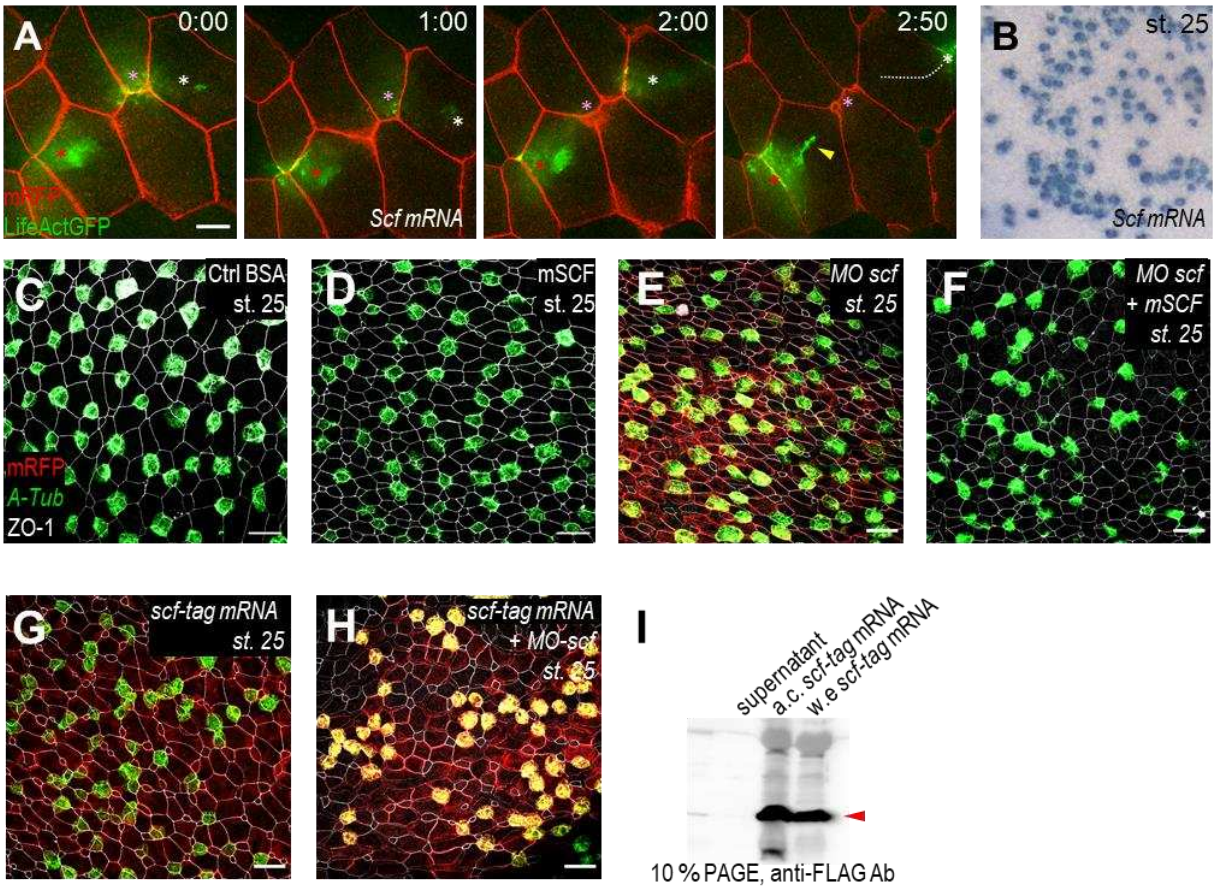

Figure T3: Does the cleaved version of Scf stimulate the mutual dispersion of MCCs?

A) Still frames from movie T3 recorded with Spinning disk confocal video microscopy in embryo injected with 0,1 ng of *scf mRNA* showing α-tub::LifeActGFP-labelled MCC and mRFP labelled outer layer cells. Red, purple and white asterisks show 3 different MCCs position, white dot-line show the trajectory of the white asterisk labeled MCC. Yellow arrowhead shows abnormal protrusion oriented toward the bottom of an outer layer cell.
B) α-tubulin colorimetric *in situ* hybridizations showing the chaotic distribution of MCCs in an embryo injected with 0,1ng of *scf mRNA.* Scale bar 20µm
C-H) α-tubulin fluorescent *in situ* hybridizations (green) and ZO-1/mRFP immunofluorescence (White and red respectively) in the following conditions: control embryo injected with BSA 1% in blastocoel stage 10,5 (**C**), embryo injected with 10 ng of mouse recombinant soluble SCF (mSCF) in blastocoel stage 10,5 (**D**), embryo injected with 20 ng of *scf* ATG morpholino (**E**), embryo co-injected with 20 ng of *scf* ATG morpholino and 10 ng of (mSCF) in blastocoel stage 10,5 (**F**) embryo injected with mRNA construct coding a tagged, truncated version of Scf which is MO-resistant (*scf-tag)* (**G**) embryo co-injected with *scf-tag mRNA and scf* ATG morpholino (**H**). Scale bar 50µm
I) Wester blot with an anti-FLAG antibody of caps / embryos injected with mRNA coding for *scf-tag* or with the supernatant of these caps. Red arrowhead point to the 15kDa SCF-tag construct.
a.c = animal caps; w.e = whole embryos

6.3. Unpublished data

6.3.1. Wiskott–Aldrich syndrome protein does not regulate the mutual repulsion of MCCs

In the submitted paper, we demonstrate the role of actin cytoskeleton in both MCC mutual repulsion and in their affinity for outer-layer junctions through the use of the well-characterized pharmacological inhibitors of the two main pathways of actin polymerization: CK-666, an inhibitor of the actin-branching nucleator ARP2/3 (Hetrick et al., 2013) and SMIFH2, an inhibitor of the actin-bundling factor FORMIN(Rizvi et al., 2009). In Chapter 4 of this manuscript, I show that the Kit receptor has been linked to actin remodeling (Mani et al., 2009; Shamloo et al., 2013). Considering the similarities in the loss of mutual repulsion phenotype observed in both Arp2/3 and SCF/Kit inhibition, we searched for potential regulators of actin branching remodeling among the known targets of Kit.

Wiskott-Aldrich Syndrome Protein (WASP), a known, downstream effector of the SCF/Kit signaling pathway and an interactor of Arp2/3 with a role in actin cytoskeleton remodeling as an actin nucleation-promoting factor, appeared as potentially interesting candidate (Mani et al., 2009). We thus tested its role in MCC patterning by using its commercially available pharmacological inhibitor Wiskostatin (Peterson et al., 2004)(Peterson et al, 2004)., or a dominant-negative form (Yamaguchi et al., 2002).

FISH for α-tub coupled with ZO-1 IF on embryos treated with 40μM wiskostatin from stage 12 and fixed at stage 25 showed that most MCCs are regularly distributed, with rare events of direct mutual contact (Figure T4 A-C) and properly emerge at the outer-layer apical surface (Figure T4 A,B).

Live imaging of embryos injected with a construct carrying a GFP-tagged, dominant-negative version of WASP under the control of the α-tub promoter showed that GFP-expressing MCCs moved actively within the plane of the inner layer and show mutual repulsion upon contact (FigureT4 D). Together these results show that WASP is unlikely to be an effector of the Scf/Kit pathway in the context of Xenopus MCC patterning.

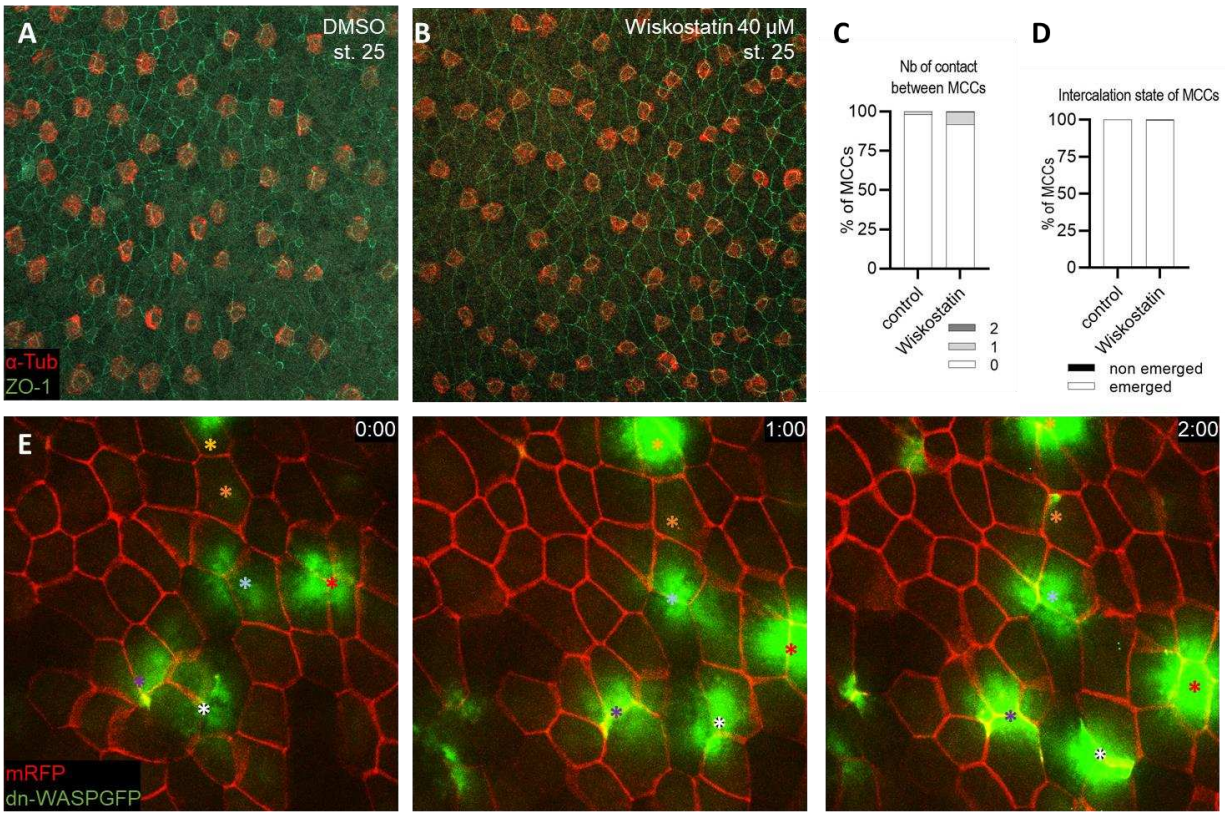

Figure T4: WASP do not regulate MCC mutual dispersion and radial intercalation.

A,B: Embryos were treated from stage 12 with 1% DMSO (**C**), 40µM wiskistatin (**D**) and analyzed at stage 25 by a-tub FISH and ZO-1 IF to examine MCC patterning. Following wiskostatin treatment, MCCs are intercalated into the outer layer and were regularly distributed. D: Graph showing the proportion of intercalated MCCs at stage 25 in control and wiskostatin -treated embryos. D: Graph showing the distribution of the number of contacts among MCCs at stage 25 in control and wiskostatin -treated embryos. E: Spinning disk confocal video microscopy was used to track a-tub::dn-WASPGFP transgenic MCCs within the inner epidermal layer. Still frames from the movie are shown. Asterisks point MCCs that moved and separate under mRFP-injected outer-layer cells to appreciate MCC dispersion.

7. Discussion

From tissue- to cell- scale, the presence of regular patterns in living beings has always been a challenge for the developmental molecular biologist since the underlying molecular mechanisms appear to be extremely dependent on the species, tissues and patterning considered. One striking characteristic of the multiciliated cells (MCCs) that cover the surface of the *Xenopus* tadpole epidermis is their nearly perfect regular spacing pattern. Over the last past two decades, this mucociliary epithelium has been set up as a model for the study of MCCs development and function. Yet, neither the developmental mechanisms that establish the regular spacing pattern of MCCs nor their physiological function during tadpole life are clearly understood.

Taking advantage of the available genetic and molecular tools, as well as of the amenability of *Xenopus* embryos to live-imaging, I focused my thesis work on characterizing the mechanisms that generate the regular spacing pattern of immature MCCs on the embryo surface. This developmental question has been little studied relative to the major efforts deployed to unravel the mechanisms of MCC specification intercalation and differentiation. Looking at the process as a whole, I followed MCCs from the earliest stage at which they can be visualized *in vivo,* as immature MCCs within the ectodermal inner layer, all the way to the moment when they have completed their intercalation and differentiate.

This discussion will further develop and enrich the "Discussion" section of the submitted manuscript, taking into consideration the ongoing experiments asked by the reviewers and not yet included in the manuscript, as well as a few additional results.

The MCCs cell specification and the regular pattern generation are not concomitant events.

A common feature of many organisms is the generation of patterns under the control of robust Gene Regulatory Networks (GRNs) that concomitantly control the specification of cell types and their position within developing embryos (Briscoe & Small, 2015; Davidson, 2010).

In *Xenopus,* pioneering studies on epidermal cell fate specification have shown that complex GNRs including the BMP and Delta/Notch pathways regulate the distribution of MCCs, ionocytes and SSCs throughout the inner layer of the epidermis with an overall control of the number of each cell type(Deblandre et al., 1999; Jennifer L. Stubbs et al., 2006; Hayes et al., 2007; Quigley et al., 2011; Cibois et al., 2015). Based on the well-characterized Delta/Notch-mediated lateral inhibition process described in *Drosophila*

and other model organisms, these studies proposed that the regularly-scatterd pattern of MCCs is established concomitantly with or immediately after their birth within the inner layer.

In their study "A two-step mechanism generates the spacing pattern of the ciliated cells in the skin of Xenopus embryos", Deblandre et al proposed a model in which the MCC regular spacing pattern is preprinted at birth and later refined by restricting the intercalation of each MCC at a single outer-layer vertex (Deblandre et al., 1999). This publication shows that Notch signal regulates the balance of the different cell types inside the inner layer and that Notch inhibition leads to the generation of supernumerary MCCs at the expense of other intercalating cell type. However, several pieces of evidence suggest that the model is not as simple as it look.

First, if the same Notch pathway regulates the fate of several cell types, why should lateral inhibition regulate the spacing pattern as a unique property of MCCs among the intercalating cells?

Second, it was shown that Notch-dependent lateral inhibition is not required for the MCCs to intercalate in a regular pattern. Indeed, upon Notch inhibition, the outer layer can accommodate twice as many MCCs with no violation of the non-contiguity rule (Deblandre et al., 1999; Stubbs et al., 2006). These results suggest that, without a tight regulation of their number, nor of their initial position, MCCs still manage to organize in a regular spacing pattern. Beside, this also indicates that, in normal conditions, vertices are in large excess with respect to incoming MCCs and that MCC spacing is not directly linked to the pattern of distribution of vertices. The fact that when the GNRs which control their fate are molecularly disrupted, MCCs can still organize in a regular distribution pattern strongly weakened the hypothesis of a GNR-dependent pre-printed patterning mechanism.

Last, the results I obtained during my thesis argue against this hypothesis. Indeed, in the submitted manuscript, we non-ambiguously show that, after they become fated, the immature MCCs are chaotically distributed throughout the whole inner layer of the epidermis (Figure 1).

In the developing embryo, we showed that MCCs transit from a chaotic distribution, characterized by extensive mutual contacts, to an orderly pattern, where they are present as isolated cells. Moreover, although it is known that MCCs intercalate each at one individual outer-layer vertex, we showed that they are initially positioned in correspondence of more than one vertex (Figure 1C). This apparent improved dispersion pattern could be explained by selective mechanisms in which only isolated cells and/or cell localized under a single vertex are selected to become MCCs or to survive However, we experimentally excluded both cell death and cell fate reversal as possible explanation (Figure S1). We then demonstrate that the immature MCCs actively move within the inner layer and that cell motility is the motor of pattern generation.

However, because of technical limits, we cannot record the spatial distribution of MCCs from the actual moment of their birth (stage 10-11) but only a few hours later in the development (from stage 14). Even if extensive cell-cell contact is observed among MCCs at stage 14, we don't know much about their behavior during the earliest stages. Yet we

known that at the time MCCs are born, the inner layer of the epidermis sustains intense remodeling from a multilayer to a monolayer through radial intercalation (Szabó et al., 2016). So, we cannot be sure if a Notch-lateral-inhibition like mechanisms regularly spaces MCCs precursor at birth. It might be possible that Notch controls very early MCC fate and dispersion, but that this spacing is subequently be lost during the inner layer thinning and that acquisition of a cell motility is required for the proper final positioning of MCCs and their intercalation. Obviously, considering the drastic change in the inner layer at the early stages, it seems probable that Notch function is to promote an even distribution of fated MCCs through the skin while, as we've shown, the regular spacing of MCCs is a self-organized cell motility-based patterning process. Yet many blind spots remain worthy to be investigated about the life of MCCs from their birth especially with regard to the highly dense MCCs distribution and low motility recorded around stage 14

The power of mathematical modeling to predict biological inputs of a self-organized MCC pattern establishment

Mathematical models such as Turing's reaction diffusion model have been an inspiration source for developmental biologists but also an intense source of disagreement until sound evidence that the model actually works *in vivo* is given. Nowadays, collaborations often emerge between physicists, mathematicians and biologists to develop prediction models, although the relevance of the modelling itself could be challenged depending on the question and the purpose of the model.

During my thesis work, the purpose of using *in silico* simulations was to easily questions the model about the relevance of candidate parameters and subsequently test them *in vivo.* Then, after assuming that the observed pattern of MCC distribution was indeed a self-organizing motility-based process, the mathematical modeling became a powerful tool to identify the minimal inputs necessary to recapitulate the final pattern in our system. This simplified mathematical model became a support to make hypotheses and test them experimentally *in vivo* or reversely test *in silico* the sufficiency of observed biological variables.

The mathematical/biological approach used during my thesis work illustrates very well the intense exchange between both fields. The *in silico* simulation defined two conditions required to evenly distribute a population of internal motile cells below epithelial vertices: 1) motile cells must repel each other, thus minimizing their mutual contacts, 2) they must maximize their contacts with outer-layer junctions, so as to stabilize at vertices, which display the highest local density of junctions.

Interestingly, both parameters emerged from biological inputs taken from the literature such as homotypic repulsion, which regularly space cells in other instances of cell motility-based regular patterns (Davis et al., 2012; Villar-Cerviño et al., 2013) and the restriction of intercalation at the outer layer cell vertices, suggesting that some mechanisms favour the cell to localize there (Deblandre et al., 1999; Jennifer L. Stubbs et al., 2006). These parameters were used to implement our model and to test their theoretical

relevance, separately or in combination. After we showed that a regular pattern can arise from the combination of mutual repulsion and junction affinity *in silico,* we later identified both parameters *in vivo.*

Another strength of the mathematical modelling approach is that it easily allows us to test the contribution of both parameters together or separately. *In vivo*, we assume a homogeneous localization of SCF along the junctions as an adhesive molecule to attract MCCs at vertices as the *in silico* model suggested. However, the fact that a mathematical model works is not a proof *per se* and we cannot exclude that the experimental approach lacks accuracy to show accumulations at vertices or the existence of other vertex-localized molecule yet to be identified.

On the other hand, mathematical models always present weaknesses and our *in silico* model is no exception. For example, the model we used does not take into account any migration speed or contact time akin to what one can measure in actual experiments. The time evolution is a succession of stationary states that make the total energy of the system decrease, but the dynamics is a succession of events where cells move according to a diffusion constant which is a free parameter on a simulation time that cannot be easily compared to the experimental one. While the direction of cells *in vivo* is dictated by the organization of their cytoskeleton, where each change of direction depends on its repolarization which depend on the previous step, the simulations are already a random walk. At each step of simulation movement of the cells are guided by the energy gradient of the system, akin to a discrete brownian motion following this energy gradient.

MCCs mutual repulsion and intercalation are cell autonomous processes which both belong to the self-organized-patterning process.

Filming live MCCs in developing embryos allowed us to visualize that the MCC behavior *in vivo* follows the two predicted parameters and revealed that actin cytoskeleton is involved in both. Immature MCCs in the inner layer extend unpolarized basolateral actin-rich protrusions with which they move and explore the surrounding environment. Whenever two such MCCs come into direct contact, the actin-rich protrusions involved in the contact are retracted, while others are deployed in different regions of the cell body, thus resulting in the two cells moving away from each other. Concomitantly, immature MCCs also emit apically-polarized actin-rich protrusions towards junctions between outer-layer cells. Despite the fact that both basolaterally- and apically-directed actin protrusions largely coexist within each MCC, a clear temporal shift between the two is observed: over time, the basolateral protrusive activity decreases, while the apically-directed one gains in intensity and stability (see example in Figure 2B and movie 2). This shift correlates with a progressive decrease of MCC motility within the inner layer and enhanced stabilization under individual vertices (as shown by Figure T2). When we analyzed the instant speed of a large cohort of MCCs from stage 14 up to approximately stage 22 (based on theoretical developmental table, since the developmental stage cannot be seen after inclusion in agar), we observed a large variety of behaviors. On average, the

MCC speed appears low for the first 40 minutes, suggesting that MCCs have only recently acquired their motile properties and start to efficiently separate only from stage 15. Then, we observed a period of maximal speed that spans stage 15 to stage 18. Interestingly, this correspond to the period in which most MCCs separate (Figure 1 A,B) thus improving the most the system order (Figure 1 D). The phase in which we observed a significant decrease of MCC speed corresponds to the time when most MCCs have already separated and started their association to vertices. Remarkably, the heterogeneous behaviors among MCCs revealed by the large error bars in the graph suggest that a lack of synchronization among MCCs is required to allow for the fine-tuning of the spacing pattern over time (Figure T2A). The intercalation of an individual MCC lasts approximately 1,5 hours while the time window in which we observe intercalation events last twice longer. Together this means that mutual repulsion and radial intercalation are overlapping events.

Stochastically, MCCs will slow down as their lateral protrusions decrease and apically-polarized protrusions are extended towards junctions between outer-layer cells. At the same time, other MCCs will continue to migrate within the inner layer plane until they find an isolated position. Consistent with this idea, we found evidence that MCC specification itself may be asynchronous (Figure S1). As a result, by early tailbud stage, all MCCs end up finding a free vertex at regular intervals, to which they anchor and through which they subsequently intercalate.

Surprisingly, we observed that the migration range of a given MCC might be reversely correlated to the number of other MCC it can encounter in its migration path (Figure T2 C). We often observed MCCs with higher speed after separating from another cells but this tendency decreases as the embryos age. Indeed, when contacts among MCCs arise later in the movies we still observed movement allowing the cells to separate but most of the cells will stop at the closest vertex. This suggests that the potential of migration of cells decrease over time.

Interestingly, the stage of intercalation has been recently correlated with microtubules and the number of centrioles (Collins et al 2020). Since centriole amplification happened when most MCCs are still within the inner layer, we can assume that the faster cells to amplify centrioles will be the first to intercalate, while cells with fewer centrioles will remain competent to mutual repulsion for a longer time. This asynchronous centriole amplification among MCCs will then play a crucial role in the generation of the spacing pattern. An open question remains to known wether mutual repulsion affects microtubule organization and thus the timing of intercalation.

Self-organized generation of a regular cellular pattern by mutual repulsion and homing.

Our data show that within the inner layer of the developing Xenopus epidermis, immature MCCs move in a partially random fashion. While the mathematical models assume a pure Brownian diffusive motion of MCCs, *in vitro* experiments of a limited

number of MCCs on a free substrate would be required to test the real nature of this random movement. Interestingly, the free displacement of the MCCs were constrained by mutual repulsion and affinity for outer-layer intercellular junctions both *in silico* and *in vivo* and these constrained movements are required for the establishment of a regularly-dispersed MCC pattern. This observation prompts analogies with other instances of developmental patterns emerging from the semi-stochastic movements of cell populations. Phenomena of contact-dependent homotypic repulsion in which mutually contacting cells withdraw projections and/or change their direction of movement underlie the regular distribution of Cajal-Retzius (CR) neurons (Villar-Cervino et al., 2013) and Retinal Horizontal (RH) cells (Galli-Resta et al., 2002) in mammals, pigment cells in zebrafish (Walderich et al., 2016) and haemocytes in Drosophila (Davis et al., 2012). The case of Xenopus MCC patterning shows nevertheless some specificities. Most notably, MCCs are already present throughout most of the developing epidermis at the start of the patterning process, such that their scattering relies almost exclusively on short-range "wobbling" random movements, without need for a concomitant long-range directional migration, as is the case for CR neurons. As a consequence, MCCs lack a well-defined leading process but rather present a multipolar protrusive activity. Moreover, unlike Danio pigment cells, scattering MCCs are post-mitotic and the patterning system may not need to adjust to variations in absolute cell numbers. Finally, in sharp contrast with Drosophila haemocytes, which continue moving and repelling each other at every encounter, even after regular distribution is reached, dispersed MCCs become fixed by anchoring and intercalating into outer-layer vertices. Interestingly, to our knowledge, the only other described case of (semi-) orderly epithelial intercalation of a population of individually dispersed motile cells occurs during the development of the peripheral nervous system in the cephalochordate Amphioxus (Benito-Gutiérrez et al., 2005; Kaltenbach et al., 2009), but the underlying mechanisms are unknown. Overall, our work reveals a new instance of self-organized tissue-wide developmental patterning, emerging from the interplay of stochastic short-range repulsive and stabilizing intercellular interactions, rather than relying on tightly controlled GRNs and classical guidance mechanisms. This is probably the most information-parsimonious strategy to optimize the distribution of a cell population whose function requires that its area of dispersion be covered completely but non-redundantly. Our identification of a molecular pathway responsible for controlling MCC dispersion, independently of cell numbers and differentiation, will make it possible to functionally explore the physiological meaning of such a pattern and the possible outcome of its perturbation.

The mutual repulsion of MCCs, a new case of contact inhibition of locomotion?

All examples of contact-dependent homotypic repulsion mentioned above rely on a common principle upon which colliding cells instantly reorganize their cytoskeleton and withdrew from each other, the so-called phenomenon of contact inhibition of locomotion (CIL) (Roycroft & Mayor, 2016). Interestingly, even if the dispersing MCCs lack a clear

polarity, they share many similarities with the archetypal CIL description made by Abercrombie (Abercrombie & Heaysman, 1954).

(1) Randomly migrating MCCs initially enter in contact. Even if our characterization lacks evidence of a molecular recognition of cells through conventional adhesion molecule such as E-cadherin, these molecules are indeed expressed in MCCs.
(2) The protrusive activity is inhibited at the contact site, as we showed by quantifying the time of contact between cells and looking at actin cytoskeleton and Arp2/3 dynamic with LifeAct and p41 fluorescent reporters, respectively.
(3) We then showed that colliding cells forms new p41/actin rich accumulations away from the contact site, suggesting a repolarization of the actin cytoskeleton.
(4) Finally, cells separate by moving away with a 180° turn in their direction.

Moreover, we showed that individual MCCs show a reverse correlation between their velocity and the amount of contacts made with other cells and a transient increase of velocity immediately after collision, similarly to how CIL was initially characterized in fibroblast (Abercrombie & Heaysman, 1953).

Altogether, we can assume that the MCC mutual repulsion is a CIL event. However, we have to take in account the severe lack of clear polarization of the MCCs as well as the low range of cell migration and low celerity. In future experiments, it should be possible to test the polarization of actin cytoskeleton through the study of Rho GTPases. These proteins are known to play crucial roles in the organization of MCC actin cap during muticiliogenesis (Chevalier et al., 2015) and are likely to be implicated in MCC mutual repulsion.

Although microtubules play crucial role in CIL (Stramer et al., 2010; Davis et al., 2015), their functions during mutual repulsion in MCCs remain to be demonstrated. Preliminary data from our team has shown that depletion of ODF2, a centrosomal protein involved in the microtubule organization in MCCs (Kunimoto et al., 2012) affects the regular spacing of the xenopus MCCs (A. Nommick, unpublished data). Thus, one can assume that microtubules take part in the mutual repulsion of MCCs as well. Besides, microtubule and centriole numbers regulate the timing of intercalation (Collins et al, 2020). Taking in account the tight interplay between actin and microtubules (Etienne-Manneville, 2013), it would be interesting to look at how contact between MCCs affect the timing of their intercalation.

Implementation of Xenopus MCC patterning by the SCF/KIT pathway.

The molecular mechanisms controlling homotypic repulsion-mediated patterning have been clearly identified in few cases only. The Eph RTKs and their ephrin ligands control the dispersion of CR neurons in the mammalian cortex (Villar-Cervino et al., 2013). Protocadherins and the immunoglobulin-superfamily proteins Dscams have been involved in the homotypic repulsion phenomena underlying mammalian RH cells tiling (Fuerst et al., 2008; Ing-Esteves et al., 2018), while the scattering of zebrafish pigment cells appears to rely on a variety of cell surface molecules, among which connexins and a

potassium channel (Iwashita et al., 2006; Irion et al., 2014). Our data show that the signal triggered by the interaction between the RTK Kit and its ligand Scf is required to establish the regularly dispersed pattern of Xenopus MCCs. Although this notoriously pleiotropic signaling pathway has been involved in many instances of cell migration, cell movement, cell adhesion, axonal guidance and cytoskeletal rearrangement, this is the first time that it has been shown to play a role in controlling the tissue-wide regular dispersion of a large cellular population. Remarkably, kit appears to be a direct transcriptional target of the multiciliogenesis master controller Multicilin/Mcidas (Stubbs et al., 2012; Ma et al., 2014; Kim et al., 2018). Such integration, through a common regulator, of fate determination and motility behavior may explain how thousands of individual cells of the same type can self-organize to achieve a global collective pattern. Our results are also remarkable in showing that the activity of a single receptor/ligand couple can result in the two opposite but temporally coexisting biological outcomes of MCC mutual repulsion and affinity for outer-layer junctions. Although these two phenomena might seem difficult to reconcile, the SCF/KIT signaling system has already been shown to promote apparently contrasting cell behaviors, such as migration and homing/adhesion, for example in melanoblasts (Jordan and Jackson, 2000; Wehrle-Haller and Weston, 1995), Hematopoietic Stem Cells (HSCs) (Tajima et al., 1998; Heissig et al., 2002), Primordial Germ Cells (PGCs) (Runyan et al., 2006; Gu et al., 2009, 2011) and dental pulp progenitors (Pan et al., 2013). Currently, the simplest and most widely accepted explanation, supported by in vivo, ex vivo and in vitro data, is that the membrane-bound and the soluble forms of the SCF ligand can both bind to and activate the KIT receptor, but with different kinetics, therefore triggering distinct, probably antagonistic signaling pathways and eliciting multiple cellular responses. In relevance to our work, soluble SCF has been shown to lead to transient activation of the KIT intrinsic TK activity, and to promote cell motility (Jordan and Jackson, 2000; Tabone-Eglinger et al., 2014; Tabone-Eglinger et al., 2012). Conversely, membrane-bound or immobilized SCF leads to formation of long-lived adhesive SCF/KIT complexes at the cell surface, independently of KIT TK activity (Tabone-Eglinger et al., 2014; Tabone-Eglinger et al., 2012). Our data show that the transmembrane Scf can be cleaved in Xenopus epidermis, thus raising the possibility that the dichotomy between membrane-associated and soluble Scf-dependent signals also controls the balance between adhesion and repulsion required for correct MCC patterning. It is easy to picture that the basolateral localization of transmembrane Scf in outer-layer cells might favor/stabilize the interaction of Kit-expressing MCCs with intercellular junctions, and even more so with vertices, where the density of the Scf signal is expected to be highest. This view is supported by our observations that MO-mediated depletion of Scf or Kit altered MCC migration along outer-layer junctions. In contrast, axitinib treatment did not cause the same defect, suggesting that TK activity is dispensable for MCC/outer cell interaction, consistent with published evidence (Tabone-Eglinger et al., 2014). Our ectopic expression assay also clearly demonstrated that full-length Scf can act as a potent adhesive cue towards Kit-expressing MCCs. Incidentally, it also revealed that the patterning system cannot afford Scf to be expressed in MCCs, consistent with our double FISH data, and with transcriptomic analysis suggesting that Mcidas negatively regulates

scf (Ma et al., 2014). By contrast, it is less simple to imagine how soluble Scf could promote MCC mutual repulsion. One possible explanation is that soluble Scf permeating the inner layer provides a motogenic signal, as described for example for mouse melanoblasts (Jordan and Jackson, 2000), thus keeping MCCs constantly moving around and dispersing until they are anchored to a free vertex by the strongly adhesive signal of membrane-bound Scf.

More support for the idea that the Scf/Kit pathway can control apparently antagonistic behaviours comes from *in vitro* experiment on Kit-expressing bone marrow-derived mast cells (BMMC), In this system, the use of a microfluidic device revealed a bimodal response to SCF signal intensity (Shamloo et al.,2013): BMMCs show a complex time-dependent chemotactic response to SCF, which can be alternatively attractive or repulsive depending on the time and the concentration of soluble SCF. Beside, we observed a switch in MCC behavior through time suggesting that the cells response to SCF might also be time dependent, regardless of the presence of cleaved or transmembrane forms of Scf. Together, these data could explain why we have not been able to promote the mutual repulsion of MCCs by reintroducing full length SCF nor the extracellular domain of SCF in SCF-depleted morphant embryos. If Kit responds to SCF in a dose dependent manner, recovering a regular MCC pattern following MO-mediated depletion of Scf and its rescue by mRNA injection seems impossible unless we could reintroduce SCF on its membrane bounded and cleaved forms in both its right place and at physiological concentrations. Unfortunately, all three independent attempts shown in figure T3 failed to promoteMCC regular spacing.

Alternatively, we can assume that the interaction between soluble Scf and Kit might initiate a cross-talk with other molecules expressed at the MCC surface. In BMMCs, the Kit dependent chemoattractive/chemorepulsive response to Scf signal requires the action of G-protein coupled receptors (Shamloo et al. 2013). It would be interesting to test in the future if the Kit-dependent MCC mutual repulsion synergizes with other known regulator of CIL-like process such as ephrins and Ephs. However, the remarkable finding that the overexpression of wild-type Kit is sufficient to induce the dispersion of ionocytes suggests that the repulsive activity relies largely on the activity of Kit itself, without the need for other, MCC-specific cell surface molecules. It is thus likely that the signaling cascade connecting Kit to the cytoskeletal effectors of cell repulsion and adhesion is a rather direct and short one.

Scf/Kit signaling and MCC actin cytoskeletal dynamics.

Our data from pharmacological inhibition experiments suggest that different modes of actin polymerization, required for the formation of distinct types of cellular protrusions, control separate aspects of MCC behavior. Following treatment with CK-666, an inhibitor of the actin-branching factor ARP2/3, MCCs present more filopodia-like extensions, show decreased mutual repulsion and major patterning defects, but no intercalation abnormalities. On the other hand, treatment with the actin bundling inhibitor SMIFH2

strongly delays intercalation without affecting patterning. The SCF/KIT pathway has been shown to control ARP2/3 activation (Mani et al., 2009) and in our model system its inhibition indeed results in defects similar to those due to CK 666 treatment: MCCs make filopodia-like protrusions and present patterning defects but are able to insert into the outer layer. Both CK-666 treatment and Scf/Kit pathway inhibition also increase the duration of MCC mutual contacts. Arp2/3 -/- fibroblasts, in which motility only relies on filopodia, show defects in the mutual repulsion-dependent collective cell movements, such as those involved in wound healing (Suraneni et al., 2012). We can thus propose a model in which the main role of the Scf/Kit pathway in Xenopus immature MCCs is the promotion of actin-based protrusions: Kit activation by soluble Scf would induce transient basolateral lamellipodia, required for redirecting MCC movements away from each other after mutual contact; membrane bound SCF would stabilize the more persistent apical protrusions required for anchoring MCCs to the vertices.

Interestingly, studies on Neural crest cells (NCCs) has shown that restricted cells completely surrounded by similar cells such as those in clusters would have their protrusion inhibited on all sides (Mayor & Carmona-Fontaine, 2010; Theveneau et al., 2010). The capacity of NCCs to extend protrusion away from other contacting NCCs is acquired after the premigratory NCCs sustain EMT (Theveneau & mayor, 2012; Scarpa et al, 2015). Before EMT, premigratory NCCs often show protrusion directed toward other NCCs (Scarpa et al., 2015). Upon inhibition of the Scf/kit signaling pathway such as depletion of the Kit receptor (Figure 5B,B' and movie 9), MCCs in clusters completely surrounded by other MCCs show no obvious polarity and emit protrusion in all direction such as those observed in premigratory NCCs (Scarpa et al, 2015). Together, these results suggest that the Scf/Kit pathway enhances the CIL of colliding MCCs and the repolarization of their protrusions away from the contact site.

A missing data in our experiment was the identification of the Kit effector(s) in charge of the regulation of actin cytoskeleton remodeling. In many Kit-expressing migrating cells, the Wiskott-Aldrich syndrome protein WASP is a downstream effector of Kit signaling which regulates cytoskeletal rearrangements and which is notably necessary for blood cell chemiotaxis (Mani et al, 2009; Shamloo et al 2013). We tried to test its function by overexpression of a dominant negative form of WASP and pharmacological inhibition, but neither approache affected MCCs regular spacing. This suggests that Kit signaling requires other intermediate downstream effectors than WASP. Among the known regulators of Arp2/3, Rho-GTPases such as RhoA and CDC42 would be ideal candidates since they are already known to participate to the regulation of actin architecture in the later differentiation of MCCs (Sedzinski et al, 2017) and are key player of CIL-like processes (Shoval & Kalcheim, 2012). Such a model warrants future validation by cell biological and biochemical approaches.

Could the SCF/Kit signaling promote other cell dispersion process?

In the previous section we illustrate how the Scf/Kit signaling pathway can trigger both cell migration and their homing to a target tissue through several example such as in melanoblasts (Jordan and Jackson, 2000; Wehrle-Haller and Weston, 1995), Hematopoietic Stem Cells (HSCs) (Tajima et al., 1998; Heissig et al., 2002), Primordial Germ Cells (PGCs) (Gu et al., 2009; Gu et al., 2011; Runyan et al., 2006) and dental pulp progenitors (Pan et al., 2013). While these cells are not characterized by regular distribution patterns as is the case for MCCs, the way the SCF/Kit signaling pathway regulates the cell migration might share common principles. Taking the example of melanocytes, before cells accumulate within follicles, they must first spread evenly throughout the skin and proliferate, both mechanisms depending on the Kit receptor (Vandamme & Berx, 2019). Interestingly, a mechanism by which cells repel each other would be ideal to regulate such a large dissemination throughout the whole body. CIL events have been proposed for the dispersion of other cell populations such as *Drosophila* hemocytes (Stramer et al., 2010) and NCCs (Carmona-Fontaine et al., 2008). It is worth mentioning that piebaldism, a pathology associated with irregular melanocyte repartition and their absence in some specific area of the skin and hair, results from mutation of the *KIT* gene (Oiso et al., 2013; R A Spritz et al., 1992; Richard A. Spritz et al., 1992). Although this pathology has been mostly associated with migration defect of melanocytes, it would be interesting to test in the future if melanocytes migration stems from CIL-like behavior that would include Kit receptor as a potent regulator. Thus the SCF/Kit signaling pathway would regulate cell scattering/regular spacing through the binding of the soluble form of SCF while, when the melanoblasts reach their target tissue, they would become trapped there through specific homing/adhesion mechanisms.

Under pathological conditions, a complete failure in CIL would result in cells crawling on top of or beneath one another such at what observed in malignant cells. Conversely, excessive CIL would trigger increased cell dissemination as is likely to happen to metastatic cancer cells (Stramer and Mayor, 2017). Although mutations of the *kit* gene are often associated with malignant cells (Lenartsson & Ronstrand., 2012), it would be interesting to investigate in the future if the loss of function of the *kit* gene is associated with tumor growth and reversely if constitutively active *kit* gene is a marker of metastasis dissemination. However, this analysis would require experiment run independently of both cell survival and proliferation, two common markers of cancer cells (Lenartsson & Ronstrand., 2012),

Does SCF regulate MCC intercalation?

The study of intercalation has always been addressed from the MCCs perspective and the outer layer was considered as simply permissive until RhoA expression levels in outer layer cells were shown to affect the outer layer rigidity and thus contribute to the MCC intercalation

rate (Sedzinski et al., 2016). On their side, Stubbs and colleagues have discussed the potential mechanisms played by outer layer cells in restricting MCCs intercalation as single cells (Stubbs et al 2006). While it was initially suggested that the intercalation at vertices results from the large size of the MCCs relative to ionocytes and SSCs, we showed that membrane-bound-SCF/Kit interactions provide a molecular guidance for MCCs toward vertices. Interestingly, among the intercalating cells observed in *Xenopus*, the restricted intercalation at vertices looks specific for MCCs since we can observe non-ciliated cells intercalated at bicellular cells junctions (figure 35B, yellow arrow head). When we inhibit the Scf-Kit signaling pathway, the disruption of the regular MCC distribution pattern results from the intercalation of several joined MCCs on a single vertex. However, preliminary results suggested that, upon depletion of the SCF ligand, MCCs can also intercalate at bicellular junctions (unpublished data). These results raise the possibility that Scf regulates the intercalation as a gatekeeper of outerlayer intercellular junction. Indeed, the Scf-Kit interaction can also transduce a signal within the Scf-expressing cells through the short Scf intracellular domain whose function remains largely unexplored. It was shown *in vitro* that Scf-Kit interactions trigger a bi-directional signaling (Buono et al., 2018). The model proposed in our manuscript proposes that soluble Scf released by proteolytic cleavage catalyze MCCs mutual repulsion while the membrane-bound form of Scf favors the MCC positioning at vertices. Together these results raise the possibility that the Scf/Kit signaling pathway regulates the spacing pattern of MCCs at a third level by restricting the intercalation of MCCs. This hypothesis has not been tested yet and might explain the restriction of intercalation in the model proposed by Stubbs and colleagues.

Interestingly, mammalian MCCs, like *Xenopus* MCCs, arise from basally positioned precursors (Evans & Moller, 1991; Rock et al., 2010). Moreover, it has been suggested that Kit has an important function in maintaining the integrity of lung tissue in mammals (Lennartson and Ronnstand, 2012). Although MCCs in mammalian airways do not present a regular spacing pattern, it would be interesting in the future to test if the Scf/Kit signaling pathway plays a role in the migration of MCCs from the basal layer toward the outer layer of differentiated lung epithelium.

The physiological function of MCC regular pattern

Ciliated epithelia have been characterized in a wide variety of living beings and biological contexts in which they commonly generate directed fluid flows. The outcome of such fluid flow can be very diverse such as ovum transport in the phallopian tube, cerebrospinal fluid circulation in the ventricle of the brain and mucociliary clearance in the airways (Werner & Mitchell, 2012; Brooks & Wallingford, 2014). Interestingly, the regular distribution of multiciliated cells throughout the tadpole epidermis is a common trait of most anurans (Nokhbatolfoghaihai et al, 2005), yet its physiological functions remain unknown. One can assume that such a regular distribution is made on the purpose of optimizing the fluid flow on the surface of the whole embryo (Figure Annex), however, the function of such a flow remains unknown.

Platyhelminthes use MCCs located on the ventral surface of the body as a locomotion system (Rompolas et al., 2009) and substratum gliding after hatching may also have a role in *Xenopus* embryo (Nokhbatolfoghaihai et al, 2005).

So far, most hypotheses attribute to the MCCs transient embryonic/juvenile functions that would be later performed by other organs of not yet developed organs/cells. Indeed, the ciliated epithelium of Xenopus is transient and the MCCs transdifferentiate into goblet cells at the moment when respiratory and immune systems become functional. Thus, one possibility would be that the fluid flow on the surface of anuran tadpole optimizes the oxygen absorption since gas exchange at the surface of embryo is the only way of respiration before the gills become functional (Nokhbatolfoghaihai et al, 2005). The second possibility would be that, together with the mucus that cover the surface of *Xenopus* embryos, the cilia-generated fluid flow would contribute to the antimicrobial defense by restricting pathogens from anchoring to the embryo surface, analogously to the mucociliary clearance in the airways.

Interestingly, the irregular distribution of MCCs upon disruption of the SCF/Kit signaling pathway would be the perfect way to experimentally explore the function and reason of their patterning. Indeed, except from the abnormal distribution of MCCs upon *dn-kit* mRNA injection, we didn't observe any defect in cilia structure on differentiated MCCs by SEM (Figure S4 F' from manuscript). Furthermore, upon disruption of the Scf/Kit signaling pathway, I observed ciliary beat and movement of particles on the surface of the embryo (data not shown) suggesting that MCCs are still functional. In the future, this approach could allow to test the biological relevance of such a regular pattern in the establishment of a tissue-wide polarization of cilia beat direction and its biological relevance for antimicrobial and oxygen exchange.

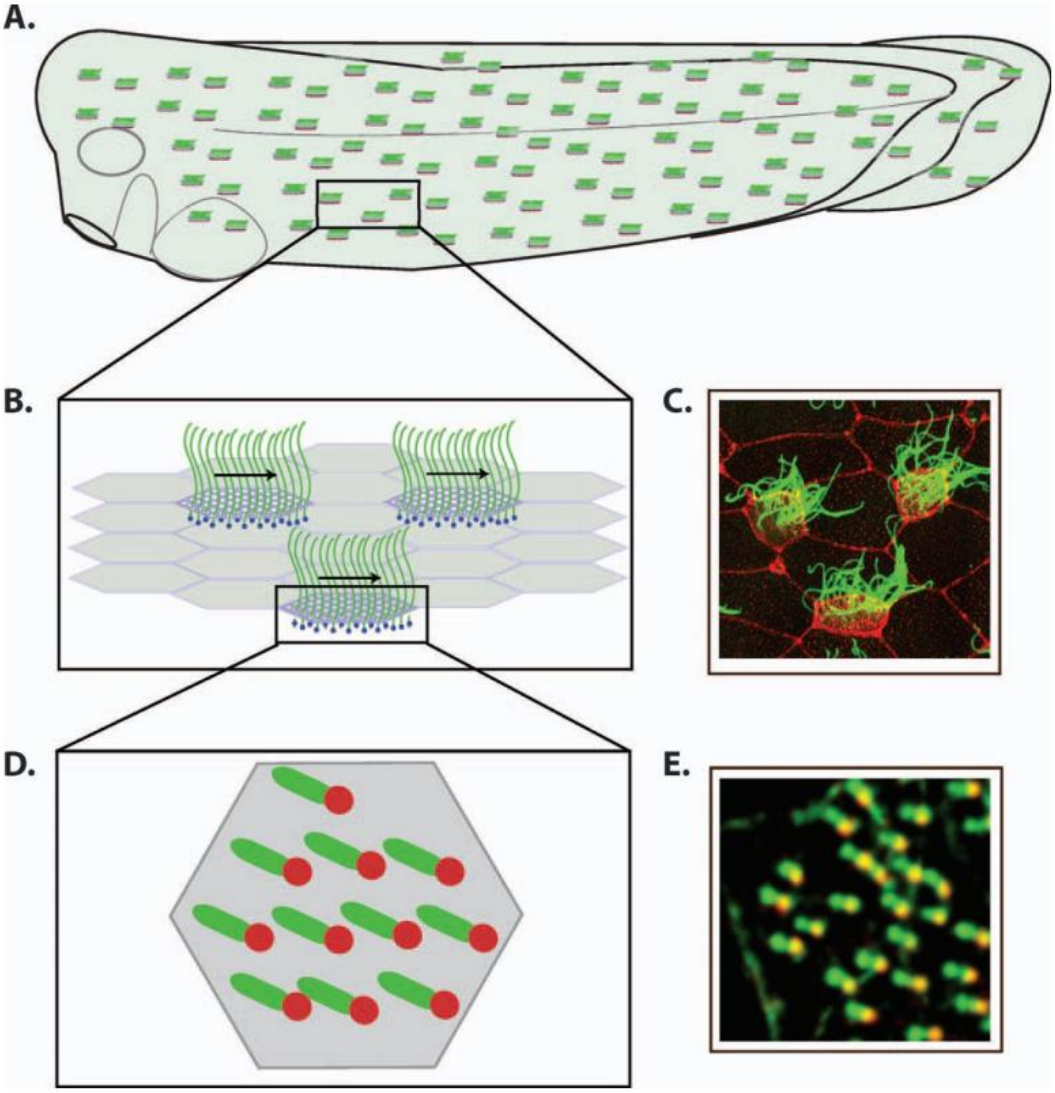

Figure annex: The Xenopus embryo: a model system for studying multiciliated epithelia.

A: Image of a Xenopus embryo showing the punctate pattern of ciliated cells that cover the surface. (B) Enlarged inlay of (A) indicating that individual ciliated cells must be coordinately polarized. C: Xenopus embryo stained with anti Beta-tubulin antibody to mark the cilia (green) and Rhodamine labeled phalloidin to mark actin (Red). D: Enlarged inlay of (B) indicating that individual cilia must be coordinately polarized within each ciliated cell. E: Portion of a cell from a Xenopus embryo injected with the basal body marker, Centrin-RFP (red) and the rootlet marker GFP-CLAMP (green) which is used to score the orientation of individual cilia (Park et al., 2008). (taken from Werner and Mitchel, 2012)

8. Conclusion and perspectives

Over the last twenty years, the MCCs that cover the Xenopus embryo surface has emerged as a major model of ciliated epithelia biology, particularly suitable for studying the mechanisms of ciliogenesis and radial intercalation. Compared to these two aspects of MCC biology, the mechanisms that generate their regular spacing pattern remained very poorly studied. Generally, regular spacing patterns are extensively studied, yet this specific example was not particularly analyzed. Many facts can explain this lack of attention. First, the physiological significance of such a regular pattern remains unknown; second, the Notch pathway was known to control MCC specification in pioneering studies, leading to the assumption that MCCs spacing pattern is specified at cell birth through lateral inhibition (Deblandre et al., 1999); third, only very few instances of phenotypes of MCC irregular distribution on tadpole epidermis have been described so far.

The work done during my thesis non-ambiguously shows that the MCC spacing pattern stems from more than just a tight regulation of cell specification. Instead, we showed that this pattern arises from a cell movement-based self-organizing process. These results have required the development of new live-imaging techniques to image MCCs through the thickness of two epidermal layers in a growing embryo and the development of *in silico* tools to analysed the resulting films.

We show here that, during development, seemingly complex and highly ordered cell patterns can be obtained by the combination of two relatively simple cell behaviors, without need for a highly regulated patterning system. Moreover, deployment of the same signaling system, presumably activated with different kinetics by soluble and membrane-anchored forms of a single ligand, can control both behaviors. This further stresses the importance of self-organizing systems in developmental biology.

Also, the Scf/Kit signaling pathway has been highly studied in medical trials, yet its functions in a developmental context remain elusive.

In this context, we characterized a hitherto unknown bimodal function of the Scf/Kit signaling pathway. At the same time, this pathway can stimulate homotypic repulsion between Kit-expressing MCCs while trigger heterotypic affinity between MCCs and outer layer cells junctions. These observations raise the question of bidirectional communication between MCCs and outer layer cells to control junction remodeling during radial intercalation of MCCs. Also, Scf has been shown to induce intracellular signaling in mouse SCF-expressing cells *in vitro* (Buono et al., 2018), and *Xenopus* Scf contains a small intracellular domain. However, no catalytical sites in Scf intracellular domains have been identified so far, and further experiments are required to explore such a potential effect in junction remodeling by outer layer cells.

On the other hand, we have been able for the first time to alter the distribution of intercalated MCCs by blocking the Scf/Kit signaling pathway either by pharmacological inhibition and by *scf* or *kit* morpholino-mediated knock-down. In all experimental conditions, MCCs succeed at their intercalation and they can produce motile cilia. The proper ciliogenesis, cilia beat and tissue polarization of cilia beat will require further characterization upon disruption of the Scf/Kit signaling pathway in the future. Interestingly, the Kit pharmacological inhibition appears as an easy way to test the physiological function of the spacing pattern of MCCs in fluid flow generation and eventually in antimicrobial defense, one of the hypothetical functions of MCC ciliary beat.

9. Material and method

This material and method is a complement from the one presented in the submitted manuscript to present additional experiment presented in the result section.

Plasmids

pαTub::EGFP-dnWASP	pCS2+	NotI	50-60pg	Made in the lab

αTubulin promoter-based constructs were generated from pαTub::GFP (a gift from C. Kintner), with the In-Fusion^{R} HD Cloning Kit (Takara Bio).

To generate pαTub:: EGFP-dnWASP, the EGFP-dnWASP ORF was PCR amplified from the dn-WASP construct (Miki & Takenawa, 1998; Yamaguchi et al., 2002) with the Phusion^{R} High-Fidelity DNA Polymerase and the primers InFuEGFPfor:5'-CAGATCCACCGGTCGTATGGTGAGCAAGGGCGGCGAGGAG -3' and InFu DN-WASP rev:5'-GATGATGAATGGGAAGACTGATCTAGAACTATAGTG -3'

mRNA synthesis

Sense mRNAs were synthesized from linearized plasmids with the Ambion mMessage mMachine kit® (Life Technologies) according to the details provided in the table below, then purified with Macherey-Nagel TM NucleoSpinTM RNA Clean-up kit. After determination of the concentration, aliquots were kept at -80°C.

Plasmid name	Vector	Linearised with	Transcribed with	Amount injected /blastomere	Reference
pCS2+SCF	pCS2+	NotI	Sp6 RNA pol	0,1 ng	
pCS2+SCF-tag	pCS2+	NotI	Sp6 RNA pol	0,1 ng	

Pharmacological inhibitors

Stock solutions of pharmacological inhibitors (all from Sigma-Aldrich®) were prepared in DMSO and added to embryos cultured in MBS 0,1X at the stages and concentrations and for the times shown in the following table.

Drugs	Source	Reference	Concentration in 0,1X MBS	Incubation time and stage
Wiskostatin	Sigma-Aldrich	W2270	40µM	From stage 12

Recombinant proteins

10 ng of soluble SCF recombinant protein (mouse) (from sigma) diluted in BSA 1% - PBS 1X, was injected into the blastocoel of stage 10.5 embyos. A similar volume of BSA 1% was injected as a negative control. Injected embryos were cultivated as usualy in MBS 0.1X.

Western blot

The western blot shown in Figure T3I was done in similar condition as westerblot decribed in the submitted paper but with an anti FLAG tag rat Monoclonal antibody (Sigma)

Caps were cultured in 96 wells plate with minimal volume of MBS 0.1X culture media (total of 440µl). The total supernatant was used for western-blot separately from caps.

Image analysis

The tissue growth-induced lateral drift wich occur in all our movies was removed by post_imaging treatment to stablize the tissue and only concider movement from MCCs themselves. We concider no-significant movements of the outer relative to the inner layer and used the outer layers junctions as a reference to stabilize the sum or max entensity projection movies. This approach requieres a vertex of reference manually tracked using "manual tracking" pluggin from ImageJ. We use an *in silico* approache using a Deep Learning coupled to a Kanade-Lucas algorithm applied to each movie and its vertex of reference coordinates to create a stabilized movie. The result give a reconstitution of the movie with the constant part on the center and deformed cluctuated potion on the borders. We then foccused our attention of the constant portion of the movies.

Stabilized movies were used with a manual tracking of MCCs centroid over time to extract information about the instantaneous speed of the MCCs.

We also used stabilized movie to analyse the outer cells junction following behavior. To control if the observed behavior is not a radom effect consequent of the overlap between MCCs and outerlayer cell junctions, we rotate the channel of mRFP which label outer layer cell junctions by 90° and quantify. As initionaly done in the submetted manuscript, we considered cells as following junction when the bevavior respect the following criteria: MCC emits protrusions in correspondence of outer-layer cells junctions; overlap between MCC shape and outer-layer cells junctions; correlation between direction of MCC migration and orientation of the outer-layer cells junctions. Cells already engaged in radial intercalation with permanent contact with vertices and ambiguous cases were removed from quantification.

Bibliographie

Abbaspour Babaei, M., Kamalidehghan, B., Saleem, M., Huri, H. Z., & Ahmadipour, F. (2016). Receptor tyrosine kinase (c-Kit) inhibitors : A potential therapeutic target in cancer cells. *Drug Design, Development and Therapy*, *10*, 2443-2459. https://doi.org/10.2147/DDDT.S89114

Abercrombie, M. (1970). Contact inhibition in tissue culture. *In Vitro*, *6*(2), 128-142. https://doi.org/10.1007/BF02616114

Abercrombie, M., & Ambrose, E. J. (1958). Interference microscope studies of cell contacts in tissue culture. *Experimental Cell Research*, *15*(2), 332-345. https://doi.org/10.1016/0014-4827(58)90034-X

Abercrombie, M., & Heaysman, J. E. M. (1953). Observations on the social behaviour of cells in tissue culture : I. Speed of movement of chick heart fibroblasts in relation to their mutual contacts. *Experimental Cell Research*, *5*(1), 111-131. https://doi.org/10.1016/0014-4827(53)90098-6

Abercrombie, M., & Heaysman, J. E. M. (1954). Observations on the social behaviour of cells in tissue culture : II. "Monolayering" of fibroblasts. *Experimental Cell Research*, *6*(2), 293-306. https://doi.org/10.1016/0014-4827(54)90176-7

Akhmanova, A., & Steinmetz, M. O. (2008). Tracking the ends : A dynamic protein network controls the fate of microtubule tips. *Nature Reviews. Molecular Cell Biology*, *9*(4), 309-322. https://doi.org/10.1038/nrm2369

Alvarez-Medina, R., Cayuso, J., Okubo, T., Takada, S., & Martí, E. (2008). Wnt canonical pathway restricts graded Shh/Gli patterning activity through the regulation of Gli3 expression. *Development*, *135*(2), 237-247. https://doi.org/10.1242/dev.012054

Anderson, D. M., Williams, D. E., Tushinski, R., Gimpel, S., Eisenman, J., Cannizzaro, L., Aronson, M., Croce, C., Huebner, K., Cosman, D., & others. (1991). Alternate splicing of mRNAs encoding human mast cell growth factor and localization of the gene to chromosome 12q22-q24. *Cell Growth Differ*, *2*(8), 373–8.

Andersson, E. R., Sandberg, R., & Lendahl, U. (2011). Notch signaling : Simplicity in design, versatility in function. *Development*, *138*(17), 3593–3612.

Aragón, J., Varea, C., Barrio, R., & Maini, P. (1998). Spatial patterning in modified Turing systems : Application to pigmentation patterns on marine fish. *Forma*, *13*(3), 213–221.

Artavanis-Tsakonas, S., Matsuno, K., & Fortini, M. E. (1995). Notch signaling. *Science*, *268*(5208), 225–232.

Baker, R. E., Schnell, S., & Maini, P. K. (2009). Waves and patterning in developmental biology : Vertebrate segmentation and feather bud formation as case studies. *The International journal of developmental biology*, *53*(0), 783-794. https://doi.org/10.1387/ijdb.072493rb

Barber, M., Arai, Y., Morishita, Y., Vigier, L., Causeret, F., Borello, U., Ledonne, F., Coppola, E., Contremoulins, V., Pfrieger, F. W., Tissir, F., Govindan, S., Jabaudon, D., Proux-Gillardeaux, V., Galli, T., & Pierani, A. (2015). Migration Speed of Cajal-Retzius Cells Modulated by Vesicular Trafficking Controls the Size of Higher-Order Cortical Areas. *Current Biology*, *25*(19), 2466-2478. https://doi.org/10.1016/j.cub.2015.08.028

Barber, M., & Pierani, A. (2016). Tangential migration of glutamatergic neurons and cortical patterning during development : Lessons from Cajal-Retzius cells. *Developmental Neurobiology*, *76*(8), 847-881. https://doi.org/10.1002/dneu.22363

Bardet, P.-L., Guirao, B., Paoletti, C., Serman, F., Léopold, V., Bosveld, F., Goya, Y., Mirouse, V., Graner, F., & Bellaïche, Y. (2013). PTEN Controls Junction Lengthening and Stability during Cell Rearrangement in Epithelial Tissue. *Developmental Cell*, *25*(5), 534-546. https://doi.org/10.1016/j.devcel.2013.04.020

Barriga, E. H., Franze, K., Charras, G., & Mayor, R. (2018). Tissue stiffening coordinates morphogenesis by triggering collective cell migration in vivo. *Nature*, *554*(7693), 523-527. https://doi.org/10.1038/nature25742

Barton, L. J., LeBlanc, M. G., & Lehmann, R. (2016). Finding their way : Themes in germ cell migration. *Current Opinion in Cell Biology*, *42*, 128-137. https://doi.org/10.1016/j.ceb.2016.07.007

Basu, R., & Chang, F. (2007). Shaping the actin cytoskeleton using microtubule tips. *Current Opinion in Cell Biology*, *19*(1), 88-94. https://doi.org/10.1016/j.ceb.2006.12.012

Batson, J., Maccarthy-Morrogh, L., Archer, A., Tanton, H., & Nobes, C. D. (2014). EphA receptors regulate prostate cancer cell dissemination through Vav2–RhoA mediated cell–cell repulsion. *Biology Open*, *3*(6), 453-462. https://doi.org/10.1242/bio.20146601

Benito-Gutiérrez, È., Nake, C., Llovera, M., Comella, J. X., & Garcia-Fernàndez, J. (2005). The single AmphiTrk receptor highlights increased complexity of neurotrophin signalling in vertebrates and suggests an early role in developing sensory neuroepidermal cells. *Development*, *132*(9), 2191-2202. https://doi.org/10.1242/dev.01803

Bertet, C., Sulak, L., & Lecuit, T. (2004). Myosin-dependent junction remodelling controls planar cell intercalation and axis elongation. *Nature*, *429*(6992), 667-671. https://doi.org/10.1038/nature02590

Billett, F. S., & Gould, R. P. (1971). Fine structural changes in the differentiating epidermis of Xenopus laevis embryos. *Journal of Anatomy*, *108*(Pt 3), 465-480.

Blanchoin, L., Boujemaa-Paterski, R., Sykes, C., & Plastino, J. (2014). Actin Dynamics, Architecture, and Mechanics in Cell Motility. *Physiological Reviews*, *94*(1), 235-263. https://doi.org/10.1152/physrev.00018.2013

Blum, M., & Ott, T. (2018). Xenopus : An Undervalued Model Organism to Study and Model Human Genetic Disease. *Cells Tissues Organs*, *205*(5-6), 303-313. https://doi.org/10.1159/000490898

Blume-Jensen, P., Claesson-Welsh, L., Siegbahn, A., Zsebo, K. m., Westermark, B., & Heldin, C. h. (1991). Activation of the human c-kit product by ligand-induced dimerization mediates circular actin reorganization and chemotaxis. *The EMBO Journal*, *10*(13), 4121-4128. https://doi.org/10.1002/j.1460-2075.1991.tb04989.x

Blume-Jensen, P., Siegbahn, A., Stabel, S., Heldin, C. h., & Rönnstrand, L. (1993). Increased Kit/SCF receptor induced mitogenicity but abolished cell motility after inhibition of protein kinase C. *The EMBO Journal*, *12*(11), 4199-4209. https://doi.org/10.1002/j.1460-2075.1993.tb06104.x

Bonaventure, J., Domingues, M. J., & Larue, L. (2013). Cellular and molecular mechanisms controlling the migration of melanocytes and melanoma cells. *Pigment Cell & Melanoma Research*, *26*(3), 316-325. https://doi.org/10.1111/pcmr.12080

Boutin, C., & Kodjabachian, L. (2019). Biology of multiciliated cells. *Current Opinion in Genetics & Development*, *56*, 1-7. https://doi.org/10.1016/j.gde.2019.04.006

Bray, S. J. (2006). Notch signalling : A simple pathway becomes complex. *Nature Reviews Molecular Cell Biology*, *7*(9), 678-689. https://doi.org/10.1038/nrm2009

Bray, S. J. (2016). Notch signalling in context. *Nature reviews Molecular cell biology*, *17*(11), 722.

Brinkmann, F., Mercker, M., Richter, T., & Marciniak-Czochra, A. (2018). Post-Turing tissue pattern formation : Advent of mechanochemistry. *PLoS computational biology*, *14*(7), e1006259.

Briscoe, J., & Small, S. (2015). Morphogen rules : Design principles of gradient-mediated embryo patterning. *Development*, *142*(23), 3996-4009. https://doi.org/10.1242/dev.129452

Briscoe, J., & Thérond, P. P. (2013). The mechanisms of Hedgehog signalling and its roles in development and disease. *Nature Reviews Molecular Cell Biology*, *14*(7), 416-429. https://doi.org/10.1038/nrm3598

Brooks, E. R., & Wallingford, J. B. (2014). Multiciliated Cells. *Current Biology*, *24*(19), R973-R982. https://doi.org/10.1016/j.cub.2014.08.047

Brunet, T., Bouclet, A., Ahmadi, P., Mitrossilis, D., Driquez, B., Brunet, A.-C., Henry, L., Serman, F., Béalle, G., Ménager, C., & others. (2013). Evolutionary conservation of early mesoderm specification by mechanotransduction in Bilateria. *Nature communications*, *4*(1), 1–15.

Buono, M., Thézénas, M.-L., Ceroni, A., Fischer, R., & Nerlov, C. (2018). Bi-directional signaling by membrane-bound KitL induces proliferation and coordinates thymic endothelial cell and thymocyte expansion. *Nature Communications*, *9*(1), 4685. https://doi.org/10.1038/s41467-018-07024-0

Carmona-Fontaine, C., Matthews, H. K., Kuriyama, S., Moreno, M., Dunn, G. A., Parsons, M., Stern, C. D., & Mayor, R. (2008). Contact inhibition of locomotion in vivo controls neural crest directional migration. *Nature*, *456*(7224), 957-961. https://doi.org/10.1038/nature07441

Carroll, S. B. (2005). *Endless forms most beautiful : The new science of evo devo and the making of the animal kingdom*. WW Norton & Company.

Castellani, V., Chédotal, A., Schachner, M., Faivre-Sarrailh, C., & Rougon, G. (2000). Analysis of the L1-Deficient Mouse Phenotype Reveals Cross-Talk between Sema3A and L1 Signaling Pathways in Axonal Guidance. *Neuron*, *27*(2), 237-249. https://doi.org/10.1016/S0896-6273(00)00033-7

Chalmers, A. D., Pambos, M., Mason, J., Lang, S., Wylie, C., & Papalopulu, N. (2005). APKC, Crumbs3 and Lgl2 control apicobasal polarity in early vertebrate development. *Development*, *132*(5), 977-986. https://doi.org/10.1242/dev.01645

Chalmers, A. D., Strauss, B., & Papalopulu, N. (2003). Oriented cell divisions asymmetrically segregate aPKC and generate cell fate diversity in the early Xenopus embryo. *Development*, *130*(12), 2657-2668. https://doi.org/10.1242/dev.00490

Chevalier, B., Adamiok, A., Mercey, O., Revinski, D. R., Zaragosi, L.-E., Pasini, A., Kodjabachian, L., Barbry, P., & Marcet, B. (2015). MiR-34/449 control apical actin network formation during multiciliogenesis through small GTPase pathways. *Nature Communications*, *6*(1), 8386. https://doi.org/10.1038/ncomms9386

Chrzanowska-Wodnicka, M., & Burridge, K. (1996). Rho-stimulated contractility drives the formation of stress fibers and focal adhesions. *Journal of Cell Biology*, *133*(6), 1403-1415. https://doi.org/10.1083/jcb.133.6.1403

Chugh, P., & Paluch, E. K. (2018). The actin cortex at a glance. *Journal of Cell Science*, *131*(14). https://doi.org/10.1242/jcs.186254

Chung, B.-M., Rotty, J. D., & Coulombe, P. A. (2013). Networking galore : Intermediate filaments and cell migration. *Current Opinion in Cell Biology*, *25*(5), 600-612. https://doi.org/10.1016/j.ceb.2013.06.008

Chung, M.-I., Kwon, T., Tu, F., Brooks, E. R., Gupta, R., Meyer, M., Baker, J. C., Marcotte, E. M., & Wallingford, J. B. (2014). Coordinated genomic control of ciliogenesis and cell movement by RFX2. *eLife*, *3*, e01439. https://doi.org/10.7554/eLife.01439

Cibois, M., Luxardi, G., Chevalier, B., Thomé, V., Mercey, O., Zaragosi, L.-E., Barbry, P., Pasini, A., Marcet, B., & Kodjabachian, L. (2015). BMP signalling controls the construction of vertebrate mucociliary epithelia. *Development*, *142*(13), 2352-2363. https://doi.org/10.1242/dev.118679

Cibois, M., Scerbo, P., Thomé, V., Pasini, A., & Kodjabachian, L. (2014). Induction and Differentiation of the Xenopus Ciliated Embryonic Epidermis. In *Xenopus Development* (p. 112-129). John Wiley & Sons, Ltd. https://doi.org/10.1002/9781118492833.ch7

Clark, E., Peel, A. D., & Akam, M. (2019). Arthropod segmentation. *Development*, *146*(18), dev170480.

Claxton, J. (1964). The determination of patterns with special reference to that of the central primary skin follicles in sheep. *Journal of Theoretical Biology*, *7*(2), 302–317.

Cohen, M., Georgiou, M., Stevenson, N. L., Miodownik, M., & Baum, B. (2010). Dynamic Filopodia Transmit Intermittent Delta-Notch Signaling to Drive Pattern Refinement during Lateral Inhibition. *Developmental Cell*, *19*(1), 78-89. https://doi.org/10.1016/j.devcel.2010.06.006

Collins, C., Majekodunmi, A., & Mitchell, B. (2020). Centriole Number and the Accumulation of Microtubules Modulate the Timing of Apical Insertion during Radial Intercalation. *Current Biology*, *30*(10), 1958-1964.e3. https://doi.org/10.1016/j.cub.2020.03.013

Cook, J. E., & Chalupa, L. M. (2000). Retinal mosaics : New insights into an old concept. *Trends in Neurosciences*, *23*(1), 26-34. https://doi.org/10.1016/S0166-2236(99)01487-3

Corson, F., Couturier, L., Rouault, H., Mazouni, K., & Schweisguth, F. (2017). Self-organized Notch dynamics generate stereotyped sensory organ patterns in Drosophila. *Science*, *356*(6337).

Crick, F. (1970). Diffusion in embryogenesis. *Nature*, *225*(5231), 420–422.

Crowe, R., Henrique, D., Ish-Horowicz, D., & Niswander, L. (1998). A new role for Notch and Delta in cell fate decisions : Patterning the feather array. *Development*, *125*(4), 767-775.

Cruciat, C.-M., Ohkawara, B., Acebron, S. P., Karaulanov, E., Reinhard, C., Ingelfinger, D., Boutros, M., & Niehrs, C. (2010). Requirement of Prorenin Receptor and Vacuolar H+-ATPase–Mediated Acidification for Wnt Signaling. *Science*, *327*(5964), 459-463. https://doi.org/10.1126/science.1179802

Curran, D. R., & Cohn, L. (2010). Advances in Mucous Cell Metaplasia. *American Journal of Respiratory Cell and Molecular Biology*, *42*(3), 268-275. https://doi.org/10.1165/rcmb.2009-0151TR

Davidson, E. H. (2010). Emerging properties of animal gene regulatory networks. *Nature*, *468*(7326), 911–920.

Davis, J. R., Huang, C.-Y., Zanet, J., Harrison, S., Rosten, E., Cox, S., Soong, D. Y., Dunn, G. A., & Stramer, B. M. (2012). Emergence of embryonic pattern through contact inhibition of locomotion. *Development*, *139*(24), 4555-4560. https://doi.org/10.1242/dev.082248

Davis, J. R., Luchici, A., Mosis, F., Thackery, J., Salazar, J. A., Mao, Y., Dunn, G. A., Betz, T., Miodownik, M., & Stramer, B. M. (2015). Inter-Cellular Forces Orchestrate Contact Inhibition of Locomotion. *Cell*, *161*(2), 361-373. https://doi.org/10.1016/j.cell.2015.02.015

De Felici, M. (2005). Adhesion molecules for mouse primordial germ cells. *Frontiers in Bioscience*, *10*(1-3), 542. https://doi.org/10.2741/1550

de Joussineau, C., Soulé, J., Martin, M., Anguille, C., Montcourrier, P., & Alexandre, D. (2003). Delta-promoted filopodia mediate long-range lateral inhibition in Drosophila. *Nature*, *426*(6966), 555-559. https://doi.org/10.1038/nature02157

Deblandre, G. A., Wettstein, D. A., Koyano-Nakagawa, N., & Kintner, C. (1999). A two-step mechanism generates the spacing pattern of the ciliated cells in the skin of Xenopus embryos. *Development*, *126*(21), 4715-4728.

DeLay, B. D., Corkins, M. E., Hanania, H. L., Salanga, M., Deng, J. M., Sudou, N., Taira, M., Horb, M. E., & Miller, R. K. (2018). Tissue-Specific Gene Inactivation in Xenopus laevis : Knockout of lhx1 in the Kidney with CRISPR/Cas9. *Genetics*, *208*(2), 673-686. https://doi.org/10.1534/genetics.117.300468

Dessaud, E., McMahon, A. P., & Briscoe, J. (2008). Pattern formation in the vertebrate neural tube : A sonic hedgehog morphogen-regulated transcriptional network. *Development*, *135*(15), 2489–2503.

Dogterom, M., & Koenderink, G. H. (2019). Actin–microtubule crosstalk in cell biology. *Nature Reviews Molecular Cell Biology*, *20*(1), 38-54. https://doi.org/10.1038/s41580-018-0067-1

Drew, C. F., Lin, C. M., Jiang, T. X., Blunt, G., Mou, C., Chuong, C. M., & Headon, D. J. (2007). The Edar subfamily in feather placode formation. *Developmental biology*, *305*(1), 232–245.

Drysdale, T. A., & Elinson, R. P. (1992). Cell Migration and Induction in the Development of the Surface Ectodermal Pattern of the Xenopus laevis Tadpole. *Development, Growth & Differentiation*, *34*(1), 51-59. https://doi.org/10.1111/j.1440-169X.1992.00051.x

Dubaissi, E., & Papalopulu, N. (2011). Embryonic frog epidermis : A model for the study of cell-cell interactions in the development of mucociliary disease. *Disease Models & Mechanisms*, *4*(2), 179-192. https://doi.org/10.1242/dmm.006494

Dubaissi, E., Rousseau, K., Hughes, G. W., Ridley, C., Grencis, R. K., Roberts, I. S., & Thornton, D. J. (2018). Functional characterization of the mucus barrier on the Xenopus tropicalis skin surface. *Proceedings of the National Academy of Sciences*, *115*(4), 726-731. https://doi.org/10.1073/pnas.1713539115

Dubaissi, E., Rousseau, K., Lea, R., Soto, X., Nardeosingh, S., Schweickert, A., Amaya, E., Thornton, D. J., & Papalopulu, N. (2014). A secretory cell type develops alongside multiciliated cells, ionocytes and goblet cells, and provides a protective, anti-infective function in the frog embryonic mucociliary epidermis. *Development*, *141*(7), 1514-1525. https://doi.org/10.1242/dev.102426

Eglen, S. J. (2006). Development of regular cellular spacing in the retina : Theoretical models. *Mathematical Medicine and Biology: A Journal of the IMA*, *23*(2), 79-99. https://doi.org/10.1093/imammb/dql003

Etienne-Manneville, S. (2013). Microtubules in Cell Migration. *Annual Review of Cell and Developmental Biology*, *29*(1), 471-499. https://doi.org/10.1146/annurev-cellbio-101011-155711

Etienne-Manneville, S. (2018). Cytoplasmic Intermediate Filaments in Cell Biology. *Annual Review of Cell and Developmental Biology*, *34*(1), 1-28. https://doi.org/10.1146/annurev-cellbio-100617-062534

Evans, M. J., & Moller, P. C. (1991). Biology of Airway Basal Cells. *Experimental Lung Research*, *17*(3), 513-531. https://doi.org/10.3109/01902149109062862

Fox Keller, E. (1999). Making Sense of Life. In *Fundamental Changes in Cellular Biology in the 20th Century. Biology of Development, Chemistry and Physics in the Life Sciences: Vol. 43 (NS 6)* (p. 173-178). Brepols Publishers. https://doi.org/10.1484/M.DDA-EB.4.00586

Friedl, P., & Gilmour, D. (2009). Collective cell migration in morphogenesis, regeneration and cancer. *Nature Reviews Molecular Cell Biology*, *10*(7), 445-457. https://doi.org/10.1038/nrm2720

Fuerst, P. G., Koizumi, A., Masland, R. H., & Burgess, R. W. (2008). Neurite arborization and mosaic spacing in the mouse retina require DSCAM. *Nature*, *451*(7177), 470-474. https://doi.org/10.1038/nature06514

Funkhouser, C. H., Kinsler, V. A., & Frieden, I. J. (2019). Striking contiguous depigmentation across the lower limbs in piebaldism and its implications for understanding melanocytic migration and development. *Pediatric Dermatology*, *36*(4), 511-513. https://doi.org/10.1111/pde.13831

Galli-Resta, L., Novelli, E., & Viegi, A. (2002). Dynamic microtubule-dependent interactions position homotypic neurones in regular monolayered arrays during retinal development. *Development*, *129*(16), 3803-3814.

Galli-Resta, L., Resta, G., Tan, S.-S., & Reese, B. E. (1997). Mosaics of Islet-1-Expressing Amacrine Cells Assembled by Short-Range Cellular Interactions. *Journal of Neuroscience*, *17*(20), 7831-7838. https://doi.org/10.1523/JNEUROSCI.17-20-07831.1997

Ghysen, A., & Richelle, J. (1979). Determination of sensory bristles and pattern formation in Drosophila : II. The achaete-scute locus. *Developmental biology*, *70*(2), 438–452.

Gierer, A., & Meinhardt, H. (1972). A theory of biological pattern formation. *Kybernetik*, *12*(1), 30-39. https://doi.org/10.1007/BF00289234

Glover, J. D., Wells, K. L., Matthäus, F., Painter, K. J., Ho, W., Riddell, J., Johansson, J. A., Ford, M. J., Jahoda, C. A., Klika, V., & others. (2017). Hierarchical patterning modes orchestrate hair follicle morphogenesis. *PLoS biology*, *15*(7), e2002117.

Goldman, D. C., Berg, L. K., Heinrich, M. C., & Christian, J. L. (2006). Ectodermally derived steel/stem cell factor functions non–cell autonomously during primitive erythropoiesis in Xenopus. *Blood*, *107*(8), 3114-3121. https://doi.org/10.1182/blood-2005-09-3930

Gommerman, J. L., Sittaro, D., Klebasz, N. Z., Williams, D. A., & Berger, S. A. (2000). Differential stimulation of c-Kit mutants by membrane-bound and soluble Steel Factor correlates with leukemic potential. *Blood, The Journal of the American Society of Hematology*, *96*(12), 3734–3742.

Gore, B. B., Wong, K. G., & Tessier-Lavigne, M. (2008). Stem Cell Factor Functions as an Outgrowth-Promoting Factor to Enable Axon Exit from the Midline Intermediate Target. *Neuron*, *57*(4), 501-510. https://doi.org/10.1016/j.neuron.2008.01.006

Goudarzi, M., Banisch, T. U., Mobin, M. B., Maghelli, N., Tarbashevich, K., Strate, I., van den Berg, J., Blaser, H., Bandemer, S., Paluch, E., Bakkers, J., Tolić-Nørrelykke, I.

M., & Raz, E. (2012). Identification and Regulation of a Molecular Module for Bleb-Based Cell Motility. *Developmental Cell*, *23*(1), 210-218. https://doi.org/10.1016/j.devcel.2012.05.007

Gough, K. C., Maddison, B. C., Shikotra, A., Moiseeva, E. P., Yang, W., Jarvis, S., & Bradding, P. (2015). Evidence for a novel Kit adhesion domain mediating human mast cell adhesion to structural airway cells. *Respiratory Research*, *16*(1), 86. https://doi.org/10.1186/s12931-015-0245-z

Grebe, M. (2012). The patterning of epidermal hairs in Arabidopsis—Updated. *Current Opinion in Plant Biology*, *15*(1), 31-37. https://doi.org/10.1016/j.pbi.2011.10.010

Green, J. B. A., & Sharpe, J. (2015). Positional information and reaction-diffusion : Two big ideas in developmental biology combine. *Development*, *142*(7), 1203-1211. https://doi.org/10.1242/dev.114991

Grueber, W. B., & Sagasti, A. (2010). Self-avoidance and Tiling : Mechanisms of Dendrite and Axon Spacing. *Cold Spring Harbor Perspectives in Biology*, *2*(9), a001750. https://doi.org/10.1101/cshperspect.a001750

Gu, Y., Runyan, C., Shoemaker, A., Surani, A., & Wylie, C. (2009). Steel factor controls primordial germ cell survival and motility from the time of their specification in the allantois, and provides a continuous niche throughout their migration. *Development*, *136*(8), 1295-1303. https://doi.org/10.1242/dev.030619

Gu, Y., Runyan, C., Shoemaker, A., Surani, M. A., & Wylie, C. (2011). Membrane-Bound Steel Factor Maintains a High Local Concentration for Mouse Primordial Germ Cell Motility, and Defines the Region of Their Migration. *PLOS ONE*, *6*(10), e25984. https://doi.org/10.1371/journal.pone.0025984

Guillot, C., & Lecuit, T. (2013). Mechanics of Epithelial Tissue Homeostasis and Morphogenesis. *Science*, *340*(6137), 1185-1189. https://doi.org/10.1126/science.1235249

GUPTON, Stephanie L. et GERTLER, Frank B. Filopodia: the fingers that do the walking. Science's STKE, 2007, vol. 2007, no 400, p. re5-re5.

Gurdon, J. B., & Hopwood, N. (2000). The introduction of Xenopus laevis into developmental biology : Of empire, pregnancy testing and ribosomal genes. *International Journal of Developmental Biology*, *44*(1), 43–50.

Hagiwara, H., Shibasaki, S., & Ohwada, N. (1992). Ciliogenesis in the Human Oviduct Epithelium during the Normal Menstrual Cycle. *Journal of Electron Microscopy*, *41*(5), 321-329. https://doi.org/10.1093/oxfordjournals.jmicro.a050974

Halova, I., Draberova, L., & Draber, P. (2012). Mast Cell Chemotaxis – Chemoattractants and Signaling Pathways. *Frontiers in Immunology*, *3*. https://doi.org/10.3389/fimmu.2012.00119

Hamada, H., Watanabe, M., Lau, H. E., Nishida, T., Hasegawa, T., Parichy, D. M., & Kondo, S. (2014). Involvement of Delta/Notch signaling in zebrafish adult pigment stripe patterning. *Development*, *141*(2), 318-324. https://doi.org/10.1242/dev.099804

Han, C., Wang, D., Soba, P., Zhu, S., Lin, X., Jan, L. Y., & Jan, Y.-N. (2012). Integrins Regulate Repulsion-Mediated Dendritic Patterning of Drosophila Sensory Neurons by Restricting Dendrites in a 2D Space. *Neuron*, *73*(1), 64-78. https://doi.org/10.1016/j.neuron.2011.10.036

Hayes, J. M., Kim, S. K., Abitua, P. B., Park, T. J., Herrington, E. R., Kitayama, A., Grow, M. W., Ueno, N., & Wallingford, J. B. (2007). Identification of novel ciliogenesis factors

using a new in vivo model for mucociliary epithelial development. *Developmental Biology*, *312*(1), 115-130. https://doi.org/10.1016/j.ydbio.2007.09.031

Heasman, J. (2002). Morpholino Oligos : Making Sense of Antisense? *Developmental Biology*, *243*(2), 209-214. https://doi.org/10.1006/dbio.2001.0565

Heisenberg, C.-P., & Bellaïche, Y. (2013). Forces in Tissue Morphogenesis and Patterning. *Cell*, *153*(5), 948-962. https://doi.org/10.1016/j.cell.2013.05.008

Heissig, B., Hattori, K., Dias, S., Friedrich, M., Ferris, B., Hackett, N. R., Crystal, R. G., Besmer, P., Lyden, D., Moore, M. A. S., Werb, Z., & Rafii, S. (2002). Recruitment of Stem and Progenitor Cells from the Bone Marrow Niche Requires MMP-9 Mediated Release of Kit-Ligand. *Cell*, *109*(5), 625-637. https://doi.org/10.1016/S0092-8674(02)00754-7

Held, L. I. (1991). Bristle patterning in Drosophila. *BioEssays*, *13*(12), 633-640. https://doi.org/10.1002/bies.950131203

Henrique, D., & Schweisguth, F. (2019). Mechanisms of Notch signaling : A simple logic deployed in time and space. *Development*, *146*(3). https://doi.org/10.1242/dev.172148

Hetrick, B., Han, M. S., Helgeson, L. A., & Nolen, B. J. (2013). Small Molecules CK-666 and CK-869 Inhibit Actin-Related Protein 2/3 Complex by Blocking an Activating Conformational Change. *Chemistry & Biology*, *20*(5), 701-712. https://doi.org/10.1016/j.chembiol.2013.03.019

Higashi, T., & Miller, A. L. (2017). Tricellular junctions : How to build junctions at the TRICkiest points of epithelial cells. *Molecular Biology of the Cell*, *28*(15), 2023-2034. https://doi.org/10.1091/mbc.e16-10-0697

Higashida, C., Kiuchi, T., Akiba, Y., Mizuno, H., Maruoka, M., Narumiya, S., Mizuno, K., & Watanabe, N. (2013). F- and G-actin homeostasis regulates mechanosensitive actin nucleation by formins. *Nature Cell Biology*, *15*(4), 395-405. https://doi.org/10.1038/ncb2693

Higgs, H. N. (2018). A fruitful tree : Developing the dendritic nucleation model of actin-based cell motility. *Molecular Biology of the Cell*, *29*(25), 2969-2978. https://doi.org/10.1091/mbc.E18-07-0426

Ho, W. K. W., Freem, L., Zhao, D., Painter, K. J., Woolley, T. E., Gaffney, E. A., McGrew, M. J., Tzika, A., Milinkovitch, M. C., Schneider, P., Drusko, A., Matthäus, F., Glover, J. D., Wells, K. L., Johansson, J. A., Davey, M. G., Sang, H. M., Clinton, M., & Headon, D. J. (2019). Feather arrays are patterned by interacting signalling and cell density waves. *PLOS Biology*, *17*(2), e3000132. https://doi.org/10.1371/journal.pbio.3000132

Hohmann, T., & Dehghani, F. (2019). The Cytoskeleton—A Complex Interacting Meshwork. *Cells*, *8*(4), 362. https://doi.org/10.3390/cells8040362

Howard, J., Grill, S. W., & Bois, J. S. (2011). Turing's next steps : The mechanochemical basis of morphogenesis. *Nature Reviews Molecular Cell Biology*, *12*(6), 392-398. https://doi.org/10.1038/nrm3120

Huang, Y.-L., & Niehrs, C. (2014). Polarized Wnt Signaling Regulates Ectodermal Cell Fate in Xenopus. *Developmental Cell*, *29*(2), 250-257. https://doi.org/10.1016/j.devcel.2014.03.015

Huber, F., Boire, A., López, M. P., & Koenderink, G. H. (2015). Cytoskeletal crosstalk : When three different personalities team up. *Current Opinion in Cell Biology*, *32*, 39-47. https://doi.org/10.1016/j.ceb.2014.10.005

Huckfeldt, R. M., Schubert, T., Morgan, J. L., Godinho, L., Di Cristo, G., Huang, Z. J., & Wong, R. O. L. (2009). Transient neurites of retinal horizontal cells exhibit columnar tiling

via homotypic interactions. *Nature Neuroscience*, *12*(1), 35-43. https://doi.org/10.1038/nn.2236

Hultman, K. A., Bahary, N., Zon, L. I., & Johnson, S. L. (2007). Gene Duplication of the Zebrafish kit ligand and Partitioning of Melanocyte Development Functions to kit ligand a. *PLOS Genetics*, *3*(1), e17. https://doi.org/10.1371/journal.pgen.0030017

Ibañez-Tallon, I., Heintz, N., & Omran, H. (2003). To beat or not to beat : Roles of cilia in development and disease. *Human Molecular Genetics*, *12*(suppl_1), R27-R35. https://doi.org/10.1093/hmg/ddg061

Ikenouchi, J., Furuse, M., Furuse, K., Sasaki, H., Tsukita, S., & Tsukita, S. (2005). Tricellulin constitutes a novel barrier at tricellular contacts of epithelial cells. *Journal of Cell Biology*, *171*(6), 939-945. https://doi.org/10.1083/jcb.200510043

Inaba, M., Harn, H. I.-C., & Chuong, C.-M. (2019). Turing patterning with and without a global wave. *PLOS Biology*, *17*(3), e3000195. https://doi.org/10.1371/journal.pbio.3000195

Inaba, M., Yamanaka, H., & Kondo, S. (2012). Pigment Pattern Formation by Contact-Dependent Depolarization. *Science*, *335*(6069), 677-677. https://doi.org/10.1126/science.1212821

Ing-Esteves, S., Kostadinov, D., Marocha, J., Sing, A. D., Joseph, K. S., Laboulaye, M. A., Sanes, J. R., & Lefebvre, J. L. (2018). Combinatorial Effects of Alpha- and Gamma-Protocadherins on Neuronal Survival and Dendritic Self-Avoidance. *Journal of Neuroscience*, *38*(11), 2713-2729. https://doi.org/10.1523/JNEUROSCI.3035-17.2018

Inomata, H. (2017). Scaling of pattern formations and morphogen gradients. *Development, growth & differentiation*, *59*(1), 41–51.

Irion, U., Frohnhöfer, H. G., Krauss, J., Çolak Champollion, T., Maischein, H.-M., Geiger-Rudolph, S., Weiler, C., & Nüsslein-Volhard, C. (2014). Gap junctions composed of connexins 41.8 and 39.4 are essential for colour pattern formation in zebrafish. *eLife*, *3*, e05125. https://doi.org/10.7554/eLife.05125

ISHIDA, T., TADOKORO, H., TAKAHASHI, H., YOSHIKAWA, H., & SAKAI, H. (2019). Constructing Models to Reproduce the Skin Color Patterns of Takifugu Species, Including Hybrids. *Journal of Fisheries Engineering*, *56*(1), 15–26.

Iwashita, M., Watanabe, M., Ishii, M., Chen, T., Johnson, S. L., Kurachi, Y., Okada, N., & Kondo, S. (2006). Pigment Pattern in jaguar/obelix Zebrafish Is Caused by a Kir7.1 Mutation : Implications for the Regulation of Melanosome Movement. *PLOS Genetics*, *2*(11), e197. https://doi.org/10.1371/journal.pgen.0020197

Jayatilaka, H., Giri, A., Karl, M., Aifuwa, I., Trenton, N. J., Phillip, J. M., Khatau, S., & Wirtz, D. (2018). EB1 and cytoplasmic dynein mediate protrusion dynamics for efficient 3-dimensional cell migration. *The FASEB Journal*, *32*(3), 1207-1221. https://doi.org/10.1096/fj.201700444RR

Jiang, T. X., Jung, H. S., Widelitz, R. B., & Chuong, C. M. (1999). Self-organization of periodic patterns by dissociated feather mesenchymal cells and the regulation of size, number and spacing of primordia. *Development*, *126*(22), 4997-5009.

Jiggins, C. D., Wallbank, R. W. R., & Hanly, J. J. (2017). Waiting in the wings : What can we learn about gene co-option from the diversification of butterfly wing patterns? *Philosophical Transactions of the Royal Society B: Biological Sciences*, *372*(1713), 20150485. https://doi.org/10.1098/rstb.2015.0485

Jordan, S. A., & Jackson, I. J. (2000). MGF (KIT ligand) is a chemokinetic factor for melanoblast migration into hair follicles. *Developmental biology*, *225*(2), 424–436.

Jung, H. S., Francis-West, P. H., Widelitz, R. B., Jiang, T. X., Ting-Berreth, S., Tickle, C., Wolpert, L., & Chuong, C. M. (1998). Local inhibitory action of BMPs and their relationships with activators in feather formation : Implications for periodic patterning. *Developmental Biology*, *196*(1), 11-23. https://doi.org/10.1006/dbio.1998.8850

Jung, H.-S., Akita, K., & Kim, J.-Y. (2003). Spacing patterns on tongue surface-gustatory papilla. *International Journal of Developmental Biology*, *48*(2-3), 157–161.

Kaddour, H., Coppola, E., Di Nardo, A. A., Le Poupon, C., Mailly, P., Wizenmann, A., Volovitch, M., Prochiantz, A., & Pierani, A. (2020). Extracellular Pax6 Regulates Tangential Cajal–Retzius Cell Migration in the Developing Mouse Neocortex. *Cerebral Cortex*, *30*(2), 465-475. https://doi.org/10.1093/cercor/bhz098

Kaltenbach, S. L., Yu, J.-K., & Holland, N. D. (2009). The origin and migration of the earliest-developing sensory neurons in the peripheral nervous system of amphioxus. *Evolution & Development*, *11*(2), 142-151. https://doi.org/10.1111/j.1525-142X.2009.00315.x

Kania, A., & Klein, R. (2016). Mechanisms of ephrin–Eph signalling in development, physiology and disease. *Nature reviews Molecular cell biology*, *17*(4), 240. https://doi.org/10.1038/nrm.2015.16

Kapur, R., Chandra, S., Cooper, R., McCarthy, J., & Williams, D. A. (2002). Role of p38 and ERK MAP kinase in proliferation of erythroid progenitors in response to stimulation by soluble and membrane isoforms of stem cell factor. *Blood*, *100*(4), 1287-1293. https://doi.org/10.1182/blood.V100.4.1287.h81602001287_1287_1293

Kay, J. N., Chu, M. W., & Sanes, J. R. (2012). MEGF10 and MEGF11 mediate homotypic interactions required for mosaic spacing of retinal neurons. *Nature*, *483*(7390), 465-469. https://doi.org/10.1038/nature10877

Kelsh, R. N. (2004). Genetics and evolution of pigment patterns in fish. *Pigment Cell Research*, *17*(4), 326–336.

Kessel, R. G., Beams, H. W., & Shih, C. Y. (1974). The origin, distribution and disappearance of surface cilia during embryonic development of Rana pipiens as revealed by scanning electron microscopy. *American Journal of Anatomy*, *141*(3), 341-359. https://doi.org/10.1002/aja.1001410306

Kim, J.-Y., Cho, S.-W., Song, W.-C., Lee, M.-J., Cai, J., Ohk, S.-H., Song, H.-K., Degan, A., & Jung, H.-S. (2005). Formation of spacing pattern and morphogenesis of chick feather buds is regulated by cytoskeletal structures. *Differentiation*, *73*(5), 240–248.

Kim, K., Lake, B. B., Haremaki, T., Weinstein, D. C., & Sokol, S. Y. (2012). Rab11 regulates planar polarity and migratory behavior of multiciliated cells in Xenopus embryonic epidermis. *Developmental Dynamics*, *241*(9), 1385-1395. https://doi.org/10.1002/dvdy.23826

Kim, S., Ma, L., Shokhirev, M. N., Quigley, I., & Kintner, C. (2018). Multicilin and activated E2f4 induce multiciliated cell differentiation in primary fibroblasts. *Scientific Reports*, *8*(1), 12369. https://doi.org/10.1038/s41598-018-30791-1

Kirshenbaum, A. S., Goff, J. P., Semere, T., Foster, B., Scott, L. M., & Metcalfe, D. D. (1999). Demonstration That Human Mast Cells Arise From a Progenitor Cell Population That Is CD34+, c-kit+, and Expresses Aminopeptidase N (CD13). *Blood*, *94*(7), 2333-2342. https://doi.org/10.1182/blood.V94.7.2333.419k30_2333_2342

Klein, R. (2012). Eph/ephrin signalling during development. *Development*, *139*(22), 4105-4109. https://doi.org/10.1242/dev.074997

Klos Dehring, D. A., Vladar, E. K., Werner, M. E., Mitchell, J. W., Hwang, P., & Mitchell, B. J. (2013). Deuterosome-Mediated Centriole Biogenesis. *Developmental Cell*, *27*(1), 103-112. https://doi.org/10.1016/j.devcel.2013.08.021

Kobia, F., Duchi, S., Deflorian, G., & Vaccari, T. (2014). Pharmacologic inhibition of vacuolar H+ ATPase reduces physiologic and oncogenic Notch signaling. *Molecular Oncology*, *8*(2), 207-220. https://doi.org/10.1016/j.molonc.2013.11.002

Koma, Y., Ito, A., Watabe, K., Hirata, T., Mizuki, M., Yokozaki, H., Kitamura, T., Kanakura, Y., & Kitamura, Y. (2005). Distinct role for c- kit receptor tyrosine kinase and SgIGSF adhesion molecule in attachment of mast cells to fibroblasts. *Laboratory Investigation*, *85*(3), 426-435. https://doi.org/10.1038/labinvest.3700231

Komiya, Y., Bai, Z., Cai, N., Lou, L., Al-Saadi, N., Mezzacappa, C., Habas, R., & Runnels, L. W. (2017). A Nonredundant Role for the TRPM6 Channel in Neural Tube Closure. *Scientific Reports*, *7*(1), 15623. https://doi.org/10.1038/s41598-017-15855-y

Kondo, S., & Miura, T. (2010). Reaction-Diffusion Model as a Framework for Understanding Biological Pattern Formation. *Science*, *329*(5999), 1616-1620. https://doi.org/10.1126/science.1179047

Kong, D., Wolf, F., & Großhans, J. (2017). Forces directing germ-band extension in Drosophila embryos. *Mechanisms of Development*, *144*, 11-22. https://doi.org/10.1016/j.mod.2016.12.001

Krause, M., Dent, E. W., Bear, J. E., Loureiro, J. J., & Gertler, F. B. (2003). Ena/VASP Proteins : Regulators of the Actin Cytoskeleton and Cell Migration. *Annual Review of Cell and Developmental Biology*, *19*(1), 541-564. https://doi.org/10.1146/annurev.cellbio.19.050103.103356

Krause, M., & Gautreau, A. (2014). Steering cell migration : Lamellipodium dynamics and the regulation of directional persistence. *Nature Reviews Molecular Cell Biology*, *15*(9), 577-590. https://doi.org/10.1038/nrm3861

Kulkarni, S. S., Griffin, J. N., Date, P. P., Liem, K. F., & Khokha, M. K. (2018). WDR5 Stabilizes Actin Architecture to Promote Multiciliated Cell Formation. *Developmental Cell*, *46*(5), 595-610.e3. https://doi.org/10.1016/j.devcel.2018.08.009

Kunimoto, K., Yamazaki, Y., Nishida, T., Shinohara, K., Ishikawa, H., Hasegawa, T., Okanoue, T., Hamada, H., Noda, T., Tamura, A., & Tsukita, S. S. (2012). Loss of basal feet on Odf2 deletion perturbs polarization of basal bodies. *Cilia*, *1*(1), O26. https://doi.org/10.1186/2046-2530-1-S1-O26

Kuriyama, S., Theveneau, E., Benedetto, A., Parsons, M., Tanaka, M., Charras, G., Kabla, A., & Mayor, R. (2014). In vivo collective cell migration requires an LPAR2-dependent increase in tissue fluidity. *Journal of Cell Biology*, *206*(1), 113-127. https://doi.org/10.1083/jcb.201402093

Kurosawa, K., Miyazawa, K., Gotoh, A., Katagiri, T., Nishimaki, J., Ashman, L. K., & Toyama, K. (1996). Immobilized anti-KIT monoclonal antibody induces ligand-independent dimerization and activation of Steel factor receptor : Biologic similarity with membrane-bound form of Steel factor rather than its soluble form. *Blood*, *87*(6), 2235-2243. https://doi.org/10.1182/blood.V87.6.2235.bloodjournal8762235

Kurrle, Y., Kunesch, K., Bogusch, S., & Schweickert, A. (2020). Serotonin and MucXS release by small secretory cells depend on Xpod, a SSC specific marker gene. *Genesis*, *58*(2), e23344. https://doi.org/10.1002/dvg.23344

Landge, A. N., Jordan, B. M., Diego, X., & Müller, P. (2020). Pattern formation mechanisms of self-organizing reaction-diffusion systems. *Developmental Biology*, *460*(1), 2-11. https://doi.org/10.1016/j.ydbio.2019.10.031

Lang, T., Klasson, S., Larsson, E., Johansson, M. E. V., Hansson, G. C., & Samuelsson, T. (2016). Searching the Evolutionary Origin of Epithelial Mucus Protein Components—Mucins and FCGBP. *Molecular Biology and Evolution*, *33*(8), 1921-1936. https://doi.org/10.1093/molbev/msw066

Lecuit, T., & Yap, A. S. (2015). E-cadherin junctions as active mechanical integrators in tissue dynamics. *Nature Cell Biology*, *17*(5), 533-539. https://doi.org/10.1038/ncb3136

Leduc, C., & Etienne-Manneville, S. (2015). Intermediate filaments in cell migration and invasion : The unusual suspects. *Current Opinion in Cell Biology*, *32*, 102-112. https://doi.org/10.1016/j.ceb.2015.01.005

Lennartsson, J., & Rönnstrand, L. (2012). Stem cell factor receptor/c-Kit : From basic science to clinical implications. *Physiological Reviews*, *92*(4), 1619-1649. https://doi.org/10.1152/physrev.00046.2011

Levayer, R., Pelissier-Monier, A., & Lecuit, T. (2011). Spatial regulation of Dia and Myosin-II by RhoGEF2 controls initiation of E-cadherin endocytosis during epithelial morphogenesis. *Nature Cell Biology*, *13*(5), 529-540. https://doi.org/10.1038/ncb2224

Liao, B.-K., & Oates, A. C. (2017). Delta-Notch signalling in segmentation. *Arthropod Structure & Development*, *46*(3), 429-447. https://doi.org/10.1016/j.asd.2016.11.007

Lin, C.-M., Jiang, T. X., Baker, R. E., Maini, P. K., Widelitz, R. B., & Chuong, C.-M. (2009). Spots and stripes : Pleomorphic patterning of stem cells via p-ERK-dependent cell chemotaxis shown by feather morphogenesis and mathematical simulation. *Developmental biology*, *334*(2), 369–382.

Lin, C.-M., Jiang, T. X., Widelitz, R. B., & Chuong, C.-M. (2006). Molecular signaling in feather morphogenesis. *Current opinion in cell biology*, *18*(6), 730–741.

Lyons, R. A., Saridogan, E., & Djahanbakhch, O. (2006). The reproductive significance of human Fallopian tube cilia. *Human Reproduction Update*, *12*(4), 363-372. https://doi.org/10.1093/humupd/dml012

Ma, L., Quigley, I., Omran, H., & Kintner, C. (2014). Multicilin drives centriole biogenesis via E2f proteins. *Genes & Development*, *28*(13), 1461-1471. https://doi.org/10.1101/gad.243832.114

MacDonald, R. B., Charlton-Perkins, M., & Harris, W. A. (2017). Mechanisms of Müller glial cell morphogenesis. *Current Opinion in Neurobiology*, *47*, 31-37. https://doi.org/10.1016/j.conb.2017.08.005

Mackenzie, M. A. F., Jordan, S. A., Budd, P. S., & Jackson, I. J. (1997). Activation of the Receptor Tyrosine Kinase Kit Is Required for the Proliferation of Melanoblasts in the Mouse Embryo. *Developmental Biology*, *192*(1), 99-107. https://doi.org/10.1006/dbio.1997.8738

Mani, M., Venkatasubrahmanyam, S., Sanyal, M., Levy, S., Butte, A., Weinberg, K., & Jahn, T. (2009). Wiskott-Aldrich syndrome protein is an effector of Kit signaling. *Blood*, *114*(14), 2900-2908. https://doi.org/10.1182/blood-2009-01-200733

Marcon, L., & Sharpe, J. (2012). Turing patterns in development : What about the horse part? *Current Opinion in Genetics & Development*, *22*(6), 578-584. https://doi.org/10.1016/j.gde.2012.11.013

Martin, B. L., & Harland, R. M. (2004). The developmental expression of two Xenopus laevis steel homologues, Xsl-1 and Xsl-2. *Gene Expression Patterns*, *5*(2), 239-243. https://doi.org/10.1016/j.modgep.2004.07.010

Mattila, P. K., & Lappalainen, P. (2008). Filopodia : Molecular architecture and cellular functions. *Nature Reviews Molecular Cell Biology*, *9*(6), 446-454. https://doi.org/10.1038/nrm2406

Mayor, R., & Carmona-Fontaine, C. (2010). Keeping in touch with contact inhibition of locomotion. *Trends in Cell Biology*, *20*(6), 319-328. https://doi.org/10.1016/j.tcb.2010.03.005

Mayor, R., & Etienne-Manneville, S. (2016). The front and rear of collective cell migration. *Nature Reviews Molecular Cell Biology*, *17*(2), 97-109. https://doi.org/10.1038/nrm.2015.14

Mayor, R., & Theveneau, E. (2014). The role of the non-canonical Wnt–planar cell polarity pathway in neural crest migration. *Biochemical Journal*, *457*(1), 19-26. https://doi.org/10.1042/BJ20131182

McLennan, R., Dyson, L., Prather, K. W., Morrison, J. A., Baker, R. E., Maini, P. K., & Kulesa, P. M. (2012). Multiscale mechanisms of cell migration during development : Theory and experiment. *Development*, *139*(16), 2935-2944. https://doi.org/10.1242/dev.081471

Meinhardt, H., & Gierer, A. (2000). Pattern formation by local self-activation and lateral inhibition. *BioEssays*, *22*(8), 753-760. https://doi.org/10.1002/1521-1878(200008)22:8<753::AID-BIES9>3.0.CO;2-Z

Meininger, C. J., Yano, H., Rottapel, R., Bernstein, A., Zsebo, K. M., & Zetter, B. R. (1992). The c-kit receptor ligand functions as a mast cell chemoattractant. *Blood*, *79*(4), 958-963. https://doi.org/10.1182/blood.V79.4.958.958

Metcalfe, D. D., Baram, D., & Mekori, Y. A. (1997). Mast cells. *Physiological Reviews*, *77*(4), 1033-1079. https://doi.org/10.1152/physrev.1997.77.4.1033

Michon, F., Charveron, M., & Dhouailly, D. (2007). Dermal condensation formation in the chick embryo : Requirement for integrin engagement and subsequent stabilization by a possible notch/integrin interaction. *Developmental dynamics: an official publication of the American Association of Anatomists*, *236*(3), 755–768.

Michon, F., Forest, L., Collomb, E., Demongeot, J., & Dhouailly, D. (2008). BMP2 and BMP7 play antagonistic roles in feather induction. *Development*, *135*(16), 2797-2805. https://doi.org/10.1242/dev.018341

Mierke, C. T., Ballmaier, M., Werner, U., Manns, M. P., Welte, K., & Bischoff, S. C. (2000). Human Endothelial Cells Regulate Survival and Proliferation of Human Mast Cells. *Journal of Experimental Medicine*, *192*(6), 801-812. https://doi.org/10.1084/jem.192.6.801

Mills, K. R., Kruep, D., & Saha, M. S. (1999). Elucidating the Origins of the Vascular System : A Fate Map of the Vascular Endothelial and Red Blood Cell Lineages inXenopus laevis. *Developmental Biology*, *209*(2), 352-368. https://doi.org/10.1006/dbio.1999.9245

Mishra, A. K., Campanale, J. P., Mondo, J. A., & Montell, D. J. (2019). Cell interactions in collective cell migration. *Development*, *146*(23). https://doi.org/10.1242/dev.172056

Miyazawa, K., Williams, D. A., Gotoh, A., Nishimaki, J., Broxmeyer, H. E., & Toyama, K. (1995). Membrane-bound Steel factor induces more persistent tyrosine kinase activation and longer life span of c-kit gene-encoded protein than its soluble form. *Blood*, *85*(3), 641-649. https://doi.org/10.1182/blood.V85.3.641.bloodjournal853641

Molyneaux, K. A., Zinszner, H., Kunwar, P. S., Schaible, K., Stebler, J., Sunshine, M. J., O'Brien, W., Raz, E., Littman, D., Wylie, C., & Lehmann, R. (2003). The chemokine

SDF1/CXCL12 and its receptor CXCR4 regulate mouse germ cell migration and survival. *Development*, *130*(18), 4279-4286. https://doi.org/10.1242/dev.00640

Montoro, D. T., Haber, A. L., Biton, M., Vinarsky, V., Lin, B., Birket, S. E., Yuan, F., Chen, S., Leung, H. M., Villoria, J., Rogel, N., Burgin, G., Tsankov, A. M., Waghray, A., Slyper, M., Waldman, J., Nguyen, L., Dionne, D., Rozenblatt-Rosen, O., … Rajagopal, J. (2018). A revised airway epithelial hierarchy includes CFTR-expressing ionocytes. *Nature*, *560*(7718), 319-324. https://doi.org/10.1038/s41586-018-0393-7

Moody, S. A. (1987a). Fates of the blastomeres of the 16-cell stage Xenopus embryo. *Developmental Biology*, *119*(2), 560-578. https://doi.org/10.1016/0012-1606(87)90059-5

Moody, S. A. (1987b). Fates of the blastomeres of the 32-cell-stage Xenopus embryo. *Developmental Biology*, *122*(2), 300-319. https://doi.org/10.1016/0012-1606(87)90296-X

Mort, R. L., Jackson, I. J., & Patton, E. E. (2015). The melanocyte lineage in development and disease. *Development*, *142*(4), 620-632. https://doi.org/10.1242/dev.106567

Munjal, A., & Lecuit, T. (2014). Actomyosin networks and tissue morphogenesis. *Development (Cambridge, England)*, *141*(9), 1789-1793. https://doi.org/10.1242/dev.091645

Murray, J. D. (1988). How the Leopard Gets Its Spots. *Scientific American*, *258*(3), 80-87. JSTOR.

Murrell, M., Oakes, P. W., Lenz, M., & Gardel, M. L. (2015). Forcing cells into shape : The mechanics of actomyosin contractility. *Nature Reviews Molecular Cell Biology*, *16*(8), 486-498. https://doi.org/10.1038/nrm4012

Nagata, S. (2005). Isolation, characterization, and extra-embryonic secretion of the Xenopus laevis embryonic epidermal lectin, XEEL. *Glycobiology*, *15*(3), 281-290. https://doi.org/10.1093/glycob/cwi010

Nagata, S., Nakanishi, M., Nanba, R., & Fujita, N. (2003). Developmental expression of XEEL, a novel molecule of the Xenopus oocyte cortical granule lectin family. *Development Genes and Evolution*, *213*(7), 368-370. https://doi.org/10.1007/s00427-003-0341-9

Nishikawa, S., Kusakabe, M., Yoshinaga, K., Ogawa, M., Hayashi, S., Kunisada, T., Era, T., Sakakura, T., & Nishikawa, S. (1991). In utero manipulation of coat color formation by a monoclonal anti-c-kit antibody : Two distinct waves of c-kit-dependency during melanocyte development. *The EMBO Journal*, *10*(8), 2111-2118. https://doi.org/10.1002/j.1460-2075.1991.tb07744.x

Nogare, D. D., & Chitnis, A. B. (2017). Self-organizing spots get under your skin. *PLOS Biology*, *15*(12), e2004412. https://doi.org/10.1371/journal.pbio.2004412

Nokhbatolfoghahai, M., Downie, J. R., Clelland, A. K., & Rennison, K. (2005). The surface ciliation of anuran amphibian embryos and early larvae : Patterns, timing differences and functions. *Journal of Natural History*, *39*(12), 887-929. https://doi.org/10.1080/00222930400002937

Nokhbatolfoghahai, M., Downie, J. R., & Ogilvy, V. (2006). Surface ciliation of anuran amphibian larvae : Persistence to late stages in some species but not others. *Journal of Morphology*, *267*(10), 1248-1256. https://doi.org/10.1002/jmor.10469

Noramly, S., Freeman, A., & Morgan, B. A. (1999). Beta-catenin signaling can initiate feather bud development. *Development*, *126*(16), 3509–3521.

Ochoa-Espinosa, A., Yu, D., Tsirigos, A., Struffi, P., & Small, S. (2009). Anterior-posterior positional information in the absence of a strong Bicoid gradient. *Proceedings of*

the National Academy of Sciences, *106*(10), 3823-3828. https://doi.org/10.1073/pnas.0807878105

Ohta, S., & Schoenwolf, G. C. (2018). Hearing crosstalk : The molecular conversation orchestrating inner ear dorsoventral patterning. *WIREs Developmental Biology*, *7*(1), e302. https://doi.org/10.1002/wdev.302

Oiso, N., Fukai, K., Kawada, A., & Suzuki, T. (2013). Piebaldism. *The Journal of Dermatology*, *40*(5), 330-335. https://doi.org/10.1111/j.1346-8138.2012.01583.x

Okayama, Y., & Kawakami, T. (2006). Development, migration, and survival of mast cells. *Immunologic Research*, *34*(2), 97-115. https://doi.org/10.1385/IR:34:2:97

Okumura, N., Tsuji, K., Ebihara, Y., Tanaka, I., Sawai, N., Koike, K., Komiyama, A., & Nakahata, T. (1996). Chemotactic and chemokinetic activities of stem cell factor on murine hematopoietic progenitor cells. *Blood*, *87*(10), 4100-4108. https://doi.org/10.1182/blood.V87.10.4100.bloodjournal87104100

Ossipova, O., Chu, C.-W., Fillatre, J., Brott, B. K., Itoh, K., & Sokol, S. Y. (2015). The involvement of PCP proteins in radial cell intercalations during Xenopus embryonic development. *Developmental Biology*, *408*(2), 316-327. https://doi.org/10.1016/j.ydbio.2015.06.013

Ossipova, O., Tabler, J., Green, J. B. A., & Sokol, S. Y. (2007). PAR1 specifies ciliated cells in vertebrate ectoderm downstream of aPKC. *Development*, *134*(23), 4297-4306. https://doi.org/10.1242/dev.009282

Owen, M. R., Sherratt, J. A., & Wearing, H. J. (2000). Lateral Induction by Juxtacrine Signaling Is a New Mechanism for Pattern Formation. *Developmental Biology*, *217*(1), 54-61. https://doi.org/10.1006/dbio.1999.9536

Pan, S., Dangaria, S., Gopinathan, G., Yan, X., Lu, X., Kolokythas, A., Niu, Y., & Luan, X. (2013). SCF Promotes Dental Pulp Progenitor Migration, Neovascularization, and Collagen Remodeling – Potential Applications as a Homing Factor in Dental Pulp Regeneration. *Stem Cell Reviews and Reports*, *9*(5), 655-667. https://doi.org/10.1007/s12015-013-9442-7

Parichy, D. M., Rawls, J. F., Pratt, S. J., Whitfield, T. T., & Johnson, S. L. (1999). Zebrafish sparse corresponds to an orthologue of c-kit and is required for the morphogenesis of a subpopulation of melanocytes, but is not essential for hematopoiesis or primordial germ cell development. *Development*, *126*(15), 3425-3436.

Park, T. J., Mitchell, B. J., Abitua, P. B., Kintner, C., & Wallingford, J. B. (2008). Dishevelled controls apical docking and planar polarization of basal bodies in ciliated epithelial cells. *Nature Genetics*, *40*(7), 871-879. https://doi.org/10.1038/ng.104

Pasquale, E. B. (2008). Eph-Ephrin Bidirectional Signaling in Physiology and Disease. *Cell*, *133*(1), 38-52. https://doi.org/10.1016/j.cell.2008.03.011

Pesce, M., Di Carlo, A., & De Felici, M. (1997). The c-kit receptor is involved in the adhesion of mouse primordial germ cells to somatic cells in culture. *Mechanisms of Development*, *68*(1), 37-44. https://doi.org/10.1016/S0925-4773(97)00120-2

Peterson, J. R., Bickford, L. C., Morgan, D., Kim, A. S., Ouerfelli, O., Kirschner, M. W., & Rosen, M. K. (2004). Chemical inhibition of N-WASP by stabilization of a native autoinhibited conformation. *Nature Structural & Molecular Biology*, *11*(8), 747-755. https://doi.org/10.1038/nsmb796

Petrovic, J., Formosa-Jordan, P., Luna-Escalante, J. C., Abelló, G., Ibañes, M., Neves, J., & Giraldez, F. (2014). Ligand-dependent Notch signaling strength orchestrates lateral induction and lateral inhibition in the developing inner ear. *Development*, *141*(11), 2313-2324. https://doi.org/10.1242/dev.108100

Pla, P., Alberti, C., Solov'eva, O., Pasdar, M., Kunisada, T., & Larue, L. (2005). Ednrb2 orients cell migration towards the dorsolateral neural crest pathway and promotes melanocyte differentiation. *Pigment Cell Research*, *18*(3), 181-187. https://doi.org/10.1111/j.1600-0749.2005.00230.x

Placzek, M., & Briscoe, J. (2018). Sonic hedgehog in vertebrate neural tube development. *International Journal of Developmental Biology*, *62*(1-3), 225-234.

Plasschaert, L. W., Žilionis, R., Choo-Wing, R., Savova, V., Knehr, J., Roma, G., Klein, A. M., & Jaffe, A. B. (2018). A single-cell atlas of the airway epithelium reveals the CFTR-rich pulmonary ionocyte. *Nature*, *560*(7718), 377-381. https://doi.org/10.1038/s41586-018-0394-6

Poché, R. A., & Reese, B. E. (2009). Retinal horizontal cells : Challenging paradigms of neural development and cancer biology. *Development*, *136*(13), 2141-2151. https://doi.org/10.1242/dev.033175

Pollard, T. D., Blanchoin, L., & Mullins, R. D. (2000). Molecular Mechanisms Controlling Actin Filament Dynamics in Nonmuscle Cells. *Annual Review of Biophysics and Biomolecular Structure*, *29*(1), 545-576. https://doi.org/10.1146/annurev.biophys.29.1.545

Quigley, I. K., Stubbs, J. L., & Kintner, C. (2011). Specification of ion transport cells in the Xenopus larval skin. *Development*, *138*(4), 705-714. https://doi.org/10.1242/dev.055699

Raspopovic, J., Marcon, L., Russo, L., & Sharpe, J. (2014). Digit patterning is controlled by a Bmp-Sox9-Wnt Turing network modulated by morphogen gradients. *Science*, *345*(6196), 566-570. https://doi.org/10.1126/science.1252960

Raven, M. A., Stagg, S. B., Nassar, H., & Reese, B. E. (2005). Developmental improvement in the regularity and packing of mouse horizontal cells : Implications for mechanisms underlying mosaic pattern formation. *Visual Neuroscience*, *22*(5), 569-573. https://doi.org/10.1017/S095252380522504X

Rawls, J. F., & Johnson, S. L. (2003). Temporal and molecular separation of the kit receptor tyrosine kinase's roles in zebrafish melanocyte migration and survival. *Developmental Biology*, *262*(1), 152-161. https://doi.org/10.1016/S0012-1606(03)00386-5

Raymond, K., Martin, S., Aractingi, S., & Lebrin, F. (2013). The (pro)renin receptor controls Wnt signalling : Promise from *Drosophila* and *Xenopus*. *European Journal of Dermatology*, *1*(1), 0-0. https://doi.org/10.1684/ejd.2013.1975

Reig, G., Pulgar, E., & Concha, M. L. (2014). Cell migration : From tissue culture to embryos. *Development*, *141*(10), 1999-2013. https://doi.org/10.1242/dev.101451

Richardson, B. E., & Lehmann, R. (2010). Mechanisms guiding primordial germ cell migration : Strategies from different organisms. *Nature Reviews. Molecular Cell Biology*, *11*(1), 37-49. https://doi.org/10.1038/nrm2815

Richelle, J., & Ghysen, A. (1979). Determination of sensory bristles and pattern formation in Drosophila : I. A model. *Developmental biology*, *70*(2), 418–437.

Ridley, A. J., Paterson, H. F., Johnston, C. L., Diekmann, D., & Hall, A. (1992). The small GTP-binding protein rac regulates growth factor-induced membrane ruffling. *Cell*, *70*(3), 401–410.

Rizvi, S. A., Neidt, E. M., Cui, J., Feiger, Z., Skau, C. T., Gardel, M. L., Kozmin, S. A., & Kovar, D. R. (2009). Identification and Characterization of a Small Molecule Inhibitor of Formin-Mediated Actin Assembly. *Chemistry & Biology*, *16*(11), 1158-1168. https://doi.org/10.1016/j.chembiol.2009.10.006

Rock, J. R., Randell, S. H., & Hogan, B. L. M. (2010). Airway basal stem cells : A perspective on their roles in epithelial homeostasis and remodeling. *Disease Models & Mechanisms*, *3*(9-10), 545-556. https://doi.org/10.1242/dmm.006031

Rockhill, R. L., Euler, T., & Masland, R. H. (2000). Spatial order within but not between types of retinal neurons. *Proceedings of the National Academy of Sciences*, *97*(5), 2303-2307. https://doi.org/10.1073/pnas.030413497

Roeth, J. F., Sawyer, J. K., Wilner, D. A., & Peifer, M. (2009). Rab11 Helps Maintain Apical Crumbs and Adherens Junctions in the Drosophila Embryonic Ectoderm. *PLOS ONE*, *4*(10), e7634. https://doi.org/10.1371/journal.pone.0007634

Rompolas, P., Patel-King, R. S., & King, S. M. (2009). Chapter 4 - Schmidtea mediterranea : A Model System for Analysis of Motile Cilia. In S. M. King & G. J. Pazour (Éds.), *Methods in Cell Biology* (Vol. 93, p. 81-98). Academic Press. https://doi.org/10.1016/S0091-679X(08)93004-1

Rönnstrand, L. (2004). Signal transduction via the stem cell factor receptor/c-Kit. *Cellular and Molecular Life Sciences CMLS*, *61*(19), 2535-2548. https://doi.org/10.1007/s00018-004-4189-6

Roth, S., Stein, D., & Nüsslein-Volhard, C. (1989). A gradient of nuclear localization of the dorsal protein determines dorsoventral pattern in the Drosophila embryo. *Cell*, *59*(6), 1189–1202.

Roycroft, A., & Mayor, R. (2016). Molecular basis of contact inhibition of locomotion. *Cellular and Molecular Life Sciences*, *73*(6), 1119-1130. https://doi.org/10.1007/s00018-015-2090-0

Roycroft, A., & Mayor, R. (2018). Michael Abercrombie : Contact inhibition of locomotion and more. *International Journal of Developmental Biology*, *62*(1-2-3), 5-13. https://doi.org/10.1387/ijdb.170277rm

Runyan, C., Schaible, K., Molyneaux, K., Wang, Z., Levin, L., & Wylie, C. (2006). Steel factor controls midline cell death of primordial germ cells and is essential for their normal proliferation and migration. *Development*, *133*(24), 4861-4869. https://doi.org/10.1242/dev.02688

Salazar-Ciudad, I., Solé, R. V., & Newman, S. A. (2001). Phenotypic and dynamical transitions in model genetic networks II. Application to the evolution of segmentation mechanisms. *Evolution & Development*, *3*(2), 95-103. https://doi.org/10.1046/j.1525-142x.2001.003002095.x

Samayawardhena, L. A., Kapur, R., & Craig, A. W. B. (2007). Involvement of Fyn kinase in Kit and integrin-mediated Rac activation, cytoskeletal reorganization, and chemotaxis of mast cells. *Blood*, *109*(9), 3679-3686. https://doi.org/10.1182/blood-2006-11-057315

Sanson, B. (2001). Generating patterns from fields of cells. *EMBO reports*, *2*(12), 1083–1088.

Scarpa, E., & Mayor, R. (2016). Collective cell migration in development. *Journal of Cell Biology*, *212*(2), 143-155. https://doi.org/10.1083/jcb.201508047

Scarpa, E., Szabó, A., Bibonne, A., Theveneau, E., Parsons, M., & Mayor, R. (2015). Cadherin Switch during EMT in Neural Crest Cells Leads to Contact Inhibition of Locomotion via Repolarization of Forces. *Developmental Cell*, *34*(4), 421-434. https://doi.org/10.1016/j.devcel.2015.06.012

Schohl, A., & Fagotto, F. (2002). β-catenin, MAPK and Smad signaling during early Xenopus development. *Development*, *129*(1), 37-52.

Sedzinski, J., Hannezo, E., Tu, F., Biro, M., & Wallingford, J. B. (2016). Emergence of an Apical Epithelial Cell Surface In Vivo. *Developmental Cell*, *36*(1), 24-35. https://doi.org/10.1016/j.devcel.2015.12.013

Sedzinski, J., Hannezo, E., Tu, F., Biro, M., & Wallingford, J. B. (2017). RhoA regulates actin network dynamics during apical surface emergence in multiciliated epithelial cells. *Journal of Cell Science*, *130*(2), 420-428. https://doi.org/10.1242/jcs.194704

Sengel, P. (1976). Morphogenesis of skin. *Developmental and cell biology series*, 1–17.

Sengel, P. (1975). Feather pattern development. *Ciba Found Symp*, *29*, 51–70.

Session, A. M., Uno, Y., Kwon, T., Chapman, J. A., Toyoda, A., Takahashi, S., Fukui, A., Hikosaka, A., Suzuki, A., Kondo, M., van Heeringen, S. J., Quigley, I., Heinz, S., Ogino, H., Ochi, H., Hellsten, U., Lyons, J. B., Simakov, O., Putnam, N., … Rokhsar, D. S. (2016). Genome evolution in the allotetraploid frog Xenopus laevis. *Nature*, *538*(7625), 336-343. https://doi.org/10.1038/nature19840

Shamloo, A., Manchandia, M., Ferreira, M., Mani, M., Nguyen, C., Jahn, T., Weinberg, K., & Heilshorn, S. (2013). Complex chemoattractive and chemorepellent Kit signals revealed by direct imaging of murine mast cells in microfluidic gradient chambers. *Integrative Biology*, *5*(8), 1076-1085. https://doi.org/10.1039/c3ib40025e

Shellard, A., & Mayor, R. (2019a). Supracellular migration – beyond collective cell migration. *Journal of Cell Science*, *132*(8). https://doi.org/10.1242/jcs.226142

Shellard, A., & Mayor, R. (2019b). Integrating chemical and mechanical signals in neural crest cell migration. *Current Opinion in Genetics & Development*, *57*, 16-24. https://doi.org/10.1016/j.gde.2019.06.004

Sheth, R., Marcon, L., Bastida, M. F., Junco, M., Quintana, L., Dahn, R., Kmita, M., Sharpe, J., & Ros, M. A. (2012). Hox Genes Regulate Digit Patterning by Controlling the Wavelength of a Turing-Type Mechanism. *Science*, *338*(6113), 1476-1480. https://doi.org/10.1126/science.1226804

Shoval, I., & Kalcheim, C. (2012). Antagonistic activities of Rho and Rac GTPases underlie the transition from neural crest delamination to migration. *Developmental Dynamics*, *241*(7), 1155-1168. https://doi.org/10.1002/dvdy.23799

Shyer, A. E., Rodrigues, A. R., Schroeder, G. G., Kassianidou, E., Kumar, S., & Harland, R. M. (2017). Emergent cellular self-organization and mechanosensation initiate follicle pattern in the avian skin. *Science*, *357*(6353), 811-815. https://doi.org/10.1126/science.aai7868

Sick, S., Reinker, S., Timmer, J., & Schlake, T. (2006). WNT and DKK Determine Hair Follicle Spacing Through a Reaction-Diffusion Mechanism. *Science*, *314*(5804), 1447-1450. https://doi.org/10.1126/science.1130088

Sim, H. J., Kim, S.-H., Myung, K.-J., Kwon, T., Lee, H.-S., & Park, T. J. (2018). Xenopus : An alternative model system for identifying muco-active agents. *PLOS ONE*, *13*(2), e0193310. https://doi.org/10.1371/journal.pone.0193310

Simões-Costa, M., & Bronner, M. E. (2015). Establishing neural crest identity : A gene regulatory recipe. *Development*, *142*(2), 242-257. https://doi.org/10.1242/dev.105445

Sirour, C., Hidalgo, M., Bello, V., Buisson, N., Darribère, T., & Moreau, N. (2011). Dystroglycan is involved in skin morphogenesis downstream of the Notch signaling pathway. *Molecular Biology of the Cell*, *22*(16), 2957-2969. https://doi.org/10.1091/mbc.e11-01-0074

Sive, H. L., Grainger, R. M., & Harland, R. M. (2000). *Early development of Xenopus laevis : A laboratory manual*. CSHL Press.

Sjöqvist, M., & Andersson, E. R. (2019). Do as I say, Not (ch) as I do : Lateral control of cell fate. *Developmental biology*, *447*(1), 58–70.

Smrž, D., Bandara, G., Beaven, M. A., Metcalfe, D. D., & Gilfillan, A. M. (2013). Prevention of F-actin assembly switches the response to SCF from chemotaxis to degranulation in human mast cells. *European Journal of Immunology*, *43*(7), 1873-1882. https://doi.org/10.1002/eji.201243214

Song, H.-K., Lee, S.-H., & Goetinck, P. F. (2004). FGF-2 signaling is sufficient to induce dermal condensations during feather development. *Developmental dynamics: an official publication of the American Association of Anatomists*, *231*(4), 741–749.

Spassky, N., & Meunier, A. (2017). The development and functions of multiciliated epithelia. *Nature Reviews Molecular Cell Biology*, *18*(7), 423-436. https://doi.org/10.1038/nrm.2017.21

Sprinzak, D., Lakhanpal, A., LeBon, L., Garcia-Ojalvo, J., & Elowitz, M. B. (2011). Mutual inactivation of Notch receptors and ligands facilitates developmental patterning. *PLoS Comput Biol*, *7*(6), e1002069.

Sprinzak, D., Lakhanpal, A., LeBon, L., Santat, L. A., Fontes, M. E., Anderson, G. A., Garcia-Ojalvo, J., & Elowitz, M. B. (2010). Cis-interactions between Notch and Delta generate mutually exclusive signalling states. *Nature*, *465*(7294), 86–90.

Spritz, R A, Giebel, L. B., & Holmes, S. A. (1992). Dominant negative and loss of function mutations of the c-kit (mast/stem cell growth factor receptor) proto-oncogene in human piebaldism. *American Journal of Human Genetics*, *50*(2), 261-269.

Spritz, Richard A., Droetto, S., & Fukushima, Y. (1992). Deletion of the KIT and PDGFRA genes in a patient with piebaldism. *American Journal of Medical Genetics*, *44*(4), 492-495. https://doi.org/10.1002/ajmg.1320440422

Stramer, B., Moreira, S., Millard, T., Evans, I., Huang, C.-Y., Sabet, O., Milner, M., Dunn, G., Martin, P., & Wood, W. (2010). Clasp-mediated microtubule bundling regulates persistent motility and contact repulsion in Drosophila macrophages in vivo. *Journal of Cell Biology*, *189*(4), 681-689. https://doi.org/10.1083/jcb.200912134

Stubbs, J. L., Vladar, E. K., Axelrod, J. D., & Kintner, C. (2012). Multicilin promotes centriole assembly and ciliogenesis during multiciliate cell differentiation. *Nature Cell Biology*, *14*(2), 140-147. https://doi.org/10.1038/ncb2406

Stubbs, Jennifer L., Davidson, L., Keller, R., & Kintner, C. (2006). Radial intercalation of ciliated cells during Xenopus skin development. *Development*, *133*(13), 2507-2515. https://doi.org/10.1242/dev.02417

Stubbs, Jennifer L., Oishi, I., Izpisúa Belmonte, J. C., & Kintner, C. (2008). The forkhead protein Foxj1 specifies node-like cilia in Xenopus and zebrafish embryos. *Nature Genetics*, *40*(12), 1454-1460. https://doi.org/10.1038/ng.267

Sun, L., Lee, J., & Fine, H. A. (2004). Neuronally expressed stem cell factor induces neural stem cell migration to areas of brain injury. *The Journal of Clinical Investigation*, *113*(9), 1364-1374. https://doi.org/10.1172/JCI20001

Suraneni, P., Rubinstein, B., Unruh, J. R., Durnin, M., Hanein, D., & Li, R. (2012). The Arp2/3 complex is required for lamellipodia extension and directional fibroblast cell migration. *Journal of Cell Biology*, *197*(2), 239-251. https://doi.org/10.1083/jcb.201112113

Sutherland, A., Keller, R., & Lesko, A. (2020). Convergent extension in mammalian morphogenesis. *Seminars in Cell & Developmental Biology*, *100*, 199-211. https://doi.org/10.1016/j.semcdb.2019.11.002

Svitkina, T. (2018). The Actin Cytoskeleton and Actin-Based Motility. *Cold Spring Harbor Perspectives in Biology*, *10*(1), a018267. https://doi.org/10.1101/cshperspect.a018267

Szabó, A., Cobo, I., Omara, S., McLachlan, S., Keller, R., & Mayor, R. (2016). The Molecular Basis of Radial Intercalation during Tissue Spreading in Early Development. *Developmental Cell*, *37*(3), 213-225. https://doi.org/10.1016/j.devcel.2016.04.008

Szabó, A., & Mayor, R. (2018). Mechanisms of Neural Crest Migration. *Annual Review of Genetics*, *52*(1), 43-63. https://doi.org/10.1146/annurev-genet-120417-031559

Tabone-Eglinger, S., Calderin-Sollet, Z., Pinon, P., Aebischer, N., Wehrle-Haller, M., Jacquier, M.-C., Boettiger, D., & Wehrle-Haller, B. (2014). Niche anchorage and signaling through membrane-bound Kit-ligand/c-kit receptor are kinase independent and imatinib insensitive. *The FASEB Journal*, *28*(10), 4441-4456. https://doi.org/10.1096/fj.14-249425

Tabone-Eglinger, S., Wehrle-Haller, M., Aebischer, N., Jacquier, M.-C., & Wehrle-Haller, B. (2012). Membrane-bound Kit ligand regulates melanocyte adhesion and survival, providing physical interaction with an intraepithelial niche. *The FASEB Journal*, *26*(9), 3738–3753.

Tajima, Y., Moore, M. A. S., Soares, V., Ono, M., Kissel, H., & Besmer, P. (1998). Consequences of exclusive expression in vivo of kit-ligand lacking the major proteolytic cleavage site. *Proceedings of the National Academy of Sciences*, *95*(20), 11903-11908. https://doi.org/10.1073/pnas.95.20.11903

Takahashi, C., Kusakabe, M., Suzuki, T., Miyatake, K., & Nishida, E. (2015). Mab21-l3 regulates cell fate specification of multiciliate cells and ionocytes. *Nature Communications*, *6*(1), 6017. https://doi.org/10.1038/ncomms7017

Taylor, H. B., Khuong, A., Wu, Z., Xu, Q., Morley, R., Gregory, L., Poliakov, A., Taylor, W. R., & Wilkinson, D. G. (2017). Cell segregation and border sharpening by Eph receptor–ephrin-mediated heterotypic repulsion. *Journal of The Royal Society Interface*, *14*(132), 20170338. https://doi.org/10.1098/rsif.2017.0338

Theveneau, E., Marchant, L., Kuriyama, S., Gull, M., Moepps, B., Parsons, M., & Mayor, R. (2010). Collective Chemotaxis Requires Contact-Dependent Cell Polarity. *Developmental Cell*, *19*(1), 39-53. https://doi.org/10.1016/j.devcel.2010.06.012

Theveneau, E., & Mayor, R. (2011). Can mesenchymal cells undergo collective cell migration? The case of the neural crest. *Cell Adhesion & Migration*, *5*(6), 490-498. https://doi.org/10.4161/cam.5.6.18623

Theveneau, E., & Mayor, R. (2012a). Neural crest migration : Interplay between chemorepellents, chemoattractants, contact inhibition, epithelial-mesenchymal transition, and collective cell migration. *Wiley Interdisciplinary Reviews. Developmental Biology*, *1*(3), 435-445. https://doi.org/10.1002/wdev.28

Theveneau, E., & Mayor, R. (2012b). Neural crest delamination and migration : From epithelium-to-mesenchyme transition to collective cell migration. *Developmental Biology*, *366*(1), 34-54. https://doi.org/10.1016/j.ydbio.2011.12.041

Theveneau, E., Steventon, B., Scarpa, E., Garcia, S., Trepat, X., Streit, A., & Mayor, R. (2013). Chase-and-run between adjacent cell populations promotes directional collective migration. *Nature Cell Biology*, *15*(7), 763-772. https://doi.org/10.1038/ncb2772

Thomas, A. J., & Erickson, C. A. (2008). The making of a melanocyte : The specification of melanoblasts from the neural crest. *Pigment Cell & Melanoma Research*, *21*(6), 598-610. https://doi.org/10.1111/j.1755-148X.2008.00506.x

Toyofuku, T., Yoshida, J., Sugimoto, T., Yamamoto, M., Makino, N., Takamatsu, H., Takegahara, N., Suto, F., Hori, M., Fujisawa, H., Kumanogoh, A., & Kikutani, H. (2008). Repulsive and attractive semaphorins cooperate to direct the navigation of cardiac neural crest cells. *Developmental Biology*, *321*(1), 251-262. https://doi.org/10.1016/j.ydbio.2008.06.028

Troost, T., Schneider, M., & Klein, T. (2015). A Re-examination of the Selection of the Sensory Organ Precursor of the Bristle Sensilla of Drosophila melanogaster. *PLOS Genetics*, *11*(1), e1004911. https://doi.org/10.1371/journal.pgen.1004911

Turing, A. M. (1952). The Chemical Basis of Morphogenesis. *Philosophical Transactions of the Royal Society of London. Series B, Biological Sciences*, *237*(641), 37-72. JSTOR.

Vaccari, T., Duchi, S., Cortese, K., Tacchetti, C., & Bilder, D. (2010). The vacuolar ATPase is required for physiological as well as pathological activation of the Notch receptor. *Development*, *137*(11), 1825-1832. https://doi.org/10.1242/dev.045484

Van Lommel, A. T. L. (2003). Tissues. In A. T. L. Van Lommel (Éd.), *From Cells to Organs : A Histology Textbook and Atlas* (p. 59-122). Springer US. https://doi.org/10.1007/978-1-4615-0353-8_4

Vandamme, N., & Berx, G. (2019). From neural crest cells to melanocytes : Cellular plasticity during development and beyond. *Cellular and Molecular Life Sciences*, *76*(10), 1919-1934. https://doi.org/10.1007/s00018-019-03049-w

Villar-Cerviño, V., Molano-Mazón, M., Catchpole, T., Valdeolmillos, M., Henkemeyer, M., Martínez, L. M., Borrell, V., & Marín, O. (2013). Contact Repulsion Controls the Dispersion and Final Distribution of Cajal-Retzius Cells. *Neuron*, *77*(3), 457-471. https://doi.org/10.1016/j.neuron.2012.11.023

Vladar, E. K., & Axelrod, J. D. (2008). Dishevelled links basal body docking and orientation in ciliated epithelial cells. *Trends in Cell Biology*, *18*(11), 517-520. https://doi.org/10.1016/j.tcb.2008.08.004

Wagner, O. I., Rammensee, S., Korde, N., Wen, Q., Leterrier, J.-F., & Janmey, P. A. (2007). Softness, strength and self-repair in intermediate filament networks. *Experimental Cell Research*, *313*(10), 2228-2235. https://doi.org/10.1016/j.yexcr.2007.04.025

Walck-Shannon, E., & Hardin, J. (2014). Cell intercalation from top to bottom. *Nature Reviews Molecular Cell Biology*, *15*(1), 34-48. https://doi.org/10.1038/nrm3723

Walentek, P., Bogusch, S., Thumberger, T., Vick, P., Dubaissi, E., Beyer, T., Blum, M., & Schweickert, A. (2014). A novel serotonin-secreting cell type regulates ciliary motility in the mucociliary epidermis of Xenopus tadpoles. *Development*, *141*(7), 1526-1533. https://doi.org/10.1242/dev.102343

Walentek, P., & Quigley, I. K. (2017). What we can learn from a tadpole about ciliopathies and airway diseases : Using systems biology in Xenopus to study cilia and mucociliary epithelia. *Genesis*, *55*(1-2), e23001. https://doi.org/10.1002/dvg.23001

Wang, F., Shi, Z., Cui, Y., Guo, X., Shi, Y.-B., & Chen, Y. (2015). Targeted gene disruption in Xenopus laevis using CRISPR/Cas9. *Cell & Bioscience*, *5*(1), 15. https://doi.org/10.1186/s13578-015-0006-1

Wanner, A., Salathé, M., & O'Riordan, T. G. (1996). Mucociliary clearance in the airways. *American Journal of Respiratory and Critical Care Medicine*, *154*(6), 1868-1902. https://doi.org/10.1164/ajrccm.154.6.8970383

Wassle, H., & Boycott, B. B. (1991). Functional architecture of the mammalian retina. *Physiological Reviews*, *71*(2), 447-480. https://doi.org/10.1152/physrev.1991.71.2.447

Wässle, H., Riemann, H. J., & Boycott, B. B. (1978). The mosaic of nerve cells in the mammalian retina. *Proceedings of the Royal Society of London. Series B. Biological Sciences*, *200*(1141), 441-461. https://doi.org/10.1098/rspb.1978.0026

Watanabe, M., & Kondo, S. (2015). Is pigment patterning in fish skin determined by the Turing mechanism? *Trends in Genetics*, *31*(2), 88-96. https://doi.org/10.1016/j.tig.2014.11.005

Weber, G. F., Bjerke, M. A., & DeSimone, D. W. (2012). A mechanoresponsive cadherin-keratin complex directs polarized protrusive behavior and collective cell migration. Developmental Cell, 22(1), 104-115. https://doi.org/10.1016/j.devcel.2011.10.013

Wehrle-Haller, B., & Weston, J. A. (1995). Soluble and cell-bound forms of steel factor activity play distinct roles in melanocyte precursor dispersal and survival on the lateral neural crest migration pathway. *Development*, *121*(3), 731-742.

Wehrle-Haller, Bernhard, & Imhof, B. A. (2003). Actin, microtubules and focal adhesion dynamics during cell migration. *The International Journal of Biochemistry & Cell Biology*, *35*(1), 39-50. https://doi.org/10.1016/S1357-2725(02)00071-7

Wehrle-Haller, Bernhard, Meller, M., & Weston, J. A. (2001). Analysis of Melanocyte Precursors in Nf1 Mutants Reveals That MGF/KIT Signaling Promotes Directed Cell Migration Independent of Its Function in Cell Survival. *Developmental Biology*, *232*(2), 471-483. https://doi.org/10.1006/dbio.2001.0167

Wells, K. L., Hadad, Y., Ben-Avraham, D., Hillel, J., Cahaner, A., & Headon, D. J. (2012). Genome-wide SNP scan of pooled DNA reveals nonsense mutation in FGF20 in the scaleless line of featherless chickens. *BMC Genomics*, *13*(1), 257. https://doi.org/10.1186/1471-2164-13-257

Werner, M. E., & Mitchell, B. J. (2012). Understanding ciliated epithelia : The power of Xenopus. *Genesis*, *50*(3), 176-185. https://doi.org/10.1002/dvg.20824

Werner, Michael E, Hwang, P., Huisman, F., Taborek, P., Yu, C. C., & Mitchell, B. J. (2011). Actin and microtubules drive differential aspects of planar cell polarity in multiciliated cells. *Journal of Cell Biology*, *195*(1), 19-26. https://doi.org/10.1083/jcb.201106110

Werner, Michael E., Mitchell, J. W., Putzbach, W., Bacon, E., Kim, S. K., & Mitchell, B. J. (2014). Radial intercalation is regulated by the Par complex and the microtubule-stabilizing protein CLAMP/Spef1. *Journal of Cell Biology*, *206*(3), 367-376. https://doi.org/10.1083/jcb.201312045

Widelitz, R. B., & Chuong, C.-M. (1999). Early events in skin appendage formation : Induction of epithelial placodes and condensation of dermal mesenchyme. *Journal of Investigative Dermatology Symposium Proceedings*, *4*(3), 302–306.

Wigglesworth, V. (1940). Local and General Factors in the Development of" Pattern" in Rhodnius Prolixus (Hemiptera). *Journal of Experimental Biology*, *17*(2), 180–201.

Wigglesworth, Vb. (1953). The origin of sensory neurones in an insect, Rhodnius prolixus (Hemiptera). *Journal of Cell Science*, *3*(25), 93–112.

Wilson, Y. M., Richards, K. L., Ford-Perriss, M. L., Panthier, J.-J., & Murphy, M. (2004). Neural crest cell lineage segregation in the mouse neural tube. *Development*, *131*(24), 6153-6162. https://doi.org/10.1242/dev.01533

Winder, S. J. (1997). REVIEW : The membrane--cytoskeleton interface: the role of dystrophin and utrophin. *Journal of Muscle Research & Cell Motility*, *18*(6), 617-629. https://doi.org/10.1023/A:1018627705273

Winkelman, J. D., Suarez, C., Hocky, G. M., Harker, A. J., Morganthaler, A. N., Christensen, J. R., Voth, G. A., Bartles, J. R., & Kovar, D. R. (2016). Fascin- and α-Actinin-Bundled

Networks Contain Intrinsic Structural Features that Drive Protein Sorting. *Current Biology*, *26*(20), 2697-2706. https://doi.org/10.1016/j.cub.2016.07.080

Wolpert, L. (1969). Positional information and the spatial pattern of cellular differentiation. *Journal of Theoretical Biology*, *25*(1), 1-47. https://doi.org/10.1016/S0022-5193(69)80016-0

Wolpert, Lewis. (1998). Pattern formation in epithelial development : The vertebrate limb and feather bud spacing. *Philosophical Transactions of the Royal Society of London. Series B: Biological Sciences*, *353*(1370), 871–875.

Wu, S. K., & Priya, R. (2019). Spatio-Temporal Regulation of RhoGTPases Signaling by Myosin II. *Frontiers in Cell and Developmental Biology*, *7*, 90. https://doi.org/10.3389/fcell.2019.00090

Yamaguchi, H., Miki, H., & Takenawa, T. (2002). Neural Wiskott-Aldrich Syndrome Protein Is Involved in Hepatocyte Growth Factor-induced Migration, Invasion, and Tubulogenesis of Epithelial Cells. *Cancer Research*, *62*(9), 2503-2509.

Yamanaka, H., & Kondo, S. (2014). In vitro analysis suggests that difference in cell movement during direct interaction can generate various pigment patterns in vivo. *Proceedings of the National Academy of Sciences*, *111*(5), 1867-1872. https://doi.org/10.1073/pnas.1315416111

Yoon, J., Hwang, Y.-S., Lee, M., Sun, J., Cho, H. J., Knapik, L., & Daar, I. O. (2018). TBC1d24-ephrinB2 interaction regulates contact inhibition of locomotion in neural crest cell migration. *Nature Communications*, *9*(1), 3491. https://doi.org/10.1038/s41467-018-05924-9

Zagorski, M., Tabata, Y., Brandenberg, N., Lutolf, M. P., Tkačik, G., Bollenbach, T., Briscoe, J., & Kicheva, A. (2017). Decoding of position in the developing neural tube from antiparallel morphogen gradients. *Science*, *356*(6345), 1379-1383. https://doi.org/10.1126/science.aam5887

Zuo, K., Kuang, D., Wang, Y., Xia, Y., Tong, W., Wang, X., Chen, Y., Duan, Y., & Wang, G. (2016). SCF/c-kit transactivates CXCR4-serine 339 phosphorylation through G protein-coupled receptor kinase 6 and regulates cardiac stem cell migration. *Scientific Reports*, *6*(1), 26812. https://doi.org/10.1038/srep26812